Hydroclimatic variability and the integration of renewable energy in Europe : multiscale evaluation of the supply-demand balance for various energy sources and mixes

Damien Raynaud

Communauté
UNIVERSITÉ Grenoble Alpes

THÈSE

Pour obtenir le grade de

DOCTEUR DE la Communauté UNIVERSITÉ GRENOBLE ALPES

Spécialité : **Océan, Atmosphère, Hydrologie**

Arrêté ministériel : 7 Août 2006

Présentée par

Damien Raynaud

Thèse dirigée par **Benoît Hingray**

préparée au sein **Laboratoire d'étude des Transferts en Hydrologie et environnement (LTHE, UMR 5564, CNRS - Grenoble INP -IRD - UGA)**
et de **Terre Univers Environnement**

Hydroclimatic variability and the integration of renewable energy in Europe.

Multiscale evaluation of the supply-demand balance for various energy sources and mixes.

Thèse soutenue publiquement le **8 Décembre 2016**,
devant le jury composé de :

Mme Delphine Riu
Professeure, Grenoble INP, G2Elab-ENSE^3, Grenoble, Président

Mme Pascale Braconnot
Directrice de Recherche, CEA, LSCE-IPSL, Gif-sur-Yvette, Rapporteur

M Christoph Schär
Professeur, ETHZ, ICA, Zurich, Rapporteur

M Jean-Dominique Creutin
Directeur de Recherche, CNRS, LTHE, Grenoble, Examinateur

M Julien Boé
Chargé de Recherche, CNRS, CERFACS, Toulouse, Examinateur

M Guillaume Bontron
Ingénieur Expert, CNR, Lyon, Invité

M Benoît Hingray
Chargé de Recherche, CNRS, LTHE, Grenoble, Directeur de thèse

“La pensée se forme dans l’âme comme les nuages se forment dans l’air”
JOSEPH JOUBERT

Remerciements

Je tiens tout d'abord à remercier l'ensemble des membres du jury d'avoir accepté d'évaluer mon travail et de m'avoir accordé le titre de docteur de l'université de Grenoble.

En Septembre 2012, alors que je commerçais un stage d'un an au JRC, Benoît et Sandrine me téléphonaient pour me proposer de contribuer au projet COMPLEX en réalisant cette thèse au sein du LTHE. Dès le début, ils ont eu une confiance totale en moi et je les en remercie. Benoît a toujours été à mes côtés, disponible et bienveillant, pour que ces trois années de travail soient riches scientifiquement mais aussi humainement. Malgré les difficultés, qui avouons-le ont été nombreuses et diverses, ses qualités nous ont toujours permis d'avancer. Je suis très heureux que Benoît ait pu obtenir son HDR et je suis même fier qu'il apparaisse pour la première fois en tant que directeur de thèse sur mon manuscrit.

Une thèse c'est aussi un travail d'équipe. J'ai eu beaucoup de plaisir à travailler et à échanger avec tous ceux qui étaient impliqués dans le projet COMPLEX, en particulier Jean-Dominique et Baptiste, qui ont eux aussi toujours eu entièrement confiance en mon travail. Anne-Catherine, Sandrine, Jean-Philippe et Hubert Gallet ont également contribué, par leur implication dans mon comité de suivi de thèse, à faire de cette thèse ce qu'elle est aujourd'hui.

Au cours de ces trois années, j'ai également eu l'occasion de participer à l'encadrement de stagiaires. Remy, Quentin, Handriyanti et Florent ont tous contribué à cette thèse en réalisant des travaux exploratoires et me faisant ainsi gagner un temps précieux. Je remercie plus particulièrement Remy qui est pour moi le stagiaire rêvé de tout encadrant de par ses qualités scientifiques mais aussi son enthousiasme et sa gentillesse.

Lors de mon arrivée à Grenoble, mon goût et mes compétences pour la programmation étaient pour ainsi dire relatifs. Mais comme dans beaucoup de domaines, il suffit d'un déclic et surtout d'une personne pour vous faire apprécier ce qui ne m'apparaissait au début que comme une tâche parmi d'autres. Samuel, en plus d'être un co-bureau en or, a consacré un temps incalculable à m'apprendre

et à m'aider à programmer. Sans lui, il n'aurait pas été possible pour moi de vous présenter ce travail et je n'aurais pas pris autant de plaisir à développer tous les outils nécessaires. J'en profite pour remercier également la plateforme de calcul de Grenoble CIMENT sans laquelle 18 années auraient été nécésssaires pour réaliser l'optimisation de SCAMP!

Mon contrat au LTHE a commencé le 15 septembre 2013, deux semaines plus tard arrivaient deux nouveaux doctorants au sein de mon équipe, Aurélien et Saif. Il n'a pas fallu longtemps pour souder notre trio et démarrer trois années d'amitié qui laissent des souvenirs inoubliables. Merci à vous deux pour ces moments passés à rire depuis notre première soirée mémorable au O'Callaghan, jusqu'à mon pot de thèse.

Nous n'avons pas ri qu'à trois pendant ces années de thèse. Fleur, Jeremy, Stéphanie, Olivier, Melody, Nicolas, Audrey, Galateia, et Camille étaient là dès le début et ont vite été rejoints par Guillaume et Marion et toute une nouvelle génération de doctorants, Victor, François, Aude, Joseph et Louise. Merci à vous aussi pour les pauses de midi décontractées, les soirées, les randos, les sorties skis... etc.

En 2014, j'ai croisé le chemin de deux habitants des grandes plaines américaines en visite au LTHE. Grâce à eux, j'ai pu profiter d'une pause bien méritée en deuxième année, rencontrer des gens fabuleux aux États-Unis et réaliser mon rêve de devenir pour quelques jours un "chasseur de tornades". Chad, Zac, thank you so much for welcoming me in Norman and San Antonio. I had the best time with you, your friends and your families in OK and TX. I will be back soon to try my luck at stormchasing again!

Tous ceux qui me connaissent le savent. Si je me suis tant plu dans mon appartement, c'est grâce aux Voisins (avec un grand V oui!). Le 39 rue Abbé Grégoire (3ème et 4ème étages), c'est un peu comme une grande coloc. Ça a commencé avec David et Maëlle, puis le cercle a été vite élargi avec Paul et Matthieu. Merci pour ces soirées au Jules Verne, ces diners, ces coinches... J'ai bien peur de ne jamais retrouver des voisins comme vous.

J'ai aussi eu une vie avant ma thèse (il paraît même qu'il y en a une après) où je me suis fait des amis qui ont été là jusqu'à aujourd'hui dans les bons moments mais aussi quand le moral atteignait un minimum local. Merci Fred d'être toujours là et de partager tant de choses avec moi. Merci les Ariègeois: Romain, Lucie, Guillaume, Caroline et Pauline. Thank you Rachel for your support, for correcting the introduction of my manuscript and for convincing me that my English was good enough for me to write the entire thesis in English. Merci aux météos, Jonathan et Lucie. Merci à Charles, Philippe et Alex.

Enfin, si j'en suis arrivé là, c'est en grande partie grâce à mes proches qui ont toujours cru en moi. Merci à mes parents, ma sœur, ma nièce et mon grand-père. Une pensée pour Marie-Thérèse et pour ma grand-mère qui auraient été fières de m'appeler "Docteur".

Bonne lecture à tous !

Résumé étendu

1. Introduction

Le dernier rapport du GIEC [IPCC, 2013] dresse un bilan alarmant du changement climatique et de ses conséquences non seulement sur le système hydro-climatique mais aussi, plus généralement, sur l'ensemble des systèmes naturels ou socioéconomiques que comporte notre planète et qui sont de près ou de loin liés au climat. Face à ce constat, la communauté internationale s'est mobilisée, notamment lors de la dernière conférence des parties à Paris (COP21) [United-Nations, 2015]. L'objectif principal fixé par l'accord engage les pays signataires à réduire leurs émissions de gaz à effet de serre afin de limiter la hausse de la température à 1.5°C par rapport aux niveaux préindustriels. Un des bras de levier possible pour cette décarbonisation profonde de notre société consiste à accélérer "l'électrification" des systèmes énergétiques utilisant jusqu'ici des sources d'énergie fossiles. Cependant, il est également nécessaire de transformer nos modes de production d'électricité et d'augmenter la part d'énergie renouvelable.

Le système terrestre offre un large panel de sources d'énergie propres et inépuisables. On peut citer, par exemple, la géothermie et les énergies marines. D'autres contributions proviennent de l'exploitation du système hydro-climatique et rassemblent les énergies, hydro-électrique, photovoltaïque et éolienne. Ces trois sources, ci-après rassemblées sous l'acronyme (CRE - Climate Related Energy) sont déjà largement exploitées en Europe grâce aux ressources importantes mises en évidences par de nombreuses études [Von Bremen, 2010; Vautard et al., 2014]. Cependant, l'intégration directe de ces énergies dans le système de production électrique est entravée par leurs fortes fluctuations résultant des variations hydrométéorologiques à différentes échelles spatio-temporelles. Il devient alors difficile de répondre à la demande énergétique, par ailleurs aussi soumise à de fortes variations liées, pour certaines, aux fluctuations météorologiques (chauffage et climatisation). Plus la part de CRE est importante, plus ce problème d'inadéquation temporelle entre production et demande devient critique et difficile à gérer sans l'intervention de systèmes de stockage ou de sources d'énergie d'appoint.

Cette thèse a pour objectif de contribuer à l'évaluation de la faisabilité hydrométéorologique d'un système de production électrique uniquement basé sur les CRE. En particulier, les problèmes multi-

échelles d'inadéquation entre production et demande liés aux conditions hydrométéorologiques sont étudiés en Europe. Ces travaux ont contribué au projet Européen COMPLEX qui regroupe communauté scientifique et parties prenantes et vise à répondre aux nombreuses questions soulevées par la transition de l'Europe vers une société faiblement émettrice en gaz à effet de serre.

2. Cadre d'étude, hypothèses et résultats en climat passé récent

Cette étude est menée sur 12 régions européennes réparties de manière homogène sur le continent afin de capter les variations spatiales des conditions hydro climatiques. Nous nous plaçons dans un cadre volontairement caricatural et anhistorique, reposant sur différentes hypothèses dont les principales sont les suivantes :

- Chaque région est autonome énergétiquement et "isolée" du reste des régions européennes. La demande énergique locale est entièrement satisfaite par la production régionale.
- L'ensemble de la production est renouvelable et basée de surcroit sur les seules énergies pilotées par la météorologie (énergies hydro-électrique, photovoltaïque et éolienne).
- Afin de se libérer des questions de ressource et de se focaliser sur les fluctuations liées aux conditions hydro-climatiques, la production énergétique moyenne est supposée égale à la demande moyenne sur l'ensemble de la période d'étude.

Pour nos analyses, nous avons mis en place une chaîne de modélisation complète permettant la conversion de données météorologiques en données de production et demande électrique. Cette chaine a été appliquée sur l'ensemble des régions d'étude. Les données météorologiques utilisées en entrée de la chaine sont des données issues d'observations [Haylock et al., 2008 ; Müller et al., 2015] ou de pseudo observations [Vautard et al., 2014] extraites au pas de temps journalier entre 1983 et 2012 pour les 12 régions européennes. Un modèle hydrologique conceptuel proposé par [Schaefli et al., 2005] est utilisé pour générer 30 ans de séries journalières de débit régional. La conversion des variables hydrométéorologiques en production électrique journalière est faite via l'utilisation de modèles conceptuels de production basés sur des équipements génériques (ferme solaire, ferme éolienne, centrale hydroélectrique au fil de l'eau). Les séries de demande énergétique sont produites à l'aide d'un modèle simple dépendant uniquement de la température de l'air et prenant en compte l'effet de l'utilisation de système de chauffage et de climatisation.

L'analyse des séries régionales de production et de demande met en avant les fortes différences d'une source d'énergie à l'autre et entre régions européennes. La production solaire fluctue majoritairement à l'échelle saisonnière en suivant les modifications de la durée du jour. La production éolienne varie à plus haute fréquence et sa saisonnalité est moins marquée, en particulier dans les terres. Les caractéristiques des séries d'hydroélectricité sont fortement dépendantes de la région. Les zones de plaine connaissent un maximum de production hivernal alors que les régions montagneuses voient la production atteindre un pic en début d'été grâce à fonte du stock de neige. Enfin, les fluctuations de demande énergétique simulée sont limitées par rapport à celles des séries de production.

L'analyse climatologique et mono-variée de chacune des sources d'énergie prise séparément donne une vision imparfaite de leur facilité d'intégration car elle ne prend pas en compte les éventuelles

covariabilités entre production et demande. L'étude a donc été complétée grâce à l'évaluation du taux de pénétration (PE), introduit par [François et al., 2016]. PE est un critère synthétique comparant production et demande énergétique au pas de temps journalier et intégrant cet écart sur toute la période d'étude (ici 1983-2012). Pour un système idéal où la production est en moyenne égale à la demande (en moyenne sur 30 ans dans le cas présent), PE varie entre 0 et 100% ; 100% représentant l'adéquation temporelle parfaite entre production et demande.

Les résultats montrent la difficulté qu'ont les CREs à répondre seules à l'ensemble de la demande. Pour l'éolien, les taux de PE sont situés autour de 70% avec une forte homogénéité spatiale partout en Europe. Les résultats sur le photovoltaïque et l'hydroélectricité sont plus variables d'une région à l'autre mais des taux de PE très faibles sont parfois observés (eg. Solaire - Scandinavie - 55% ; Hydro - Méditerranée - 60%). Le foisonnement des sources est un facteur possible pour améliorer l'intégration des CREs. Dans l'étude de François et al., 2016, nous montrons comment un mix énergétique associant l'hydroélectricité, le photovoltaïque et l'éolienne permet d'augmenter le taux de pénétration régional, jusqu'à un mix optimal atteignant 80 à 90% suivant les régions.

En complément à cette analyse, nous regardons aussi les périodes, particulièrement problématiques, qui souffrent simultanément d'une faible production et d'une forte demande énergétique. Par analogie avec les sécheresses hydrologiques, nous définissons les sécheresses énergétiques comme des périodes pour lesquelles le taux journalier de demande satisfaite est en dessous d'un certain seuil. Nous étudions ensuite les caractéristiques de ces périodes de sécheresse en terme de fréquence annuelle et de durée moyenne pour chacune des régions d'études, des sources d'énergie et pour le mix optimal proposé par [François et al., 2016]. Les résultats associés sont présentés sur la Fig.1 pour 3 des 12 régions tests et pour un des 4 seuils des sécheresses retenus, ici 50%. Les caractéristiques des sécheresses sont très variables d'une source d'énergie à l'autre. Les sécheresses éoliennes sont particulièrement fréquentes mais de relativement courte durée (2 à 5j en moyenne). En revanche, il y a peu de sécheresse d'hydroélectricité mais ces évènements peuvent être particulièrement longs, jusqu'à 100j en moyenne (Scandinavie - hiver ; Méditerranée - été). Les sécheresses photovoltaïques ont, quant à elles, des caractéristiques intermédiaires. Une fois encore, on peut noter la forte diminution du nombre de jours en condition de sécheresse énergétique lorsque les 3 sources d'énergie sont combinées, prouvant qu'il est possible d'arriver à des systèmes de production d'électricité plus fiables grâce au foisonnement des sources.

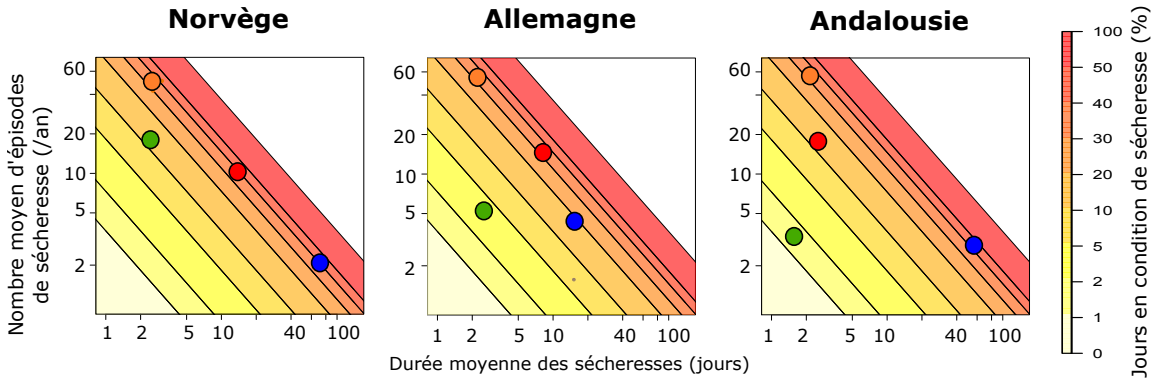

Figure .1 – **Caractéristiques des sécheresses énergétiques**. Nombre annuel moyen d'épisodes de sécheresse énergétique en fonction de leur durée moyenne. Les résultats sont présentés pour le seuil PE<50% et pour l'hydro-électricité (bleu), le photovoltaïque (rouge), l'éolien (orange) et le mix région optimal (vert). L'échelle de couleur donne la proportion totale de jours en condition de sécheresse.

Nous avons enfin évalué l'impact d'autres facteurs d'intégration (surdimensionnement, échanges d'énergie inter-régions, systèmes de stockage) sur les taux de pénétration et les sécheresses énergétiques. Dans la majorité des cas, l'utilisation de ces facteurs associée au foisonnement des sources mène à un système de production beaucoup plus fiable (PE souvent proche de 100%, rares et courtes sécheresses énergétiques).

3. Développement d'une méthode de descente d'échelle multivariée

Les résultats présentés précédemment s'appuient sur les 30 années du climat passé récent. Le climat est cependant connu pour fluctuer à des échelles temporelles plus grandes du pluriannuel au multi-décennal. De plus, dans un contexte de changement climatique, une modification des diverses variables météorologiques qui pilotent les CRE est probable. Afin d'étendre l'étude précédente à l'ensemble des 20ème et 21ème siècles, nous avons développé une méthode de descente d'échelle multivariée permettant de régionaliser l'information météorologique basse résolution issue de réanalyses climatiques et de modèles de climat. En effet, les données de ces simulations, ne peuvent pas être utilisées pour les études d'impact telles que celle réalisée ici : les données sont souvent biaisées et leur résolution spatiale est par ailleurs souvent comprise entre 1 et 3° de latitude, ce qui est n'est pas suffisant pour la génération de séries régionales de production et de demande énergétique pertinentes pour notre étude.

La méthode de descente d'échelle que nous avons mise en place pour cette étude est basée sur les analogues atmosphériques. Cette méthode statistique s'appuie sur les liens physiques existants entre les situations météorologiques synoptiques et les variables météo locales [Lorenz, 1969]. Elle a été largement explorée dans le passé pour la génération de séries locales de précipitation ou de température [Obled et al., 2002; Chardon et al., 2014]. Bien que facile d'implémentation, la méthode des analogues nécessite un effort important pour sa paramétrisation, notamment pour le choix des variables météo de grande échelle (prédicteurs) et pour celui des domaines spatiaux utilisés pour l'identification des jours analogues. De plus, le cadre spécifique de notre étude introduit d'autres contraintes en termes de cohérence physique entre les variables météo locales des scenarios régionaux générés.

La méthode des analogues que nous avons développée permet la génération de scenarios météorologiques multivariés sur nos 12 régions d'étude [Raynaud et al., 2016]. Nous comparons deux implémentations possibles de la méthode:

- "Analogues Communs": Un seul jeu de prédicteurs - optimisé pour chaque région, est retenu pour toutes les variables. Dans cette configuration, les dates analogues retenue pour un jour de prédiction donné sont les mêmes pour toutes les variables à prédire.
- "Analogues spécifiques": Chaque variable météorologique locale dispose de ses propres prédicteurs optimaux, optimisés de nouveau pour chaque région indépendamment.

Ces deux approches ont été comparées sur la période 1983-2012 pour laquelle l'information météorologique de grande échelle (réanalyses ERA-Interim) et les observations locales sont disponibles simultanément. La cohérence physique entre variables est garantie par la méthode "Analogues Communs"

mais les scénarios météo locaux sont sous-optimaux. A l'inverse, de meilleures performances mono-variées sont obtenues avec la méthode "Analogues Spécifiques" pour la prédiction de chaque variable locale. Les scénarios multivariés résultent cependant de dates analogues a priori différentes d'un prédictant à l'autre conduisant à une cohérence physique inter-variable dégradée.

L'exploration des nombreuses combinaisons de prédicteurs/domaines d'analogie pour chacune des approches a permis d'identifier une configuration intermédiaire garantissant d'une part de bonnes performances de prédiction pour chacune des variables locales et d'autre part des corrélations inter-variables pertinentes. Le modèle final, baptisé SCAMP (Sequential Constructive atmospheric Analogue for Multivariate weather Prediction) et présenté au Tab.1, combine l'approche "Analogues Communs" pour 3 variables (température, précipitation et rayonnement) et une approche "Analogues Spécifiques" pour le vent. Le premier niveau d'analogie est toujours basé sur les formes et gradients de géopotentiel à divers niveaux de référence. Une second prédicteur (humidité près du sol) vient ensuite effectuer une sous-sélection d'analogues pour les températures, les précipitations et le rayonnement. Enfin une correction de la température locale basée sur la température de grande échelle est faite. L'approche est robuste puisque cette paramétrisation optimale est identique pour toutes nos régions d'étude ; seule la position/forme du domaine d'analogie varie d'une région à l'autre.

Table .1 – **Caractéristiques de la descente d'échelle analogue multivarié SCAMP**. HGT - Géopotentiel, T - Température, Td - Température du point de rosée.

Predictand	**Méthode analogue**	**Predicteur 1**	**Predicteur 2**
Temperature	Commune	HGT500 & HGT1000	T-Td (2m) & T850 (correction)
Vent	Spécifique	HGT1000	-
Precipitation	Commune	0HGT500 & HGT1000	T-Td (2m)
Rayonnement	Commune	HGT500 & HGT1000	T-Td (2m)

4. Etude des co-fluctuations basse fréquence des CRE en climat passé

L'application de SCAMP aux réanalyses climatiques ERA20C proposées par l'ECMWF [Poli et al., 2013] a permis de générer 111 années (1900-2010) de production et demande énergétique sur nos 12 régions test. L'étude des séries brutes permet tout d'abord d'identifier des tendances de diminution de la demande (Europe entière) et de la production hydro-électrique (régions méditerranéennes). L'analyse des fluctuations basse fréquence autour de ces tendances ou du signal moyen permet de mettre en évidence les fortes différences qui existent d'une source d'énergie à l'autre. Les énergies solaire et éolienne ne fluctuent de modérément à l'échelle multi-décennale. En revanche l'hydroélectricité subit de fortes variations qui peuvent atteindre 15% d'une décennie à l'autre. Ces caractéristiques des séries de production se répercutent directement sur les fluctuations basse fréquence des taux de pénétration et des caractéristiques des sécheresses énergétiques. Pour toutes les régions, l'hydroélectricité est la source d'énergie la moins fiable à l'échelle multi-décennales avec des taux de PE subissant des variations pouvant atteindre 15% (Fig.2) et des durées moyennes de sécheresse pouvant doubler d'une décennie à l'autre.

L'analyse des corrélations entre l'Oscillation Nord Atlantique (NAO - [Trigo et al., 2002]), l'Oscillation Atlantique Multi-décennale (AMO - [Enfield et al., 2001]) et les séries annuelles de pénétration a permis de mettre en évidence les liens existants entre ces indices climatiques et les CRE. Les relations

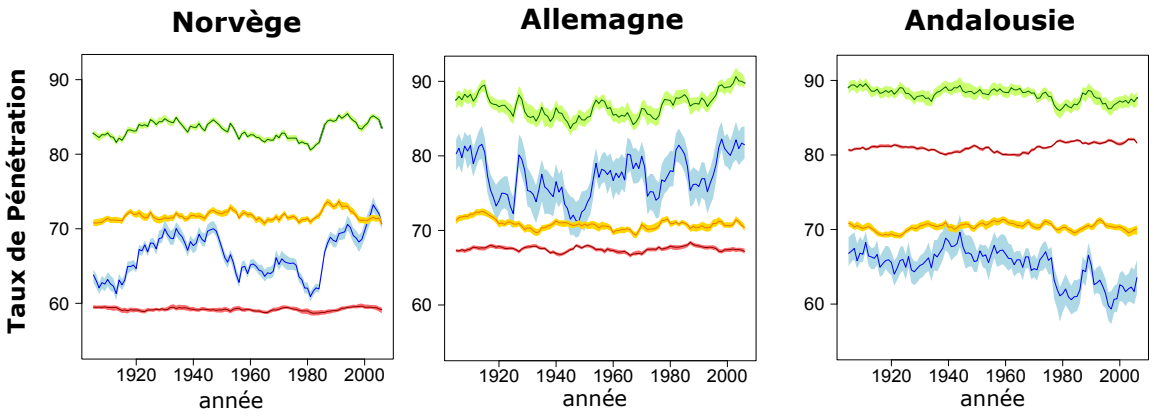

Figure .2 – **Variations multi-décénales du taux de pénération (PE - %)**. Chroniques sur 10 ans glissants du taux de PE associé à l'hydro-électricité (bleu), le photovoltaïque (rouge), l'éolien (orange) et le mix région optimal (vert) entre 1900 et 2010. Les résultats sont présentés pour trois régions: la Norvège, l'Allemagne et l'Andalousie.

les plus fortes sont sans conteste celles liant la NAO aux différents taux de PE. Les phases positives de NAO sont associées à des anomalies positives de production éolienne et hydroélectrique, des anomalies négatives de demande et de production solaire en Europe du Nord. L'inverse est observé pour les régions méditerranéennes.

5. Projections futures

La dernière partie de cette thèse présente les résultats obtenus en climat future. SCAMP a été appliqué à une sélection de modèles climatiques issus du CMIP5 pour deux scénarios d'émissions (RCP45 et RCP85). Pour chacun de ces modèles, des séries régionales météorologiques ont été produites et analysées entre 1950 et 2100. L'analyse des scenarios générés met en avant des tendances similaires pour tous les GCMs et toutes les régions d'études : Une augmentation de la température et des radiations solaires et une diminution du vent et des précipitations. Ces tendances sont plus marquées pour le scenario RCP8.5. Ces résultats ont été confrontés aux nombreuses études déjà existantes sur l'Europe, en particulier Jacob et al., 2014.

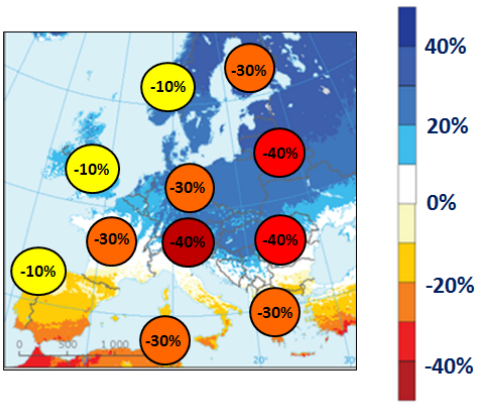

Figure .3 – **Comparaison des scénarios futurs de précipitation entre EURO-CORDEX et SCAMP.** Changements de precipitation annuelle simulés (%) par EURO-CORDEX (carte) entre 1971-2000 et 2071-2100 pour le RCP85 (Extrait et adapté de Jacob et al., 2014). Changements simulés avec SCAMP et un des modèles de climat selectionnés, ici HadGEM2-CC (pastilles).

La comparaison a permis de mettre en évidence la probable non-pertinence de nos scenarios de précipitations, en particulier en Scandinavie, où une forte hausse des précipitations moyennes est attendue dans les décennies à venir (Fig.3).

Nous terminons notre étude par une évaluation de SCAMP en climat futur afin d'identifier les possibles raisons menant des scenarios de précipitation erronés. Pour cela, les différentes hypothèses utilisées dans la méthode analogue sont testées dans un cadre dit "modèle-parfait" où des modèles de climat régionaux issus des dernières simulations EURO-CORDEX fournissent à la fois les prédicteurs et chroniques de précipitations régionales. Il en ressort une probable modification du lien entre prédicteur de grande échelle et précipitations locales pour des conditions météorologiques fortement modifiées par le changement climatique. Ces résultats laissent la porte ouverte à de possibles adaptations de la méthode analogue (ex : autres prédicteurs) ou à l'utilisation d'autres méthodes de descente d'échelle afin de poursuivre l'étude des co-fluctations des CREs en climat futur.

Contents

List of abbrevations

AMO: Atlantic Multidecadal Oscillation
AN: Andalucia (test region ID)
BE: Belarus (test region ID)
CDF: Cumulative Distribution Function
COMPLEX: Knowledge Based Climate Mitigation Systems for a Low Carbon Economy
CMIP5: Coupled Model Intercomparison Project Phase 5
COP21: 21st session of the Conference of the Parties
CORDEX: Coordinated Regional Climate Downscaling Experiment
CRE: Climate-Related Energy
CRE-Mix: Climate-Related Energy Mix model
CRPSS: Continuous Rank Probability Skill Score
DJF: December-January-February
ECA& D: European Climate Assessment & Dataset
ECMWF: European Centre for Medium-Range Weather Forecasts
EOF: Empirical Orthogonal Functions
EN: England (test region ID)
ENSEMBLE: Ensembles-Based Predictions of Climate Changes and Their Impacts
ENSO: El Niño et Southern Oscillation
ENTSOE: European Network of Transmission System Operators for Electricity
ERA-CLIM: European Reanalysis of Global Climate Observations
FI: Finland (test region ID)
FR: France (test region ID)
GA: Galicia (test region ID)
GCM: General Circulation Model
GE: Germany (test region ID)
GHG: GreenHouse Gas
GR: Greece (test region ID)

HGT...: Geopotential height at ...hPa
IPCC: Intergovernmental Panel on Climate Change
ISD-lite: Integrated Surface Database lite
IT: Italy (test region ID)
JJA: June-July-August
NAO: North Atlantic Oscillation
NCEP: National Centers for Environmental Prediction
NO: Norway (test region ID)
NWP: Numerical Weather Prediction
OM1: Optimal Mix 1 (solar - wind - hydro)
OM2: Optimal Mix 2 (solar - wind)
Pc: Convective Precipitation
PE: Penetration (rate)
PRUDENCE: Prediction of Regional scenarios and Uncertainties for Defining EuropeaN Climate change risks and Effects
Ps: Stratiform Precipitation
PSL: Sea Level Pressure
PV: Photovoltaic
Q-Q: Quantile-Quantile mapping
RCM: Regional Climate Model
RCP: Representative Concentration Pathway
RH...: Relative Humidity at ...hPa
RHS: Near Surface Relative Humidity
RMSE: Root-Mean-Square Error
RO: Romania (test region ID)
RoR: Run-of-the-River
SA: Satisfaction (rate)
SARAH: Surface Solar Radiation Data Set - Heliosat
SCAMP: Sequential Constructive atmospheric Analogues for Multivariate weather Predictions
SCAMP-FX: SCAMP - Fixed Archive
SCAMP-MV: SCAMP - Moving Archive
SDM: Statistical Downscaling Method
SST: Sea Surface Temperature
TCW: Total Column Water
T-Td: Temperature and dew-point Temperature difference
TU: Tunisia (test region ID)
TWE: Teweles-Wobus Score
VRE: Variable Renewable Energy
VV...: Vertical Velocities at ...hPa
WCRP: World Climate Research Programme
WRF: Weather Research& Forecasting model

Part I

GENERAL INTRODUCTION

Chapter I

Toward a Green Economy: The contribution of renewables

1. From Climate Change awareness to sustainability

1.1. Fifth IPCC report: Last assessments of the current global warming

Since its creation in 1988, the Intergovernmental Panel on Climate Change [1] (IPCC) has promoted and led studies on Global Warming, its consequences on the climate system and on possible mitigation strategies to curb it. A lot of effort is put into attributing the current changes in temperature to human activities [Stocker et al., 2009; Christidis et al., 2010; Ring et al., 2012; Imbers et al., 2013]. The main difficulty comes from the necessity to separate the climate change contribution to the observed modifications of climate from the natural variability of this complex system [Fogt et al., 2009; Swanson et al., 2009]. The fifth IPCC report [Bindoff et al., 2013], sums up the findings from these numerous studies and comes to the following conclusions about the recent changes in mean surface temperature:

- There is a high probability (90-100%) that the increase in green house gas concentration due to anthropogenic activities is responsible for more than half of the observed increase in global mean surface temperature.
- The natural variability of the climate system cannot account for the observed increase in temperature (probability $> 99\%$).

[1] https://www.ipcc.ch/index.htm

For other components of the climate system, the impact of Global Warming is not certain but still very likely. It is the case for the cryosphere for which both glaciers and Artic sea ice diminution are probably due to Climate Change [Stroeve et al., 2012; Marzeion et al., 2014] and contributed to the global mean sea level rise [Church et al., 2013]. The important changes at a global scale of both tropospheric and oceanic temperatures impact the entire atmospheric system and likely modify the atmospheric circulation [Graff and LaCasce, 2012]. As a consequence, local climate conditions are also experiencing fluctuating trends and changes in characteristics. Precipitation, and also the whole water cycle, are examples of local conditions becoming impacted by global warming: Despite the large spatial and temporal variability of these hydro-meteorological parameters, recent findings indicate that part of their modifications can also be attributed to climate change [Tapiador, 2010; Trenberth, 2011; Scheff and Frierson, 2012].

Another concern is related to extreme weather events which are expected to increase in both occurrence and intensity due to global warming. For temperature extremes, there is a high probability (>90%) that climate change is responsible for their increasing number and magnitude [Rahmstorf and Coumou, 2011; Christidis et al., 2011]. More uncertainty exists for extreme precipitation events. However, an increasing number of studies have concluded that anthropogenic activities have been a major contributing factor to the observed changes [Min et al., 2011; Westra et al., 2013].

1.2. International agreements on Climate Change

Over the past decade, the growing body of evidence that Global Warming is caused by human activities has led to a consensus among scientists and politicians. The climate sceptics, calling climate change a hoax because of a single and short cold event, are still getting to much attention but are becoming more marginal.

The first major step toward a sustainable society was made in 1997 with the Kyoto Protocol[1]. In the first phase of the agreement, 37 industrialized countries decided to reduce their greenhouse gas emissions by 5% compared to the level of 1990. Thereafter, some of them, including the European Union, committed to increase the reduction target to 18%. However, since then, the following agreements have failed to convince the main emitters of greenhouse gas (USA, China...) to participate in a transition toward a global green economy.

The year 2015 marks a major milestone for a global cooperation to counter climate change and its future negative impacts on our society. In December 2015, the 21^{st} session of the Conference of the Parties[2] (COP21) resulted in 181 signatories to the Paris agreement. It details higher level requirements to the reduction of greenhouse gas emissions in order to mitigate the impacts of climate change. [United-Nations, 2015]:

- Limit the global increase in mean temperature to 1.5°C above pre-industrial levels.
- Adapting their commitments every 5 years to ensure that the 1.5°C target will be achieved.
- Moving toward a balance between anthropogenic emissions by sources and removals by sinks of greenhouse gases by 2050.

[1] http://unfccc.int/kyoto_ protocol/items/2830.php
[2] http://www.cop21.gouv.fr/

- Limiting the risks of loss and damages related Climate Change (extreme events, sea level rise) and their impacts on our society.
- Providing financial support to developing countries which are more vulnerable to Climate Change and cannot meet the 1.5°C goal by themselves.

A decarbonisation of the economy can be done efficiently by taking various measures and actions. Improving the energy efficiency can contribute to a global reduction of the energy load. European countries recently agreed on an energy efficiently target of 27% or greater by 2030 [1]. The electrification of fossil based systems such as means of transport (e.g. electric cars) could also significantly lower green house gas emissions. However, it implies that the electricity production would no longer rely on fossil fuels (petroleum, gaz or coal). Nowadays, the energy sector contributes to 35% of the total anthropogenic emissions [Change, 2014]. Thus, the development of renewables is the keystone to curb the part of green house gas emissions related to electricity generation.

The range of renewable energy sources that could be developed to reduce GHG emissions is wide. Some of them take advantage of the large amount of available marine energy (tidal and wave power) [Shields, Payne, et al., 2014]. Geothermal energy is also widely used in countries where it is plentiful and easily accessible (e.g. 25% of the total electricity production in Iceland[2]). The use of biomass for electric power generation is now contemplated and developped in several country [Szarka et al., 2013]. Another family of renewables makes use of hydro-meteorological variables which can be converted into electricity, gathering solar power, wind power and hydro power. The increasing number of renewable energy power plants developed in the past 20 years has significantly reduced the cost of these energy sources and strengthened their competitiveness [Arent et al., 2011]. However, the current level of equipment in the world is not sufficient to meet the objectives of the 2015 Paris agreement [Guivarch and Hallegatte, 2011] and some further efforts will be required.

The majority of renewables presented previously (marine, solar, run-of-the-river hydro and wind power) are subject to strong temporal variations, they are often referred to as variable renewable energy (VRE). Conversely, biomass and geothermal power are controllable sources and can be harnessed when needed. In the following study, we will solely consider run-of-the-river (RoR) hydro, wind and solar power. To avoid any misunderstanding and exclude non-weather-driven intermittent sources, these three energy sources will be refereed to as Climate-Related Energy (CRE).

2. Climate-Related Energy

2.1. CRE resources

The quantity of renewable energy at global scale is considerable ; potentially able to supply several times the current global demand [Hoogwijk and Graus, 2008]. CRE resource has been widely evaluated from global to regional scales proving its abundance [De Vries et al., 2007; Adams and Keith, 2013]. Numerous studies aimed to identify hot spots in Europe for solar and wind power (Fig.I.1), with results supporting the development of new power plants [Von Bremen, 2010; Vautard

[1] https://ec.europa.eu/energy/en/topics/energy-efficiency
[2] http://www.nea.is/geothermal/

et al., 2014; Jerez et al., 2015]. They demonstrated that numerous possibilities exist to diversify and increase the green energy share in the European electricity production.

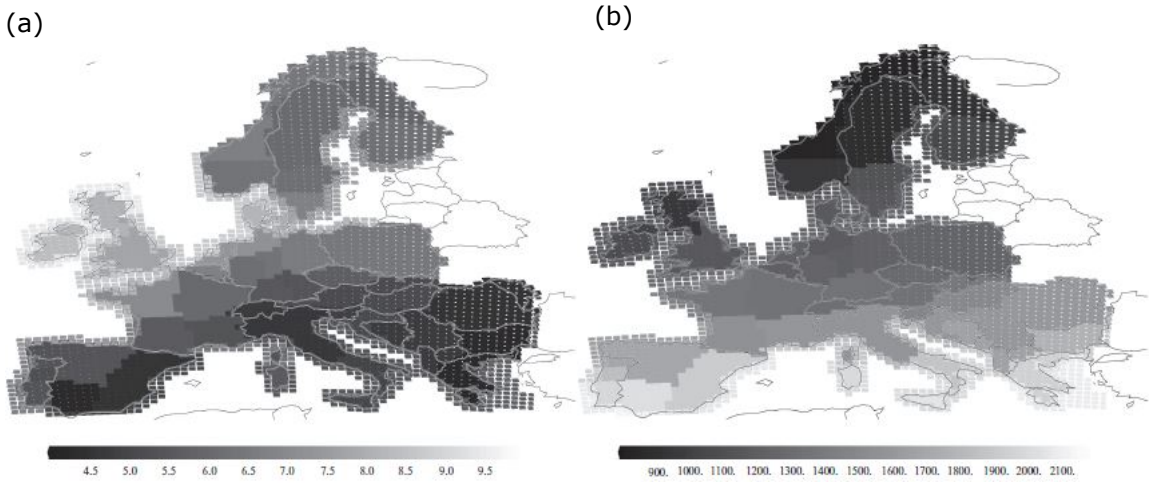

Figure I.1 – **Ressources in wind speed and solar radiation in Europe.** Average wind speed (m/s) in Europe (a) and annual resource of global radiation (kWh/m2/year) that can be used by PV converters (b) from 2000 to 2007. Extracted and adapted from Von Bremen, 2010.

The numerous mountain ranges and the wide-spread European river network has also encouraged the development hydro power plants and storage systems. Besides the conventional hydro power associated to large water reservoirs, Run-of-the-River and small hydro power plants will also play an important role in the next decades by continuing to increase the share of energy from renewable sources [ESHA, 2012; Lazzaro and Botter, 2015; Gallagher et al., 2015; François et al., 2016].

Unfortunately, quantifying the current resources in renewable energy is not sufficient to assess to the extent to which the different sources can be integrated in the global power supply system. Being driven by local meteorological conditions, CRE varies greatly in time and space. It results in a very uneven electricity production which is, on average, substantially below the maximum potential output. The temporal inconsistency of CRE generation and gap between supply and demand becomes a major obstacle to the direct use of these renewables. This issue is particularly important for power supply systems which have a large share of CRE sources. A deliberate over-sizing of power plants does not suffice for getting rid of this imbalance when a single CRE source is harnessed [François et al., 2016].

2.2. Variability of CRE

2.2.1. Intermittence

All CRE sources fluctuate at various time scales from hourly to multidecadal periods. Wind power is mainly fluctuating at a weekly time scale resulting from large atmospheric patterns and the alternation/succession of low and high pressure systems. However, it is also characterised by a strong diurnal cycle (diurnal sea/land breeze) and a large variability due to turbulence [Albadi and El-Saadany, 2010; Graabak and Korpås, 2016]. Even larger climate oscillations, such as the North Atlantic Oscillation, impact wind speed and the associated power generation [Ely et al., 2013]. Fig.I.2 (extracted and adapted from Graabak and Korpås, 2016) presents, as an illustration, the different time scales of wind power variations. Using hourly wind reanalysis data from 1950 to 2013, this figure

shows the mean annual cycle of capacity factor[1] in Scotland (blue curve) together with the mean global production. It also presents the maximum and minimum hourly/annual values. The strong intermittence of wind at small time scales results in important variations of hourly wind power (from 0 to 93% capacity factors). Seasonal and inter-annual variations also greatly contribute to the total fluctuations of wind power (capacity factor from 10 to 50% and from 22 to 35% respectively). The final mean wind power production represents only, 27% of the potential electricity production with the level of equipment in Scotland.

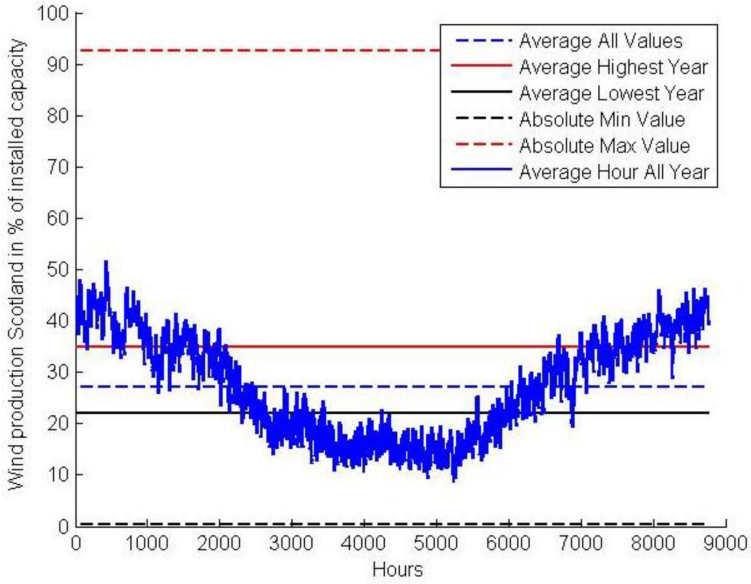

Figure I.2 – **Multi-scale time variation of wind power.** Mean annual cycle of capacity factor in Scotland (blue curve), global average value (blue dash line), maximum (red) and minimum (black) hourly (dash lines) and annual (solid lines) values. Based on hourly wind reanalysis data from 1950 to 2013 derived from the NCEP reanalysis data. Extracted and adapted from Graabak and Korpås, 2016.

Solar power is also known to fluctuate over a variety of time periods from minutes (variations in cloud cover) to seasons and decades (variations in earth inclination and solar activity). Large weather patterns are also a dominant driver, imposing several consecutive sunny or overcast days. Consequently the intermittence of this energy source is large and results from a combination of contributions from various time scales [Graabak and Korpås, 2016; Von Bremen, 2010].

River discharge and the associated hydro power mostly vary on longer periods. For most rivers, the seasonality of river flow is strong and classically determines the dimensioning and the management of reservoirs [Basso and Botter, 2012]. Multi-annual and decadal scales also play a key role to low frequency fluctuations of hydro power [Uvo and Berndtsson, 2002].

Considering that part of the energy load is also fluctuating according to both human activities and weather conditions [Isaac and Van Vuuren, 2009], the discordance between high energy load and peak power production could lead to unsatisfied energy demand.

[1] ratio of actual power generation output of a power plant to its maximum potential output

2.2.2. Extreme

Extreme events are also a threat to electricity production. During strong winter storms or flood events, wind and hydro power plants have to be shut down to preserve their integrity. These events should become more numerous and stronger in the next decades [Leckebusch et al., 2008; Makkonen et al., 2007]. Similarly, when river discharge is lower than a given threshold, no hydro power can be generated to preserve the integrity of the riverbed and its ecosystem. Extreme temperature events also greatly impact the energy demand. Long and intense cold waves result in several days of high energy load. These periods can also be associated to low solar irradiance (winter) and low wind speed making it difficult to meet the energy demand.

2.2.3. Low frequency fluctuations

In addition to extreme events, climate also fluctuates at multidecadal time scales, impacting all hydro-meterological drivers of CRE sources. For instance, multidecadal variations on river dicharge and their impacts on hydro power have been largely studied in various regions worldwide [Enfield et al., 2001; Nalley et al., 2016]. CRE sources and their associated power generation also presents low-frequency fluctuations. Few studies assessed the long-period variability of renewables, among which Jourdier, 2015 for wind power in France. An accurate estimation of the resources in renewable energy cannot be made without taking into account these fluctuations which shape the mean potential production over several consecutive years.

2.2.4. Effect of Climate Change on CRE

In sec.1.1 we discussed some of the expected consequences of Global Warming on climate. These modifications will, without doubt, impact the green energy sources and their characteristics. Over the past decade, the number of studies attempting to estimate the effects of Climate Change on wind and solar resources is continuously increasing [Fant et al., 2016; Segal et al., 2001]. In Europe, the first outcomes of future wind power assessments indicate some modifications in both mean annual resources and inter-annual variability [Tobin et al., 2015; Reyers et al., 2016]. Similarly, solar power resource should undergo some changes in Europe with more potential for electricity production in the south-eastern part of the continent [Bartók, 2010].

There is more concern about some possible variability of the hydro power resource. For some European countries, this energy source represents a large part of the electricity production (17% for France, and almost 99% for Norway[1]). The join effects of warmer temperatures and modifications in precipitation could strongly impact river discharge. Many studies highlighted the strong future decrease in hydro power resource in Southern Europe and for the Alpine power plants [Lehner et al., 2005; Schaefli et al., 2007]. The diminution of snow-pack in Scandinavia is also expected to modify the mean water resource and its seasonality.

The modifications of hydro-meteorological variables in a climate change context should not only impact the mean resources in renewable energy but also its spatio-temporal variations. Moreover, the co-variations between energy sources could also undergo important changes and lead to less or, in some instances, more synergy.

[1] http://www.statkraft.com/energy-sources/hydropower/

3. Integrating factors of CRE sources

The intermittence and variability of the different CRE sources is a major hindrance to their rapid and efficient contribution to the global power supply system. A number of different integration factors can be used to tackle these issues.

3.1. Storage

Storage systems have proved their ability to balance the temporal variability of renewables. Reservoirs have been developed for decades to provide hydro power when needed and not suffer from the strong seasonality of river discharge. These reservoirs can also be used to store the overproduction from other CRE sources thanks to pumped storage systems [Rehman et al., 2015]. The recent technological breakthroughs on batteries make the storage of intermittent energy sources conceivable [Chen et al., 2009; Beaudin et al., 2010; Luo et al., 2015]. Several past studies assessed the support of solar and wind power storage to meet the electricity demand. They all concluded that the development of additional storage capacities would efficiently balance the strong variability of these sources [Rasmussen et al., 2012; Steinke et al., 2013; Weitemeyer et al., 2015].

3.2. Multiple contributions

3.2.1. Energy mix

Betting on multiple energy types to tackle the high variability of single sources has gained currency over the past few years. It consists in taking advantage of the possible complementarity between wind, solar and hydro power. Many regional initiatives in Northern America aimed to combine several sources (wind-hydro, wind-solar) and proved that it could significantly reduce the risk of power shortage [Denault et al., 2009] and help to meet a large part of the future energy demand [Budischak et al., 2013]. Energy mixes involving even more sources (biomass, geothermal) lead to more dependable systems and reduce their reliance on fossil fuels as backup energy [Mason et al., 2010]. In Europe, recent attempts to combine solar and wind power [Von Bremen, 2010] demonstrated that an optimal mix can be found to minimize the variance of imbalances between production and energy load. However, the optimal mix depends on the time scale of interest. Furthermore, François et al., 2016 showed that even higher energy demand can be met by including hydro power in the energy mix (increase ranging from 1 to 8% depending on the region considered).

3.2.2. Spatial integration

We previously discussed the disparities in energy resources that exist from one region to another. This variability can be turned into an advantage by performing a spatial integration which consists of gathering electricity production and energy load from different regions. Thanks to this method, part of the local variability of CRE sources can be balanced. It gets more and more efficient with wider integrations which gather contributions from various regions which have different hydro-meteorological conditions.

For instance, several European studies analysed the currently urealistic, but still instructive, case known as the "European copper plate" for which power can be shared at a European scale without losses due to electricity transmission. Steinke et al., 2013 demonstrated that the spatial integration of an energy supply based only on a mix of solar and wind power could increase the amount of satisfied energy demand from 40 to 80%. Von Bremen, 2010 came to a similar conclusion with an increase by 50% of the grid power generation - energy load adequacy. The so called "super-grid" has already been widely studied [Bogdanov and Breyer, 2016; Xydis, 2013]. It proved that taking advantage of the complementarity between regions is an efficient tool for the integration of renewables in the energy supply system.

3.3. Some other options

The concept of "smart-grid" has been recently introduced and consists in managing the energy demand and adjusting it to the electricity production. Using a two way exchange of electricity and information between utilities and consumers [Fan et al., 2013], it contributes to making the power grid more reliable and efficient. Indeed, rescheduling the functioning of some non-critical household electrical goods for instance, can significantly reduce the peak demand. The information provided to costumers also helps them to manage their electricity bill and thus to lower their contribution to the total energy load [Goulden et al., 2014].

Another option to meet a larger proportion of energy demand consists in deliberately oversizing some power plants. Rasmussen et al., 2012 proved that an average wind and solar power production slightly higher than the average energy load (from 1 to 3%) leads to a conceivable 100% renewable European energy system when combined with some storage and a hydro power backup. Despite the financial cost that such a method implies, it is an efficient tool to balance moderate lack of wind or solar power due to slight wind or to the limited day length in winter.

4. Research objectives

4.1. The COMPLEX project

This PhD thesis contributes to the FP7 COMPLEX[1] project. This collaboration of 17 European partners aims to answer some key questions about the European transition to a low carbon society. It involves both scientific and stakeholder communities to tackle the various physical, technical and socio-economic issues related to this transition.

The main objective of this thesis is to complement previous studies on CRE sources in Europe. We will focus on climate variability and provide some further assessments of its impacts on the ease of integration of CRE sources. The adequacy between energy production and load being the keystone of an efficient integration of renewables, this work will not only account for the variability of each CREs sources taken independently but also on the co-variations between them and the energy demand.

[1] http://owsgip.itc.utwente.nl/projects/complex/

4.2. Outline and goals

Based on the numerous studies described previously and on their associated outcomes, this work aims to address some issues related to the integration of renewables in Europe:

⇒Variability and complementarity of renewables

In the first part of this thesis we will assess the feasibility, in terms of hydro-meteorological conditions, of a 100% renewable energy supply in Europe based on CRE sources (solar, wind and run-of-the-river hydro power). To delve deeper into this issue, we will develop and use a simple but complete simulation chain named CRE-Mix, which converts meteorological observations into proportions of satisfied energy demand. It involves an hydrological model and conversion models of weather/hydro data into electricity production and energy load. For a selection of European regions, we will evaluate the ability of each CRE source to meet the energy demand. We will also focus on the assessment of the duration and frequency of problematic sequences of days for which this energy demand remains unsatisfied. CRE-Mix also makes assessing the effects of some integration factors possible (Storage, energy mix, over-sizing and spatial integration).

⇒ Low-frequency fluctuations of CRE sources

In Part III, we will describe in detail the downscaling method, hereafter referred to as SCAMP (Sequential Constructive Atmospheric Analogues for Multivariate weather Predictions), that has been developed and evaluated to generate physically consistent multi-variate and regional weather series.

SCAMP was then used in Part IV to downscale the recently released climate reanalysis of the 20^{th} century and generate long regional series of CRE sources hydro-meteorological drivers. After converting them into energy production series, the multidecadal variability of renewables and its dependence on climate fluctuations is assessed.

⇒ Future trends and modifications of CRE sources in a Climate Change context

The last part of this work aims to assess the possible modifications of the variability of CRE sources and of their adequacy with the energy demand. Using SCAMP and a set of climate models issued from the fifth phase of the Coupled Model Inter-comparison Project[1] (CMIP5), regional series of CRE hydro-meteorological drivers will be generated for the whole 21^{th} century. Their trends and changes due to Global Warming will be analysed and compared to the results of similar studies. The outcome of this comparison highlights the difficulties that SCAMP has in simulating relevant future series of precipitation. In the last chapter we attempt to identify some possible reasons for this failure using SCAMP in a perfect-model approach and Regional Climate Models (RCM) simulations.

[1] http://cmip-pcmdi.llnl.gov/

Part II

RENEWABLES IN EUROPE: EASE OF INTEGRATION

Chapter II

Hydroclimatic and energy regimes

This study relies on a suite of models using meteorological variables as input data. It simulates time series of renewable power generation and energy demand. These simulations should draw a correct picture of the hydro-climatic variability in Europe and enable the assessment of its effects on the variations of renewables. Many simplifying assumptions have been made to reach a compromise between reasonable modelling complexity and satisfactory simulations:

H1 The studied power supply system only relies on CRE sources. The different electricity production models are only weather-driven and based on generic equipments (generic RoR station, wind farm and photovoltaic power station). This also applies to the energy demand model, which uses a unique "consumer profile" and depends only on meteorological conditions.

H2 Our main interest resides in the variability of renewables due to climate fluctuations. Therefore, the absolute value of power generation and the underlying level of equipment (number of wind turbines, solar and hydro power plants) is not crucial. The sizing of renewable power stations (c.f. Chap.III) is time-invariant, region-dependent and guarantees a balance between mean electricity production and energy load for a 33-year reference period.

H3 In order to take on board the spatial variability of climate conditions in Europe, the following analysis is performed on 12 test areas spread over the whole continent. All of them are square regions which do not respect administrative borders. The hydro-climatic regime is assumed to be relatively homogeneous within each region.

H4 Regions are located at the upstream part of river basins, thus avoiding stream flow contributions from large rivers crossing them. Then, the simulated hydro-power only results from local river discharge and from the underlying regional hydro-meteorological variability.

H5 Electricity production and energy load series are analysed at a regional scale, assuming a perfect power transmission within each region. This simplifying hypothesis implies that local power

generation and energy demand can be brought face to face even when coming from different locations.

H6 All time scales are determining factors for the assessment of the ease of integration of CRE sources. However, we will only focus on their temporal variations going from daily to multi-decadal time scales. We will disregard the sub-daily fluctuations. It implies that some daily storage systems can balance the high-frequency variations in electricity production and demand.

H7 All models (hydrological and conversion models) have a unique and constant parametrisation for all test regions. These parameters are coming either from the literature (electricity production models) or from a global optimisation using observations (hydrological model, energy load model).

Each component of this suite of models will be described in detail in a logical order from meteorology to electricity production. The associated characteristics of meteorological, hydrological and power series will also be discussed in turn.

1. Climate conditions and meteorological regimes

1.1. Definition and geographical features of the test regions

12 regions in Europe and Maghreb are targeted in this study. Their boundaries are presented on Fig.II.1. Each of them is identified thanks to two letters, these IDs will be used thereafter. The spatial distribution of these regions gives a balanced coverage of the European continent. The represented latitudes range from 35° (Tunisia - TU) to 64° (Finland - FI). Similarly, Galicia (GA) and Romania (RO) give the minimum and maximum longitudes, 9°W and 29°E respectively.

Moreover, the topography greatly changes between regions. Some of them, located in plains, have a limited altitude difference between their highest and lowest points (England - EN, Belarus - BE, Finland - FI). On the opposite, Italy (IT), Andalusia (AN) and Greece (GR) contain major mountain ranges and the highest points often exceed 2500m in altitude. The main geographical features are gathered in Tab.II.1.

This variety of topography and positioning within Europe induces strong differences in climate conditions and hydro-meteorological regimes.

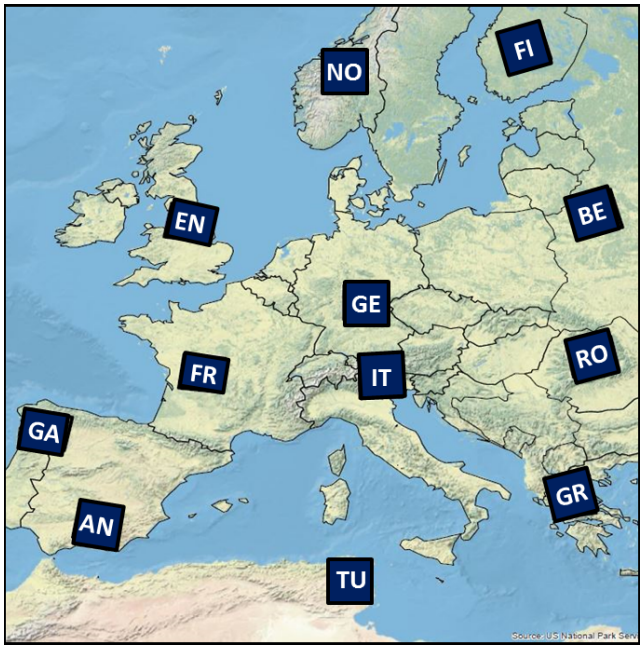

Figure II.1 – **Test regions boundaries** and regional IDs.

1.2. Climate conditions

The climate conditions greatly change from one Euroepan region to the other. Peel et al., 2007 proposed a global and updated climate classification. Their results in Europe and Northern Africa are presented on Fig.II.2. 4 out of the 5 main world climate classes are represented in Europe.

Maghreb and part of the Iberian Peninsula experience an arid climate. The remainder of the Mediterranean basin has a temperate climate with dry and hot summer. Western Europe (France, British Isles, Benelux and Western Germany) are mostly influenced by the Atlantic Ocean giving a

Table II.1 – Geographical features of the 12 studied regions

Region ID	Mean latitude (°)	Mean longitude (°)	Min altitude (m)	Max altitude(m)	Mean altitude (m)
EN	53.75	-1.625	0	720	130
NO	62	9.25	0	2290	1010
FI	62.5	25.5	60	270	140
FR	46.25	0.875	5	940	220
GE	50.25	10.75	0	1010	390
BE	53.5	27.125	100	360	180
GA	42.25	-7.375	0	2140	720
IT	46.5	11.625	1	3640	810
RO	46.5	24.5	170	2160	620
AN	38	-3.5	110	2730	800
TU	35.875	9.875	0	1340	290
GR	39.5	21.75	0	2710	610

temperate, moist climate with relatively warm summer. Central and Eastern Europe have a typical continental climate with cold and long winter whereas warm conditions return during summer. For higher latitudes (Scandinavia), summer remains chilly. Finally the numerous and high mountain ranges in Europe, whose climate has been classified as "Polar", are characterised by frequent and heavy snowfall in winter and a recurrent diurnal convection cycle in summer leading to a broad panel of possible weather conditions across the year.

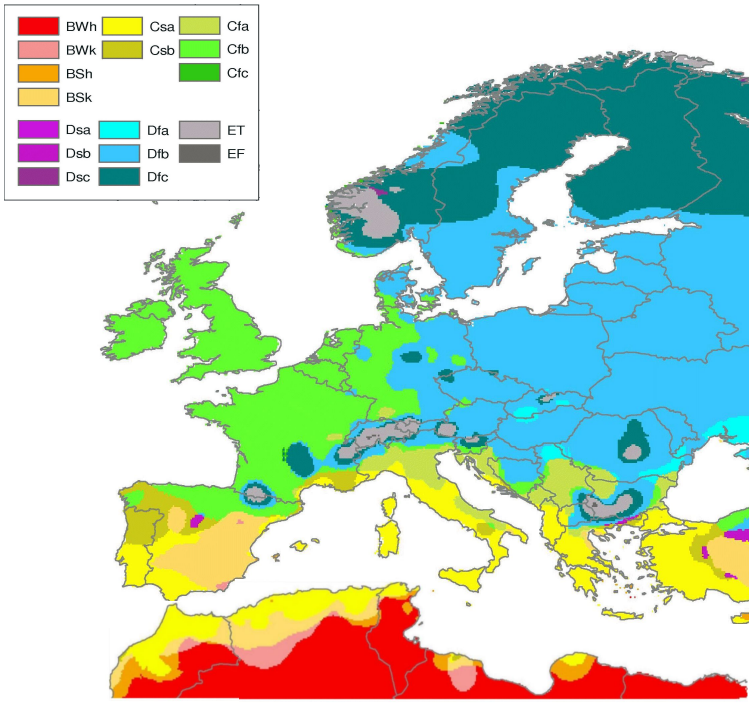

Figure II.2 – **Climate classification in Europe and Northern Africa.** Extracted and adapted from Peel et al., 2007. B=Arid, C=Temperate, D=Cold, E=Polar, W=Desert, S=Steppe, T=Tundra, F=Frost, s=Dry Summer, f=Without Dry Season, h=Hot, k=Cold, a=Hot Summer, b=Warm Summer, c= Cold Summer

1.3. Meteorological regimes

1.3.1. Meteorological datasets

The most ancient meteorological records for temperature in Europe date back to the 17th century. Unfortunately, it is only since the second half of the 20th century that weather stations started multiplying and offering a more complete coverage of the European continent. For some other variables, the historical records are even shorter (wind, sun radiation) and the density of stations does not give accurate information on their spatio-temporal variations.

To meet the requirements of many studies in need of a global spatial and temporal coverage, gridded weather reanalysis data have been developed. For temperature and precipitation, the density of stations suffices to build such a dataset from on-site measurements. Satellite-based observations of sun radiation, available since the 80s, provide increasingly accurate information on weather conditions. They lent support to on-site measurements and helped developing sun radiation gridded data. Unfortunately, neither weather stations nor satellite data can be directly used to produce satisfactory wind speed gridded data over a long period of time. Consequently, wind pseudo-observations, obtained from regional atmospheric models, are frequently used as a substitute for "real" observations.

Here, we present the different datasets which were used as observations (or pseudo-observations) to describe the recent past climate conditions in Europe.

1.3.1.a. Temperature and precipitation: ECAD

As part of the EU-FP6 ENSEMBLE and ECA& D (European Climate Assessment & Dataset) projects [Haylock et al., 2008], observed weather time series were collected and converted into gridded data using a three-steps methodology similar to universal kriging. A description of the the gridding methodology can be found in Haylock et al., 2008; Hofstra et al., 2008. Five daily variables (minimum, maximum and mean temperature, precipitation and sea level pressure) are available on a 0.25° grid from 1952 and cover the entire Europe, Turkey and part of Maghreb.

This dataset provides a complete and regular coverage of Europe. However, it must be underlined that it is not temporally and spatially homogeneous. Indeed, as shown in Fig.II.3, the density and length of the observed time series change greatly from one country to another. It probably leads to an underestimation of precipitation for mountainous regions (Alps, Pyrenees...) where this variable has a strong spatial variability and elevation dependency. Precipitation and temperature data were directly extracted from this dataset from 1983 to 2012. Daily temperature range was also computed from minimum and maximum temperature series.

1.3.1.b. Sun radiation: Heliosat (SARAH)

On-site solar radiation measurements are relatively scarce and their associated time series are often short. Thus, no gridded dataset using weather stations such as the one developed in the ECA& D project could be built for this variable. Nevertheless, since the early 80s, satellite measurements have helped bridging this gap.

The Surface Solar Radiation Data Set - Heliosat (SARAH) was selected to provide daily surface sun radiation data for the 12 regions of this study. This dataset, based on measurements from

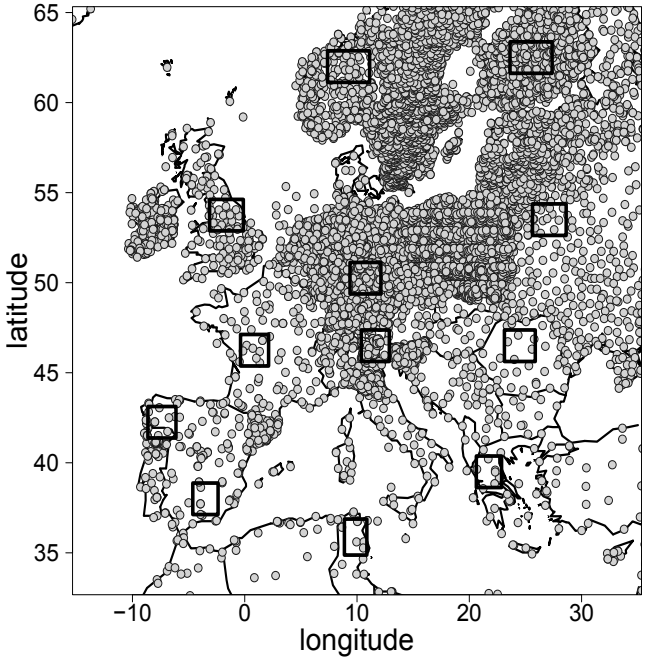

Figure II.3 – **Locations of the weather stations used in the ECA& D project** (grey dots). Test regions (black squares).

the geostationary Meteosat satellites, extends from 1983 to 2013. It has a rather high resolution (0.05° grid). Due to the high angle of incidence from geotationnary satellites toward high latitudes, measurements are expected to be more accurate near the Equador. A detailed evaluation is available in Müller et al., 2015. The comparison with ground measurements at a selection of stations, including several European ones (France, Spain, Netherlands, Germany, UK, Switzerland, Estonia), proved the relevance of these satellite data. The uncertainty associated to these data is of the same order of magnitude as the one of ground-based measurements.

1.3.1.c. Wind speed: Pseudo-observations using the WRF model

Surface observations of wind speed suffer from the same limitations as solar radiation ones. It would be difficult to build correct regional series of this variable for some of our studied areas where weather stations are rare or relatively new. The only gridded dataset of wind speed that exist are usually outputs of dynamical downscaling methods from regional climate models. The obvious advantage of these data is that they provide a continuous temporal and spatial coverage. However, their quality (realistic and accurate wind speed) is not guaranteed and has to be evaluated. Indeed, regional models often suffer from large biases. Even if wind is usually one of the most accurately simulated variables (unlike thermodynamic ones), the coarse European topography in the model prevents it from simulating local effects, especially in mountainous regions. In this study, we use wind outputs from the WRF model forced by the ERA-INTERIM reanalysis data [Vautard et al., 2014]. The resolution is about 50km and data are available on a 3h time step.

We performed an evaluation of the model outputs comparing them with some available wind stations. The associated analysis and results are presented in Appendix.A. All in all, this evaluation highlighted uneven performances of the WRF model in Europe. Despite a good consistency between observed and simulated wind series over plains, the rather low resolution for the current model set-up leads to poorer results in mountainous areas. Using these simulations in this study has the advantage

of guaranteeing a complete coverage of the tested regions but some of our results must be analysed with caution. This is especially the case when a region contains a high mountain range such as the Italian (IT), the Norwegian (NO) and the Romanian (RO) test areas.

1.3.2. Meteorological regimes

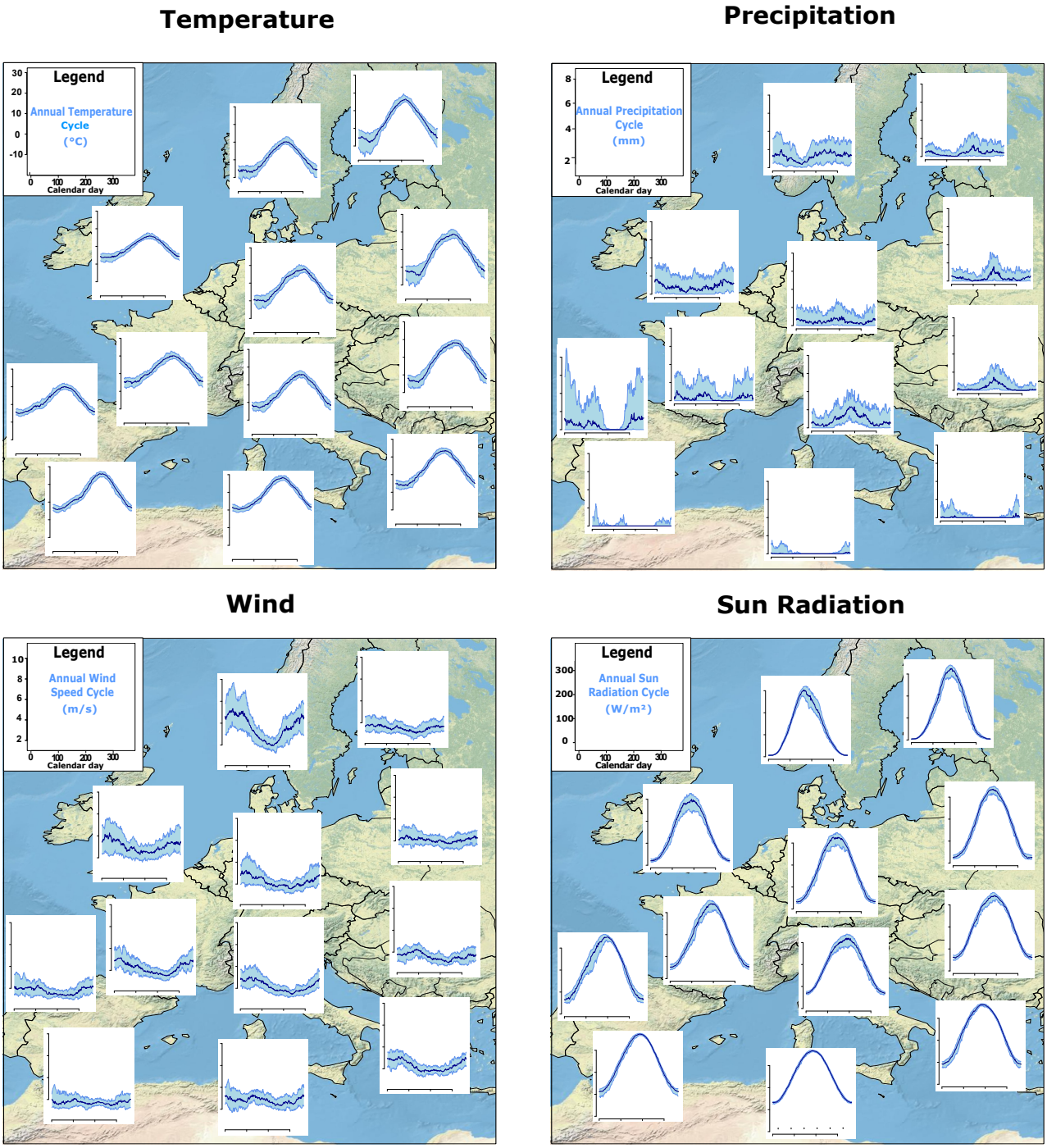

Figure II.4 – **Climatological seasonal cycles of temperature, precipitation, wind and sun radiation for the 12 test regions**. Cycles were computed using the meteorological data described in sec.1.3.2 from 1983 to 2012 (30-day moving average). Information about both median cycles (dark blue line) and 10^{th}-90^{th} percentiles ranges (light blue shading) is provided.

To complement the information provided in sec.1.2, Fig.II.4 presents the seasonal median cycles of meteorological predictands (30-day moving average) for the 12 test regions and based on the datasets described previously. It highlights the spatial variations of climate conditions in Europe.

Additionally, the blue shading also gives an assessment of the inter-annual variability (10^{th} and 90^{th} percentiles).

Temperature cycles vary in two different ways across Europe. Firstly, temperature is obviously higher in southern regions leading to a translation of cycles toward higher temperature values from North to South. The contrast between oceanic and continental climates induces also a gradual transition from western regions to central European ones. In GA, FR and EN, winter is relatively mild and summer reasonably hot. Conversely, BE and RO experience some intense cold waves in winter while summer can be sweltering sometimes. The inter-annual variability of temperature is also larger for these last regions, especially in winter, revealing an alternating of freezing and relatively mild cold seasons.

Precipitation exhibits 3 main types of annual cycle in Europe. In EN, GE, NO, and to a lesser extent in FR, there is a weak seasonality in precipitation (constant median cycles and 10^{th}-90^{th} percentiles ranges). In the Mediterranean basin (AN, TU, GR), rainfall is rare and most days are dry. Some more humid winters occur in these regions but they are relatively infrequent. GA has the more pronounced seasonal cycle and inter-annual variability in precipitation. In this region, summer is dry but more humid conditions return from September. The variability in winter precipitation is high with a large 10^{th}-90^{th} percentiles range from September to May. For continental/mountainous regions (BE, FI, RO, IT), the seasonality of precipitation is inverted with a peak precipitation during summer, indicating numerous and strong convective weather disturbances. The inter-annual variability is also higher in summer. In these regions (plus NO and FI), most of the late autumn - early spring precipitation is solid, leading to snow accumulation.

Wind seasonality has homogeneous characteristics across Europe with higher but also more variable wind speed values in winter. However, the distance of a region from the Atlantic Ocean or the Mediterranean determines the amplitude of the seasonal cycle with fewer differences from summer to winter in continental regions. One can also notice that the average wind speed is higher in North-western Europe where most atmospheric low pressure systems circulate.

Solar radiation is mostly driven by the Earth inclination and day duration. Logically, the amplitudes of the seasonal cycles are higher in Northern Europe than for Mediterranean regions. Moreover, the inter-annual variability is rather different from one region to the other. The 10^{th}-90^{th} percentiles range is larger from winter to early summer in FR and GA. For Mediterranean regions (AN, TU and GR) the inter-annual variability is weak but slightly higher in winter. Conversely, more variability in solar radiation is observed in summer for all other regions.

In conclusion, the 4 meteorological drivers of river discharge, CRE sources and of the weather-dependent part of energy load manifest strong seasonal and regional variations in Europe. These fluctuations are expected to strongly influence all power series and lead to a variety of characteristics in our 12 test regions.

2. Hydrological regimes

2.1. Hydrological modelling

To go from weather to discharge, we use a simple conceptual hydrological model inspired from what is proposed by Schaefli et al., 2005. Its structure is illustrated in Fig.II.5.

The snow module simulates the whole spatio-temporal dynamic of snow pack. It uses, on one hand, a temperature threshold to convert precipitation into rainfall and snowfall and on the other hand, a classic degree-day method for snow-melt. Part of the resulting equivalent precipitation (P_{eq}) is then intercepted by plants and trees. The potential evapo-transpiration (PET) model gathers information on the atmospheric state (Temperature amplitude, wind, humidity and sun radiation) and converts it into PET using the Penman Monteith equation [Monteith, 1965]. The combination of these two first outputs (PET and P_{eq}) leads to a first loss of water through the actual evapo-transpiration (ET_1).

Then, the remaining part of P_{eq} is split up and contributes to infiltration into the upper ground layer S_1 and to a quick hydrological response through run-off. This first ground layer is also subject to evapo-transpiration (ET_2). Water percolation from S_1 supplies the deep ground layer which consists of two sub-reservoirs. The deeper one, S_3, drives the slow hydrological response of the basin. The regional discharge is obtained summing the contributions of all grid cells (no flow routing is performed). In a first approximation, we assume that the region is small enough to make the routing time from any grid cell to the region outlet shorter than one day.

This simple model must be seen as a hydrological filter simulating a realistic regional hydrological cycle and taking into account most of the non-linear processes converting precipitation into river discharge (interception by vegetation, snow-pack, several components of ground storage...). It gives a simplified representation of snow-pack dynamics and of both slow and rapid-flow components of discharge. Moreover, we decided to use a single set of parameters for all regions. It makes the model simulations only sensible to the different meteorological regimes and to the geomorphological characteristics of each region. With such choices, one cannot expect the model to give entirely satisfactory discharge simulations on any region considered individually. However, its relatively simple structure leads to correct simulations of river discharge for the 12 regions.

The calibration/validation of the model was performed using a stepwise technique for all 12 regions simultaneously. We do not detail this process here. Some supplementary information can be found in Appendix.B.

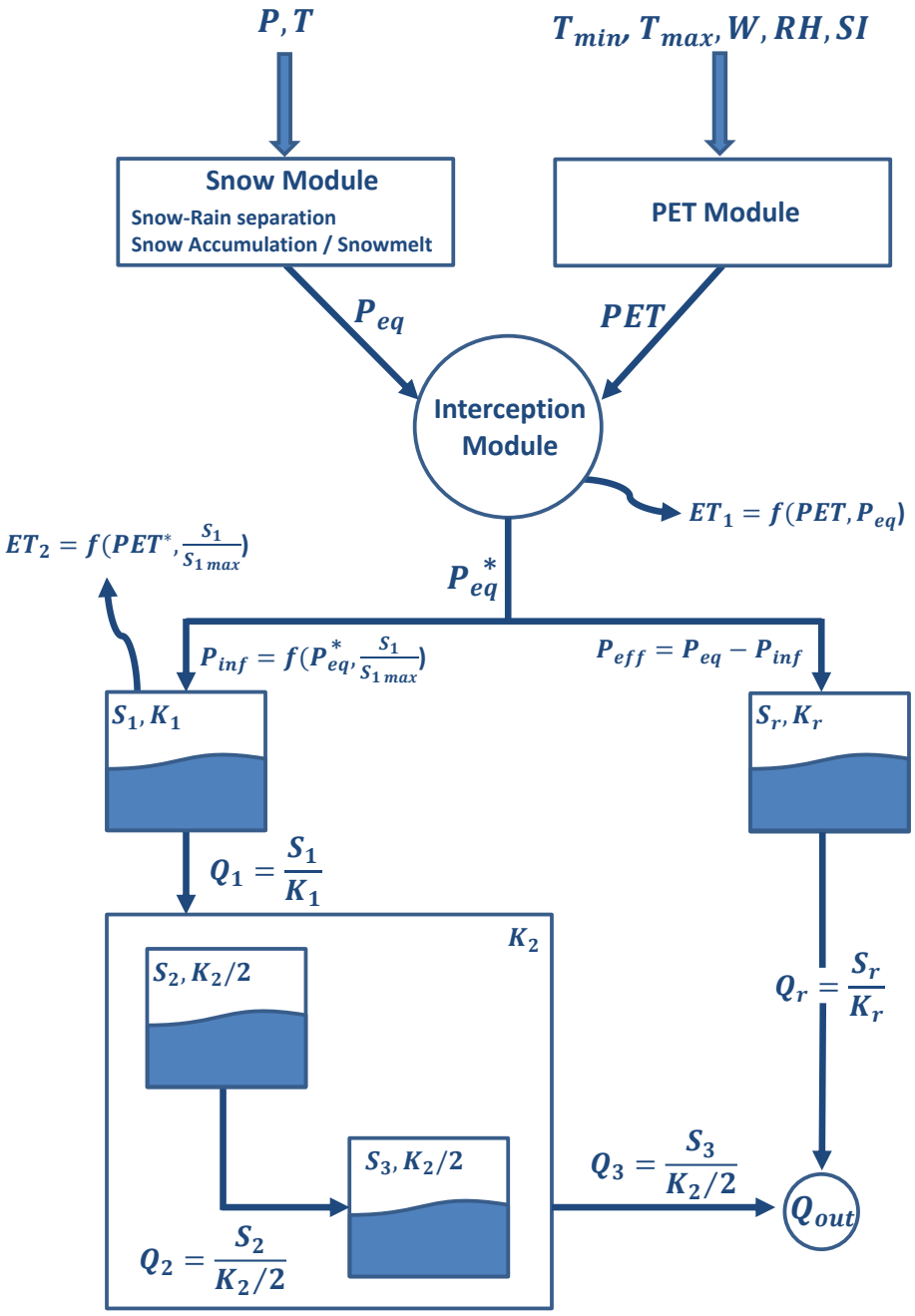

Figure II.5 – **Hydro model structure and functioning.** P (Precipitation), T (Temperature), W(Wind speed), RH(Near-surface relative humidity), SI (Solar Irradiance), P_{eq} (Equivalent precipitation), PET (Potential evapo-transpiration), P_{eff} (Runoff contribution of precipitation), P_{inf} (Infiltration), ET_i (Evapo-transpiration), S_i (Current storage), S_{imax} (Storage capacity of soil reservoir) K_i (Time constant), Q_{tot} (Outlet discharge).

2.2. Hydrological regimes in Europe

Using the hydrological model described in Sec.2.1 and the observed weather data of Sec.1.3.2, the discharge time series were computed for the 12 test regions from 1983 to 2012. Fig.II.6 presents the resulting climatological seasonal cycles of river discharge. They can be classified into two main hydrological regimes:

- For most regions (GA, AN, FR, EN, TU, GE, GR) river discharge values reach a maximum in winter whereas low flows are generally observed from July to early September. This is typical of the pluvial regime. The dry and hot summer season, as part of the Mediterranean climate characteristics, results in extremely low discharge values or even dry rivers in AN TU, and GR. The inter-annual variability (10^{th}-90^{th} percentiles range) is larger in winter for these regions (and in GA as well). It is rather constant across the year for the others.
- NO, IT and to some extent FI, present discharge cycles which are characterised by a main peak in river discharge in spring due to snow-melt and a secondary one in late autumn resulting from large precipitation amounts. The snow-melt related peak has a large inter-annual variability. For these regions, the low-flow period occurs in winter when most of precipitation is solid (snow accumulation).
- The two remaining regions, BE and RO, seem to have more complex regimes. No clear peak in discharge can be seen. These discharge cycles have a very weak seasonally compared to what has been described for the other European regions.

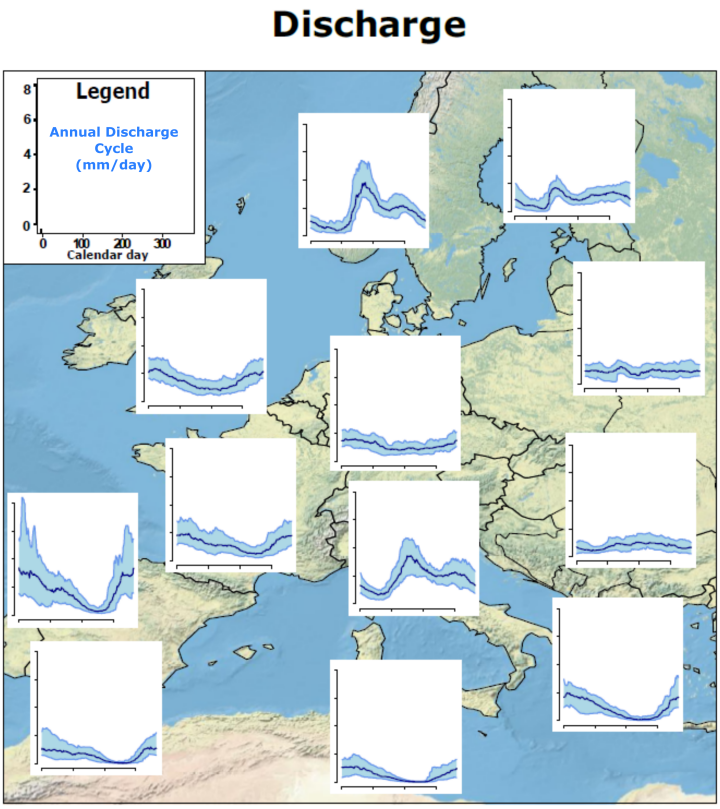

Figure II.6 – **Climatological seasonal cycles of discharge in the 12 test regions**. Cycles were computed using the hydro model described in II.5. Input data are taken from the datasets described in Sec.1.3.2 from 1983 to 2012 (30-day moving average). Information about both median cycles (dark blue line) and 10^{th}-90^{th} percentiles ranges (light blue shading) is provided.

3. Power generation

3.1. Weather-Energy conversion models

The weather and hydrological data presented previously are converted into power generation series using the simple models described hereafter.

3.1.1. Solar power

As proposed by Perpinan et al., 2007, solar power generation is driven by Eq.II.1. It depends on two meteorological variables: global solar irradiance SI and, to a lesser extent, air temperature T. All the other parameters are constants. This simple conversion model does not take into account the orientation of solar panels and their inclination is set to 0°. Finally, in order to make the solar power series directly comparable between regions, the solar panels area is set to $10^4 m^2$ for all regions, corresponding to a nominal power of $1MW_p$ under standard test conditions (i.e. $1MW$ for a solar irradiance of 1000 $W.m^2$, with a spectrum similar to sunlight hitting the earth's surface (standard airmass) and hitting the positioned solar cells perpendicularly. The standard temperature is set to $T_{c,STC}$=25°C).

$$\mathrm{P_{PV}(t)} = \mu_{al} \cdot A \cdot r \cdot SI(t) \cdot [1 - \mu \cdot (T(t) - T_{c,STC}) - \mu \cdot C \cdot SI(t)] \quad \text{(II.1)}$$

Where

- P_{PV}: Power generation from a photovoltaic generator (W)
- μ_{al}: Power losses coefficient due to the transition from direct to alternative current (dimensionless)
- μ: Temperature-dependent efficiency reduction factors (dimensionless)
- A: Surface area of the PV array $10^4 \cdot m^2$
- r: Efficiency under standard conditions (dimensionless)
- SI: Global solar ($W.m^2$) irradiance
- T: Air temperature (°C)
- $T_{c,STC}$: cell temperature ($25°C$) corresponding to standard test conditions [Duffie and Beckman, 1991]
- C: Radiation-dependent efficiency reduction factors (dimensionless)

3.1.2. Wind power

The instantaneous wind power generation equation is presented on Eq.II.3. To trigger the turbine rotation, a minimum wind speed is necessary (v_{in}). Then, wind power is proportional to the cube of wind speed. For wind values higher than v_{nom} the power production is limited to P_{nom}, the nominal power. For strong wind ($> v_{out}$), the production has to be shut down to avoid damages to the turbine.

$$\mathrm{p_w(t)} = \begin{cases} 0 & \text{if } w(t) < w_{in} \\ \frac{1}{2} \cdot \rho \cdot (w(t) - w_{in})^3 & \text{if } w_{in} \leq w(t) < w_{nom} \\ P_{nom} & \text{if } w_{nom} \leq w(t) < w_{out} \\ 0 & \text{if } w_{out} < w(t) \end{cases} \tag{II.2}$$

Where

- p_w: Instantaneous power generation from the wind turbine
- ρ: air density. $\rho = 1.225 kg.m^2$
- w: instantaneous wind speed at 80m ($m \cdot s^{-1}$)

In order to convert daily wind speed into wind power, Eq.II.3 needs to be adapted. To do so, we use an estimation of the probability density function of the infra-daily wind speed f_W which depends on daily wind speed W. Then the daily wind power generation $P_w(W)$ is given by the convolution of this function with the instantaneous power curve $p(w)$. We estimate this integral $P_w(W)$ using a set of daily wind speed values and the 3h data coming from the WRF model (sec.1.3.1.c). Daily wind speed values range from 0 to $35 m \cdot s^{-1}$. Finally, f_W was estimated using the Weibull density function. Fig.II.7 illustrates the initial (instantaneous) and final (daily) conversion curves. For more details, see François et al., 2016.

$$\mathrm{P_w(W)} = \int_0^\infty f_W(w) \cdot p(w) \cdot dw \tag{II.3}$$

Where

- $P_w(W)$: Daily power generation from the wind turbine (Watt)
- f_W: Probability density function of the infra-daily wind speed. Function of the daily wind speed
- w: instantaneous wind speed ($m \cdot s^{-1}$)

Wind data are available at 10m. An estimate of wind speed at 80m (chosen as turbine height) is obtained with a classic scaling relationship presented in Eq.II.4. This simple relationship uses a roughness-dependent scaling factor set to $\frac{1}{7}$. Wind speed is supposed to be homogeneous on the whole propeller.

$$W_{80m(t)} = W_{10m}(t) \cdot (\frac{H_{80m}}{H_{10m}})^{\alpha} \tag{II.4}$$

Where

- W_{80m}: wind speed at 80m ($m \cdot s^{-1}$)
- W_{10m}: wind speed at 10m ($m \cdot s^{-1}$)
- H: altitude (here 80m or 10m)
- α: roughness-dependent scaling factor. Here set to $\frac{1}{7}$ (dimensionless)

3.1.3. Run-of-the-river hydro-power

Run-of-the-river (RoR) hydroelectricity can make a significant contribution to the total hydro power generation. Actually, it represents 26% of the total hydroelectric production in France, 24% in Italy and 26% in Switzerland. As run-of-the-river hydro power is directly related to discharge, it is

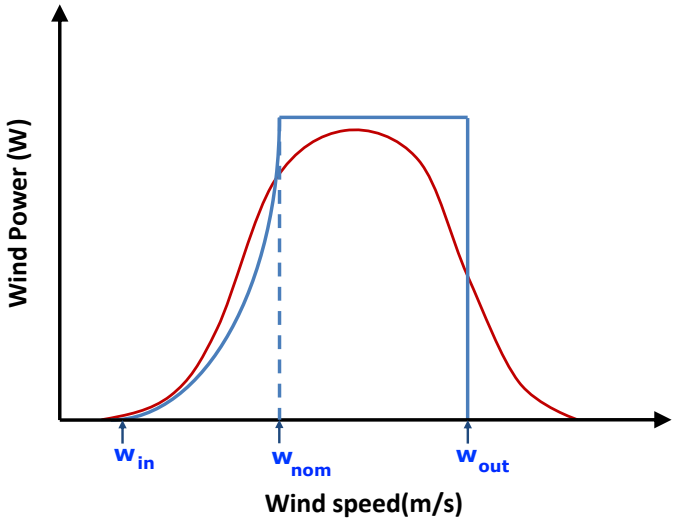

Figure II.7 – **Daily and instaneneous wind power curves.** Instantaneous wind power curve as a function of instantaneous wind speed (blue). Modelled daily power curve as a function of mean daily wind speed (red). w_{in}, w_{nom}, w_{out} represent respectively the cut-in, nominal and cut-out instantaneous wind speed values

very sensible to hydro-meteorological fluctuations. In this study, we not take into account any water storage reservoirs in order to isolate the most weather-related part of hydro power production.

To estimate RoR hydro power from river discharge, we use a classic conversion function (Eq.II.5) using the water head (H) which represents the altitude difference between the current grid cell and the lowest point of the region. Since no water routing is done in our simple hydrological model, we assume that the regional hydro power generation can be estimated summing the contribution of all grid cells.

$$P_h(t) = r_h \cdot \rho \cdot g \cdot H \cdot Q(t) \tag{II.5}$$

Where

- P_h: Power generation from the hydro-electric generator (Watt)
- r_h: Standard efficiency of the generator
- ρ: liquid water density. $\rho = 1000kg.m^2$
- g: gravitational acceleration. $g = 9.81m^3.s^{-1}$
- H: Water head (m)
- Q: River discharge ($m^3.s^{-1}$)

As for wind power, some discharge thresholds determine the final hydro power generation. Hydro-electricity can only be produced when river discharge is greater than a given threshold Q_{min} which represents the minimum flow that should not be diverted to preserve the integrity of the river bed and its ecosystems. The design flow Q_d is the maximum discharge that can be converted into power. This parameter depends on the size and characteristics of the hydro-power plant. Finally, Q_{max}, the upper discharge threshold, gives the discharge value above which it is not possible to produce hydro power due to high-flows. Q_{min}, Q_d and Q_{max}, have been set to the 95^{th}, 25^{th} and 2^{nd} percentiles

of discharge values. Those choices are based on some previous studies [Hänggi and Weingartner, 2012]. The final equations, defining the actual hydro power generation from these 3 thresholds, are presented in Eq:II.6.

$$\mathrm{P_h(t)} = \begin{cases} 0 & \text{if } Q(t) < Q_{min} \\ r_h \cdot \rho \cdot g \cdot H \cdot (Q(t) - Q_{min}) & \text{if } Q_{min} \leq Q(t) < Q_d \\ r_h \cdot \rho \cdot g \cdot H \cdot (Q_d - Q_{min}) & \text{if } Q_d \leq Q(t) < Q_{max} \\ 0 & \text{if } Q(t) > Q_{max} \end{cases} \tag{II.6}$$

Where

- P_h: Power generation from the hydro-electric generator (Watt)
- r_h: Standard efficiency of the generator
- ρ: liquid water density. $\rho = 1000kg.m^2$
- g: gravitational acceleration. $g = 9.81m^3.s^{-1}$
- H: Water head (m)
- Q: River discharge ($m^3.s^{-1}$)
- Q_{min}: Minimum discharge for power generation ($m^3.s^{-1}$)
- Q_{max}: Maximum discharge for power generation ($m^3.s^{-1}$)
- Q_d: Design discharge ($m^3.s^{-1}$)

3.1.4. Energy load

Energy load depends on both meteorological and socio-economic parameters. On a daily basis, the energy consumption peaks twice, in the morning (7-8am) and in the late afternoon (5-7pm). Similarly, energy load usually drops during week-ends and school holidays. In the "real world", this variable exhibits low frequency fluctuations and trends resulting from various factors related to economy, demography and/or political choices (electricity price, energy efficiency...). Here, we only take into account weather-related factors: Our energy load model is only driven by temperature. In this way, results from different regions are easily comparable whatever the population or their economic development.

To develop this simple model, national load data, available since 2006, have been downloaded from the ENTSOE[1]. Before being used, these data have been preprocessed in order to remove trends or break points due to changes in population or to the 2008 economic crisis (which created a drop in electricity consumption for some country). The detailed methodology applied for the standardisation of load data can be found in Pustitrarini, 2015.

Fig.II.8, also extracted and adapted from Pustitrarini, 2015, presents the national standardized daily energy load values as a function of daily temperature. There is a strong relationship between energy demand and air temperature for all European regions. Despite rather large differences between regions, three distinct temperature intervals appear with 1) decreasing energy load with higher temperature from -30 to 15°C, 2) rather constant energy load from 15 to 20°C and 3) increasing daily

[1] https://www.entsoe.eu/db-query/country-packages/production-consumption-exchange-package

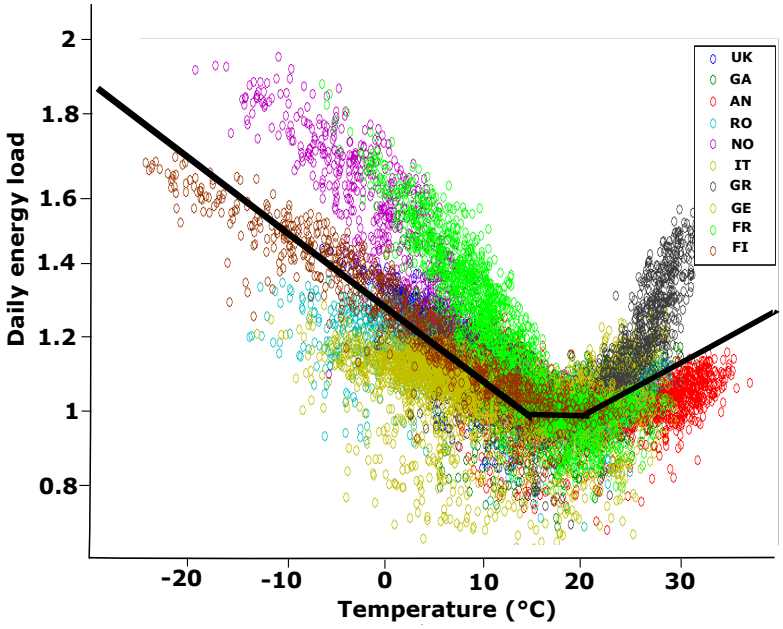

Figure II.8 – **Relationship between daily energy load and temperature.** Daily standardized energy load (dimensionless) as a function of temperature for each country (color classes). The global piecewise linear model, corresponding to three linear regressions from -30 to 15°C, from 15 to 20°C and from 20 to 40°C is presented in black.

energy load for temperature higher than 20°C. As before, we decided to develop a unique temperature-load conversion model for our 12 regions. A global piecewise linear model, corresponding to three linear regressions using all data below 15°C, from 15 to 20°C and above 20 C has been applied and is also presented on Fig.II.8. Eq.II.7 presents this simple model. The piecewise linear function takes on board heating systems for temperature lower than $15°C$ and air conditioning when then mean daily temperature exceeds $20°C$.

$$\mathrm{D} = \begin{cases} a_{cold} \cdot T + b_{cold} & \text{if } T < 15°C \text{ with } a_{cold} = -0.02\,T^{-1} \text{ and } b_{cold} = 1.31 \\ 1 & \text{if } 15°C \leq T \leq 20°C \\ a_{hot} \cdot T + b_{hot} & \text{if } T > 20°C \text{ with } a_{hot} = -0.01\,T^{-1} \text{ and } b_{hot} = 0.79 \end{cases} \tag{II.7}$$

Where D is the standardized energy load and T the air temperature (°C).

To illustrate how this stepwise linear function is going to impact the regional energy load series depending on their climate characteristics, Fig.II.9 presents the seasonal and annual density function of temperature for three representative regions (NO, GE, AN). In NO, winter and late/early autumn/spring are cold. Large energy load values are expected from heating systems. Summer is generally mild and do not require air conditioning. The same comments apply to GE despite less extreme temperature values in winter and a few days for which air conditioning is going to impact the daily energy load in summer. Conversely, in AN, winter is generally not cold enough to significantly increase the regional energy load. However, air conditioning systems are coming into play for most summer days and a large proportions of autumn ones. All in all, the seasonal variations and the

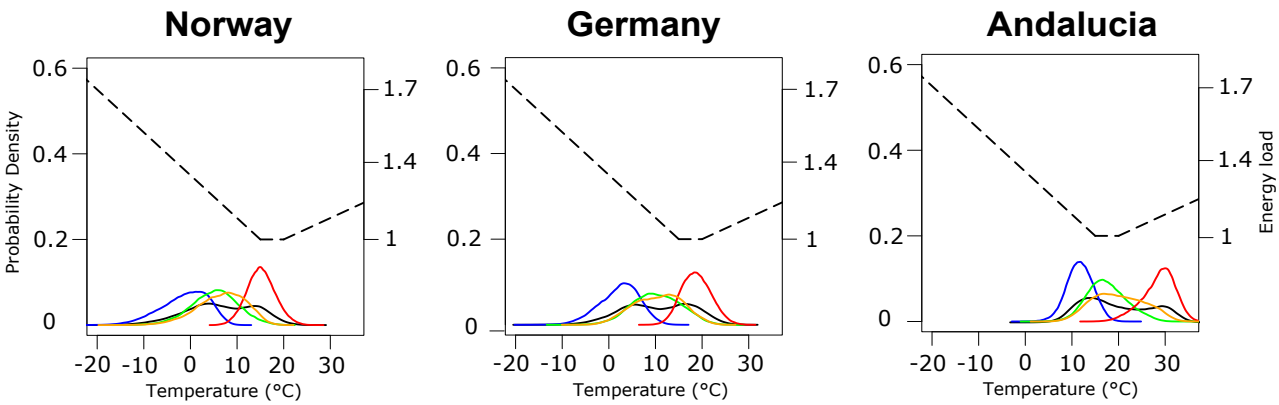

Figure II.9 – **Regional temperature probability distributions and temperature-demand model.** Piecewise linear function for converting daily temperature (x-axis - Celsius degrees) into energy demand (y-axis, left, dimensionless). The seasonal and annual distributions of daily temperature (DJF-blue, MAM-green, JJA-ref, SON-orange) are also displayed.

regional differences of temperature will have repercussions on the energy load series and lead to a variety of characteristics.

3.2. Power generation and energy load regimes

The conversion models presented previously were used to simulate regional series of power generation and energy load from 1983 to 2012 in Europe. Undoubtedly, it is not possible to discuss the absolute values of production and energy demand as a result of the simplifications and normalizations applied in all models (same parametrisation in the hydrological model, same level of equipment in the energy weather-conversion models, no dependence to population density and/or development level in the energy load equations). However, the relative differences between regions are expected to be realistic. Fig.II.10 presents the mean daily power generation for the three CRE sources together with the mean daily energy load.

Despite its dependence on discharge, the potential for run-of-the-river hydro power generation is much higher in mountainous regions where a high elevation difference provides a large water head. Thus, IT clearly stands out from the crowd. Hydro power is much smaller but still significant compared to other regions for GA and NO. Despite their high mean altitudes, AN, GR and RO do not have high electricity production values due to relatively low discharge.

Wind power production is emboldened over flat regions close to the sea (i.e. where wind has not eased off because of the ground roughness yet). North-Western Europe is consequently the place where the higher production values can be found. The preferential mid-latitude cyclones pathway guarantees strong and frequent wind over EN and NO. However, the Tunisian coast also seems to experience significant wind leading to a rather high wind power production.

Solar power depends mainly on latitude. The North-South gradient in production is strong with values almost twice higher in TU than in FI. For regions at the same latitude (e.g FR-RO, EN-BE), higher productions are achieved in the East as a likely consequence of less cloudy conditions on average for continental climate.

There is a SW-NE oriented gradient of weather-driven energy load in Europe. The long and tough winter in northern continental regions results in large energy demand values in FI, NO and BE. Despite the contribution of air-conditioning in summer, southern Europe and Maghreb still have the lowest values of climate-related energy demand. These regional differences are a direct consequence of the seasonal probability density functions discussed in sec.3.1.4 for Fig.II.9.

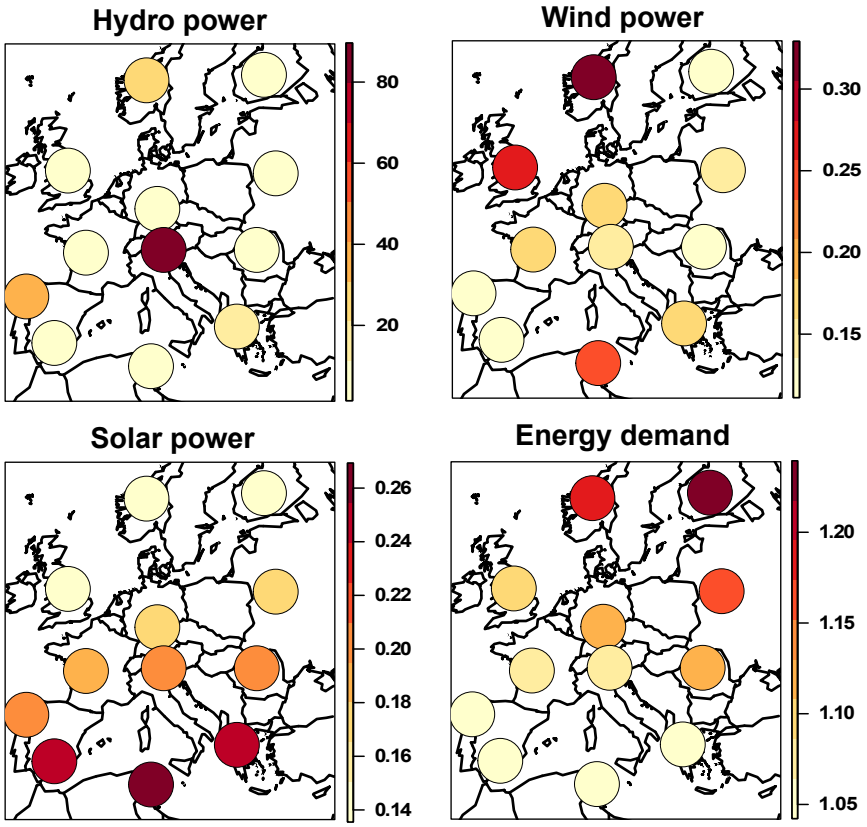

Figure II.10 – **Regional mean daily power generation and energy demand.** Spatial pattern of mean simulated power generation (MW) and of weather-related energy load (dimensionless). Mean values were computed using the whole 1983-2012 period.

Mean daily production hides the seasonal and inter-annual variations of CRE sources. Fig.II.11 shows the regional seasonal cycles of power productions and energy load. These cycles have been standardized using the regional daily mean production values presented in Fig.II.10.

The hydro power cycles mainly correlate with the river discharge ones (cf. Fig. II.6). However, the snowmelt-related high flows in IT and NO have been cut off as a result of discharge values often exceeding Q_d or Q_{max} during the snow-melt period. These two regions, together with RO, have a peak in hydro power production in summer whereas this season is generally a low production period elsewhere. Following the Earth axial tilt, solar power is obviously lower in winter. Cycles are more pronounced in northern Europe where day length varies the most across the year. Wind power seasonality is weaker than for the other CRE sources. However, regions at a reasonable distance from the Atlantic Ocean have more wind power potential in winter, resulting from higher wind speed values. Finally, the energy load cycles are relatively flat, especially in FR and GA where both summer and winter are mild. Nevertheless a peak in energy demand is noticeable in winter in north-eastern Europe whereas Mediterranean regions consume more power from June to September.

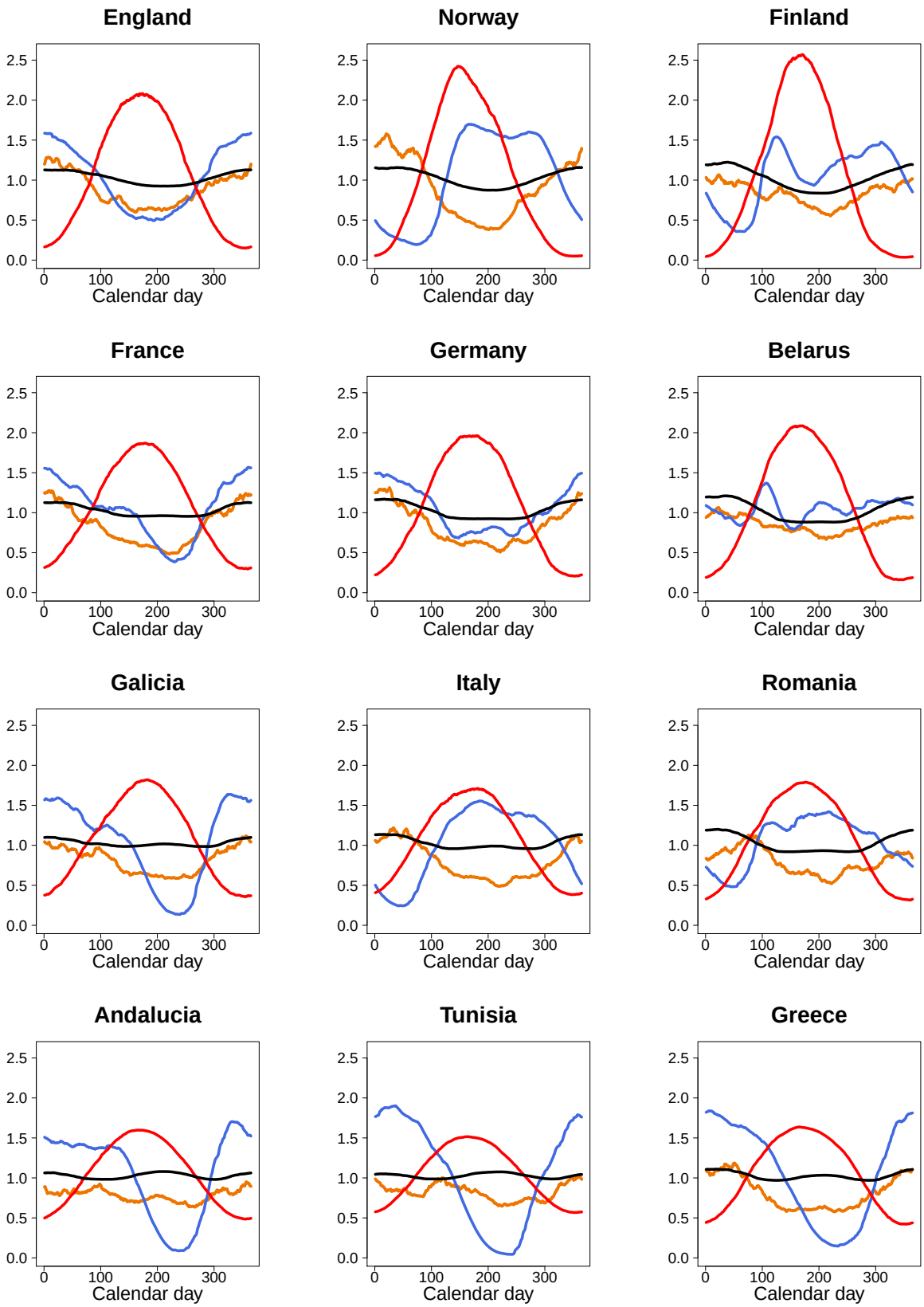

Figure II.11 – **Seasonality in electricity production and energy load.** Standard mean seasonal cycles of power generation for solar (red), wind (orange), hydro (blue) energy sources. Standard mean seasonal cycle energy demand (black). Cycles were computed using a 30-day moving window and the whole period of observations (1983-2012). The standardisation was performed by diving the initial cycles by the mean productions over the entire 1983-2012 period

Tab.II.2 gives the inter-annual coefficients of variability of the three CRE sources and of energy demand. Hydro power changes greatly from one year to another in all regions. The lower coefficients in NO and IT could result from the effect of the snow-pack dynamics. Wind power and solar power coefficients of variation, range from 0.06 to 0.14 and from 0.02 to 0.10, respectively. The inter-annual variability is stronger in Northern Europe as a likely consequence of the North-Atlantic-Oscillation (NAO). Finally, energy load does not vary much from one year to the other.

By way of conclusion, the previous results indicate that:

- Energy load exhibits unquestionably the smallest variability, either in terms of seasonality or inter-annual fluctuations.
- Solar power presents a large seasonality but a very small inter-annual variability
- Hydro power is characterized by both high seasonality and the highest inter-annual variability.
- Regarding wind power, both seasonality and inter-annual variability are moderate.

Table II.2 – CREs and energy load inter-annual coefficient of variability

Region ID	Hydro Power	Wind Power	Solar Power	Energy Load
EN	0.22	0.11	0.06	0.01
NO	0.15	0.14	0.07	0.01
FI	0.21	0.12	0.10	0.02
FR	0.28	0.06	0.06	0.01
GE	0.26	0.08	0.06	0.01
BE	0.26	0.09	0.06	0.02
GA	0.23	0.08	0.05	0.01
IT	0.15	0.07	0.04	0.01
RO	0.27	0.10	0.06	0.01
AN	0.32	0.07	0.03	0.01
TU	0.34	0.09	0.02	0.01
GR	0.29	0.07	0.03	0.01

Chapter III

Penetration rate of CRE sources and energy droughts

The ease of integration of CRE sources depends on their spatio-temporal fluctuations and on their temporal match with the energy load. In this chapter we will evaluate the ability of single CRE sources to meet the demand.

Previously, we discussed the inter-sources and inter-regional disparities which exist in Europe. These differences can be turned to our advantage if one contemplates the possibility of a multi-sources, pan-European integration of renewables. We will illustrate how the integration CRE sources could be improved, making use of these possible complementary contributions. We will use an evaluation criterion quantifying the mean balance between power generation and energy load.

The mean percentage of satisfied demand is a relevant measurement. However, it does not inform on more problematic events for which an energy source is not able to meet the demand for a long period. Using a daily measurement of satisfied energy load, we will define sequences of energy shortage and analyse how their characteristics (duration, frequency of occurrence) vary between sources and regions. Finally, the impact of storage, over-sizing, spatial integration and multi-sources on the global percentage of satisfied demand and on these problematic events will be assessed. It gives a first evaluation of the contributions of these tools to a more relevant integration of intermittent renewables in Europe.

1. Single energy sources

1.1. Penetration rate

1.1.1. Definition

The daily amount of power that a renewable power plant produces is not a sufficient measurement of its relevance. Actually, this evaluation criterion does not take into account the temporal mismatch that exist between electricity production and energy load. Eq.III.1 defines the global penetration rate definition (PE) which will be used to assess the ability of each CRE source to fulfil the energy demand. This measurement quantifies the percentage of energy load that is met by the considered energy source production. It sums up, over the entire period of interest (1983-2012 in or case), the daily unsatisfied energy load and compares it to the total demand. In this evaluation, the daily oversupply that may occur, is lost. As a result, PE ranges from 0 to 100%, this last value representing the ideal configuration for which there is a perfect match between daily power generation and energy load.

The higher the level of equipment, the easier it gets to fulfil the energy load. The relationship between level of equipment and penetration rate has been illustrated in François et al., 2016. To free ourself from this dependence and to characterize only the effects of the temporal mismatch between power generation and energy load on PE, the power production $P_i(t)$ has been standardised. For all regions and energy sources, the power generation time series are scaled using the ratio between mean energy load $\langle D(t) \rangle$ and mean power generation $\langle P_i(t) \rangle$ over the entire 1983-2012 period. Thus, the 33-yr standardised electricity production is equals to the total 1983-2012 energy demand.

$$\begin{aligned} PE &= (1 - \frac{\sum max(D(t) - P_i(t) \cdot \frac{\langle D(t) \rangle}{\langle P_i(t) \rangle}, 0)}{\sum D(t)}) \cdot 100 \\ &= (1 - \frac{\sum max(D(t) - p_i(t), 0)}{\sum D(t)}) \cdot 100 \end{aligned} \tag{III.1}$$

Where

- $PE(t)$: Penetration rate of energy source i
- $D(t)$: Energy load
- $P_i(t)$: Power production of energy source i
- $p_i(t)$: Standardized power production of energy source i
- $\langle P_i(t) \rangle$: Mean production from 1983 to 2012
- $\langle D(t) \rangle$: Mean energy load from 1983 to 2012

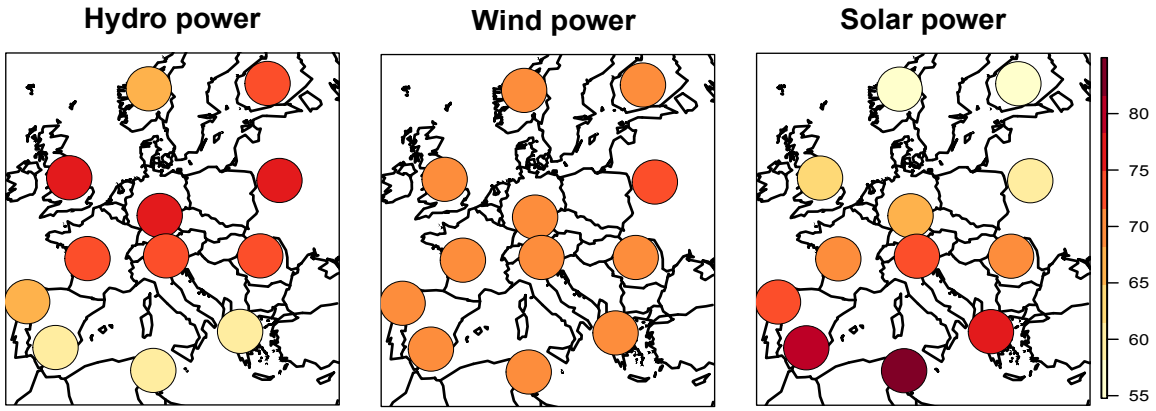

Figure III.1 – **Global Peneration rate (%) for the three single energy sources in Europe.** Computed from 1983 to 2012.

1.1.2. Mean penetration rate in Europe

The penetration rate of all single energy sources is presented in Fig.III.1. Results are very uneven from one source to the other:

- Hydro power gives low penetration rates (<60%) in Mediterranean regions as a likely consequence of the co-occurrence of low discharge and high energy load due to air conditioning in summer. The highest penetration rates are found from EN to BE (>75%). For Scandinavian regions, the match between energy load and power generation decreases again as a result of high energy load but relatively low hydro power generation in winter.
- No clear spatial patter exists for wind power. The regional penetration rates range from 70 to 80%. These values are higher than the ones of hydro power in southern Europe.
- There is a strong North-South gradient in solar power penetration. In northern regions, PE values are rather low (<60%). In the Mediterranean basin, summer months gather both high energy demand (air conditioning) and maximum electricity production from photovoltaic power stations leading to PE values exceeding 80%.

From these first results, one can notice the inter-sources complementarity that may exist for some regions. In TU, for instance, the high penetration rate achieved using solar can probably balance the low value associated to hydro power. Similarly hydro and wind power can complement each other in FI and NO and compensate for the match between energy load and solar power series.

1.2. Energy droughts

1.2.1. Definition

For a given energy source, the penetration rate estimates the mean daily proportion of satisfied energy demand. Thus, it quantifies the long-term match between energy generation and energy load. It does not inform on the chronology of days for which the production does not meet the energy demand. More precisely, it does not inform on the occurrence of long lasting sequences of both power shortage and high energy load. In this section, we will present the concept of energy droughts, following the classic definition of hydrological droughts used for long lasting sequences of days with extreme low river discharge values [Hannaford et al., 2011].

A first approach would be to define energy droughts considering only low power generation sequences. However, in order to take into account energy demand, we define energy droughts as uninterrupted sequences of days characterized by concomitant low power production and high energy load. Here, we focus on another aspect of the production/demand balance issue, exploring the critical asynchronism between them. These problematic sequences can result from various situations: very low power generation vs. moderate demand ; moderate power generation vs. high demand ; low power generation vs. high energy load. This criterion disregards periods for which both electricity production and energy demand are low, which are considered as non-critical. We will estimate the statistical characteristics (duration, frequency of occurrence) of energy droughts for the different energy sources and test regions in Europe.

To perform this analysis, we consider time series of daily satisfaction rate (SA) which quantifies the day-to-day percentage of energy load which can be met by the daily electricity production. SA is a similar measure to PE. It gives a daily estimation of the mismatch between energy load and power generation rather an integrated one over long periods (Eq:III.2):

$$\begin{aligned} SA(t) &= (1 - \frac{max(D(t) - P_i(t) \cdot \frac{\langle D(t) \rangle}{\langle P_i(t) \rangle}, 0)}{D(t)}) \cdot 100 \\ &= (1 - \frac{max(D(t) - p_i(t), 0)}{D(t)}) \cdot 100 \end{aligned} \tag{III.2}$$

Where

- $SA(t)$: Daily satisfaction rate of energy source i
- $D(t)$: Energy load
- $P_i(t)$: Power production of energy source i
- $p_i(t)$: Standardized power production of energy source i
- $\langle P_i(t) \rangle$: Mean production from 1983 to 2012
- $\langle D(t) \rangle$: Mean energy load from 1983 to 2012

Energy droughts, as hydrological or agro-meteorological droughts [Vidal et al., 2012], are fully determined by the chronology of weather conditions. Many different methods are used to characterize hydro-related droughts. The usual estimated features are the frequency of occurrence, the intensity and the duration of droughts sequences. Consequently, it is necessary to decide on a relevant threshold (usually related to discharge values in hydrology) which separates normal conditions from droughts.

In the following analysis, an energy drought sequence is defined as one or several consecutive days for which SA is lower than a given threshold. In order to consider different droughts intensities, we use 4 different thresholds of satisfied demand (100%, 80%, 50% and 20%). The 100% threshold corresponds to a simple case for which the daily energy load is not fully satisfied by the power generation. The 20% threshold corresponds to what could be called "extreme mismatch events". Usually, the term of "droughts" is reserved to extreme events. It would be more accurate to speak of periods of "under-production" for the less restrictive SA thresholds (100, 80 and 50%) and limit the

usage of "energy droughts" to the most severe one (20%). However, for the sake of simplicity, the same terminology is used for all thresholds.

1.2.2. Droughts characteristics

Fig.III.2 presents the droughts characteristics for all regions, single energy sources and thresholds. The frequency of occurrence of drought sequences (y-axis, mean number of sequences per year) is plotted against the mean drought duration (x-axis, in days). The proportion of days (%) undergoing drought conditions is also presented via the background color scale. For a given energy source, the drought characteristics corresponding to different SA thresholds (dots of the same color) are connected in a logical order from 100% (corresponding to the higher proportion of days under drought conditions) to 20%.

- Hydro-power droughts are not frequent but have large mean durations (from 20 days in FR to 80 days in NO). In GR, TU, AN and GA, the droughts characteristics are not much impacted by the satisfaction rate threshold. Anywhere else in Europe, both droughts number and mean droughts duration decrease with lower thresholds (i.e. severe droughts are less frequent and have a smaller duration). However, in NO and IT, going from the 100% threshold to the 80% one, induces a provisional increase in mean drought duration. This result comes from the removal of short and weak droughts giving the upper hand to long duration ones.
- For most regions (except in Scandinavia), solar-power related drought sequences consists of days with very low satisfaction rates. As a consequence, lowering the SA threshold reduces their mean duration, cutting days off at the starting and ending points of the sequences, but leaves the mean number of droughts unchanged. There seems to be a clear relationship between solar power droughts and latitude: On one hand, GR, TU and AN have few and short periods of SA rates below 20%, and on the other hand, droughts in FI and NO have the same characteristics whatever the SA threshold.
- Wind power droughts are rather short (never exceeding 5 days) but numerous (From 10 to 60 sequences per year depending on the SA threshold). Similarly to solar power droughts, lowering the SA threshold first reduces the mean droughts duration. It is only with the 20% satisfaction rate that the frequency of occurrence also drops.

Following the seasonality of mean power generation series, energy droughts characteristics change in the course of the year. Naturally, they are much less numerous and long for seasons with higher mean production (e.g. solar power - summer). The seasonal characteristics of energy droughts are presented on Fig.III.3 for the three CRE sources and three representative regions.

Wind power droughts have a weak seasonality. Both mean droughts durations and numbers are similar from one season to the other. Conversely, the intra-annual variations of solar power droughts are strong: the simultaneity between low solar power production and high energy demand due to heating systems, in winter, leads to much longer droughts in NO and GE. There are very few events (NO, GE and most regions) or even no solar droughts (AN and all Mediterranean regions) in summer. The seasonality of hydro power droughts is highly region-dependent. In Scandinavia and high-mountain regions, the accumulation of snow in winter results in low winter and early spring discharge. Consequently, hydro power cannot balance the energy demand during the cold season

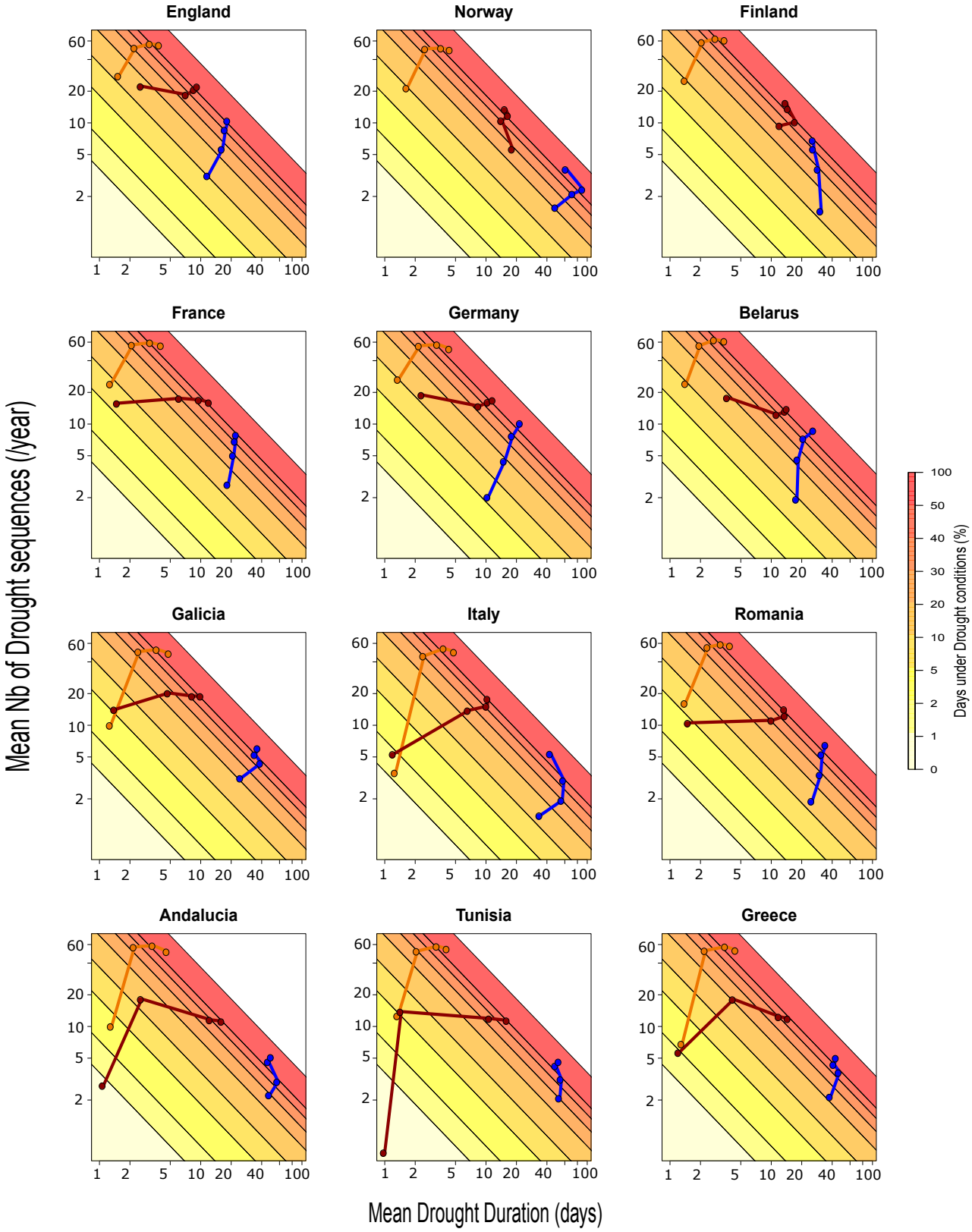

Figure III.2 – **Droughts characteristics associated to different SA threshold**. Mean number of drought episodes versus mean drought duration. Results are displayed for hydro-power (blue), solar-power (red), wind-power (orange). The points associated to different thresholds but from the same energy source have been connected in a logical order from 100% to 20%. The color scale gives the mean annual number of days experiencing droughts conditions.

and the associated droughts sometimes last for the whole 3-month period. Regions located in plains and close to the Mediterranean suffer from low hydro power production combined with high energy demand due to air conditioning in summer. It often results in a single but extremely long energy drought sequence from June to August.

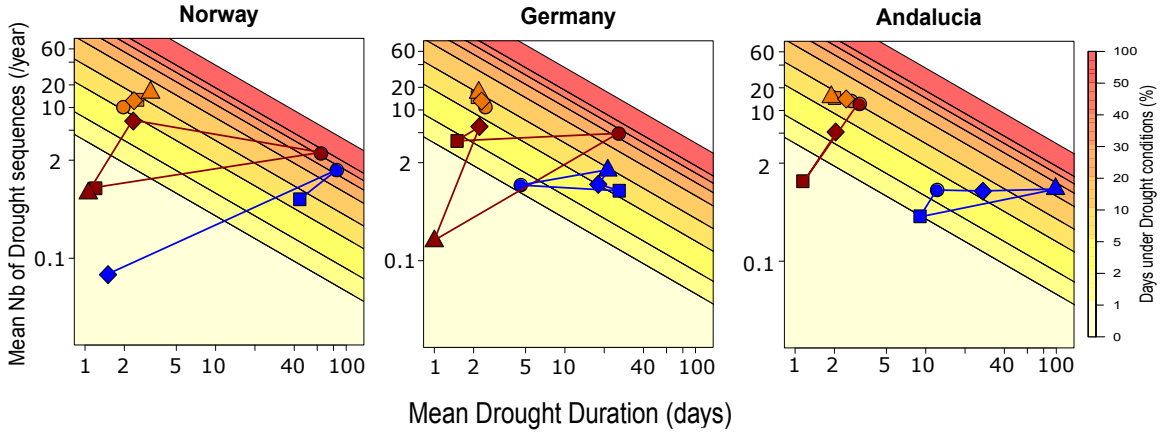

Figure III.3 – **Seasonality in droughts characteristics**. Seasonal mean number of drought episodes versus mean drought duration associated to the 50% SA threshold. Results are displayed for hydro-power (blue), solar-power (red), wind-power (orange). The color scale gives the mean annual number of days under droughts conditions. Dot=Winter, Square=Spring, Triangle=Summer, Diamond=Autumn.

This analysis reveals that energy droughts have various characteristics from one power source to the other. Hydro power droughts are long but relatively infrequent whereas wind power ones are numerous but never exceed a week. Solar power droughts characteristics are intermediate. Furthermore, the seasonality is particularly strong for both solar and hydro power droughts but it is rather limited for wind power ones.

Drought characteristics have a strong spatial consistency in Europe. In most cases, both duration and frequency of occurrence of energy droughts are similar from one region to the neighbouring one, especially for the 100% and 80% SA thresholds.

2. Multi-sources

The PE rates associated single CRE sources can be quite low (e.g. solar power - Scandinavia, hydro power - Mediterranean basin, cf. Fig.III.1) and some long period of energy generation/load mismatch often occur (e.g. hydro power, cf. Fig.III.2). In this section, we investigate how combining different energy sources could improve their integration in Europe.

2.1. Inter-sources correlations

As a first step in evaluating the complementarity between renewables in Europe, we analyse the Spearman correlation between seasonal series of power generation and energy load. It highlights the synchronism/asynchronism between sources and hence their potential counterbalance at a seasonal time scale.

The regional Spearman correlation coefficients between CRE sources are presented on Fig.III.4 for both winter and summer months. In addition, this figure presents the correlation coefficients between power generation and energy load series. On one hand, high anti-correlations between CRE sources are desirable as they would guarantee some asynchronism between production series. Then, seasons of weak power generation from one energy source may be balanced by another source. On the other hand, and whatever the energy source, the higher the correlation with the energy demand, the better.

Generally speaking, there is a strong spatial consistency between the correlation coefficients obtained for neighbouring regions. In winter and for all regions (except TU, IT, GR), wind and hydro power are always positively correlated and thus likely cannot complement each other. Moreover, these two energy sources are not synchronized with the energy demand and cannot efficiently balance it at seasonal scale. On the other hand, solar power seems much more relevant: It has not only negative correlation coefficients with the other energy sources, but also positive ones with the energy demand. However, this result must be looked at in context as solar radiation is very low in winter in northern regions.

In the three remaining regions (TU, IT, GR), the conclusions are more heterogeneous. The correlation coefficients between wind power and energy demand are positive for all of them. In TU, hydro power and energy demand are also correlated and the coefficient between solar power and the energy demand is negative.

In most cases, summer correlation coefficients are similar to winter ones. Nevertheless, some noteworthy changes in sign exist for correlation coefficients between energy demand and all energy sources in EN, NO and FI. On the other hand, the synergy of renewable with the energy load undergoes a reversal in summer.

Analysing correlation coefficients at a seasonal scale is a first but coarse approximation of what could be a relevant combination of energy sources in our 12 test regions. Indeed, it does not inform on the daily complementarity between sources and hence, on their conjoint ability to fulfil the energy load. Using the penetration rate defined in Sec.1.1.1, we will now present how this criterion can be optimised combining all three hydro, wind and solar power sources.

2.2. Optimal mixes: Definition and penetration rates

Hydro, solar and wind power exhibit different characteristics at all time scales. Thus, considering a mix of those sources rather than single univariate ones is expected to reduce the variability of power generation and to increase its match with energy load.

Following François et al., 2016, we now explore how PE and energy droughts characteristics can be improved mixing CRE sources. To go from univariate power generation to energy mix, we use three sharing coefficients representing the proportion of each energy source in the final mix (Hydro power: s_H ; Wind power: s_W ; Solar power: s_H). These coefficients fulfil the following condition: $s_{PV} + s_W + s_H = 1$. Then, a daily power generation series P_{mix} is computed following Eq.III.3.

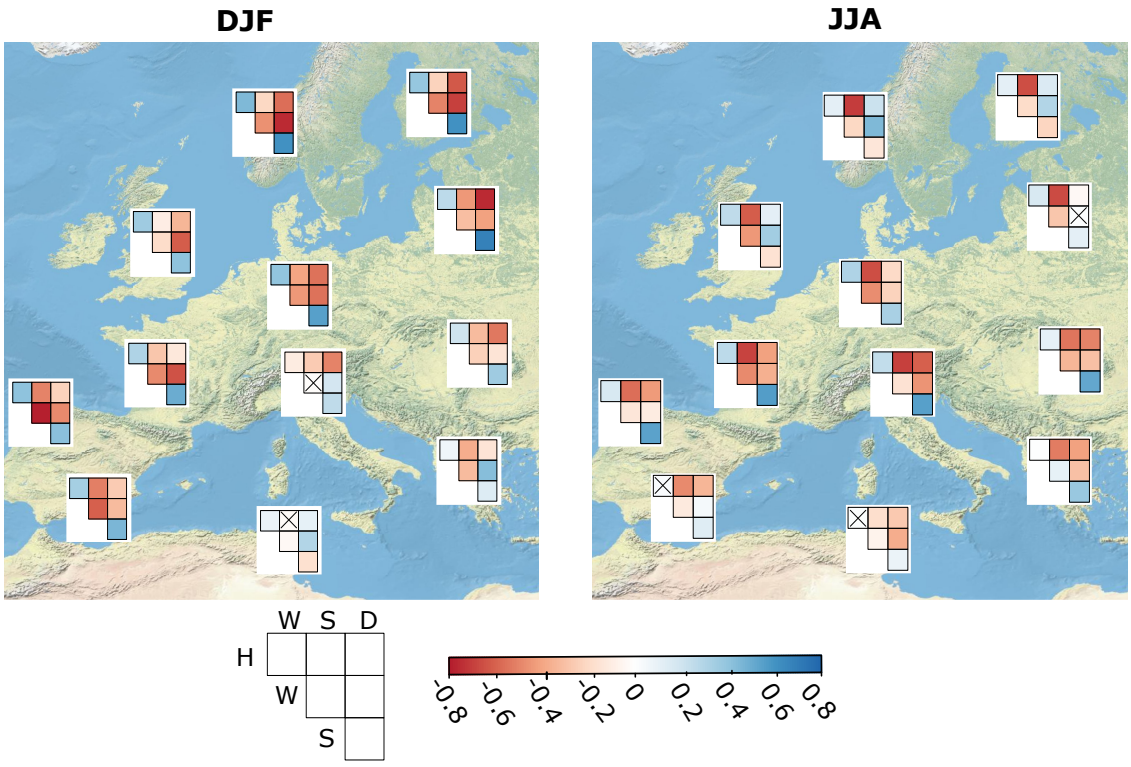

Figure III.4 – **Regional inter-energy sources and energy-demand Spearman correlation coefficients.** Non-significant correlation coefficients (95% confidence interval) are highlighted with a cross symbol.

We will consider all possible combinations of energy sources, testing all values of each sharing coefficient from 0 to 1. It includes the usual univariate options (e.g $s_{PV} = 1$, $s_W = s_H = 0$) but also the bivariate combinations (e.g $s_{PV} = 0.5$, $s_W = 0.5$, $s_H = 0$) and trivariate series (e.g $s_{PV} = 0.33$, $s_W = 0.33$, $s_H = 0.33$).

$$P_{mix}(t, s_{PV}, s_W, s_H) = s_{PV} \cdot p_{PV}(t) + s_W \cdot p_W(t) + s_H \cdot p_H(t) \tag{III.3}$$

Where

- $P_{mix}(t)$: Power production from the energy mix
- $p_i(t)$: Standardized production of energy source i
- s_i: Sharing coefficient of energy source i

Various indicators could be used to measure the relevance of all possible energy mixes. We use here the penetration rate defined previously (Eq.III.1). Comparing the P_{mix} series associated to all possible s_{PV}-s_W-s_H, the optimal sharing coefficients are the ones maximizing PE.

Here, we present the penetration rates of all possible energy mixes for the 12 European test regions. The optimal CRE combinations, regarding this criterion, and their associated penetration rates are also discussed. These results and figures are have been published in François et al., 2016 (Appendix.C).

First, Fig.III.5 illustrates, as an example, the penetration rates obtained with all possible CRE combinations in GA. The optimal mix is identified with a black dot. The three dash lines show how

to find the three sharing coefficients from the maximum penetration rate point. In the current case, it corresponds to $s_{PV} = 0.45$, $s_W = 0.1$ and $s_H = 0.45$. From this graph, the univariate penetration rates associated to the three energy sources can also be found at vertices. In GA, for instance, investing on hydro power seems to be the most relevant single-energy option. Finally, the triangle sides give the penetration rates of the bi-variate energy scenarios. For wind-solar power mixes for instance (i.e. $s_H = 0$), the best mix is reached combining 40% of wind power and 60% of solar power. In GA, the optimal bivariate mix is achieved for a hydro-wind power mix ($s_W = 0$, $s_H = 0.5$ and $s_W = 0.5$, bottom side).

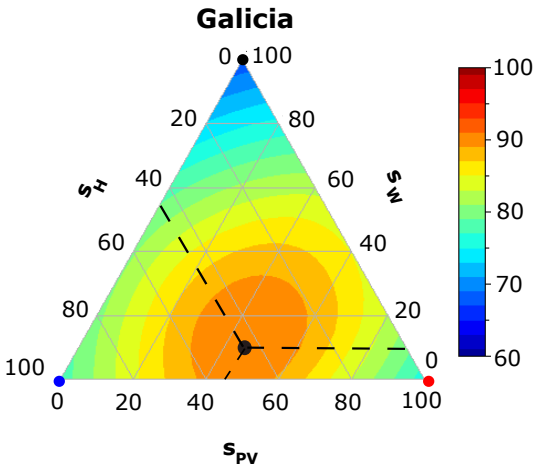

Figure III.5 – **CRE penetration rates (%) for all possible wind/solar/hydro power combinations in Galicia.** The energy production is supposed to be only based on CRE sources. The bottom axis gives the share of solar power (s_{PV} %), the left one the share of hydro power (s_H %), and the right one the share of wind power (s_W %). Red, black and blue bullets correspond respectively to a 100% solar, 100% wind and 100% hydro mix scenario. Horizontal gray lines show mixes with the same wind share. 60° increasing (resp. decreasing) gray lines shows mixes with the same solar power share (resp. hydro power share). The black dot corresponds to the optimal mix, i.e. the mix giving the highest penetration rate. The dash lines indicate the sharing coefficient of this optimal mix. Extracted and adapted from François et al., 2016

We discuss now the results for all 12 test areas and the inter-regional variability of the optimal energy mix. On Fig.III.14 are displayed the penetration rates of all energy sources combinations in Europe. Firstly, one can see that the maximum penetration rate is not constant across the continent. There is a NE-SW gradient with values going from 80% in FI to 90% in AN and 92% in GR. Similarly, the three sharing coefficients also vary in a logical way between regions. From the Mediterranean basin (GR, TU, AN) to western continental Europe (GA, FR, GE), hydro and solar power share most of the electricity production out and the contributions of wind turbines range only from 10 to 20%. Two regions, IT and RO, have a rather balanced distribution of power production between sources. In northernmost regions s_{PV} drops, reaching only 5% in BE. These low values of s_{PV} are balanced with higher hydro power contributions in BE, EN and FI. Finally, NO is the only region where s_W prevails over the other sharing coefficients. The optimal regional coefficients and their associated penetration rates are summed up in Tab.III.1. In the following study, they will be referred to as the "optimal mixes 1" (OM1). Many past studies focused on combining solar and wind power [Denault et al., 2009; Von Bremen, 2010]. The analysis performed by François et al., 2016 and presented here proved that introducing a third energy source (run-of-the-river hydro

power) significantly improves the penetration rate. Thus, regarding our evaluation criterion, a multi-sources integration of renewable energy in Europe leads to a more efficient energy supply system. It contributes to achieving a better synergy between energy generation and power load.

To further compare single sources, bi- and trivariate energy mixes, we will also evaluate the regional energy combination proposed by Von Bremen, 2010 and hereafter refered to as OM2. Based only on wind and solar power, this optimal energy share has been computed minimizing the variability of energy load residuals (load minus production) at the European scale. Gridded data of electricity production in Europe have been used in an unlimited cross-border power transmission context. In this configuration, the entire European continent has been considered as a whole, allowing also a spatial balance. The detailed methodology can be found in Von Bremen, 2010. We will use the best sharing coefficients corresponding to the optimised daily residual load (OM2): s_{PV}=0.6 and s_W=0.4. The associated penetration rates are presented in Tab.III.1. As expected, there are (from 1 to 8%) lower than for OM1.

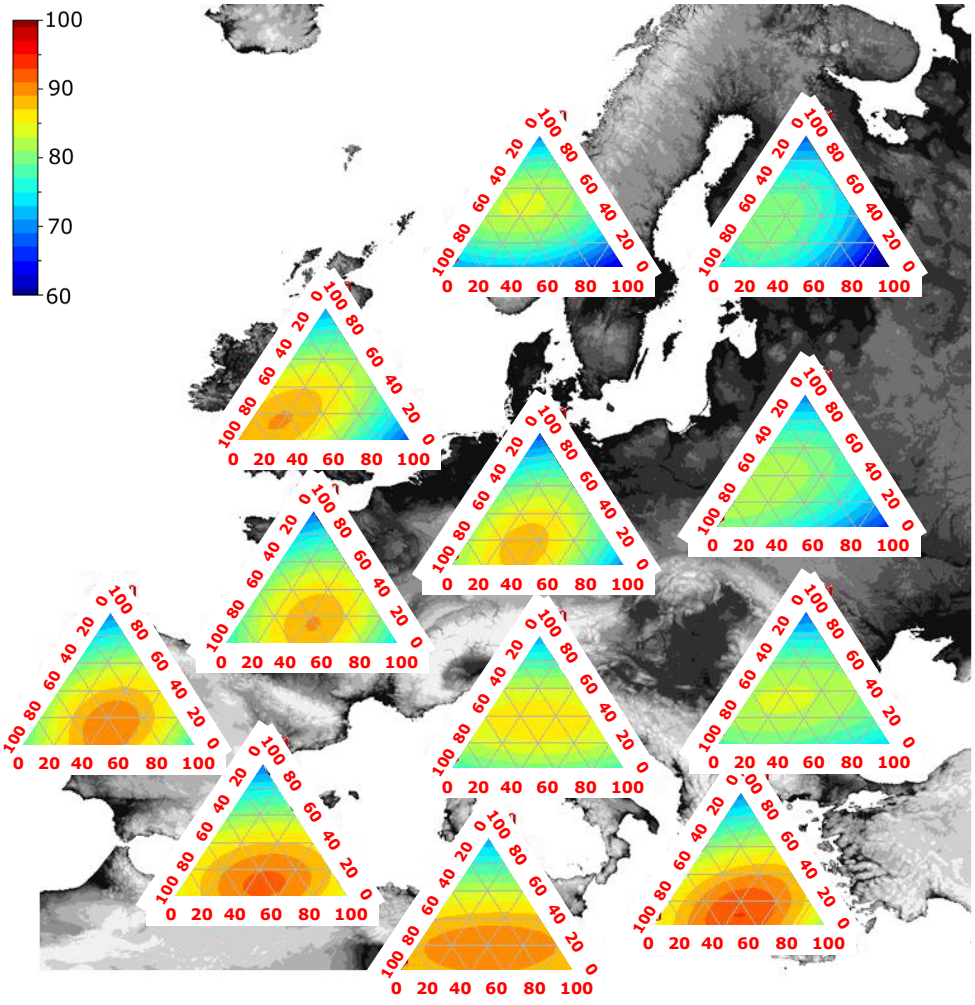

Figure III.6 – **CRE penetration rate (%) as a function of the wind/solar/hydro mix for all 12 European regions.** See Fig.III.5 for caption details. Extracted and adapted from François et al., 2016

Table III.1 – Optimal energy sharing coefficients and regional penetration rates (%) for OM1 (wind/solar/hydro and OM2 (wind/solar).

Region ID	**OM1**				**OM2**		
	s_{PV}	s_W	s_H	PE_{OM1}	s_{PV}	s_W	PE_{OM2}
EN	0.2	0.15	0.65	88	0.4	0.6	80
NO	0.15	0.50	0.35	82			78
FI	0.15	0.35	0.5	80			72
FR	0.45	0.15	0.4	88			83
GE	0.35	0.15	0.5	87			80
BE	0.05	0.3	0.65	82			76
GA	0.45	0.1	0.45	89			84
IT	0.3	0.35	0.35	85			84
RO	0.25	0.35	0.4	82			80
AN	0.5	0.1	0.4	90			86
TU	0.4	0.2	0.4	89			87
GR	0.45	0.1	0.45	92			87

2.3. Optimal mixes: Effects on energy droughts

The results presented in Sec.2.2 proved the relevance of combining multiple power sources to fulfil the energy demand. However, this "climatological" analysis does not account for the energy droughts defined previously.

To assess the effect of a multi-sources integration on energy droughts, Fig.III.7 shows for three representative regions and three of our droughts thresholds (100, 50 and 20%), the droughts characteristics of all single sources (hydro, wind and solar power) and mixes (OM1 and OM2). In addition to the mean duration and frequency of these droughts, the 10^{th} and 90^{th} percentiles provide information on the inter-annual variability.

The first significant result on this figure is that mixing energy sources has a positive effect on the most severe droughts. Indeed, the number and duration of severe droughts (SA $\leq$ 20%) are significantly lessened by the combinations of CRE sources. Droughts sequences become rare and short-lasting or even non-existent (AN - OM1). Considering the 50% SA threshold, OM1 leads to a slight reduction of both number and frequency of energy droughts for most regions. However, these improvements are less clear in Scandinavia (here NO). OM2 also gives weaker enhancements compared to OM1. Finally, the number of days for which the balance between energy load and electricity production is negative (100% threshold) remains unchanged, whatever the region. The duration and frequency of these underproduction periods depend on the regional sharing coefficients and are generally a compromise between the characteristics of all single sources involved in the energy mix.

The assessment of inter-annual variations of energy droughts is a key element to quantify the risks associated to renewable sources. Strong fluctuations from one year to the other could be hidden when considering only the mean characteristics. The moderate 10^{th}-90^{th} percentiles intervals for solar and wind power prove that these sources have a rather small inter-annual variability in droughts

characteristics. Conversely, following the strong inter-annual fluctuations of river discharge, droughts duration and number vary greatly for hydro power. Mixing energy sources, despite a reduction of mean droughts number and duration, does not necessarily result in a reduction of the inter-annual variability, especially when hydro-power comes into play (OM1).

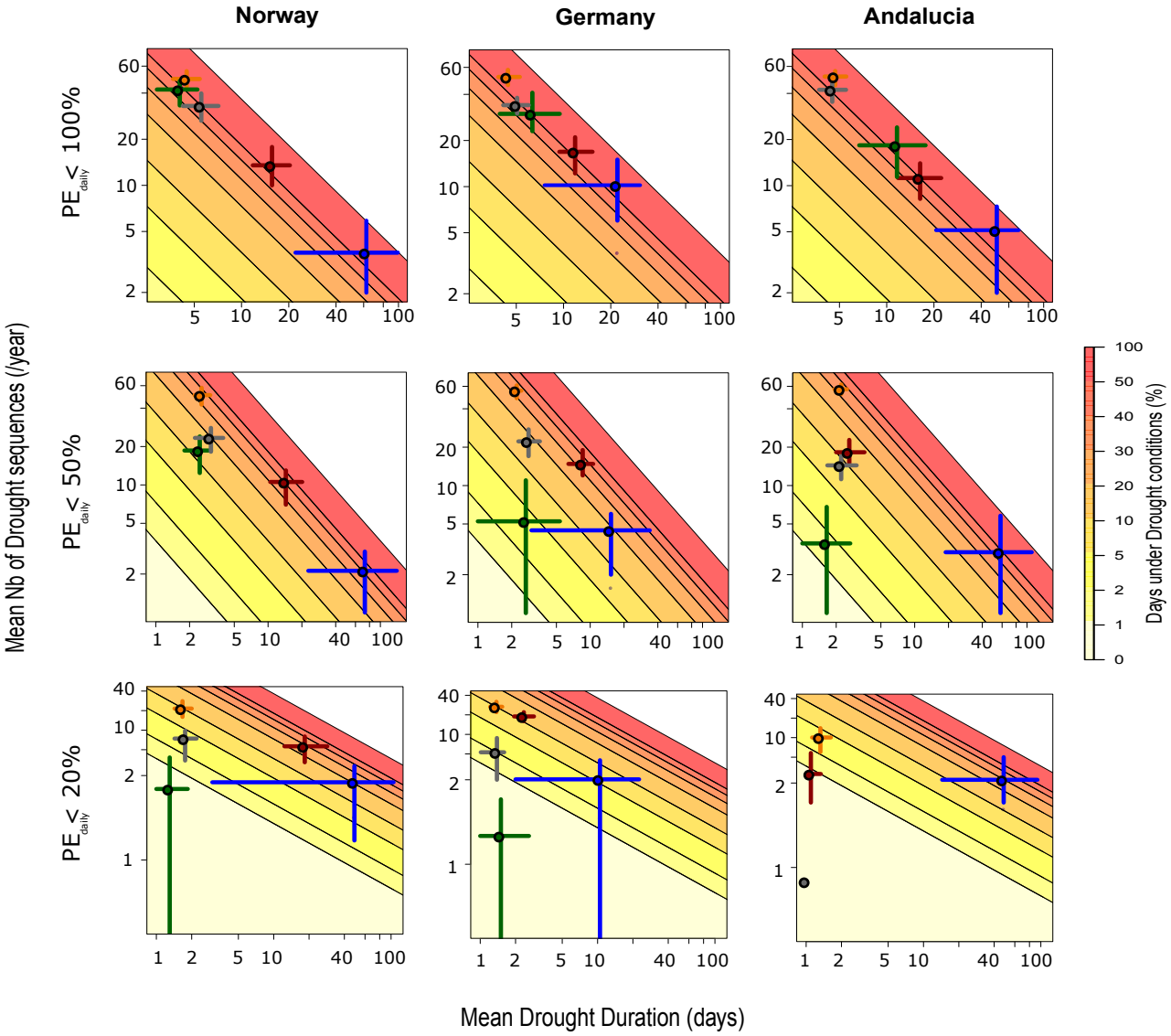

Figure III.7 – **Effect of using multi-sources on energy droughts.** Mean number of drought episodes versus mean drought duration associated to the 100, 80 and 50% SA thresholds. Results are displayed for hydro-power (blue), solar-power (red), wind-power (orange), OM1 (green) and OM2 (grey). The color scale gives the mean annual number of days under droughts conditions. The vertical and horizontal bars give the 10^{th} and 90^{th} percentiles of mean annual drought duration and number of drought sequences.

In addition to the mean and 10^{th}-90^{th} percentiles range, the annual maxima of droughts duration have been computed for all regions, sources and mixes. As an illustration, the associated results are presented (for NO, GE and AN) on Fig.III.8.

From a univariate point of view, the longest duration of hydro power droughts can change greatly from one year to the other, with differences exceeding 100 days in most regions. For solar power, the maximum annual drought duration seems to be mainly driven by day length. Consequently, it has a limited inter-annual variability. Finally, the mismatch between wind power and energy demand never exceeds two weeks and is relatively homogeneous in time and space.

The longest droughts associated to energy mixes are generally shorter than the ones of single CRE sources. OM1 often gives the best results but its inter-annual variability is rather high.

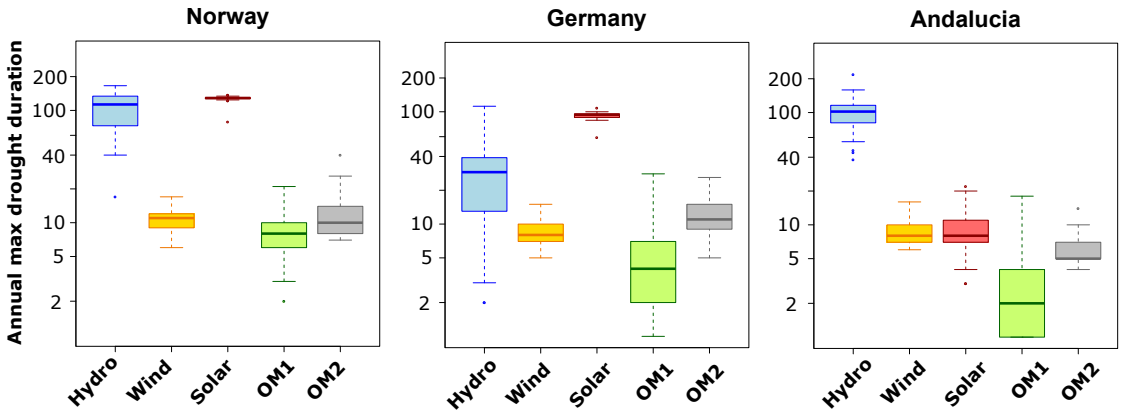

Figure III.8 – **Boxplot of annual maximum drought duration (days) in NO, GE and AN.** Results are displayed for hydro-power (blue), solar-power (red), wind-power (orange), OM1 (green) and OM2 (grey).

3. Spatial integration

As a second method to combine renewables in Europe, we will now assess how a spatial integration can help building a more reliable energy supply system.

Similarly to what has been presented for the multi-source approach, we will first use inter-region correlations to highlight some possible complementarity. Subsequently, we will evaluate the effects of a spatial integration on both penetration rates and energy droughts.

3.1. Inter-regions correlations

3.1.1. Seasonal correlation coefficients

As a consequence of the natural spatial variations of climate, electricity production series from non-neighbouring regions could complement one another. Firstly, using univariate inter-regions correlation coefficients of seasonal series, we coarsely evaluate the spatial synchronism of energy sources within Europe. Results are presented on Fig.III.9 for winter and summer seasons separately. For each sub-plot, the arrangement of regions is optimised in order to cluster correlation coefficients of the same sign.

- Winter
  Only a few regions couples show anti-correlated hydro power series in winter. Nonetheless, high levels of seasonal production in Scandinavian regions (FI and NO) could balance low ones in souther Europe (AN-GR-GA and GR-GA-RO-FR). GA and GE but also BE and AN also seem complementary.
  Winter wind power generation is more region-dependent, leading to numerous anti-correlated couples of regions. NO, GA, and AN are all involved in 5 possible regional combinations and thus could balance seasons of low productions from many of other regions. GR and FI also

take part in 4 anti-correlated region couples.
12 combinations of regions have a significant anti-correlation in winter solar power generation. GR and NO are brought to the forefront once again with respectively 5 and 4 negative correlations.
Considering energy load, most European regions are significantly correlated and no relevant combination of region can be established.

- Summer
  The number of significant positive or negative correlation coefficients drops in summer. It is more difficult to find a seasonal balance between regions. Only two couples are slightly anti-correlated for summer hydro power: AN-EN and TU-EN. It is pretty much the same for wind power with only NO being negatively correlated with FR and GE, or EN and GR balancing each other. More possible combinations of regions exit for solar power. They generally bring face to face one northern region (NO, FI or BE) with a Mediterranean one (TU, AN, IT).
  Contrary to what has been said in winter, some significant inter-regions anti-correlation coefficients can be found for summer energy load. Almost all the associated combinations involve the electricity demand in EN which is negatively correlated to TU, AN, IT, FR and GA.

3.1.2. Combining regions

These results suggest that groups of regional energy generation or load series, with on one hand significant intra-group correlations, and on the other hand significant inter-groups anti-correlation, exist in Europe. Such groups of regions would present an attractive complementarity and would make the integration of CRE sources easier.

Some conceivable options are presented on Fig.III.9, on maps highlighting two possible complementary groups of regions. These combinations have been built with a simple automatic stepwise algorithm which uses the inter-regional correlation coefficients discussed previously to construct 2 complementary groups of regions as large as possible. The process abides to the following rules:

- It considers successively each couple of region from the highest anti-correlation coefficient to the lowest.
- The highest anti-correlation determines to starting point of the process and thus, the first member of each group.
- The integration of an additional couple of regions is validated if there is a configuration for which each region is:
  - In its own group:
    i. correlated or non-significantly correlated with the other regions
  - In its complementary group:
    i. anti-correlated with at least one region
    ii. anti-correlated or non-significantly correlated with all the others

The groups sizes and the regions making them up are very uneven from one energy source to the other and also change from winter to summer. The most interesting results are for winter hydro and solar power which involve respectively 8 and 9 regions and have balanced groups. In any other case,

the total number of regions is much smaller (Hydro and wind power, JJA) or else there is a strong disequilibrium between the sizes of the two groups (Wind power, DJF ; energy demand JJA). It should be noted that, due to the restrictive requirement of the stepwise construction, not all couples showing anti-correlated series are included. Considering the summer energy load for instance, GE has been excluded, despite its anti-correlation with AN, due to its positive correlation with IT, FR and GA.

The previous analysis confirmed that a balance between renewables can be found using the partial complementarity between European regions at seasonal time scale. However, it is necessary to go further and assess the impact of this spatial integration on penetration rates and energy droughts.

3.2. Spatial aggregation: Functionning and penetration rate

Integrating the whole European continent in a single energy supply system would likely increase the production/load match and thus lower the frequency and duration of energy droughts. We now explore here these possible improvements.

We use a European energy mix gathering the electricity production and energy load from all 12 regions. We assume that there is no power loss due to energy transmission from one region to the other. This simple "copper plate" hypothesis has already been used in some previous works such as in Von Bremen, 2010. Eq.III.4 presents how the European power integration was performed. The 12 regional power and energy load time series, used in the previous sections (i.e all normalised to 1), are simply summed up. The European production and load time series are then used to calculate both PE and SA as following:

$$PE_{Euro} \quad = \quad (1 - \frac{\sum max(D_{Euro}(t) - p_{i,Euro}(t), 0)}{\sum D_{Euro}(t)}) \cdot 100$$

Where

- PE_{Euro}: European penetration rate of energy source i
- $D_{Euro}(t) = \sum_{Europe}^{Europe} D(t)$: European energy load
- $p_{i,Euro}(t) = \sum_{Europe} p_i(t)$: European power production with energy source i

A comparison between the PE rates of independent regions (average of 12 regional PE rates) and of the "European copper plate" is presented in Tab.III.2. For all energy sources and mixes, using the complementarity between regions improves the match between production and load. However the magnitude of these changes is uneven from one source to the other. Solar power does not benefit much from the spatial integration. This variable suffers from a strong spatial synchronism of low production periods which are mainly driven by day length. Hydro power, wind power and OM1 exhibit a large improvement of their penetration rates (+8%). It now reaches 94% for OM1, proving the efficiency of both multi-sources and spatial integration to build a reliable energy supply system. The PE rate of OM2 has also been increased but only by 5% due to the large proportion of solar power in this mix.

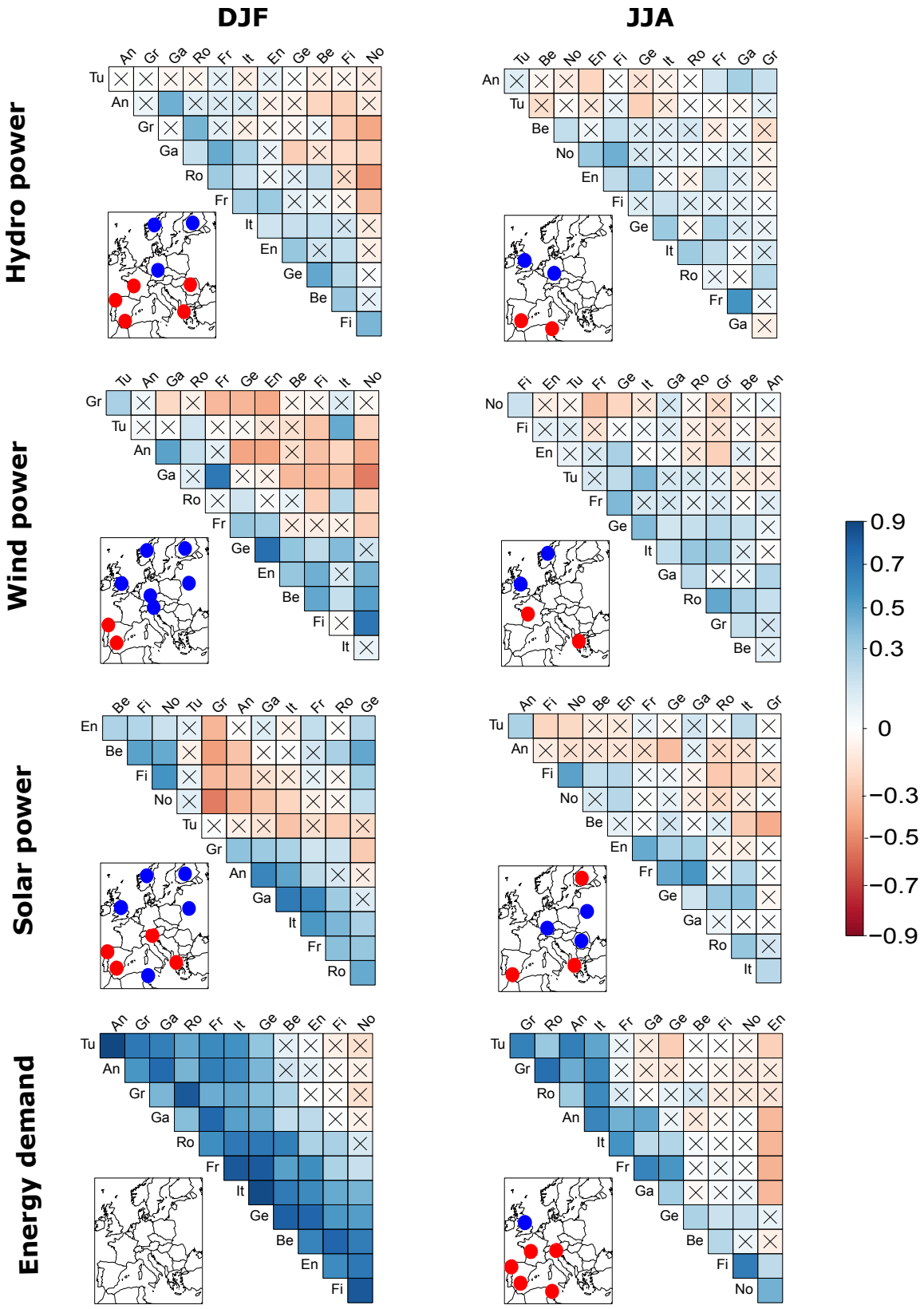

Figure III.9 – **Inter-regions correlation coefficients for the three CRE sources and energy demand.** Non-significant correlation coefficients (95% confidence interval) are highlighted with the cross symbol.

Table III.2 – Penetration rate (PE) at a European scale considering independent regions (average of the 12 regional PE) and an European perfect grid. Results are presented for all energy sources and mixes.

Energy source	PE (%) - Independent regions	PE (%) - European grid
Hydro	73	91
Wind	69	87
Solar	73	74
OM1	86	94
OM2	81	87

3.3. Spatial aggregation: Effects on energy droughts

On Fig.III.10 are presented the droughts characteristics of both regional and European series associated to the 50% SA threshold for all energy sources and mixes.

- There are rather few regional hydro power droughts but their durations range from 15 to 80 days on average. Integrating at a European scale greatly reduces the mean drought duration to a week. The number of occurrence also drops to one sequence per year.
- Wind power droughts have very similar characteristics from one region to the other with about 50 2-day long episodes per year. The spatial integration helps to balance the European energy load and leads to much fewer droughts episodes ($\simeq 10$).
- Spatially integrating solar power production reduces the number of energy droughts. However, the remaining ones are long lasting and their mean duration exceed a month. In most European regions, energy droughts occur in winter and are driven by day length. Logically, they are mostly synchronised. Southern regions (AN, TU, GR), which have a moderate day length annual cycle, are not able to balance the low solar power production in northern Europe.
- Considering the energy mix OM2, gathering both solar and wind power at a European scale moderately improves the droughts attributes.
- Including also hydro power (OM1), leads to very short and rare drought episodes. Their frequency drops to 0.1, meaning that several years can flow by between two drought sequences. This very last result proves that the more integrated electricity production series are (i.e multi-variate and at a European scale), the better for reducing the drought hazard.

In conclusion, these results demonstrate the efficiency of the spatial integration to increase PE and limit the risks associated to energy droughts. For all sources and mixes (except solar power) all the evaluation criteria are improved. The ones of OM1, which rely on all energy sources (hydro/wind/solar), are particularly satisfactory, encouraging to use both methods of integration, spatial and multi-sources.

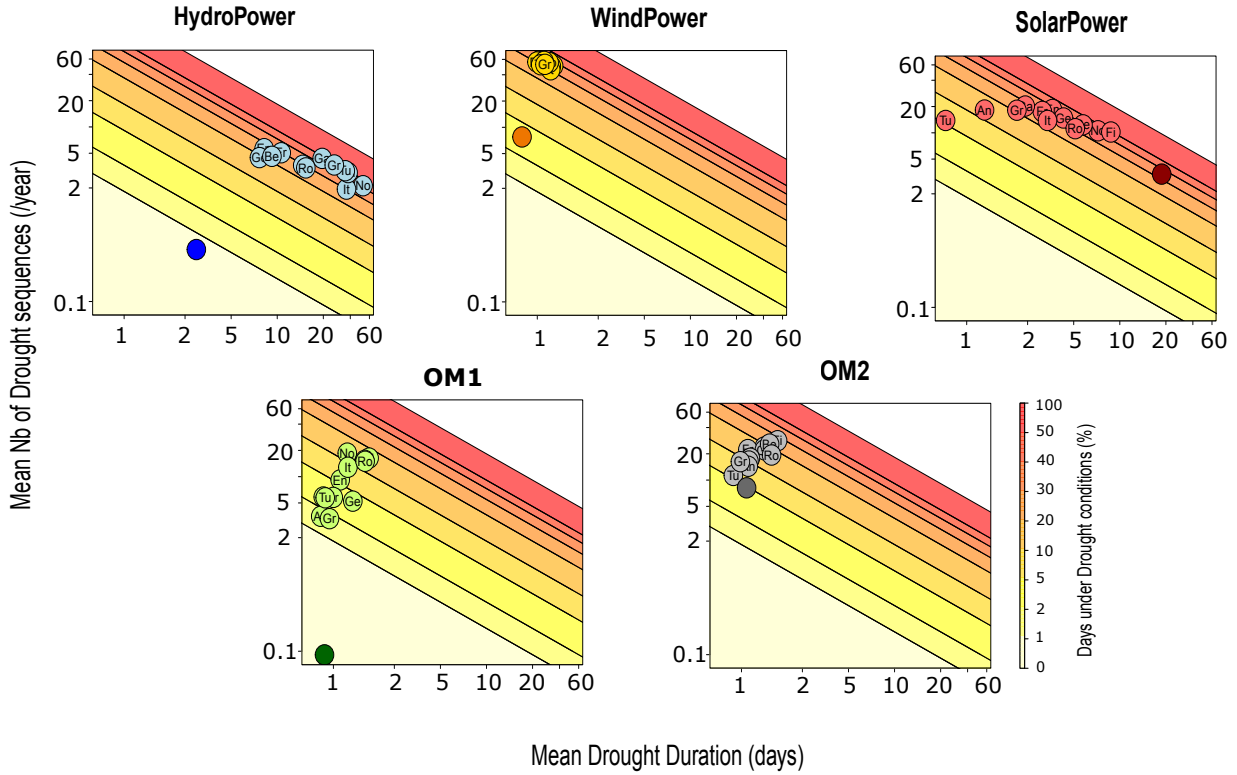

Figure III.10 – **Effect of a spatial integration on drought characteristics.** Mean number of drought episodes versus mean drought duration associated to the 50% SA rate threshold. Results are displayed for hydro-power (blue), solar-power (red), wind-power (orange), OM1 (green) and OM2 (grey). The color scale gives the mean annual number of days under droughts conditions. Light colors correspond to regional droughts while dark ones are associated to European droughts.

4. Storage

4.1. Functioning ans penetration rates

The intermittence of CRE sources and the mismatch that exists between them and energy load either leads to over or underproduction. Storage systems, such as water reservoirs (for hydro power) and batteries, are another option to balance low production values with the energy surplus from previous days. As mentioned in Chap.I, many past studies explored this option for the integration of renewables. In this subsection, we assess the effects of energy storage on the penetration rates of all energy sources and mixes. We will also focus on energy droughts and on the possible lowering of their mean frequency and duration.

We consider 4 different storage systems with different storage capacities corresponding respectively to 1, 7, 30 and 90 days of mean energy load (Eq.III.4.a). The energy transfer from and toward the storage system is done on a daily basis. Depending on both current electricity production and energy load, the storage system either fills up or runs out (Eq.III.4.c). When necessary and possible, it supports the daily power generation and helps to meet the daily energy load (Eq.III.4.d).

(a) $$S_{max} = \lambda \cdot \langle D(t) \rangle$$

(b) $$\Delta(t) = P_i(t) - D(t)$$

(c) $$\mathrm{S(t)} = \begin{cases} min(S(t-1) + \Delta(t),\ S_{max}) & \text{if } \Delta(t) > 0 \\ max(S(t-1) + \Delta(t)),\ 0) & \text{if } \Delta(t) < 0 \end{cases}$$

(d) $$\mathrm{SA(t)} = \begin{cases} 1 & \text{if } \Delta(t) > 0 \\ 1 & \text{if } \Delta(t) < S(t-1) \\ 1 - \frac{\Delta(t) + S(t-1)}{D(t)} & \text{if } \Delta(t) > S(t-1) \end{cases} \quad \text{(III.4)}$$

Where

- $D(t)$: Daily energy load
- $\langle D(t) \rangle$: Mean daily energy load from 1983 to 2012
- $\lambda \in \{1, 7, 30, 90\}$: dimensioning
- $P_i(t)$: Daily energy generation
- $\Delta(t)$: Power mismatch
- $S(t)$: Storage level
- S_{Max}: Maximum storage capacity
- $SA(t)$: Daily satisfaction rate

The changes in PE using storage systems of different sizes are presented on Fig.III.11. Note that these simplified systems do not account for the energy loss due their limited technical efficiency.

Both solar and hydro power are weakly sensible to small storage capacities (1 and 7 days). It is only using a 30-day or 90-day based storage that a large increase in penetration rate is noticeable. This result is consistent with the previous analysis revealing that PE has a strong seasonality for both hydro and solar power. In southern regions (AN, TU, IT, GR) a solar based energy supply paired with a large storage capacity (90-day) achieves penetration rates close to 100%. On the other hand, 90% PE rates are barely reached with a seasonal storage of hydro power in Scandinavia and in the Mediterranean basin.

Wind power penetration rates increase quickly and from the daily-based storage capacity. PE values greater than 90% are already reached with a 7-day based storage system. The seasonal storage gives an almost perfect match between energy generation and energy load.

OM1 and OM2 had much higher global penetration rates than single energy sources when no storage was used. Logically, the increase in PE due to the introduction some storage is more gradual. However it still leads to PE values close to 100% for a seasonal capacity. In some regions (FI, BE,

RO), when a weekly to a seasonal storage capacity is used, it is also interesting to note that the single wind power source gives better penetration rates than OM1 and OM2.

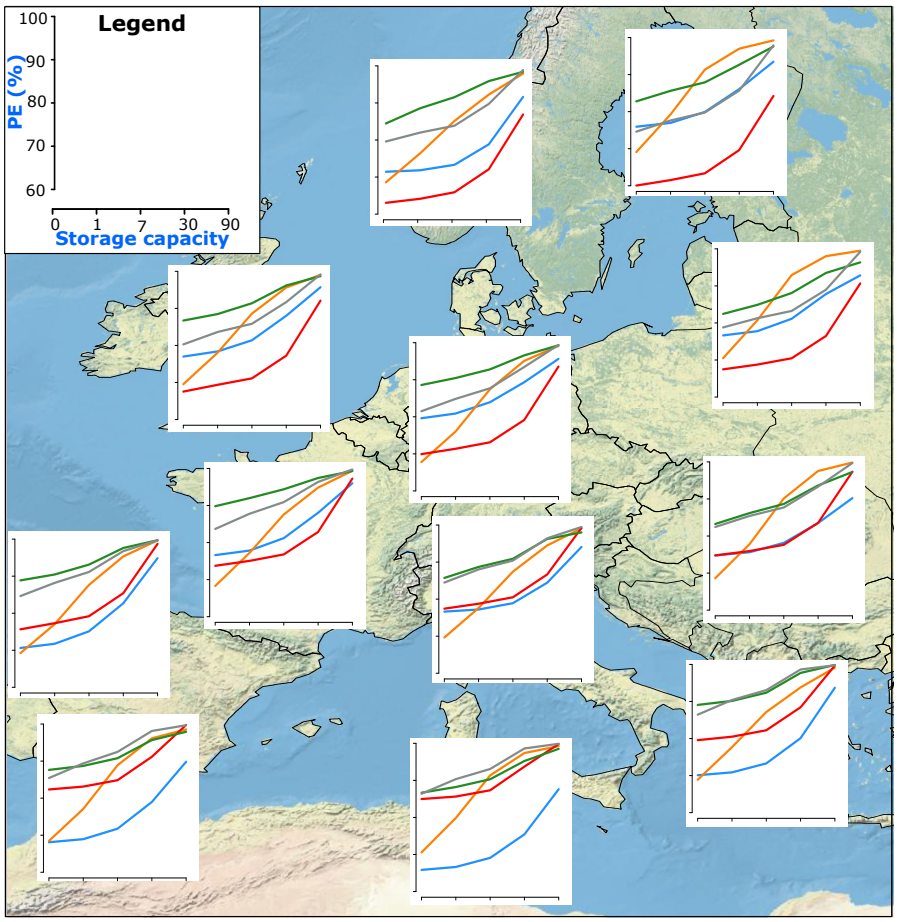

Figure III.11 – **Effects of storage on global penetration rate.** Results are displayed for hydro-power (blue), solar-power (red), wind-power (orange), OM1 (green) OM2 (grey). The storage capacity varies from 0 to 90-day (cf. Eq.III.4).

4.2. Storage: Effects on energy droughts

Fig.III.12 presents the effect of storage on the energy droughts attributes.

In most regions, hydro power droughts are persistent. Small size storage systems do not lead to a significantly reduction of droughts severity. Nevertheless, the seasonal based size ($\lambda = 90$) is more efficient and lowers both duration and number of drought sequences. The same comments can be made about solar power. However, regions in northern Europe still suffer from long and numerous solar power droughts even with large storage systems. Conversely, these critical periods are almost all removed in IT, AN, TU and GR.

For all three wind power, OM1 and OM2, storage systems help reducing the number of drought episodes. Only a few of them remain with $\lambda = 90$. When large storage are involved, results are very similar for OM1 and the univariate solar or wind power sources (FI, BE, RO, AN, TU). The hydro power contributions in the tri-variate energy mixes slightly limit the positive effects of storage systems for OM1.

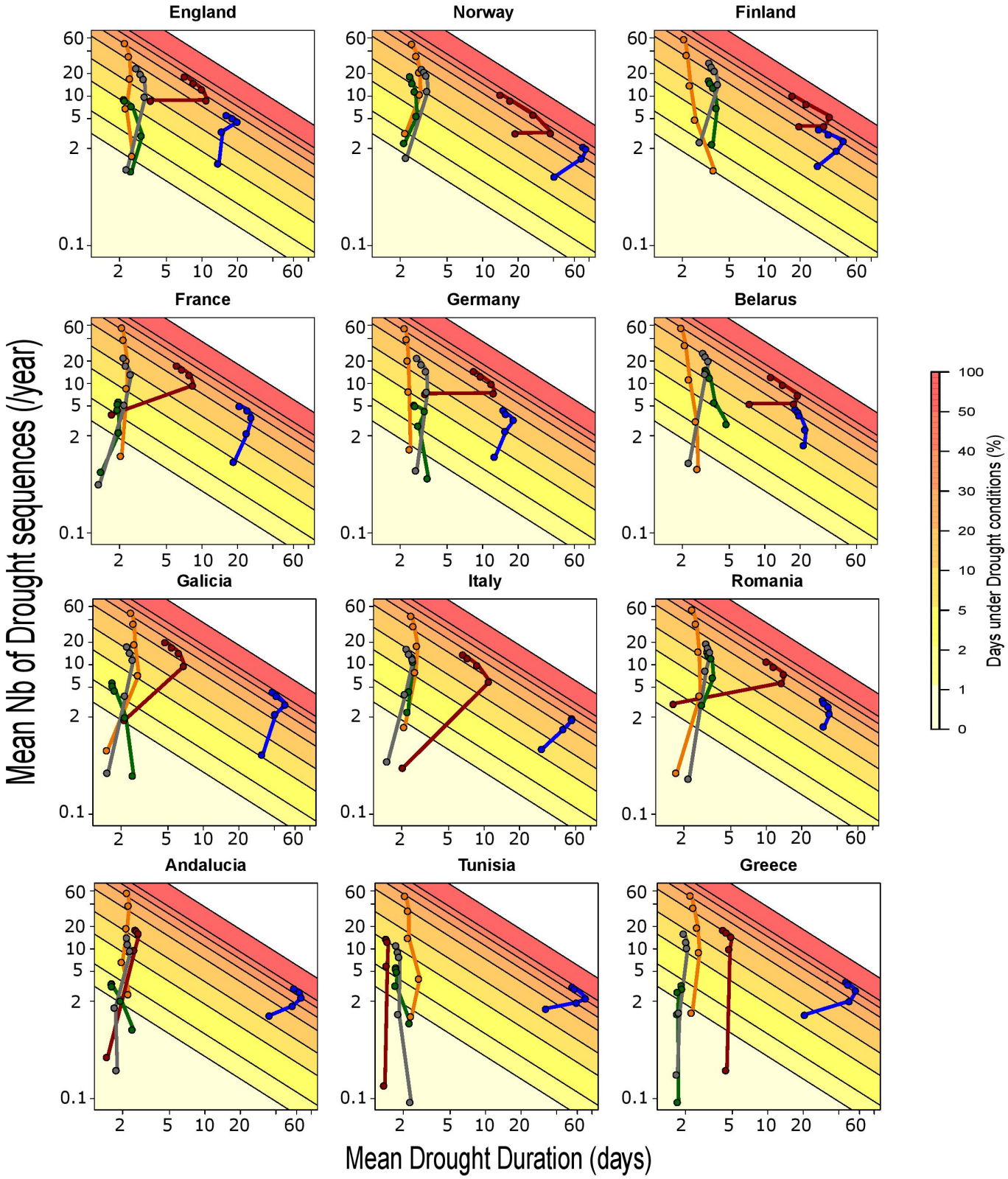

Figure III.12 – **Effect of storage on droughts characteristics.** Mean number of drought episodes versus mean drought duration associated to the 50% SA threshold. Results are displayed for hydro-power (blue), solar-power (red), wind-power (orange), optimal mix (green) and wind-solar European mix (grey). The points associated to the same energy source but to different storage capacities have been connected in a logical order from from $\lambda = 1$ to $\lambda = 90$. The color scale gives the mean annual number of days under droughts conditions.

5. Over-sizing

5.1. Functioning ans penetration rates

Previously, we performed a standardization of the electricity production series considering a balance between mean production and mean energy load over the 1983-2012 period. Hence, we implicitly chose and fixed the power plants dimensions. Deliberately over-sizing the power stations is another option that can be used to increase the penetration rate of CREs and reduce the duration and number of drought sequences.

Eq.III.5 shows how the penetration rate computation is modified when changing the size of power plants. The μ coefficient varies from 1 (no over-sizing) to 2 (double power production).

$$PE = (1 - \frac{\sum max(D(t) - \mu \cdot p_i(t), 0)}{\sum D(t)}) \cdot 100 \tag{III.5}$$

Where

- $PE(t)$: Penetration rate of the energy source i
- $D(t)$: Energy load
- $\mu \in \{1,\ 1.1,\ 1.2,\ 1.5,\ 2\}$: Over-sizing coefficient
- $p_i(t)$: Standardized power production with energy source i

The penetration rates associated to the different over-sizing coefficients are presented on Fig.III.13 for all regions, all energy sources and mixes. Generally speaking, the increase in PE is gradual and very similar for all energy sources/mixes. Doubling the equipment size leads to 15% higher penetration rates. The ranking between sources is usually not changed. The highest PE values are always found for OM1 and exceed 95%. It should be noted that, for $\mu > 1.2$, the penetration rates associated to wind power often increase more rapidly than with the other energy sources (GA, AN, IT, TU, NO and GR).

5.2. Oversizing: Effects on energy droughts

Hydro power droughts are very faintly sensitive to the power plant size. Even for $\mu = 2$, neither the mean duration nor the number of droughts are significantly lowered. Low SA periods appear to be severe and associated to very low daily SA values that cannot be balanced by adding more power conversion equipments. Similarly, solar power droughts are weakly modified by larger power plants in the most northern regions (EN, NO, FI and BE). However, their mean duration is lowered with large equipments ($\mu \geq 1.5$) in central and western Europe. Their numbers drop for Mediterranean regions. Low SA periods associated to wind power are rather brief. Thus, increasing the number of wind turbines mainly impacts the number of droughts. This effect is more noteworthy for southern regions. Finally, combining CRE sources on one hand and over-sizing their associated power plants

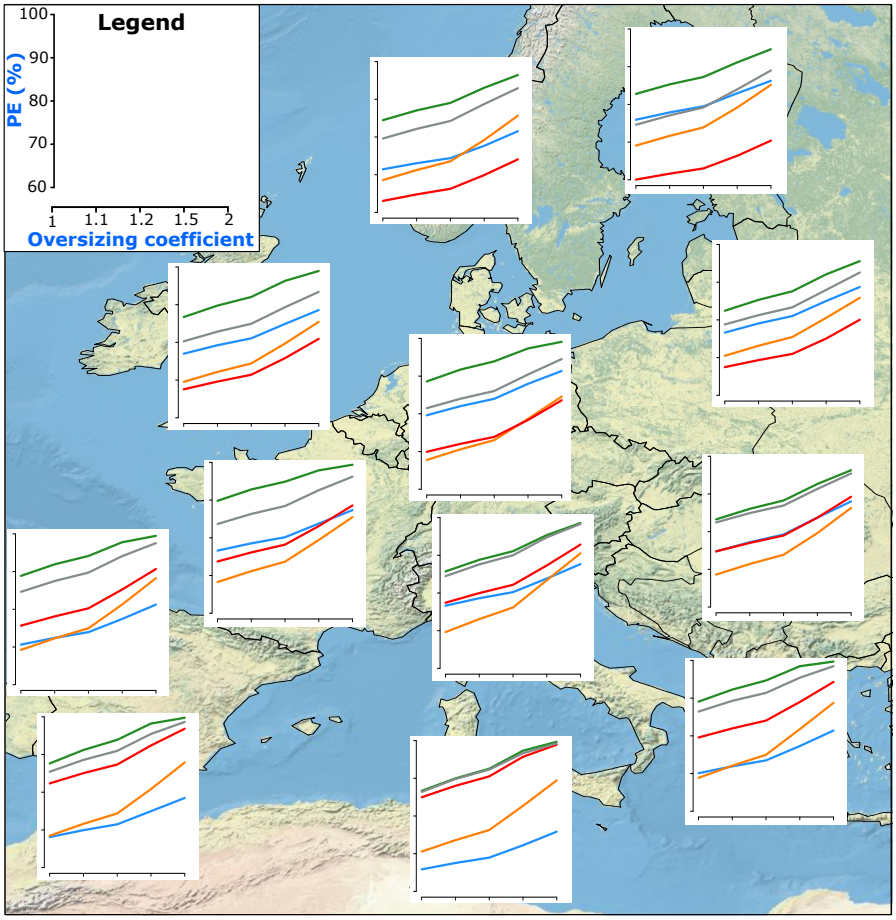

Figure III.13 – **Effect of over-sizing on penetration rate.** Results are displayed for hydro-power (blue), solar-power (red), wind-power (orange), OM1 (green) OM2 (grey). The over-sizing coefficient varies from 1 to 2 based (cf. Eq.III.5).

on the other hand, efficiently lowers the number of energy droughts. The tri-variate mix (OM1) is again the best choice for limiting low SA periods.

All in all, this assessment of the contribution of over-sized power plant to a more reliable integration of renewables in Europe showed that it is a rather efficient tool. However, it is necessary to increase by 50 to 100% the equipment size to reach significant improvements of both penetration rates and energy droughts characteristics. Even so, for some variables, over-sizing fails to reduce both frequency and duration of energy droughts (Hydro power ; solar power - EN-NO-FI-BE). It is only when combined with a multi-sources approach that most of these problematic periods are counterbalanced.

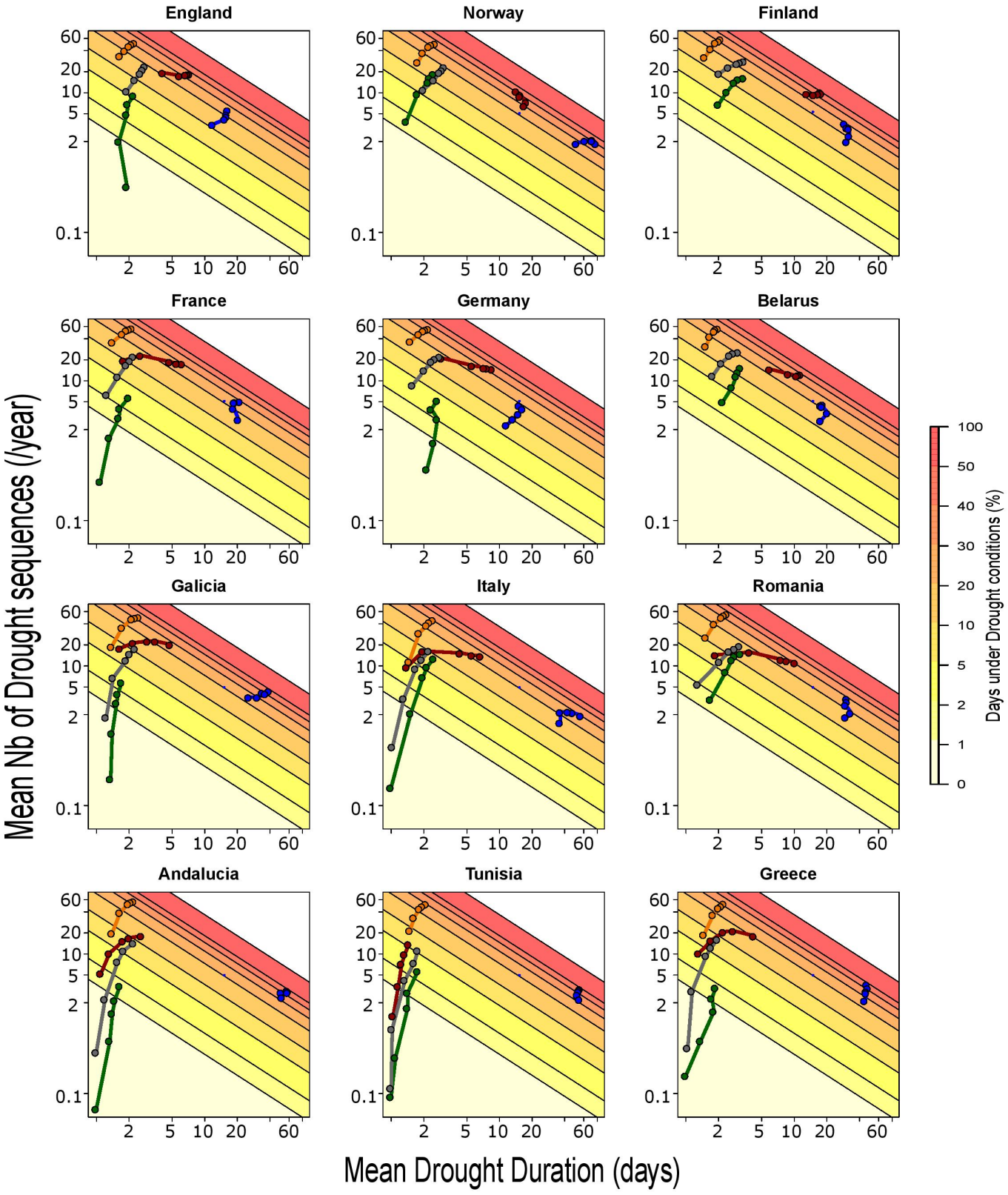

Figure III.14 – **Effects of over-sizing on energy droughts characteristics.** Mean number of drought episodes versus mean drought duration associated to the 50% SA threshold. Results are displayed for hydro-power (blue), solar-power (red), wind-power (orange), optimal mix (green) and wind-solar European mix (grey). The points associated to different oversized power plant but from the same energy source have been connected in a logical order from $\mu = 1$ to $\mu = 1.5$. The color scale gives the mean annual number of days under drought conditions.

Overview

In the two previous chapters, we presented the components and analysed the outputs of a suite of models simulating CRE power production from weather observations (wind solar and RoR hydro power). Combining an hydrological model, weather-energy and temperature-load conversion models, it simulates the spatio-temporal fluctuations of electricity production and energy load resulting from the hydro-climatic variability. Based on these simulations, we explore for 12 European regions how several integration methods could take advantage of this spatio-temporal variability.

Hydro-climatic and renewables variability in Europe

The analysis of meteorological data, issued from gridded observations (temperature, precipitation, sun radiation) or reanalysis from regional dynamic models (wind speed), highlighted the strong spatial and temporal fluctuations of the CRE meteorological drivers.
These important variations are logically transmitted to the associated CRE sources. All time scales (from daily to inter-annual periods) are impacted and there are also some large disparities between European regions. These results suggest that some integration factors should be used to improve the ability of CRE sources to meet the energy demand.

The integration of renewables

We used two criteria to evaluate the energy supply-load match and the possible improvements obtained with a selection of integration methods. First, we considered the penetration rate (PE) which quantifies the global proportion of satisfied energy demand. Then, we introduced the concept of energy droughts, defined as a sequence of one or several consecutive days for which the percentage of daily satisfied load is lower than a given threshold. The frequency and duration of these problematic sequences were compared for all CRE sources and integration options. These analyses led to the following conclusions:

- Hydro and solar power give uneven and region-dependent penetration rates in Europe, ranging from less than 60% to more than 80%. Their associated energy droughts are long lasting, especially for hydro power and have strong seasonal and inter-annual variations.
- Wind power penetration rates are very similar between regions but limited (75%). The energy droughts related to this source last less than a week but are also particularly numerous. Wind power is weakly sensible to seasonal and inter-annual fluctuations.
- Combining CRE sources considerably improves the penetration rate. The regional PE values associated to the optimal mix range from 80 to 92% and are significantly higher than for single sources. The proportion of each energy source in the optimal mix changes a lot from one region to the other, with a larger contributions of solar power in the Mediterranean basin and of hydro power in northern and central Europe. However, it must be emphasised that the energy mix only accounts for the temporal adequacy between electricity production and energy load and not for the absolute resources in CRE. A multi-sources mix greatly reduces both number and duration of the most severe energy droughts ($SA < 50\%$)

- Integrating CRE sources and energy load at a European scale increases the global penetration rate by 8% for hydro power, wind power and OM1 (3-sources mix). It has weak effects on solar power and OM2 (solar-wind mix) due to a strong seasonality and spatial synchronism of solar radiation at a continental scale.
- Storage systems can contribute to a more reliable renewable integration. However, large storage capacities (up to 3 months of mean daily load) are required if one wants to balance the strong seasonality in both PE and energy droughts of hydro and solar power.
- Deliberately over-sizing regional power plants to balance the intermittence of CRE sources gives moderate and gradual improvements in penetration rate. It does not lead to a reduction of the duration and frequency of energy droughts, except if this method is combined with an energy mix approach.

Part III

MULTI-VARIATE ANALOGUE DOWNSCALING: DEVELOPMENT AND EVALUATION

Chapter IV

Downscaling methods

Since the development of numerical weather prediction models (NWP), global circulation models (GCM) and climate reanalysis datasets, downscaling methods have been used to bridge the gap between large scale and regional weather conditions. Indeed, the low spatial/temporal resolution and the coarse surface topography of some climate models, prevent them from solving explicitly small scale processes such as convection. As a consequence of these limitations, large biases often exist in the models outputs. Thermodynamic variables such as precipitation and cloud cover are particularly affected, as they result from complex and fine-scale processes. For most impact studies, information about local weather conditions is required to drive other models (e.g hydrological models, energy conversion models) or to taking into account the small scale variations of meteorological parameters.

All downscaling methods assume that synoptic meteorology affects regional conditions and use this strong interdependence to predict local meteorological parameters. These methods can be used to perform a temporal downscaling (going from daily to hourly data for instance) or a spatial one (determining the weather at a specific station or increasing the spatial resolution over a limited area).

In this chapter, we present the main hypothesis and the functioning of the most classic downscaling methods, either dynamical or statistical. We will particularly focus on the analogue method which has been selected for the purpose of this thesis.

1. Dynamical downscaling

Dynamical downscaling consists in using Regional Climate Models (RCMs) over a limited area. RCM have a much higher resolution (classically raging from 10 to 50km) than GCMs and are consequently able to reproduce smaller scale phenomena. Fig.IV.1 illustrates how a RCM is nested within the global model grid. For non-spectral regional models, only a few large scale cells are used to force its simulations at the domain boundaries. In the inner part, no synoptic information is assimilated and the model is entirely free.

The main advantage of using RCMs for weather and climate downscaling is that it gives spatially and temporally consistent information. RCMs simulations are based on physics equations for synoptic and larger scale phenomenon. However, these models still include a large number of parametrisations to take on board micro-scale and some meso-scale processes. They can still suffer from relatively large biases and often need to be calibrated and/or post-processed (e.g. bias correction) so that their outputs can be used in impact studies (e.g. in Hagemann et al., 2011; Teutschbein and Seibert, 2012). Dynamically downscaled climate reanalysis datasets and future scenarios from GCM also require large computing resources. Despite the wide range of possibilities offered by clusters and computing grids, the large number of GCMs, members and Representative Concentration Pathways (RCPs) still makes running an RCM with all possible forcing data a demanding task.

Dynamical downscaling has been widely developed and used in past decades either from individual initiatives or as part of collaborative projects. In a climate change framework, the PRUDENCE project (Prediction of Regional scenarios and Uncertainties for Defining EuropeaN Climate change risk and Effects) was the first collaboration that aimed to produce high resolution scenarios from GCM data over Europe. The ENSEMBLE project (ENSEMBLE-based predictions of climate change and their impacts) took over from 2004 to 2009. It aimed to "help inform researchers, decision makers, businesses and the public by providing them with climate information obtained through the use of the latest climate modelling and analysis tools". The multi-model approach used in this project also enabled the assessment uncertainty regarding climate scenarios. The outcomes of the project have been published in a large number of specific international publications [Déqué et al., 2005; Christensen and Christensen, 2007; Blenkinsop and Fowler, 2007; Boberg et al., 2009] and in a final report [Linden, 2009]. The European branch of the CORDEX project (COordinated Regional climate Downscaling EXperiment), supports the development of numerous downscaled climate scenarios using 10 different RCMs and a large variety of GCMs and RCPs as input data. Simulations are performed at 0.11°or 0.44° resolution for a domain covering the entire European continent and the Mediterranean basin. The production of regional scenarios in the frame of EURO-CORDEX is still ongoing but many of them are already available for use or presented in publications [Jacob et al., 2014; Kotlarski et al., 2014].

2. Statistical methods

As an alternative to dynamical downscaling, statistical approaches have been widely used in recent years. Despite the initial effort that has to be made for their construction, they allow users to

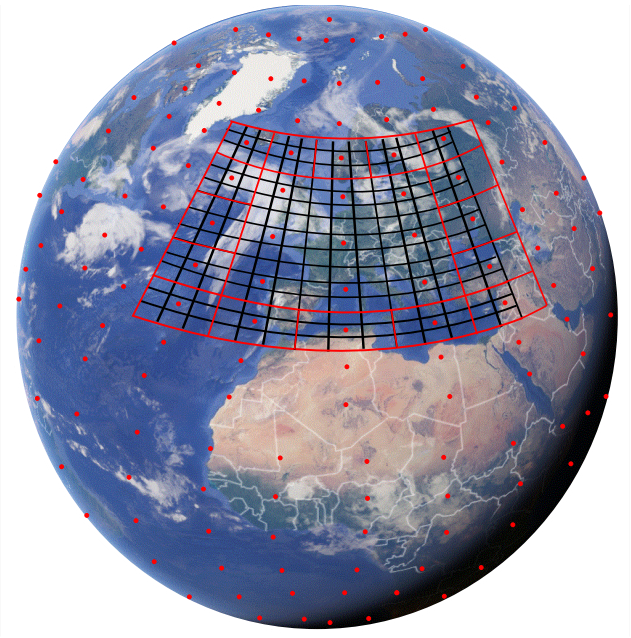

Figure IV.1 – **Nesting of a Regional Climate Model (RCM) into a Global Circulation Model (GCM)**. The black grid corresponds to the RCM. The red grid, belonging to the GCM, is used as boundary conditions to drive the RCM. The others nodes (red dots) are not used as forcing data. Initial globe picture from Google Maps.

downscale without too much computational effort, a large amount of climate data. They are based on the strong connections that exist between large scale meteorological information and regional weather. The establishment of these relationships requires a long historical period for which both synoptic weather and local observations are available. After identifying which large scale variables are the most relevant for the prediction of local weather (i.e the ones having the strongest predictive skills for the local variables of interest) on this historical period, local meteorological parameters can be estimated for past and future decades from GCMs or climate reanalysis datasets. In statistical downscaling studies, these optimal large scale variables are called predictors while the local weather parameters that have to be predicted are referred to as predictands.

The simple implementation of statistical downscaling should not detract attention from the assumptions that have to be made to use these methods in a climate change context. Indeed, it is assumed that the GCMs predictors are of good quality and that they carry the climate change signal. Moreover, to be relevant under different climate conditions, the relationships between predictors and predictands must be stationary. Some statistical method such as the analogue method (described in the following section), also use the historical predictands database to generate future regional series. In consequence, this approach makes the hypothesis that the past probability distributions of predictands are still relevant in a warmer climate. These different assumptions will be examined in the last chapter of this manuscript.

There are three main categories of statistical downscaling methods:

- Weather generators are used to construct, via a stochatic generation process, single or multi-sites time series of predictands based on the distributional properties of observed data. These

characteristics, and consequently the weather generator paramatrisation, are usually determined on a monthly or seasonal basis to take seasonality into account. They can also be estimated for different families of atmospheric states, often reffered to as weather types. A state of the art of the most common methods which have been used for the downscaling of precipitation (single or multi-site) is presented in Wilks and Wilby, 1999 and more recently in Maraun et al., 2010. More recent publications gather detailed reviews of some sub-categories of weather generators ([Ailliot et al., 2015] - hierarchical models). An increasing number of studies also focus on the generation of multivariate downscaled series of predictands [Steinschneider and Brown, 2013; Srivastav and Simonovic, 2015]. However, the development of weather generators and their calibration using observed distributions can become tricky when several sites and/or predictands are involved. The spatial and multivariate cross correlations are not systematically well represented and the weather generator often has to be adapted.

- Transfer functions directly exploit the statistical link between predictors and predictands. Various functions can be used to model this relationship from a predictor-predictand simple linear regression [Goyal, Ojha, et al., 2010] to Generalized Linear Model [Pulquério et al., 2015] and non-linear regression such as Generalized Additive Model [Vrac et al., 2007] and more complex ones [Olsson et al., 2001]. The method enables the adaptation and the interpolation of the predictands simulations to predictors values that would exceed the historical range. Various predictands have been downscaled using regressions such as temperature and precipitation[Jeong et al., 2012], radiation and evapo-transpiration [Fealy and Sweeney, 2008], wind speed [Kirchmeier et al., 2014] and even extreme precipitation indices [Hertig et al., 2014]. However, using transfer functions simultaneously for several predictands and/or sites becomes a tough task if one wants to preserve spatial and cross-predictands correlations.

- The last family of statistical downscaling methods is based on weather classification [Willems and Vrac, 2011; Goodess and Palutikof, 1998]. The information on the synoptic atmospheric state, enclosed in the chosen set of predictors, is used to identify similar large-scale situations in the historical database. The observed local weather on these meteorologically similar days are then assumed to be relevant predictands values on the target day. The additional requirement of these downscaling approaches, compared to weather generators or transfer functions, is that the historical database must be long enough to represent the full variety of possible synoptic weather patterns. When the historical database is first scanned in order to perform a clustering of synoptic situations, the method is based on weather types. In this case, each target day is assigned to one group and all predictands values within this group are considered as plausible local scenarios. An extension of this method, which does not use weather classes, consists in 1) identifying the most similar large-scale situations to the target day in the whole archive and 2) using their associated local observations of predictand as plausible predicted values. It is referred as the analogue method.

Using statistical downscaling methods, the relationship between synoptic information and local weather that we take advantage of is not univocal. For the same large scale atmospheric state, several values of predictand are plausible. Indeed, some mesoscale or even smaller phenomena also come into play and affect local weather conditions. The best illustration of this small scale variability

is probably the example a typical summer day in a mountain area. A local storm driven by mountain breeze results in strong temperature and precipitation gradients over a short distance. For the same synoptic conditions, this local storm is equally likely to affect two neighbouring valleys. It is possible to take into account the small scale variability of local weather with ensemble or probabilistic versions of downscaling methods. Using the weather classification approach, it consists in selecting several days from the same weather class. Using an analogue method, the ensemble prediction of any target day is obtained from the k-nearest analogues and not only from the best one.

3. Zoom in on the Analogue method

3.1. Functioning and state-of-the-art

As part of the statistical downscaling methods group, the analogue approach hypothesises that local weather parameters are steered by synoptic meteorology. A set a relevant large scale predictors is used to describe synoptic weather conditions. Fig.IV.2 illustrates how local weather predictions are generated. From the atmospheric state vector, characterizing the synoptic weather of the target day, analogues are identified in the available climate archive. Then, the analogue method makes the assumption that similar large scale conditions have the same effect on local weather. The key element of the analogue method is that it does not require making assumption on the probability distributions of predictands. This is a noteworthy advantage for predictands, such as precipitation, which have a non-normal distribution with a mass in zero. However, resampling observations induces a restriction of the range of predicted values. This can be problematic in a climate change context and will likely lead to erroneous projections if large scale climatic conditions undergo strong modifications.

Since the description of the concept of analogy by Lorenz, 1969, the analogue method has gained popularity over time, for climate or weather downscaling. Table.IV.1 sums up, over the 5 last years, a selection of studies which used the analogue method. Many regions worldwide are represented but most of these studies focused on mid-latitudes areas, where the relationship between synoptic and local weather is often more robust. Nervertheless, Hwang and Graham, 2013 and Farajzadeh et al., 2015 applied this method in humid and dry sub-tropical zones respectively. Surmaini et al., 2015 even used analogues in Java, where tropical conditions prevail. Many studies also focused on the mediterranean area. Their main findings have been gathered and summed up by Jacobeit et al., 2014.

Initially focusing on precipitation and temperature downscaling, analogues are increasingly used for other local variables such as wind, humidity or even more complex indices related to wild fire [Abatzoglou and Brown, 2012; Casanueva et al., 2014]. They put emphasis either on efficiently reproducing the predictands time series or on accurately simulating the occurence and intensity of extreme events (e.g. in Horton et al., 2012).

These studies are addressing a wide range of questions from past climate variability to future scenarios. They also focused on the operational forecasting of predictands, extreme events or more complex weather-driven phenomena, such as flood [Marty et al., 2012; Marty et al., 2013], wild fire and agricultural production [Surmaini et al., 2015].

Table IV.1 – Selection of recent studies (last 5 years) using the analogue method for downscaling. The table gathers the test regions, the predictands, the predictors and the main objectives of these studies. Pr-Precipitation ; T-Temperature ; WS-Wind Speed; ET-Evapo-transpiration ; Tmin-Minimum Temperature ; Tmax-Maximum Temperature ; EPT-Equivalent Potential Temperature ; DIV-Horizontal Divergence ; VV-Vertical Velocity, SLP-Sea Level Pressure ; LCL-Lifting Condensation Level ; Q-Specific humidity ; QFX-Module of Moisture Flux ; TTI-Totals Total Index ; RH-Relative humidity; Z-Geopotential, U-Zonal Wind ; V-Meridional Wind ; SKT-Surface Skin Temperature; TCW-Total Column Water ; PW-Precipitable Water ; VOR-Vorticity

Reference	**Studied region**	**Predictand(s)**	**Predictor(s)**	**Prediction type**	**Context**
Caillouet et al., 2016	France	Pr, T	T925, T600, Z500, Z1000, VV850, PW, RH850, T2m (Common)	Probabilistic	20th century reconstruction
Daoud et al., 2016	SE France	Pr	EPT, DIV, VV	Probabilistic	probabilistic quantitative precipitation forecasting
Dayon et al., 2015	France	Pr	Pr, SLP, T2m, LCL, QFX850, TTI, Q850	Deterministic	Transferability in future climate
Surmaini et al., 2015	Western Java	Pr	U850, V850	Probabilistic	Drought prediction and impact on rice paddies
Chardon et al., 2014	France	Pr	Z500, Z1000, RH850	Probabilistic	Spatial transferability of analogue dates
Casanueva et al., 2014	Spain, Croatia	Fire Weather Index, Physiological Equivalent Temperature,	SLP, T2m, R850, Q850, T850, U850 and V850, Z500 (Predictand-specific)	Deterministic	Comparison of downscaling method on past decades + future trend of FWI and PET
Farajzadeh et al., 2015	Mid-West of Iran	CLIMDEX Indices (T, Pr)	HGT700, T700, U700, V700, HGT850, T850, U850, V850, Pr, Tx, Tn (Predictand-specific)	Deterministic	Comparison with several other downscaling methods
Gutmann et al., 2014	Western US	Pr	Coarsened Pr	Probabilistic	Comparison with other downscaling method for hydrological purpose
Martín et al., 2014	Ireland, Denmark, Germany	WS	SLP	Probabilistic	Wind power production estimation
Pierce et al., 2014	Western US	Pr, T	Large-scale Pr and T (Predictand-specific)	Deterministic	Produce consistent field of Pr an T for hydrological purposes
Charles et al., 2013	SE Australia	Pr	SLP, V850, Pr	Deterministic	Downscaling of GCM (historical period)
Hwang and Graham, 2013	Florida	Pr	Coarse-scale bias-corrected Pr	Deterministic	GCM downscaling. Focus on spatial-temporal correlation.
Radanovics et al., 2013	France	Pr	T925, Z1000, VV850, RH850xTCW	Probabilistic	Spatially coherent precipitation
Valero et al., 2014	Spain	Daily wind gusts	Z1000	Probabilistic	Forecasting strong wind gusts
Horton et al., 2012	Swiss Alps	Pr	Z500, Z1000, RH	Probabilistic	Local precipitation forecasting. Extreme events.
Tian and Martinez, 2012	South-Eastern USA	ET	Large-scale ET	Both	Comparison of two analog methods
Abatzoglou and Brown, 2012	Western US	Tx Tn T, Td, WS, Pr (Predictand-specific)	Predictands at low resolution	Probabilistic	WildFire prediction
Marty et al., 2012	Cevennes - France	Pr	Z500, Z1000, PW, RH850	Probabilistic	Flash flood forecasting

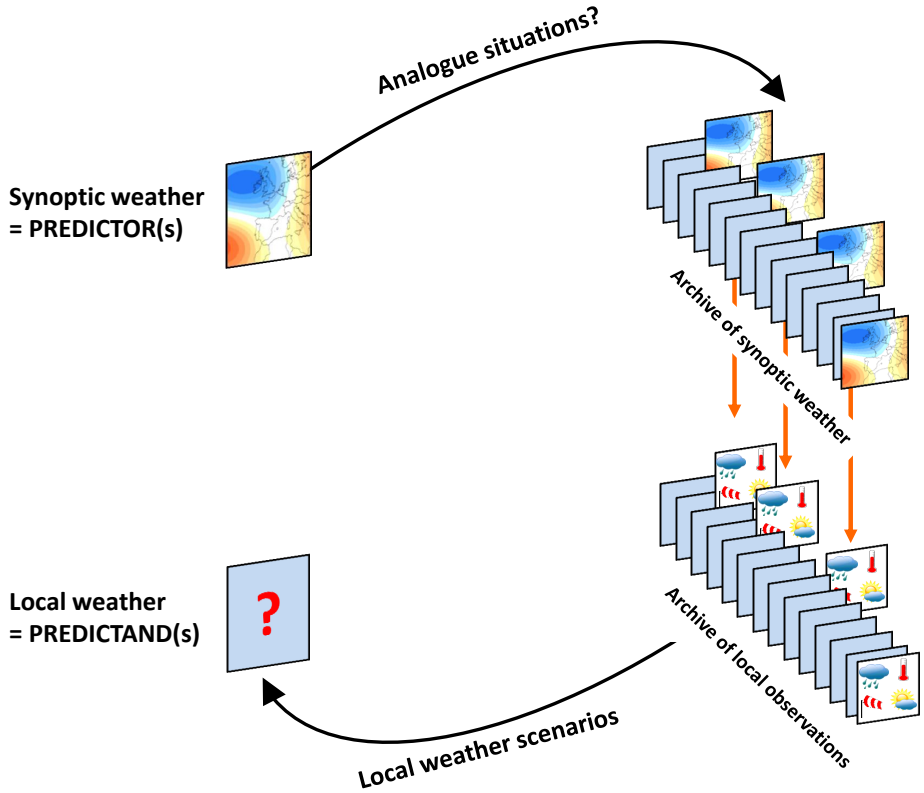

Figure IV.2 – **Principles of the analogue method.** From the synoptic weather of the target day, analogues are identified within the available climate archive. The local weather on these analogue days are then used as weather scenarios for the target day.

3.2. The choice of the predictors set

The keystone of an effective downscaling with analogues lies in a relevant choice of predictors. The most pertinent large scale information is expected to depend on the predictand, the climate conditions over the test region and possibly on the season. Two main branches about the choice of the predictors set exist. The first one consists in using the large-scale values and/or fields of predictand as predictors. This can be done, for instance, comparing the precipitation fields from GCMs with the coarsened ones from observations [Gutmann et al., 2014]. Consequently, it assumes that two similar synoptic precipitation patterns give similar local rainfall (or snowfall) amounts. This choice has been made for other variables such as temperature [Pierce et al., 2014], evapotranspiration [Tian and Martinez, 2012], dew point temperature and wind speed [Abatzoglou and Brown, 2012].

The second option for the choice of predictors takes advantage of some other meteorological parameters whose large scale features drive the predictand of interest. Classically, these parameters are also expected to be better simulated than low-resolution predictands, as synoptic and larger scale phenomena are explicitly modelled (no parametrisation) by GCMs. Geopotential, sea level pressure and zonal/meridional components of wind are widely used, as they inform on air flow direction and on the positions of low and high pressure systems. Other dynamic predictors such as vertical velocities and divergence help locating fronts and are often picked up as predictors for downscaling of precipitation [Caillouet et al., 2016; Daoud et al., 2016]. Thermodynamic variables usually provide additional support, bringing information on the atmosphere water content through relative and specific humidity, total column water or precipitable water.

3.3. The small scale variability using analogues

The analogue method can be used in different ways to generate local series of predictands. If one is only interested in building a single daily prediction or regional series, the procedure consist in selecting only the best analogue of each target day. In this case, the downscaling method is deterministic (e.g in Farajzadeh et al., 2015; Pierce et al., 2014).

As the relationships between predictors and predictands are not univocal, the same large scale state can result in several local weather conditions from the intervention of small scale atmospheric processes. In order to take on board this source of variability, the analogue method can be used in a probabilistic or ensemble way. It is probabilistic when the observations associated to the k-nearest analogues are used to estimate, for each target day, the probability distributions of predictands [Bontron, 2004; Daoud et al., 2016; Chardon et al., 2014; Horton et al., 2012]. An ensemble of stochastic predictions is obtained when randomly selecting multiple analogue days from the k-nearest analogues sample and using the associated observations to generate multiple and equi-probable downscaled series of predictands [Lafaysse et al., 2014]. In the following downscaling application, we selected this approach, as it offers the possibility of working with an ensemble of regional series and of quantifying the contribution of small scale variability to the global fluctuations of climate.

4. Statistical multivariate downscaling

4.1. Tackling the multivariate issue

The simultaneous generation of time series associated to several predictands is not straightforward when using statistical downscaling methods. Contrary to RCMs, which guarantee the physical consistency between local meteorological variables, statistical methods are often optimised in a predictand specific way.

Weather generators have usually tackled the multivariate issue performing first a downscaling of precipitation and conditioning the other variables to this prediction [Abdulharis et al., 2010; Fatichi et al., 2011]. Yet, some weather generators account for the inter-dependency between local predictands [Steinschneider and Brown, 2013; Srivastav and Simonovic, 2015] but require an accurate knowledge of the covariation between these variables. It is often difficult to assess these relationships from observations and subsequently to take them into account in the model.

Copula can be used to adapt transfer functions for the simulation of correct inter-variable correlations [Alaya et al., 2014] but this method still needs to be further explored. Some regression-based methods also handled multivariate downscaling by combining univariate predictors-predictand relationships with a stochastic component which aims to reproduce the co-variations between local variables [Khalili et al., 2013]. This was also done to obtain correct multi-sites or temporal correlations in [Mezghani and Hingray, 2009]. In spite of everything, these methods require a large amount of preliminary work to ensure correct interdependence between variables.

Weather classification and analogue methods offer a simple way of generating consistent multivariate series: For a given target day, if all predictands are sampled from the same analogue, their physical consistency is automatically guaranteed. Several studies used this approach to ensure the relevance

of their multivariate predictions (e.g. in Boé et al., 2006; Lafaysse et al., 2014, or Abatzoglou and Brown, 2012 for minimum, maximum and dew point temperatures). However, to use such a method, it is necessary to find a set of relevant common predictors to avoid a deterioration of the prediction skills.

4.2. Motivation and requirements for this study

In the context of the integration of renewables, climate reanalysis datasets and GCMs can help characterising both low frequency variations and future trends of CRE sources. Downscaling methods are required to generate scenarios of meteorological drivers at a relevant spatial scale.
The main challenge to take up is that the downscaled regional series must guarantee both relevant probability distributions of predictands and correct inter-variables correlations. In this way, power production coming from different energy sources can be compared and analysed simultaneously (cf. Chap.III). As mentioned previously, building a multi-variate linear regression for downscaling is an arduous task. Thus, our choice leaned in the direction of the analogue method. This method requires some preliminary effort on the choice of predictors. Thus, we will explore for the 12 test regions, the setting up of a multivariate downscaling, using the analogue method. We will look for the best configuration regarding both prediction skills and inter-predictands consistency. The associated results have been published in Raynaud et al., 2016, Int. J. Climatology. This article is presented in the following chapter. The outcomes of this study lie in the development of SCAMP (Sequential Constructive Atmospheric Analogues for Multivariate weather Predictions). SCAMP is a hybrid analogue downscaling method based on multiple analogue sub-models. It is able to generate accurate multivariate predictions of local predictands. SCAMP is used in Chap.VI to explore the past climate variability of the 20^{th} century and in Chap.VIII/IX to generate future scenarios of local weather conditions.

Chapter V

Multivariate analogue dowsncaling

1. IJOC publication

Atmospheric analogues for physically consistent scenarios of surface weather in Europe and Maghreb.

RAYNAUD Damien[1,2], HINGRAY Benoit[1,2], ZIN Isabella[1,3], ANQUETIN Sandrine[1,2], DEBIONNE Samuel[1,2], VAUTARD Robert[4]

1: Univ. Grenoble Alpes, LTHE UMR 5564, Grenoble, F-38000, France
2: CNRS, LTHE UMR 5564, Grenoble, F-38000, France
3: Grenoble-INP, LTHE UMR 5564, Grenoble, F-38000, France
4: LSCE/IPSL, Laboratoire CEA/CNRS/UVSQ, F-91191 Gif/Yvette, France

Corresponding author: HINGRAY Benoît, benoit.hingray@ujf-grenoble.fr, LTHE Domaine Universitaire 1025 rue de la piscine 38 400 Saint Martin d'Hères FRANCE

Acknowledgments

This work has been carried out within the European COMPLEX Project on Knowledge Based Climate Mitigation Systems for a Low Carbon Economy (European Collaborative Project FP7-ENV-2012 number: 308601; http://www.complex.ac.uk/). It partly contributes to the VALUE COST Action funded by the European Community to develop and evaluate downscaling strategies for Europe (COST Action ES1102; http://www.value-cost.eu/). We thank Charles Obled, Anne-Catherine Favre and Jean-Dominique Creutin (LTHE) for the interesting discussions we shared with them about this work as well as Isabelle Tobin (LSCE/IPSL) for providing with wind observation data from the ISD-LITE data base. We also thank Casey Brown and the two anonymous reviewers for their constructive comments and suggestions. Most of our figures have been generated using a "color blind safe" panel from http://colorbrewer2.org/.

Key words: statistical downscaling, analogue, multivariate, precipitation, temperature, radiation, wind, correlation

1.1. Abstract

The present study compares the multivariate predictions of daily temperature, temperature range, precipitation, surface wind and solar radiation of a single-model analogue approach with an original multi-model analogy over 12 regions in Europe and Maghreb. Both approaches are based on two-level analogue models where atmospheric predictors are either dynamic or thermodynamic. In the multi-model approach, independent analogue models with predictand-specific predictors are used. In the single-model one, a unique analogue model and its associated set of predictors is applied to all predictands.

Testing numerous large scale predictors, we first identify the best predictor sets for each modelling strategy. Those obtained for the single-model approach are significantly different from those of the predictand-specific models. This is especially the case for local temperature and wind speed. Both methods perform similarly for precipitation, temperature range and radiation.

We next assess the ability of both approaches to simulate physically coherent multivariate weather scenarios. With the single-model method, weather scenarios are obtained for each prediction day from observations sampled simultaneously on one analogue day. The physical consistency between variables is thus automatically fulfilled each day. This allows the single-model method to reproduce well the observed inter-predictand correlations, especially the significant correlations between radiation and precipitation and between radiation and temperature range. These results suggest a hybrid analogue model using a single-model for radiation, temperature range and precipitation, combined with a univariate approach for wind. Two options are proposed for temperature for which either the predictand-specific method or a single-model approach with an additional correction are conceivable. This hybrid approach leads to a possible compromise between reasonable univariate prediction skills and realistic inter-predictands correlations, both classically required for many impact studies.

1.2. Introduction

Characterizing and understanding the impact of climate variability on regional environmental systems has received increasing attention in different fields of Geosciences, such as Hydrology, Agroforestry or Ecology. Other domains such as Green Energy are also coming into play as a result of the massive development of renewables. In addition, numerous regional studies aim to assess the future long-term effects of climate change resulting from anthropogenic forcing [IPCC, 2013]. Other studies focus on past decades or on the 20th century to better describe and understand the multi-decadal variations which are characteristic of Climate internal variability [Kuentz et al., 2014]. Toward this goal, global reanalysis of the Earth system for the whole 20th century [Compo et al., 2011; Poli et al., 2013] and general circulation models (GCM) are used and provide useful information on weather at synoptic scale. However, their coarse spatial resolution prevents them from simulating relevant local weather conditions credibly. Consequently, reanalysis data and GCM outputs are of limited use for a number of regional studies without adjustments. Downscaling and bias correction methods are used to tackle the scale issue and many of them have been developed in the recent decades (see review of Maraun et al., 2012).

Using GCM or reanalysis data as boundary conditions, dynamic downscaling allows simulation of climate conditions over a limited spatial domain with a higher resolution of typically a few dozen kilometres [Jakob et al., 2006]). Dynamical downscaling models offer physical, spatial and temporal consistency between simulated local variables. However, some of their outputs such as precipitation or incoming solar radiation often suffer from large biases resulting from the parametrizations required to simulate sub-grid atmospheric processes. Dynamical models classically also require a large computational effort when a large ensemble is downscaled. This is particularly the case for the last CMIP5 project which gathers control, historical and future climate ensemble members of numerous GCMs. This also applies to the reanalysis datasets of the 20th century for which multiple members are available to characterize the uncertainty in the reconstructions.

Statistical downscaling models (SDMs) are an alternative for constructing local weather conditions from large scale simulations with lower computational cost. SDMs are simpler and easily implementable models based on the often strong physical relationships that exist between some large scale atmospheric parameters and local weather variables. Different SDMs have been developed in recent decades, including weather generators and so-called "perfect prog" approaches such as transfer functions and analogue methods [Maraun et al., 2012]. They are used to generate regional weather series from GCMs outputs [Hanssen-Bauer et al., 2005; Timbal et al., 2009; Lafaysse et al., 2014], to reconstruct past weather conditions from atmospheric reanalysis data [Wilby and Quinn, 2013; Kuentz et al., 2015] or to produce probabilistic weather forecasts from weather forecasting models [Obled et al., 2002; Marty et al., 2012]). Other applications such as weather generation [Buishand and Brandsma, 2001; Yiou, 2014] and detection/attribution of climate trends can also benefit from SDMs [Vautard and Yiou, 2009; Stott et al., 2016]. They have also been used to detect problematic climate conditions in vulnerability analyses [Steinschneider and Brown, 2013]. Most SDMs have been developed for the simulation of precipitation and temperature time series as main hydrometeorological drivers. In recent years, SDMs often include additional meteorological variables such as relative humidity, wind speed, potential evaporation, solar radiation and extreme temperatures [Timbal et al., 2009; Fealy and Sweeney, 2008]. These parameters are useful for impact studies which are sensitive to the

variability of hydrometeorological variables. In a multivariate simulation framework, a key challenge is the generation of weather scenarios that are relevant from both statistical and physical point of views, as regards 1) space-time variability of individual predictands and 2) space-time covariability between predictands. An accurate multivariate covariability simulation is, for instance, a critical requirement for impact studies in snow dominated areas where river discharge, avalanches but also landslides and ground stability are strongly influenced by the joint effects of elevation, precipitation and temperature [Jakob et al., 2006; Jomelli et al., 2007]. The covariability between weather variables is also decisive for wildfires whose triggering ingredients are related to hydrometeorological drought conditions prior to the ignition and favourable weather conditions such as wind during an active fire [Abatzoglou and Brown, 2012]. Inter-variable covariability has also recently become a critical issue for the integration of intermittent energies (e.g. wind, small hydro, solar) which are a growing fraction of electricity sources as part of the ongoing transition to a low carbon economy [François et al., 2016].

Among the large panel of SDMs, the analogue method [Lorenz, 1969] is frequently selected for downscaling purposes. It gained popularity with a number of studies such as those of Zorita et al., 1995; Guilbaud and Obled, 1998; Timbal and McAvaney, 2001. It is easy to implement and often shows satisfactory prediction skills. Analogue models have been widely applied for precipitation and temperature downscaling in various regions [Timbal et al., 2003; Wetterhall et al., 2005]. They have also been used in recent years for other meteorological variables such as wind [Valero et al., 2014; Martín et al., 2014], radiation [Abatzoglou and Brown, 2012], surface humidity and evapotranspiration [Timbal et al., 2009; Tian and Martinez, 2012].

In the analogue method, analogues, which are days that are similar to the current target day, are identified in the historical database. To draw up a list of days with similar conditions, we use a daily state vector characterizing the current atmospheric circulation and state. Similarity is measured in terms of distance between the daily state vector of the target day and those of all other days. This state vector is classically composed of a set of large scale atmospheric predictors over some relevant spatial domain. Typically, a single day is drawn from the set of the k-most similar analogues and the local surface weather observations of that day are then used as weather scenario for the target day [Lafaysse et al., 2014].

A major advantage of the analogue method is that it does not require restrictive assumptions concerning the joint distribution of the different predictands. When a single analogue model is applied to a multivariate set of predictands, meaning that the same set of predictors (atmospheric variables and analogy domains) is used for all predictands, all surface weather variables are sampled simultaneously from historical record available for a given analogue day and used as the prediction. The resulting multivariate scenarios are then physically realistic and consistent and the simulated weather variables are bound to reproduce the correlations between the variables. This single analogue model strategy has been applied in several previous works such as Boé et al., 2006; Abatzoglou and Brown, 2012; Steinschneider and Brown, 2013; Lafaysse et al., 2014.

However, the best atmospheric predictors for identifying analogues most likely depend on the region, the predictand and the season of interest [Cavazos and Hewitson, 2005; Timbal et al., 2009; Chardon et al., 2014]. If a single analogue model is used to predict all predictands at all sites, that is, if a unique set of predictors is retained for all variables and sites, predictions are likely to be sub-optimal in comparison to individual models for individual variables and sites [Radanovics et al.,

2013; Chardon et al., 2014]. As an alternative to the single-model approach, multivariate predictions can be obtained from a suite of predictand-specific analogue models, each of them having its own predictors. With that approach, an analogue model is built for each single predictand based on the most relevant large scale predictors and their associated optimal spatial domains. The models are therefore optimal for each site and variable individually. The main drawback is that the physical consistency of the surface weather conditions is not guaranteed.
The present study proposes to explore and compare the generation of multivariate weather scenarios with these two different analogue downscaling approaches, the single and the predictand-specific model strategies. In order to ensure that results are representative of a large zone of the European continent, the analysis is performed for 12 regions of Europe and Maghreb. Five daily weather variables at the surface are targeted: precipitation, wind speed, temperature, temperature range and solar radiation. The two approaches are compared in their prediction skills for individual predictand and their ability to reproduce observed inter-predictands covariability.
The methods, data and regions tested are presented in Sec1.3. Sec.1.4 explores for each predictand the dependence of prediction skill on the predictors set and the region of interest. It also compares the ability of the two modelling approaches to reproduce the observed inter-predictand covariations. The respective advantages and drawbacks of the two methods are discussed in Sec.1.5.

1.3. Models and Data

1.3.1. Data

We use five daily surface variables (temperature, temperature range, wind speed, solar radiation and precipitation) for 12 regions in Europe and Maghreb (Fig.II.1). A large panel of possible climatic conditions are represented with 1) a West-East gradient going from climates influenced by the Atlantic Ocean to continental climates in Eastern Europe and 2) a South-North gradient from subtropical and Mediterranean climates to a subarctic one. Some regions also include major mountain ranges (Norwegian and Italian regions for instance) with frequent and heavy snowfall in winter and a recurrent diurnal convection cycle in summer leading to a broad panel of possible weather conditions across the year.
Daily time series of predictands are extracted for the 1983-2012 period from three different datasets. Temperature, temperature range and precipitation data are taken from the European Climate Assessment & Dataset (ECA&D) available at a 0.25°resolution for the whole Europe [Haylock et al., 2008]. ECA& D data have been obtained by kriging of observations from meteorological stations.
Observations of solar radiation are rare at the surface but estimates of solar radiation are available from satellites products since the mid-80s. Time series of solar radiation are here taken from the Surface Solar Radiation Data Set - Heliosat (SARAH) available at a 0.05°resolution for the 1983 - 2012 period and for a large region of the globe (±65°longitude, ±65°latitude). The dataset has been evaluated on a group of weather stations including several ones in Europe for daily and monthly time series and proves to be capable of producing relevant estimation of incoming solar radiation at the Earth's surface [Riihelä et al., 2015; Müller et al., 2015].
Surface time series of observed wind speed are scarce and usually cover rather short periods. For

many regions considered here, few wind stations were available and complete from 1983 to 2012. In a number of regional studies for which wind is a variable of interest, wind speed estimates are often taken from the outputs of regional climate models forced by some global atmospheric reanalysis [Jerez et al., 2015]. In the present case, wind data are extracted from regional simulations performed using the WRF model forced by ERA-INTERIM [Vautard et al., 2014]. Wind speed data are available on a 3h time step for a 50x50 km grid over the whole 1983-2012 period.
For all predictands, the gridded data described previously were converted into regional series of daily means averaging the values of all grey cells presented on Figure 1.
Thirteen daily atmospheric predictors were selected in this study to respond to the wide range of meteorological conditions of the twelve selected regions. The selection gathers most predictors considered in previous studies over Europe [Hanssen-Bauer et al., 2005; Wetterhall et al., 2005; Horton et al., 2012]. They were extracted from the ERA-Interim dataset [Dee et al., 2011] for the 1983-2012 period (0.75°grid). They include dynamic predictors (1000, 700 and 500hPa geopotential heights, vertical velocities in mid-troposphere at 600hPa), thermal fields (air mass temperature at 850hPa and sea surface temperature) and predictors related to the atmospheric water content (relative humidity at various levels, total column water, "distance to saturation" with T-Td where T and Td are respectively air and dew point temperatures at two meters). This very last predictor can be considered as similar to the near-surface relative humidity which is not a parameter directly available in the ERA-Interim database. All predictors, initially available on a 6-hour time step were converted into daily mean.

1.3.2. Multivariate modelling strategies based on two-level analogue models

In the following, we describe the two modelling strategies discussed previously. For the first one, a suite of predictand-specific models is used with a separate set of predictors for each single local variable. The second is a single-model method using the same set of predictors for all predictands.
For both modelling strategies, we use two-level analogue models. Following Obled et al., 2002, the first analogy level is always based on dynamic predictors to guarantee similar large scale circulation patterns for all the predictions of a given target day. Conversely, the second analogy level is based on regional thermodynamic predictors. Step by step, this procedure builds a description of the weather situation by 1) determining to which weather type, in terms of positions of lows and highs and intensity of gradients, the target day belongs to and 2) what are the thermodynamics characteristics over the target region and its surroundings. This stepwise analogue approach has been widely used in recent years [Marty et al., 2012; Horton et al., 2012; Radanovics et al., 2013; Chardon et al., 2014].
In practice, the selection of the analogues and the generation of local weather scenarios for a given target day consists of several consecutive steps. A seasonal filter, based on a 30-day moving window, is first applied in order to extract days that belong to the same period of year. The 100 best analogue days are then identified among those candidates according to the first analogy level predictors. The 30 most similar analogue dates with respect to the predictors of the second analogy level (Tab.V.1) are then selected within this 100 dates subset. The number of analogs selected for the first and the second level results from the previous work of Daoud et al., 2016. Finally, 50 multivariate time series covering the whole 1983-2012 period are generated using a random selection for each target day of one of its analogue days (sampling with replacement of the 30 best analogues). For each analogue

date, the value of the predictands of interest in the observations archive is used as local scenario for the target day. The identification of the best analogue dates uses in turn two different analogy scores. The Teweles-Wobus score (TWS) proposed by Teweles and Wobus, 1954 is used for the first analogy level. This score has been found to lead to higher performances than a more classic Euclidian distance [Guilbaud and Obled, 1998; Wetterhall et al., 2005]. It quantifies the similarity between two geopotential fields comparing their spatial gradients. It allows selecting dates that have the most similar spatial patterns in terms of atmospheric circulation at a given (or several) geopotential level(s). The root-mean-square error (RMSE) is applied as the performance metric for the second analogy level, for any other predictor.

1.3.3. Predictor sets and spatial analogy domains

As mentioned previously, the best predictors set is expected to depend on the predictand and on the region considered. Let us first consider the case of the predictand-specific modelling approach. For a given predictand and a given region, the search for the best predictor set is carried out over two steps. For the first analogy level, we compare the prediction skill of models either based on a single geopotential height (at 1000, 700 or 500 hPa) or on a combination of the 1000 and 500hPa levels (HGT500 provides information on the general meteorological situation while more intense and smaller lows and highs can be distinguished at 1000hPa). Once the best option is identified, we then look for the best thermodynamic predictor at the second analogy level.
The best spatial domain used to compute the analogy score is also expected to be predictand- and region- dependent [Chardon et al., 2014]. Optimizing the limits of the spatial analogy domain can be done using different methods. A possible technique consists in a stepwise spatial extension of an initial elementary spatial domain in one of the 4 cardinal directions until a maximum in prediction skill is reached. As shown by Chardon et al., 2014, this optimization process is not very efficient as a number of different spatial domains usually lead to very similar prediction skill scores. Additionally, the process often leads to local optima and results are very dependent on the initial position of the elementary domain [Radanovics et al., 2013]. To tackle this issue, another approach was followed (see 1.6.1 for details). For each combination of region, predictand and predictor, it consists of comparing the prediction skills obtained for a large number of analogue models based on different analogy domains. For this purpose, we consider different analogy domain types with different shapes and sizes (e.g. 9 different types in a configuration where a single geopotential height is used as predictor), and for each of them, we search for its optimal positioning over Europe. Hence, predictions are made and evaluated for all possible centres of the analogy domain within a large geographical area including the target region. Then, the most skilful configuration in terms of shape, size and positioning is retained as the best analogue model for the region-predictand-predictor combination considered.
When two-level analogy models are considered, this process is carried out successively for both levels. The best analogy domain (size, shape, positioning) obtained for the second analogy level is thus conditional on the results obtained for the first analogy level. A global optimization process, where all parameters are optimized in one single step for both analogy levels, would likely be preferable. Its technical implementation is however not straightforward and it would have been moreover highly time consuming [Horton et al., 2012]. Thus, it was not considered here. In this optimization process, the prediction skill for the considered predictand is assessed using the Continuous Ranked Probabil-

ity Skill Score (CRPSS) calculated from the 50 time series realizations simulated for the 1983-2012 period. The CRPSS (V.1) is based on the Continuous Ranked Probability Score calculated on a daily time step as described by Brown, 1974 and Matheson and Winkler, 1976.

$$\text{CRPSS} = 1 - \frac{CRPS_{analogue}}{CRPS_{clim}} \tag{V.1}$$

Where $CRPS_{analogue}$ is the Continuous Ranked Probability Score obtained with the analogue prediction and where $CRPS_{clim}$ is the Continuous Ranked Probability Score obtained with a reference prediction model. This reference is defined as a climatology based on all calendar days around the target day with a temporal extent set to ± 30 days. As a consequence, the CRPSS is normalized allowing comparison of the prediction skill obtained for different predictands and regions. The optimal CRPSS value is equal to one and a negative value indicates that the analogue model has a lower skill than the climatology

This optimisation process allows to identify the best predictor set for each predictand individually. As shown in the following section, the best predictor set (predictor variable and analogy domain) varies from one predictand to the other.
This optimisation process was also applied in the single-model strategy. Yet, in this case, a unique set of predictor is used for all 5 predictands and the performance of the model has to be assessed based on its multivariate prediction skill. It is evaluated with the average value of the univariate prediction skills scores obtained for each of the 5 local variables respectively (Eq.V.2). Thus, the best single-model reaches a compromise between the prediction skill scores of the different predictands.

$$\text{CRPSS}_{\text{all}} = \frac{1}{5} \cdot (CRPSS_{Temp} + CRPSS_{Precip} + CRPSS_{Radiation} + CRPSS_{Wind} + CRPSS_{Tx-Tn}) \tag{V.2}$$

1.4. Results

We first present the results obtained with the predictand-specific strategy. Results for the single-model method follow. In both cases, skill scores are first described for predictions obtained at the first analogy level. They are next presented for predictions resulting from the entire analogue chain using both analogy levels.

1.4.1. Predictand-specific analogue models

Fig.V.1 presents the CRPSS obtained for each predictand and region at the first analogy level using the 4 selected predictors (single geopotential heights and combination of 500 and 1000hPa). The rankings of the different predictors are also displayed with numbers ranging from 1 (for the best predictor) to 4 (for the poorest). The results are discussed in turn for each of the five predictands (precipitation, wind speed, radiation, temperature and temperature range). Furthermore, Fig.V.2 compares the prediction skill scores obtained with the combined HGT500 & 1000hPa predictor and

with the single geopotential level predictors.

For wind, the best predictor is the geopotential height at 1000hPa for all regions with rather high CRPSS values ranging from 0.4 to 0.6. This result is mainly due to the close relationship existing between wind near the surface and local gradient of geopotential in the low troposphere. The best analogy domain is always the smallest one as another consequence of this link (e.g. δLon = 6°; δLat=6°when the square shape is selected). The best scores are obtained for regions influenced by the Atlantic and for regions prone to few interactions between topography and the geostrophic wind component. The 500hPa geopotential is less relevant for surface wind and does not provide useful information. Introducing this level in a combination with HGT1000 leads to an important score decrease, whatever the location (Fig.V.2).

For precipitation, solar radiation, temperature range and temperature, the best prediction skills are obtained from the combination of the two levels of geopotential, HGT500 and HGT1000. They are significantly smaller than for wind, highlighting that dynamic circulation is a weaker predictor for these variables. Nevertheless, the scores still range from 0.27 to 0.37 for temperature, from 0.15 to 0.41 for temperature range, from 0.12 to 0.22 for solar radiation and from 0.21 to 0.46 for precipitation. In fairly all cases, the best analogy domains combine the largest spatial domain for HGT500 and the medium one for HGT1000 (eg. δLon = 16°; δLat=16°for HGT1000 and δLon = 22°; δLat=22°for HGT500 if the square shape is the most relevant). Temperature and temperature range are better simulated in southern Europe with CRPSS greater than 0.3. No clear spatial structure of the score can be seen for radiation and precipitation. However, Tunisia stands out with much lower scores compared to the other regions. This is a consequence of the high prediction skills of the climatology in this region where most days are dry and sunny. Finally, these results highlight that, when using a single geopotential height as predictor, the lower (in the troposphere) the information, the better the prediction skill for precipitation, radiation and temperature range (Fig.V.2). This is not the case for temperature which is better simulated using HGT500 and HGT700 rather than HGT1000.
Fig.V.3 presents the boxplots of CRPSS gains obtained for all regions introducing different second level predictors. For each predictand, the first level analogy is carried out with the previously identified best predictors (i.e. HGT1000 for wind and HGT1000+HGT500 for precipitation, temperature, temperature range and radiation). For temperature, air mass temperature at 850hPa as second analogy predictor boosts the CRPSS with an increase ranging from 0.12 to 0.20. TCW comes after with a mean CRPSS increment equals to 0.1. CRPSS gains are much smaller but still significant for SST and humidity parameters close to the surface (T-Td and RH1000). They drop for all other predictors. A roughly identical hierarchy of prediction skills between predictors is obtained for precipitation and wind, although the CRPSS gains are much smaller for the latter. The mid-troposphere vertical velocities lead to the highest CRPSS increase. This predictor actually allows locating large scale fronts and disturbances which concentrate most of the precipitation and potentially stronger winds. The low and mid-troposphere humidity parameters T-Td, RH700, RH1000 and their combined use also lead to a rather high CRPSS gain. They bring information about clouds and water vapor from possible different origins (fronts, stratocumulus or stratus under high...). As for TWC, this predictor can be indirectly related to precipitation amounts through precipitable water. Consequently it gives a

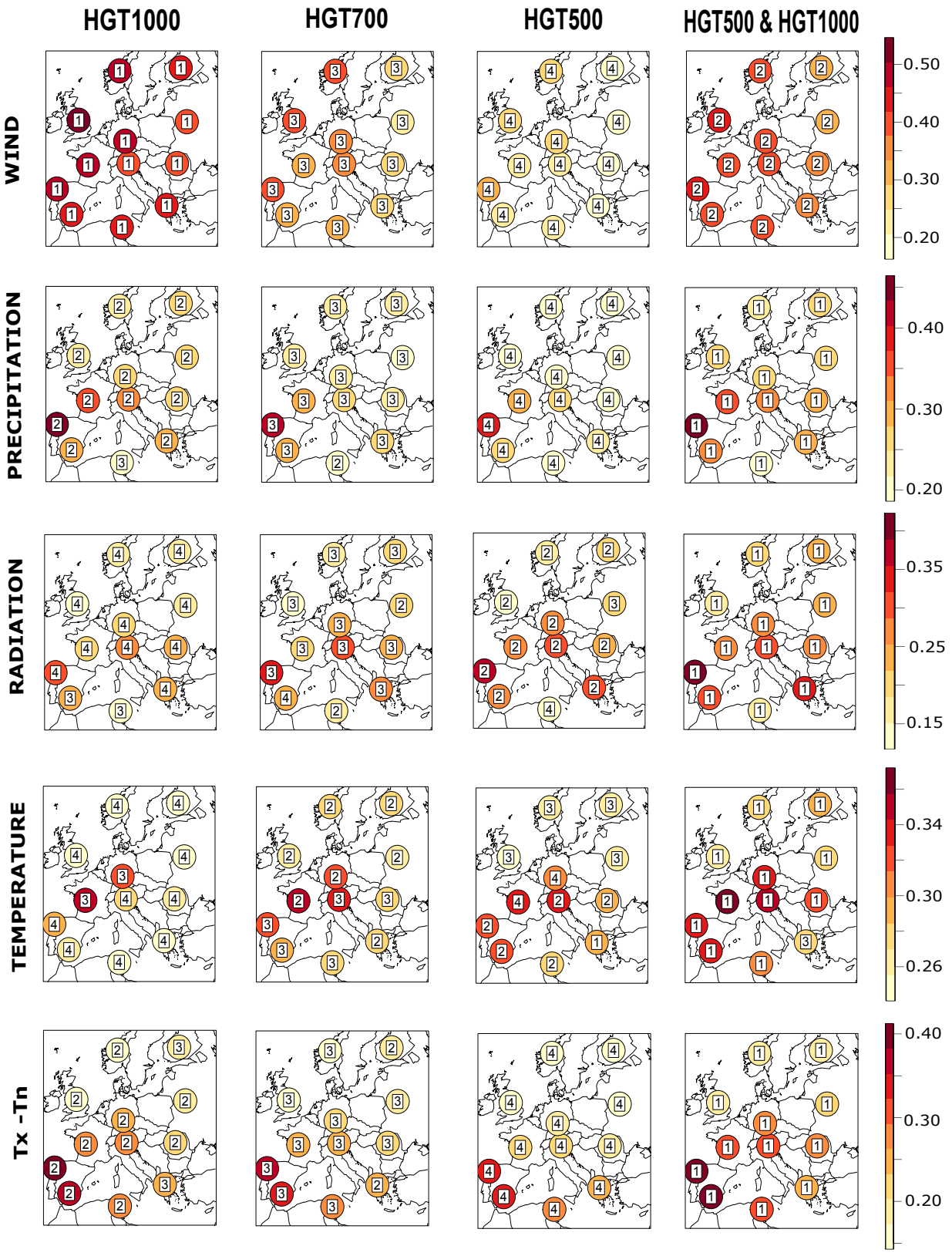

Figure V.1 – Predictand specific models. Prediction skill scores obtained with the predictand-specific models at the first level of analogy (12 regions, 5 predictands). The CRPSS values are given by the bubbles colours (with a predictand specific colour scale shown on the left side). For a given predictand and a given region, the numbers give the rankings of predictors (1 : best predictor, 4: poorest).

Table V.1 – List of predictors tested in first and second levels of analogy

Analogy Level	Predictor name	Altitude or geopotential height
Level 1	Geopotential height (HGT)	1000 hPa
		700 hPa
		500 hPa
		500 hPa & 1000 hPa
Level 2	Relative Humidity	1000 hPa
		850 hPa
		700 hPa
		400 hPa
		700 hPa & 1000 hPa
	Total Column Water	-
	Vertical Velocity (VV)	600 hPa
	Sea Surface Temperature (SST)	-
	Air Temperature (T850)	850 hPa
	Temperature-Dew point temperature difference (T-Td)	2 m

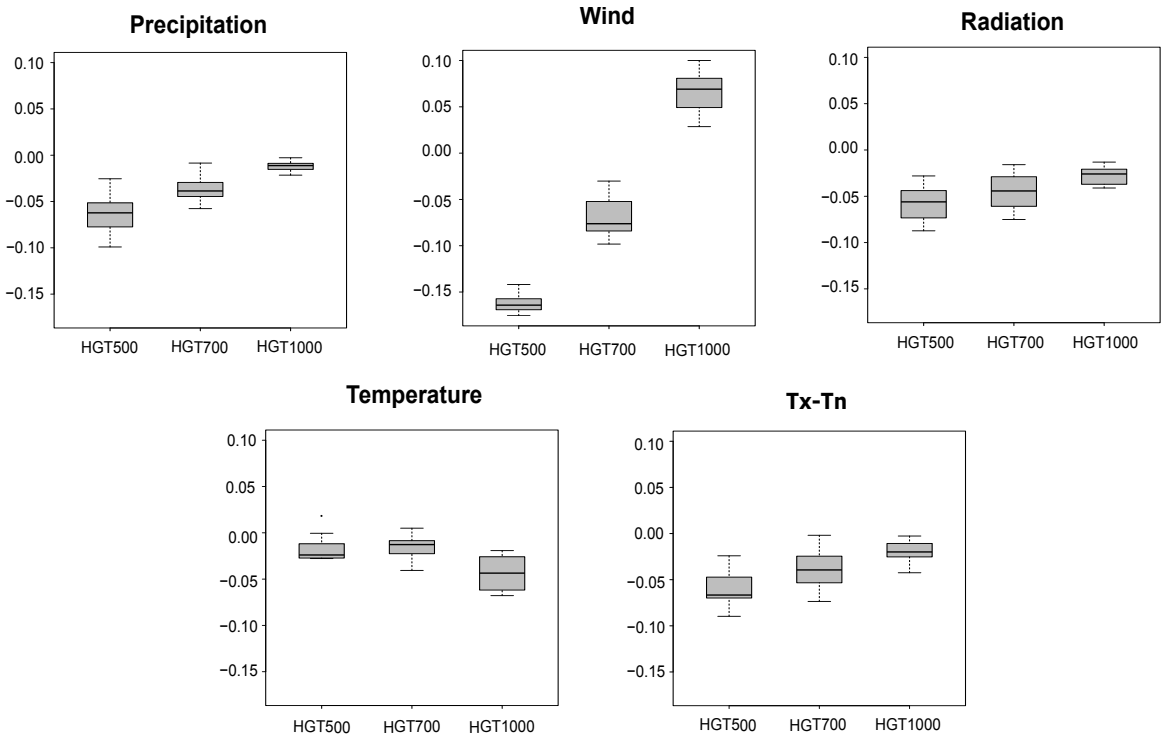

Figure V.2 – Predictand specific models. CRPSS gains (when positive) or losses (when negative) when using a single geopotential level predictor instead of a combined 500 + 1000hPa predictor. Each boxplot gather changes in CRPSS obtained with the 12 test regions.

first estimation of possible rainfall amounts when weather conditions are favourable for the triggering of precipitation and without taking into account the influence of more complex phenomena such as convergence. Despite that, it does not provide much information and it is much less relevant than all low level humidity parameters. The same assessment can be made for wind. Indeed, from the inner structure of fronts, high and mid-level humidity can be drawn far ahead from the area at the surface where precipitation and stronger winds occur. Moisture at low altitudes is in consequence often more relevant. Finally, thermic predictors (T850 and SST) are not very informative.
Solar radiation is mainly dependant on rainy or overcast days for which the atmosphere is closer to saturation. It explains the rather high CRPSS increase obtained for both solar radiation and precipitation when T-Td and to a lesser extent RH1000 is used as second level predictor. A much lower gain is achieved with the other predictors. Temperature range has a predictors ranking rather similar to radiation with the lowest levels of relative humidity being the most informative. Following the same reasoning as for radiation, these predictors provide information on cloudy and/or rainy days for which the temperature does not follow a classic diurnal cycle. Contrary to the results for temperature, T850 does not impact significantly the prediction scores of daily temperature range. SST used as a predictor for precipitation gives some noteworthy results. Although this variable is classically expected to be an important ingredient for some meteorological phenomena such as intense precipitation, it was found to bring some (small) CRPSS gain for temperature but not for the other predictands. This result was quite homogeneous among the twelve regions whatever their distance to the sea. SST is known to impact indirectly many of the other predictors tested at both analogy levels. Its information could thus be already included. Moreover, in spite of the water vapour SST provides to the atmosphere every day, it also mainly impacts the low-frequency variability of precipitation and can be considered as poorly related to its daily variations [Cattiaux et al., 2009].

The best predictors at the second analogy level were expected to be regionally dependent. Fig.V.4 presents maps of CRPSS gains achieved for four selected second level predictors. Their ranks among the 10 possible large scale variables are given as well (1 still indicating the best predictor). Some notable spatial patterns of CRPSS increase and of predictors rankings appear.

As mentioned previously, T850 is by far the best second level predictor for temperature whatever the region. Nevertheless, its prediction skill is stronger for regions far from the influence of the Atlantic Ocean. TCW, as second best predictor, shows large spatial differences with higher CRPSS gains for northern regions. For radiation, the best scores are mostly achieved with T-Td and to a less extend with RH1000 & RH700. For each predictor clear dependencies on the latitude and the distance to the Atlantic Ocean are discernible with smaller gains in central Mediterranean and continental European regions. The relative humidity at 400hPa is in most cases weakly informative with the remarkable exception of Tunisia. This region has numerous cloud-free days on one hand, and on the other one, greater proportions of high altitude clouds than low and mid-troposphere ones as a consequence of its subtropical and Mediterranean climate. The 400hPa relative humidity is the most relevant second-level predictor to catch the occurrence of cirrus and other high level clouds. This could explain the relatively high performances of this predictor but this hypothesis would require further investigation to be validated.
The CRPSS of temperature range are mainly improved by T-Td and the lowest levels of relative

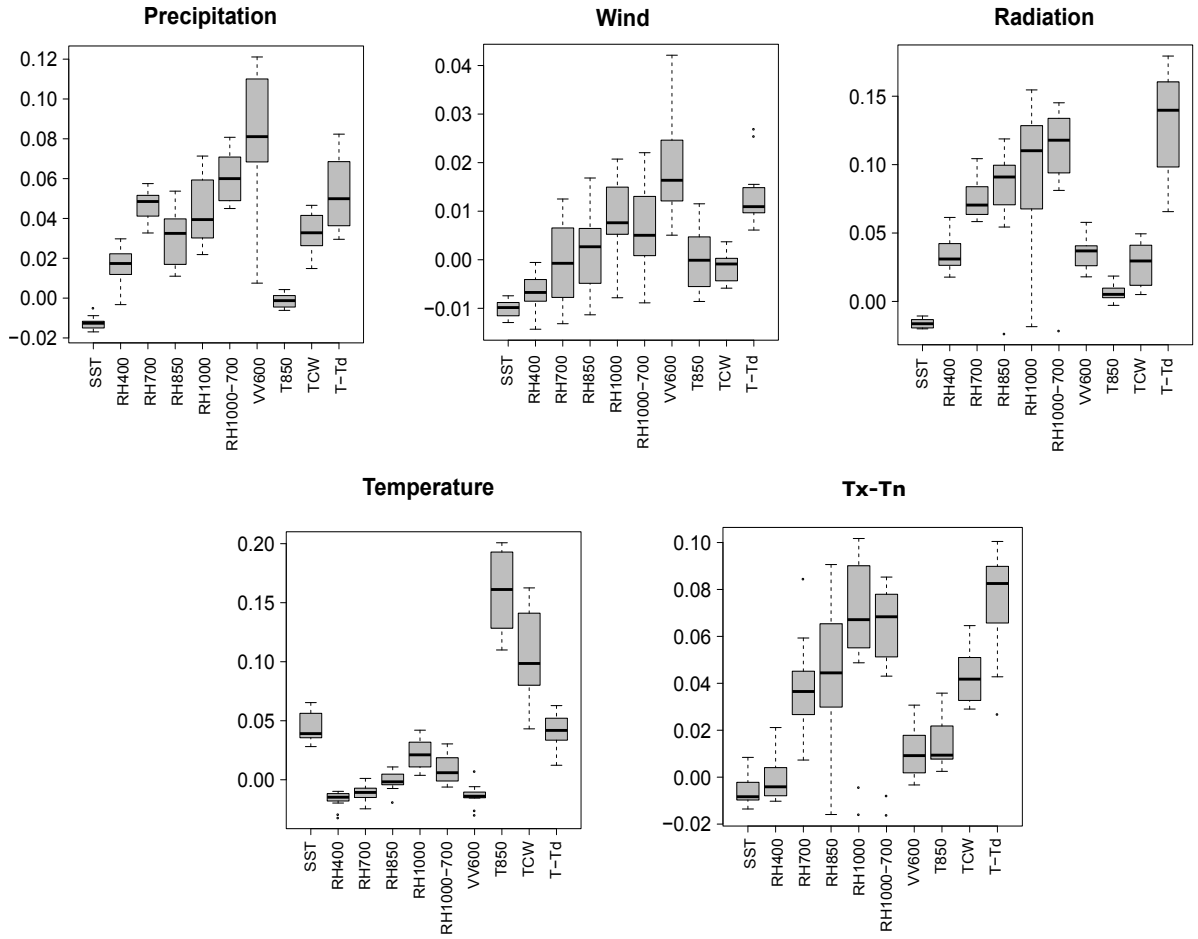

Figure V.3 – Predictand specific models. CRPSS gains obtained with the introduction of different predictors in a second analogy level. Each boxplot gathers changes in CRPSS obtained with the 12 test regions.

humidity. No obvious spatial pattern can be seen on the associated maps.
For both wind and precipitation, vertical velocities, despite their good ranking as a whole, have also some regional dependency. Predictions of precipitation are more accurate using this predictor in Scandinavian regions together with Germany and Italy. Yet, the combination of RH1000 and RH700 gives the best results in the South-eastern regions and Andalusia.
No clear spatial pattern can be put forward for wind, whatever the second level predictor. Furthermore, most of the associated CRPSS gains are small compared to what is achieved for the four other predictands.

For each couple of region and predictand, the best combinations of first and second level predictors are summed up in Tab.V.2. As highlighted previously, despite some exceptions and differences in CRPSS gains from one region to another, the best sets of predictors present a rather important spatial homogeneity over the whole European domain. For radiation and temperature, all regions have the same set of large scale variables with a combination HGT500 and HGT1000 at level one and T-Td or T850 at level 2 respectively. Both wind and precipitation also show a homogeneous selection of first level predictors over the entire continent (HGT1000 and HGT500+1000 respectively), but two predictors share out the 12 regions at the second analogue level. However, in the wind speed

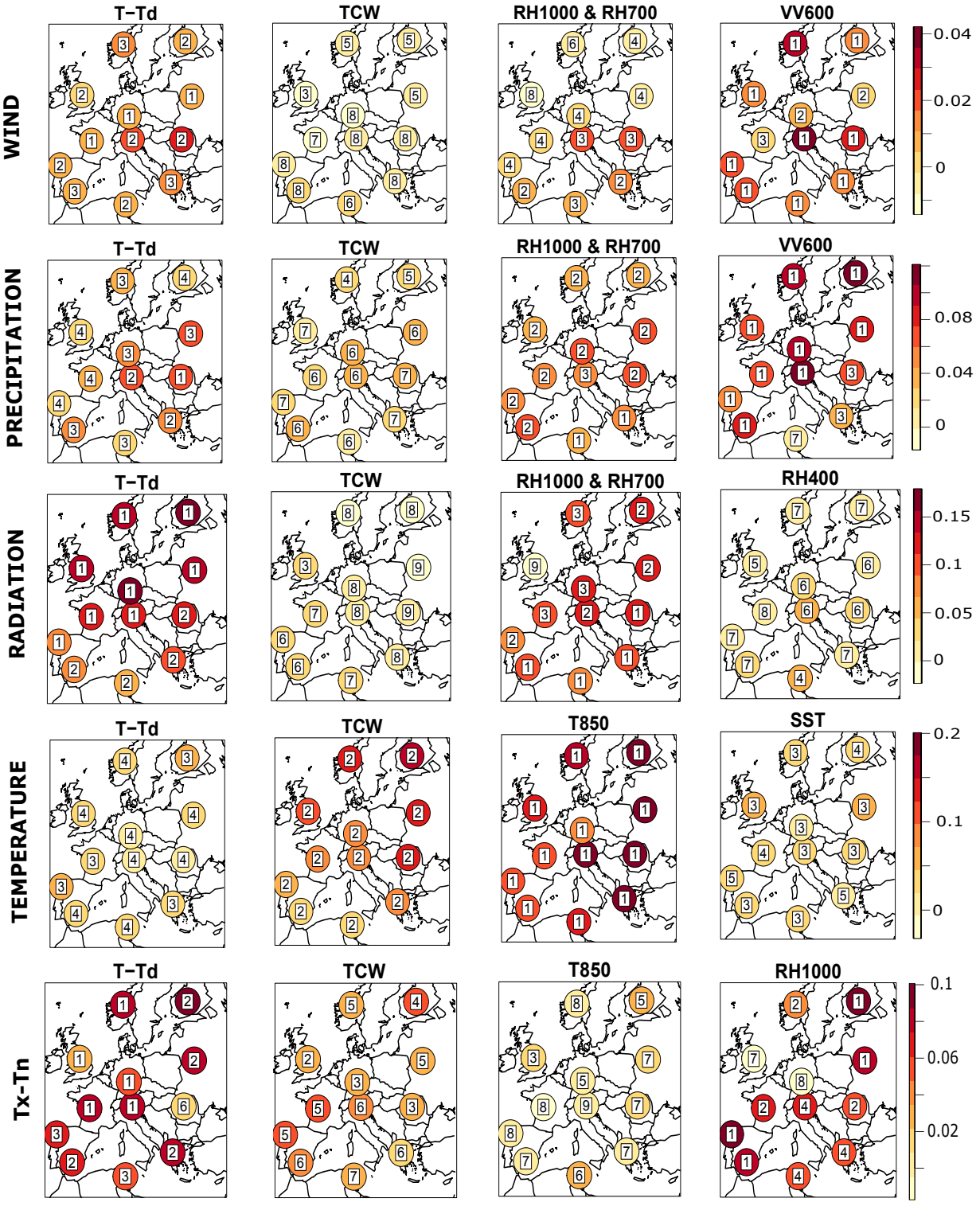

Figure V.4 – Predictand specific models. CRPSS gain obtained for each region with the introduction of different predictors in a second analogy level. Maps are shown for 4 selected predictors out of 10. The CRPSS values are given by bubbles colours. The numbers the numbers give the rankings of predictors (from 1 to 10).

case, the CRPSS gains associated to these two predictors (T-Td and VV600) are similar and low. For precipitation, VV600 does not lead to significantly better CRPSS gains than T-Td except in Norway and Finland. Finally, the temperature range seems to have higher regional differences on the secondary predictor with T-Td being voted in for North Western Europe whereas various levels of relative humidity are picked for the other regions. All in all, despite a large panel of climates across Europe, the same large scale data could be used to predict efficiently local meteorological variables.

1.4.2. Single analogue models

As mentioned in Sec.1.3, single analogue models have been optimised (predictor, analogue domain) following the same process as for the single-predictand approach but used the multivariate prediction skill as optimisation score. To make both predictand-specific and single-model approaches comparable, we present here the univariate prediction skills of the single-model approach obtained with different predictor sets.
In the single-model approach, the optimal predictor set is not found to depend on the region (Tab.V.2). It always gathers HGT500 and HGT1000 for the first analogy level and T-Td for the second one. Responding to the results obtained with the predictand-specific models, T-Td is actually the only predictor having a positive and significant impact on the CRPSS for all predictands (T-Td is almost always among the 4 best predictors as shown in Fig.V.4). Thus, the predictor set based on HGT500, HGT1000 and T-Td provides the best combination of information needed by each regional variable.
For most predictands, the prediction skills achieved with the best single analogue model is significantly lower than the ones obtained with the predictand-specific method. Fig.V.5 presents the CRPSS differences between both approaches.

For temperature, CRPSS decreases make sense because the single-model does not use information on low troposphere temperature anymore but only information on its distance to saturation. Decreases present also strong spatial contrasts, with higher drops in Eastern Europe. The further the region is from the Atlantic Ocean, the smaller the differences between the two methods.
CRPSS losses range from 0.07 to 0.12 for wind. The differences are here due to the introduction of the geopotential height at 500hPa in the first analogy level. As already discussed, this information is irrelevant for wind speed at 10m whose variability relies on low troposphere geopotential gradient. CRPSS losses are slightly smaller in South Eastern Europe.
For radiation, all single and predictand-specific models have the same set of predictors whatever the location. However, some very small differences in CRPSS can be seen for some regions. It is only due to the slight shifts in the position of the analogy domains from the predictand-specific case to the single-model one. The same comments can be made for temperature range for which T-Td was already selected for 5 out of 12 regions in a predictand-specific approach. This predictor still gives a large improvement of the CRPSS for the other test areas. There are more regional variabilities for precipitation. For regions where VV600 was selected as the best second level predictor in the precipitation specific models, CRPSS losses are significant, especially in Scandinavia. Nevertheless, for any other region, the best second level predictor, namely RH1000 & RH700 provide similar information

Table V.2 – List of predictors selected at first and second levels of analogy in a predictand-specific approach for each region and each predictand together with results of single-models (multivariate).

	Sun Radiation		Wind		Temperature		Precipitation		Tx-Tn		Multivariate	
	Level 1	**Level 2**	**Level 1**	**Level 2**	**Level 1**	**Level 2**	**Level 1**	**Level 2**	**Level 1**	**Level 2**	**Level 1**	**Level 2**
EN	HGT500 HGT1000	T-Td	HGT1000	VV600	HGT500 HGT1000	T850	HGT500 HGT1000	VV600	HGT500 HGT1000	T-Td	HGT500 HGT1000	T-Td
NO	HGT500 HGT1000	T-Td	HGT1000	VV600	HGT500 HGT1000	T850	HGT500 HGT1000	VV600	HGT500 HGT1000	T-Td	HGT500 HGT1000	T-Td
FI	HGT500 HGT1000	T-Td	HGT1000	VV600	HGT500 HGT1000	T850	HGT500 HGT1000	VV600	HGT500 HGT1000	RH1000	HGT500 HGT1000	T-Td
FR	HGT500 HGT1000	T-Td	HGT1000	T-Td	HGT500 HGT1000	T850	HGT500 HGT1000	VV600	HGT500 HGT1000	T-Td	HGT500 HGT1000	T-Td
GE	HGT500 HGT1000	T-Td	HGT1000	T-Td	HGT500 HGT1000	T850	HGT500 HGT1000	VV600	HGT500 HGT1000	T-Td	HGT500 HGT1000	T-Td
BE	HGT500 HGT1000	T-Td	HGT1000	T-Td	HGT500 HGT1000	T850	HGT500 HGT1000	VV600	HGT500 HGT1000	RH1000	HGT500 HGT1000	T-Td
GA	HGT500 HGT1000	T-Td	HGT1000	VV600	HGT500 HGT1000	T850	HGT500 HGT1000	VV600	HGT500 HGT1000	RH1000	HGT500 HGT1000	T-Td
IT	HGT500 HGT1000	T-Td	HGT1000	VV600	HGT500 HGT1000	T850	HGT500 HGT1000	VV600	HGT500 HGT1000	T-Td	HGT500 HGT1000	T-Td
RO	HGT500 HGT1000	T-Td	HGT1000	VV600	HGT500 HGT1000	T850	HGT500 HGT1000	RH700 RH1000	HGT500 HGT1000	RH700 RH1000	HGT500 HGT1000	T-Td
AN	HGT500 HGT1000	T-Td	HGT1000	VV600	HGT500 HGT1000	T850	HGT500 HGT1000	VV600	HGT500 HGT1000	RH1000	HGT500 HGT1000	T-Td
TU	HGT500 HGT1000	T-Td	HGT1000	VV600	HGT500 HGT1000	T850	HGT500 HGT1000	RH700 RH1000	HGT500 HGT1000	RH700 RH1000	HGT500 HGT1000	T-Td
GR	HGT500 HGT1000	T-Td	HGT1000	VV600	HGT500 HGT1000	T850	HGT500 HGT1000	RH700 RH1000	HGT500 HGT1000	RH850	HGT500 HGT1000	T-Td

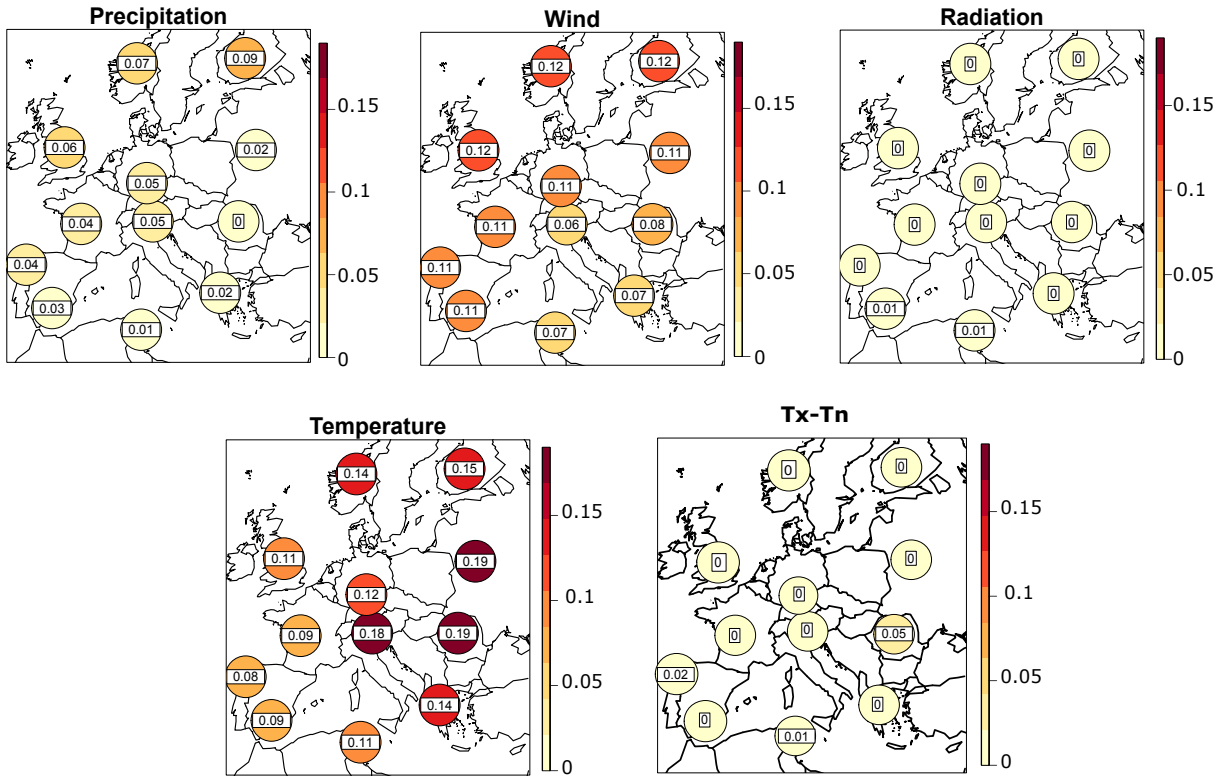

Figure V.5 – Single models. CRPSS losses when a single analogy model is used instead of each predictand-specific model. The single analogy model is region specific.

as T-Td. CRPSS decreases are therefore small to very small in most configurations (e.g. in Tunisia, Greece and Romania).

1.4.3. Inter-predictands correlations

The comparisons in the previous section show that significant drops in prediction skill occur when using the single-model approach rather than the predictand-specific one. It is particularly true for wind and temperature which cannot be efficiently simulated without their specific large scale predictors. Thus, the predictand-specific approach is potentially more appealing. However, the physical consistency of multivariate predictions in this configuration is potentially degraded in comparison to the single-model approach.

We further assess the ability of the two strategies to simulate multivariate predictions with correct temporal correlations between predictands. For each pair of predictands (e.g wind-precipitation), we estimate the Pearson correlation coefficient first from observed time series (or pseudo-observed for wind), and then from the predicted time series (generated from either the predictand-specific or the single-model strategies). For each predictand, the seasonal component is removed before estimation using a 30-day moving climatology.

Simulated correlations are presented as a function of observed correlations for winter and summer seasons on Fig.V.6. The X,Y extents of dots (or rectangles) correspond to the 95% confidence intervals of observed and simulated correlation coefficients respectively. The closer to the 1:1 bisector

a dot is, the better the performance of the model to reproduce the "observed" correlation. When the confidence intervals of a given configuration (region, season and downscaling model) include the 1:1 bisector, the simulated correlation can be considered as a good estimate of the observed one. As expected, this is achieved by the single-model approach for fairly all predictands pairs in all regions and for all seasons. A noticeable exception is for the "temperature-radiation" pair in winter. The predictand-specific approach yields contrasting results. It fails to reproduce observed correlations for most configurations except those where temperature is involved. With this approach, observed correlations are globally underestimated (the blue dots and rectangles are nearly always between the x-axis and the 1:1 bisector). If it exists, the seasonal change in correlation sign is however rather well reproduced (e.g. for all pairs involving temperature).
Generally, the single-model approach performs thus better than the predictands-specific one for most pairs of predictands, whatever the region and the season. Considering the 95% confidence intervals, the differences in performance between both approaches are particularly high for the pairs of variables for which T-Td was found to be a good second-level predictor in a predictand-specific approach (i.e. precipitation, radiation and temperature-range). This applies also in winter to wind/precipitation, wind/radiation, wind/Tx-Tn and Tx-Tn/temperature in most regions. The differences between both approaches are much lower but still important for the other configurations except for the pairs involving temperature. In these cases, both approaches show rather similar performances in one or both seasons. The unique configuration for which the predictand-specific method outperforms the single-model one is the temperature/radiation pair in winter.

1.5. Discussion and Conclusions

1.5.1. Toward a hybrid downscaling approach

As shown Sec.1.4.1, predictand-specific models lead to higher CRPSS for the univariate prediction of all surface variables. For temperature and wind, their prediction skills are much higher than that achieved using the single-model approach. On the other hand, a suite of predictand-specific models is not able to correctly simulate the correlation observed between some predictands pairs, especially the three involving precipitation, radiation and temperature range.
These complementary results suggest that a hybrid approach could gather the advantages of both single and predictand-specific models.
In Sec.1.4.3, we discussed the correlation coefficients of the predictands pairs involving wind. The single model approach presented slightly better results for the correlations between wind/radiation and wind/temperature range. However, the important CRPSS drop (of about 0.1) obtained for wind prediction tips the scales in favour of a wind specific model. The wind specific model could only rely on the first analogy level (with a single HGT1000 predictor), as the second level of analogy does not lead to significant CRPSS gains.
For precipitation, radiation and temperature range, the single-model approach is much better at reproducing the inter-predictand correlations. Luckily, the CRPSS between the single-model and the predictand-specific models are very similar for the three predictands (apart for precipitation in the Scandinavian regions). Consequently, a single-model seems to be a reasonable choice for these variables (a 2 level model with HGT500+1000 for the first level and T-Td for the second).

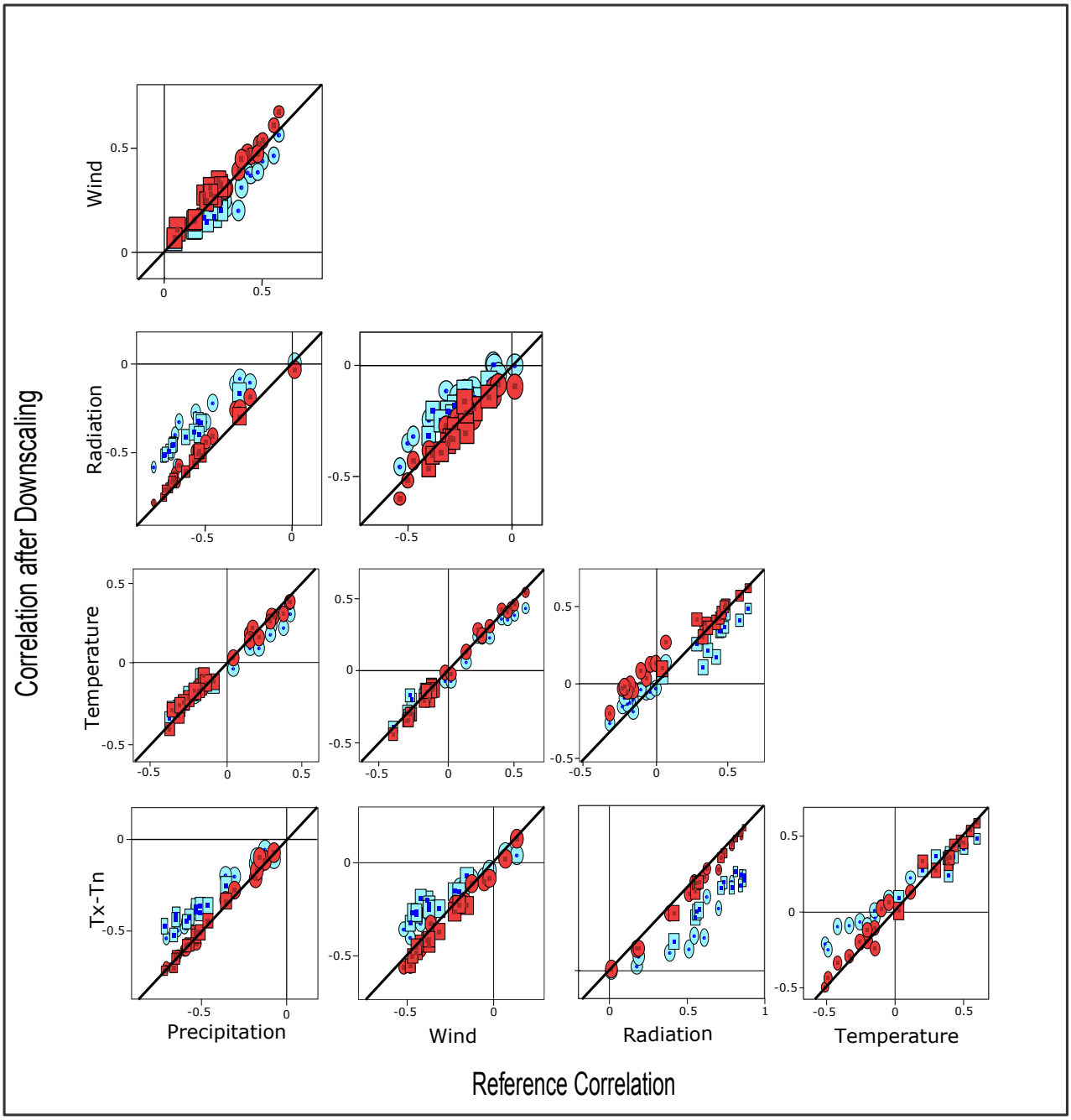

Figure V.6 – Scatterplots of seasonal Pearson correlations for each predictands couple in reference data (X axis) and in downscaled regional series (Y-axis). Blue colour (light grey in the black and white version of the paper) corresponds to downscaled time series obtained with predictand specific models and red colour (dark grey in the black and white version) refers to downscaled time series obtained with the single analogue models. Correlations are obtained from times series of daily variables for all days in the winter season (winter (DJF) correlations, ellipses symbols) and for all days in summer season (summer (JJA) correlations, rectangle symbols). The size of a given ellipse (respectively rectangle) corresponds to the 95% confidence interval of the correlation coefficient estimation. Each confidence interval is obtained via MonteCarlo simulations (for observations, the confidence interval is obtained from the 2.5th and 97.5th percentiles of correlation coefficients estimated from 10000 multivariate time series, generated from observed time series using bootstrapping with replacement. Confidence intervals of correlation for multivariate downscaled series (with either the predictand specific models or the single models) are obtained in the same way.

For temperature, the predictand-specific approach gives much higher CRPSS (about +0.14). However, the single-model approach reproduces some inter-variables correlations much better, especially for the temperature/radiation pair in summer and for the temperature/temperature range pair in winter. No entirely satisfying modelling option seems possible. Giving priority to the univariate prediction skill (and thus choosing a predictand-specific approach) would be detrimental to the reproduction of some correlations involving temperature and vice versa.

To tackle this temperature issue, we evaluated an additional modelling approach similar to the one presented in [Kuentz et al., 2015]. This method uses temperature predictions made by the single-model approach which are corrected according to some large scale temperature information thereafter. More precisely, for each prediction, the correction factor applied to the temperature predictions of the single-model approach is the difference between the large scale values of T850 on the target day and on analogue one. For instance, considering that the 850hPa temperature is 8°on the target day and its current analogue is much warmer with 10.5°, the local temperature prediction at the surface is lowered by 2.5°. This approach is expected to modify at the same time the temperature prediction skill and all inter-variable correlations involving temperature. It actually achieves CPRSS scores similar to those of the predictand-specific approach for all regions, thus outperforming the single-model approach (Fig.V.7). It also allows good reproduction of inter-variable correlations for most seasons and regions and for both temperature/wind and temperature/precipitation pairs (Fig.V.8). In the "temperature-temperature range" case, observed correlations are slightly underestimated but the distances to the 1:1 bisector are small and in all cases much more reasonable than those of the predictand-specific approach. Additionally corrections do not significantly worsen the correlations simulated with the single-model approach. The acceptability of the hybrid model with correction is more questionable in the "temperature-radiation" case where the distances to the 1:1 bisector are rather high, especially in winter, thus calling for further model refinements.

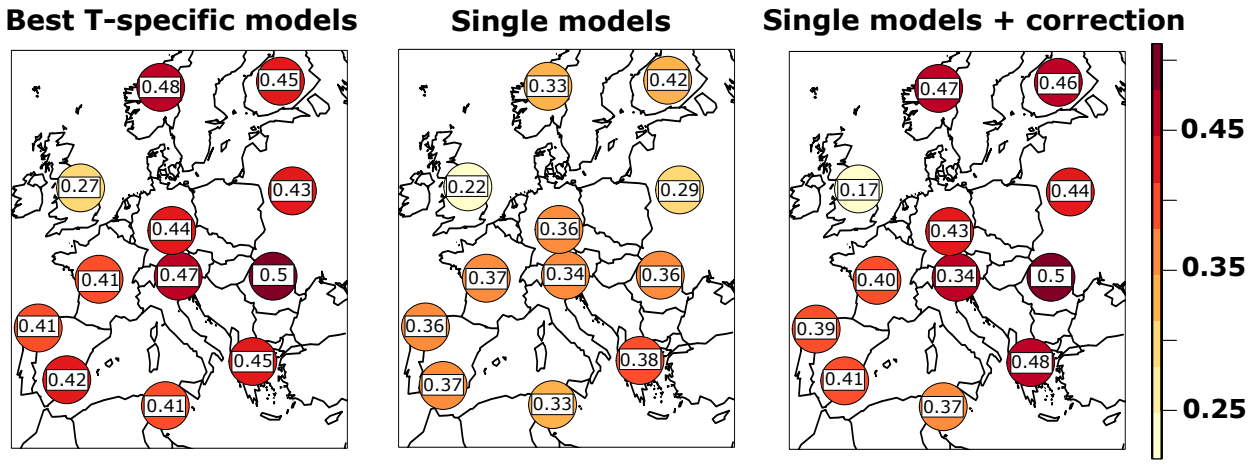

Figure V.7 – Temperature correction. Final CRPSS for the temperature predictand of T-specific models (based on HG500 & HGT1000 and T850 predictors), single models (based on HG500 & HGT1000 and T-Td predictors) and single models to which is applied a correction of temperature (the correction is based on large scale 850hPa temperature difference between the target day and the analogue one).

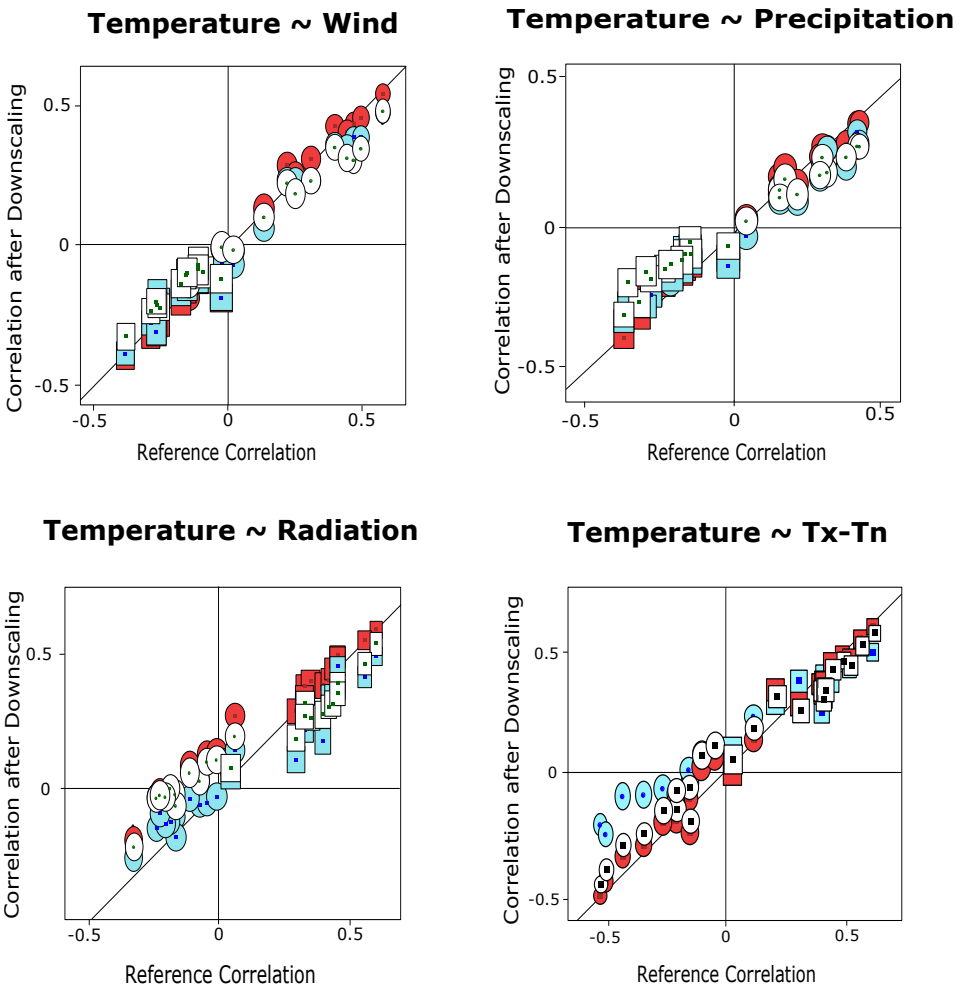

Figure V.8 – Scatterplots of seasonal Pearson correlations between temperature and the three other predictands in reference data (X axis) and in downscaled regional series (Y-axis). Blue (light grey): downscaled time series obtained with predictand specific models; red (dark grey): downscaled time series obtained with the single analogue models; white: downscaled series obtained from the single analogue models with a correction of temperature. See Fig.V.6 for captions details.

1.5.2. Some limits and perspectives

The main features of this hybrid downscaling model are summarized in Tab.V.3. As highlighted from the different results presented above, this model seems satisfactory in Europe for simulating physically consistent multivariate weather scenarios with reasonable prediction skills for all predictands. For a given local variable, there are few differences in the final sets of predictors from one region to another. Thus, the model could rely on the same large scale information for the entire continent without damaging the prediction skills too much. Of course, these results were obtained for a few regions and some spatial disparities may be revealed with a continuous spatial scanning of local weather conditions in Europe. Furthermore, the reasonable prediction scores achieved across the continent may significantly differ in other parts of the world. These results are probably non-transferable and the associated prediction skills would be lower particularly where local weather

Table V.3 – Proposition of combination of predictand-specific and single models compromising requirements of having high CRPSS and relevant inter-variables Pearson correlations.

Predictand	Downscaling type	Predictors Level 1	Predictor Level 2
Temperature	Single models	HGT500 HGT1000	T-Td (T850 used for correction)
Wind	Wind-specific	HGT1000	-
Precipitation	Single models	HGT500 HGT1000	T-Td
Radiation	Single models	HGT500 HGT1000	T-Td
Tx-Tn	Single models	HGT500 HGT1000	T-Td

conditions are driven by small scale atmospheric processes such as convection in tropical zones.

Another issue is related to the hybrid dataset supporting these analyses. Gridded observations were available for temperature, precipitation and radiation but not for wind for which model data were used as pseudo-observation instead. Wind outputs from numerical models have the strong advantage to produce pseudo-observations which are continuous over large spatial domains where few or in some cases no wind measurements exist. They are however obviously not an ideal surrogate to observations. In the present case, the medium resolution of WRF simulations induces for instance a rough representation of the European topography and consequently of its local effects on wind speed and direction. When compared to observations from the ISD-LITE data base [Smith et al., 2011], WRF wind is found to give a reasonable estimate of surface wind for a number of locations in Europe [Vautard et al., 2014]. In the present work, the covariability obtained between the WRF wind simulations and the other weather observations, used as a reference for inter-variable correlations, can be however rather different from the actual one. This limitation is mainly affecting mountainous areas as presented in Annex.A. Consequently, our results involving wind must be put into perspective for regions that suffer from the rough WRF topography. The dependence of the results to the model or to its parametrisation would be worth investigating in the future. A more accurate analysis could also be achieved with a higher resolution model.

All in all, our work highlights the necessary compromise that has to be agreed on between good prediction skills and relevant reproductions of the inter-variable correlations. If such an analogue based model has to be developed and applied, the most relevant model configuration is expected to be highly dependent on the type of application for which the weather scenario will be used. The final hybrid-model with correction that we propose here sacrifices some inter-variables correlations (e.g. wind-TxTn and wind-radiation in summer) in order to achieve much higher CRPSS. Room for model improvement obviously exists. An option could be a complete optimization of the method, on the individual prediction skill for each variable and on the reproduction of covariability between variables simultaneously. Similarly other or additional predictors could be included in the predictor sets. Finally, the number of analogues dates retained for the prediction was set arbitrary to the optimal numbers found for precipitation prediction by Daoud et al., 2016. Re-optimising these numbers for each predictand could also lead to some further improvements. The hybrid approach with correction would allow generating relevant regional scenarios of multivariate weather for the last decades or century based on the recent atmospheric reanalyses. Following for instance Kuentz et al., 2015

and Lafaysse et al., 2014, it would allow exploring the multiscale variability of a number of regional hydrometeorological variables resulting from the large scale variability of climate. Another application could be the generation of regional weather scenarios until the end of the 21st century using GCMs data. Such an application raises different issues which were not considered in the present work. First, the quality of the selected predictors in the climate models is not guaranteed. GCMs do not necessary correctly simulate all predictors and this would have to be checked [Timbal et al., 2009]. In our case, a good performance of climate models is expected for the geopotential fields shapes but not necessarily for the thermodynamic predictors, either at the surface (e.g T-Td) or at given geopotential levels. Secondly, the temporal transferability of the model is also questionable. To be applied in a changing climate context, the physical relationship between predictands and predictors has to be assumed stationary. This assumption does not probably hold or would require further validations. In our case, the first analogy level is only based on shapes and gradients of geopotential fields. This is obviously in favour of the relevance of these predictors in a warmer climate. Similarly, using T850 as a correction factor rather than as a classic secondary predictor should prevent from being limited by the range of observed values of this large scale parameter. Finally, T-Td, which could be assimilated to a relative humidity predictor, would be less sensitive to a changing climate than other water content parameters such as specific humidity or TCW. In any case, the selection of the best predictors for a climate change application would require evaluating the temporal transferability of the model. If such an evaluation is rather impossible to carry out from observations as they do not cover the whole range of possible future climates, it can be carried out in "perfect model" framework as proposed by Dayon et al., 2015.

1.6. Appendix S1. Identification of the best analogy window for a given predictand / region configuration

For each combination of predictand and region, the analogue model with the best prediction skill is searched for among a large number of analogy models. They are characterized by their predictors set and their associated analogy windows (shape, size and positioning). We here describe the procedure used to identify the best analogy window for a given predictor.

1.6.1. Size and shape of the analogy window

When a single geopotential height is used as predictor (either 500, 700 or 1000hPa), 9 different analogy window types, with 3 different shapes (rectangular shape with a EW orientation, with a NS orientation and square shape) and 3 different sizes for each shape (small, medium and large with, for instance, extensions of 6°, 12°and 22.5°for the square shape) were tested. For the configuration where both 500 and 1000hPa are used as predictors, we additionally considered 6 other options for which where the analogy windows at 1000hPa are twice smaller than the ones at 500hPa. For secondary predictors, we only tested the 3 smallest analogy domains (with 2 rectangular and one square shapes) as a consequence of the much smaller information of thermodynamic predictors to be captured compared to the one of HGT.

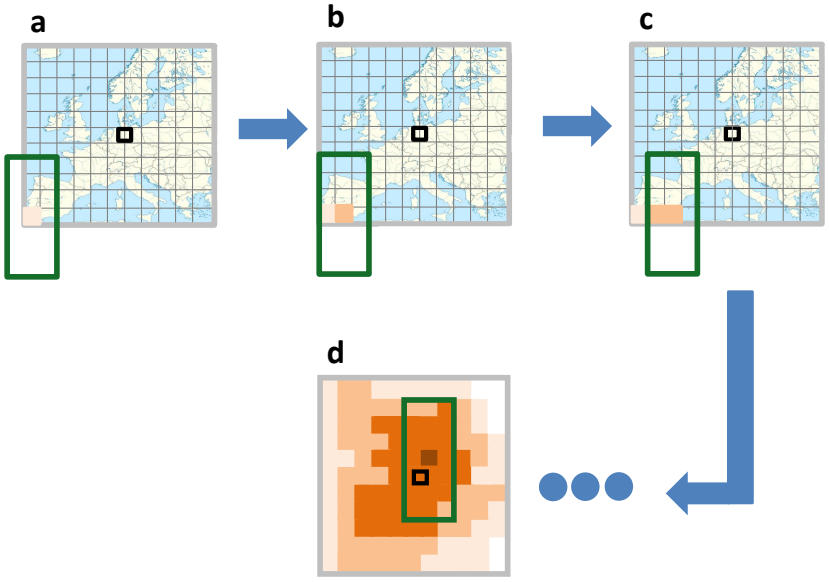

Figure V.9 – Scanning process used to identify the best position of a given analogy domain (large rectangle) with fixed shape and size for a given large scale predictor (e.g. HGT1000 predictor with a 4.5° Lon ·9° Lat extent). The skill score obtained with each analogy domain is plotted on the skill score map (map d) at the grid cell which coordinates corresponds to those of the central point of the analogy domain (see e.g. the scores obtained successively for three consecutive steps of the scanning process with three different domains represented respectively in maps a, b and c). The best position of the analogy domain, ie the one that maximizes the prediction skill score, corresponds to the dark orange pixel on the colour map d

1.6.2. Optimal positioning of the analogy window

For each predictor, predictand, and target region, a given analogy window type is evaluated at all possible positioning over Europe in order to find the one that leads to the best prediction skill. For the first analogy level, the geographical area under scanning largely covers the European continent (longitudes from -60°to +60°East, latitudes from +15°to +85°North) in order to catch some large meteorological patterns that are far from the target region but might still influence it. For all second level predictors except SST, the geographical area under scanning is much smaller (15°in longitude and latitude) and is centred on the target region as most of the predictors are thermodynamic. Fig.V.9 illustrates the process retained to optimize the positioning of a given analogy window. All central points of the analogy domain that are possible according to the ERA-Interim grid (grey grid) are considered in turn and used for the prediction of the current predictand (e.g. precipitation) in the target region (central bold square). For a chosen size and shape, the scanning procedure consists in placing the analogy window at a corner of the scanning area, and computing the associated skill score. The window is then shifted according to the predictor dataset grid and the skill score is computed once again. The procedure is repeated until the whole scanning area is evaluated. The best position of the analogy window is simply the one maximizing the skill score. For all region, predictand and predictor combinations, the most skilful shape and size of the analogy window is finally kept. This process was carried out successively for both analogy levels.

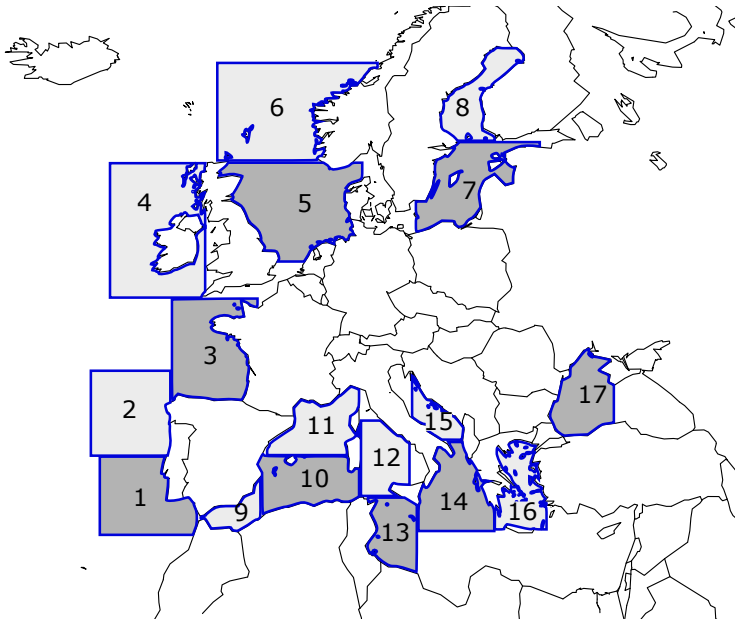

Figure V.10 – The seventeen maritime domains used for the sea surface temperature predictor. For each target region and each predictand variable, the domain retained for SST as predictor is the domain that gives the best CRPSS score of the prediction.

For SST, we more simply tested the predictive skills of 17 analogy domains corresponding respectively to different zones of the Atlantic Ocean and of the Mediterranean, the Baltic, the Black and the North Seas (Fig.V.10). The domains have been constructed to gather information from areas as homogeneous as possible (eg. Bay of Biscay, Aegean Sea, North Sea, northern and southern Baltic Sea...).

2. Complementary evaluation

In Sec.1, we proposed a hybrid analogue downscaling method (SCAMP) that compromise satisfactory prediction skills and inter-predictand correlations in our 12 test regions. It combines a predictand-specific model for wind and a common set of predictors for precipitation, temperature, radiation and temperature range (c.f. Tab.V.3). Here, we provide some complementary information on the parametrisation of SCAMP. We also perform an additional evaluation of the seasonal cycles and inter-annual variability of simulated predictands.

2.1. Regarding the analogy domains

Previously, we discussed the procedure of optimisation of the analogy domains. The final windows used in the hybrid downscaling approach (Tab.V.3) are presented in Fig.V.11.
Firstly, the downscaling of precipitation, temperature and radiation is done using the combination of HGT500 and HGT1000. For all regions, the most relevant choice consists of a large window at 500hPa and a medium one at 1000hPa, which catch both mid-troposphere large meteorological patterns and smaller structures near the surface. The windows orientation often attaches more importance to the meridian gradient of geopotential (except in RO, AN, TU and GR where both component are equally

represented). The analogy windows are generally well-centred on the target regions. However they have a slight tendency to gather more information south-westward.
Wind is downscaled with its own set of predictors. A single level of analogy, using HGT1000 as predictor, seems to be sufficient to have relevant series of regional wind. For all regions, the smaller analogy windows give, by far, the best results. Like for the HG500-HGT1000 combination described previously, most windows are West-East oriented or with a square shape. They are also well centred over the target region, underlying again the strong relationship between local wind and geopotential gradient.
For the second level of analogy, only small windows were tested. Here again, the optimal windows have either a square shape or are West-East oriented. In some cases, the window is not centred on the region of interest and tends, when it is possible, to get information about near-surface humidity over the Ocean or the Mediterranean sea (GA, AN, TU and GR).

2.2. Multi-scale variability of downscaled series

The evaluation presented in Sec.1 proved that SCAMP is able to simulate accurate daily values of univariate predictand and correct inter-predictands correlations. However, some further validation of the predictands series are required to ensure that both simulated hydrological and power generation series will have correct and relevant characteristics for this study. We illustrated in Chap.II and Chap.III that the inter and intra-annual variations of CRE sources are a key element to the integration of renewables in Europe. To complement the previous evaluation of the hybrid downscaling method on this point, we will present the seasonal cycles and annual time series of the four meteorological drivers (precipitation, temperature, wind, sun radiation). In addition, the same information will be provided for hydrological cycles and the inter-annual variability of river discharge which shape the hydro power generation. It also constitutes another way of validating the inter-predictands co-variations as physically inconsistent multivariate weather scenarios would result in inaccurate hydrological simulations. This complementary evaluation was performed for all 12 regions, 4 meteorological predictands and simulated river discharge. We only present an inner group of the associated results for 3 representative regions (NO, GE and AN).

Fig.V.12 shows the mean annual time series of daily observed (or pseudo-observed - Wind speed) predictands from 1983 to 2012. The simulated mean annual series (blue line) and the dispersion between downscaled series (10^{th} and 90^{th} percentiles of the 50 regional scenarios - blue shade) are also presented.

- For all regions the annual variations of precipitation are well simulated by the hybrid downscaling method. Unusual dry or wet years are equally well reproduced. The inter-scenarios dispersion is rather constant for the entire period and seems to be more important (about 0.5mm/day) in Northern regions.
- The performances of the downscaling method are remarkable for temperature. Whatever the region and its associated climatic conditions, simulated yearly variations in temperature always agree with observed ones. The 50 downscaled scenarios are very similar to each other and the small scale dispersion is weak.

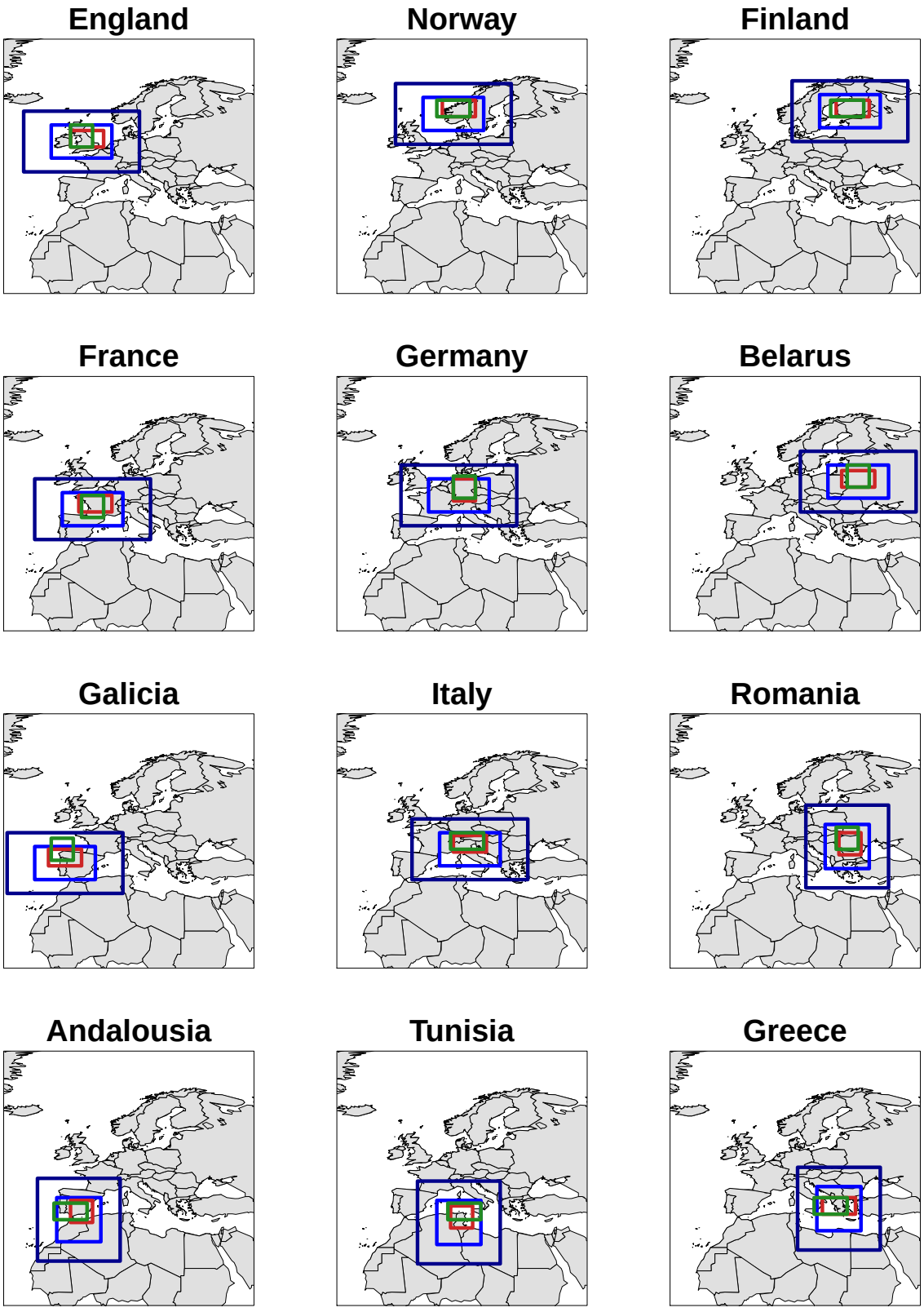

Figure V.11 – Final analogy domains used in the multi-variate downscaling method optimised and presented in Sec.1. The predictors used for the simultaneous downscaling of Precipitation, Temperature and Radiation are: HGT500 (dark blue), HGT1000 (blue) and T-Td (green). Wind is downscaling independently thanks to HGT1000 (red).

- The confrontation between observed and simulated wind series proved that the downscaled wind has a correct inter-annual variability whatever the region of interest. However, it also highlights a small positive bias in wind speed (of about $0.3m \cdot s^{-1}$ maximum) in north-western European regions (EN and NO being the most affected).
- Sun radiation inter-annual variability is well simulated by the hybrid downscaling. The 50 regional scenarios are close to each other and their dispersion usually represents from 5 to 10% of the observed mean daily sun radiation.
- Finally, river discharge shows a higher inter-scenarios dispersion as a direct consequence of the results presented for precipitation. However, the simulated mean annual discharge is of the right magnitude and both low and high flow years are correctly simulated.

High and low daily values of predictands are also an important feature that must be accurately simulated by the hybrid downscaling method. Indeed, they indirectly drive the occurrence of energy droughts or determine how much energy can be stored when storage systems are used for the integration of renewables (c.f. Chap.III).

We compare the seasonal cycles of 10^{th} and 90^{th} percentiles of daily predictands values (30-day moving window) from observations (blue and red lines) and simulated series (green and brown lines) on Fig.V.13. The dispersion between downscaled scenarios, representing the small scale variability (c.f. Chap.IV), is also illustrated thanks to the green and orange color shades. This figure also gives an evaluation of the seasonality of predictands in the simulated series. Results are only presented for NO, GE and AN. Similar comments are also valid for the median cycles of predictands and for other regions.

- The seasonal cycles of precipitation percentiles are correctly reproduced after downscaling. Both simulated and observed 10^{th} percentiles are always at 0mm/day. Similarly, the simulated 90^{th} percentile cycles also have a relevant seasonality, even for regions having a severe dry season (AN).
- The simulated seasonality of temperature is in perfect agreement with observations. Both low and high temperature values have correct annual variations.
- For all regions, the observed 10^{th} and 90^{th} percentiles cycles associated wind speed reach their maximum during winter. Simulated series have the same characteristics. However, despite an almost perfect reproduction of the upper part of the wind distribution, the 10^{th} percentile is slightly overestimated in NO and GE. It reveals that the positive bias discussed on Fig.V.12 is not seasonal and is a consequence of an under-sampling of low wind speed values.
- Annual cycles of sun radiation are rather well simulated by our downscaling method. Nonetheless, some imprecisions exist with a slight underestimation of the 10^{th} percentile in spring in NO and in early summer in AN. SCAMP also tends to flatten the 90^{th} percentile cycles, overestimating the number of high sun radiation values during inter-seasons, especially in southern Europe.
- Finally, the seasonality of river discharge is accurately simulated for both percentiles. Downscaled low discharge periods, either in late winter (NO) or summer (GE and AN) agree with the observed series. In spring, the peak in discharge for snow-dominated catchments has a correct timing even if it is slightly underestimated in the simulated scenarios.

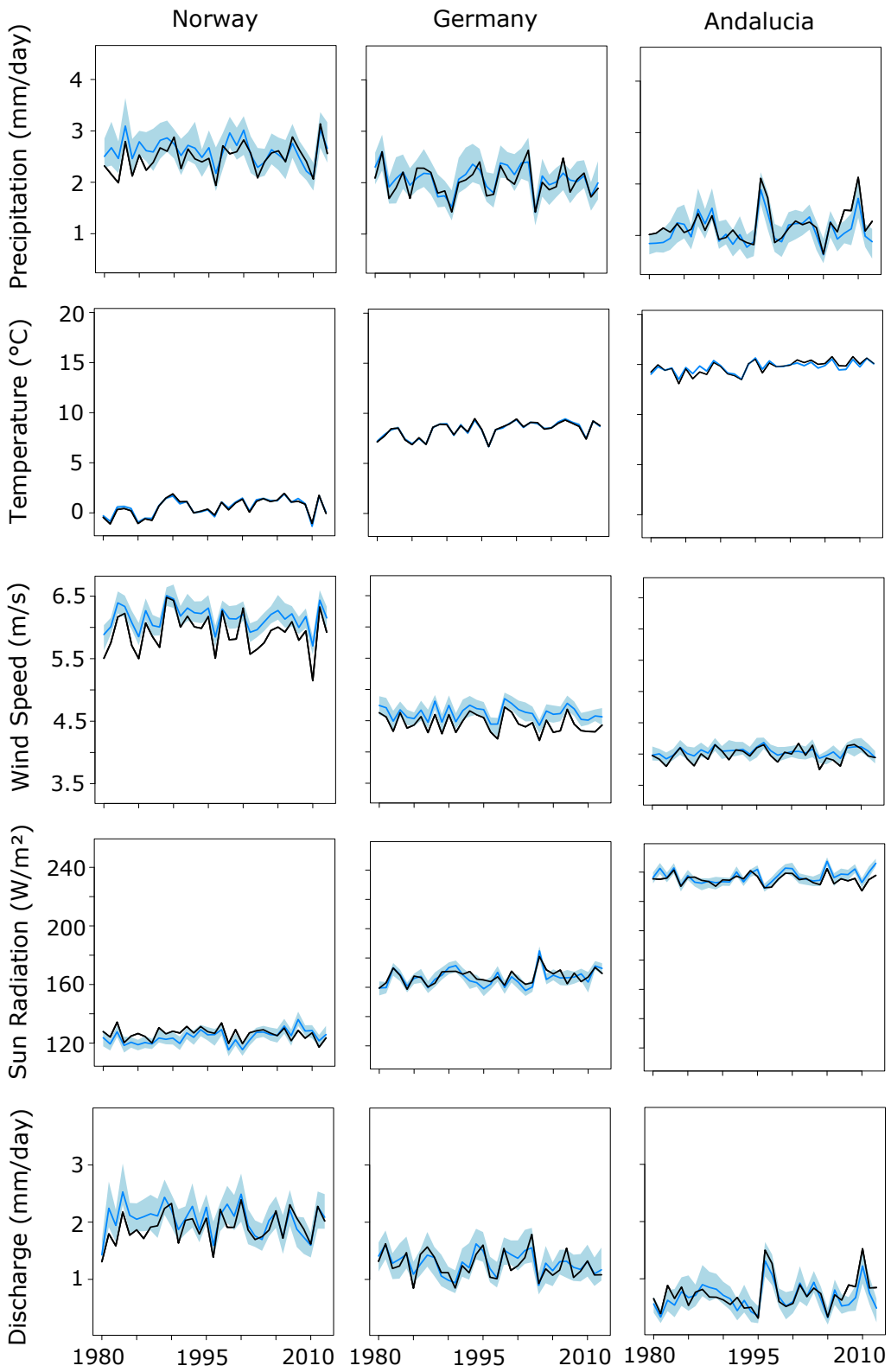

Figure V.12 – **Mean annual values of predictands from 1982 to 2012 in observed series (black) and downscaled ones (blue)**. The inter-scenarios dispersion is display thanks to the light blue shade. The media scenario is displayed in dark blue.

All in all, this complementary evaluation proved that SCAMP is largely able to simulated relevant downscaled series of predictands in terms of daily (10^{th} and 90^{th} percentiles), seasonal (seasonal cycles) and inter-annual variability (annual time series). Using its downscaled simulations seems satisfactory for generation of relevant series of regional power generation.

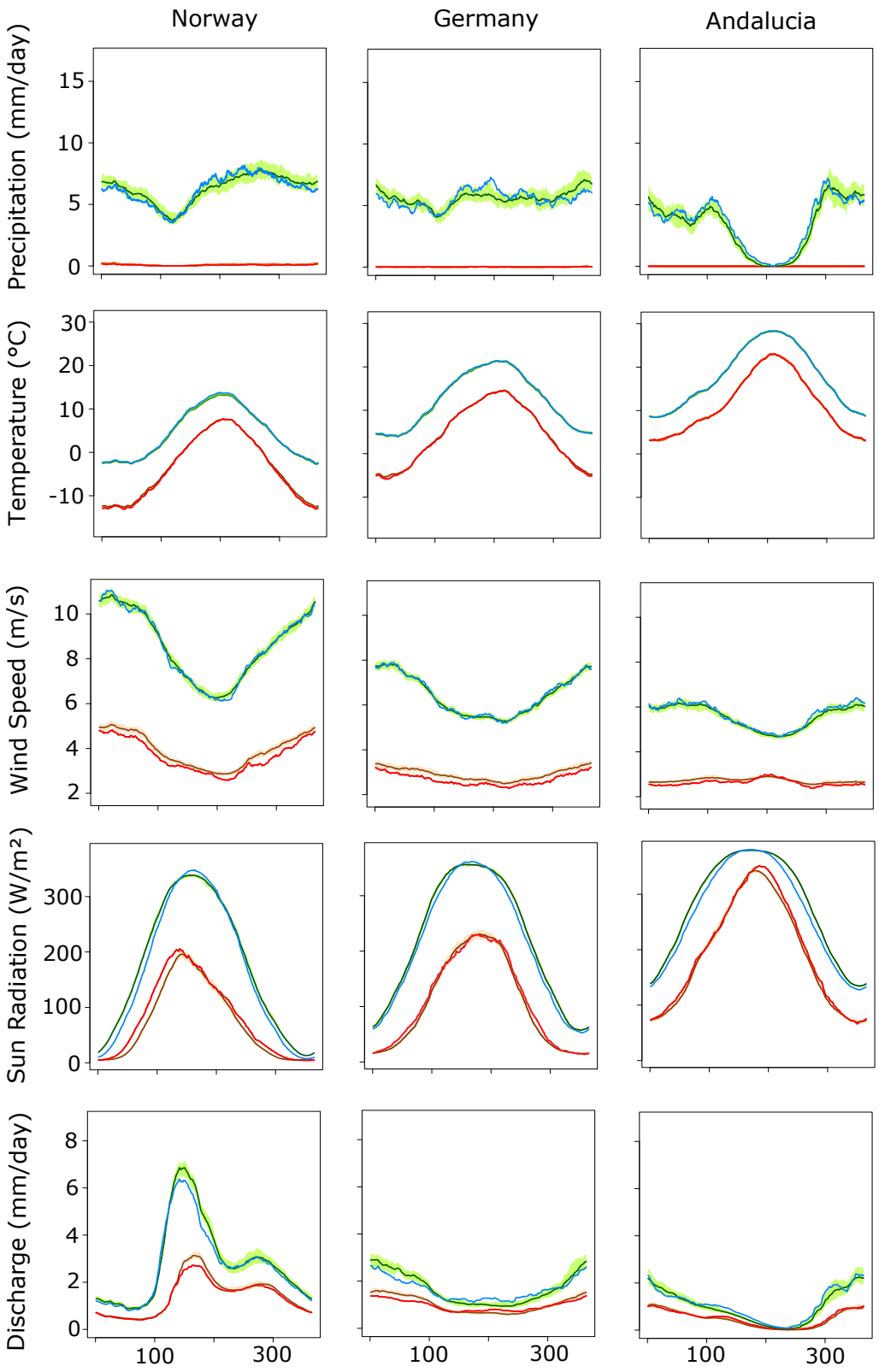

Figure V.13 – **Seasonal cycles of 10^{th} and 90^{th} percentile of daily predictands values from observed series (respectively in red and blue) and downscaled ones (respectively in orange and green)**. The inter-scenarios dispersion is display thanks to the color shading.

Overview

A complete and efficient integration of CRE sources in Europe cannot be done without assessing their past long-term fluctuations and their future trends in a climate change context. Climate reanalysis datasets and GCMs provide meteorological data at low resolution and need to be adapted before being used for the generation of regional series of power production and energy demand. Downscaling methods are usually used to bridge the gap between spatial scales. However, the demanding set of objectives of this study imposes that the downscaled outputs meet the following requirements:

- Relevant daily values of local weather variables
- Correct inter-variables correlations
- Accurate multi-scale fluctuations of weather variables

With such characteristics, the downscaled multivariate weather series should lead to correct regional power generation scenarios and ensure that co-variations between CREs sources are accurately simulated.

Among the numerous existing downscaling methods, the analogue approach seems to be suitable for the simulation of multivariate regional weather series. It requires few assumptions and prior knowledge on the inter-variables relationships. Indeed, sampling simultaneously all variables from the same analogues leads automatically to physically consistent scenarios. However, such an approach runs the risk of deteriorating the univariate skills of the analogue method unless a common set of relevant large scale predictors can be found for all local variables.

We explored, for the 12 test European regions, the possibility of constructing a multivariate analogue downscaling method that would meet the previous requirements. Testing a large number of possible predictors (dynamic and thermodynamic), we compared the performance in terms of prediction skills and inter-variable correlations of predictand-specific and single (i.e. common to all variables) analogue methods. The results call for a hybrid downscaling, SCAMP, which combines:

- A wind-specific analogue downscaling (based on geopotential gradients at 1000hPa)
- A common model for precipitation, radiation, temperature and temperature range (based on geopotential gradients at 500 and 1000hPa and near-surface humidity)
- A post-correction of local temperature (based on large scale near-surface temperature).

The evaluation of the downscaled series of temperature, precipitation, wind, sun radiation and simulated discharge, proved that SCAMP is able to provide relevant meteorological drivers for our study. Energy generation series, computed from the outputs of this analogue method are expected to exhibit correct characteristics in terms of spatio-temporal fluctuations and inter-sources co-variations.

Part IV

LOW FREQUENCY VARIATIONS: RECONSTRUCTION OF THE 20TH CENTURY CLIMATE

Chapter VI

The 20^{th} century climate

Climate is known to fluctuate on various time scales from inter-annual to multidecadal periods. Low frequency variations of climate are likely to impact many sectors including agriculture and power production. In Africa, these fluctuations are responsible for long and severe droughts leading to disastrous harvests during long periods [Rodríguez-Fonseca et al., 2015; Stige et al., 2006; Omondi et al., 2012]. In North America and Europe, their effects on the hydrological cycle and snow-pack have been largely evaluated [Enfield et al., 2001; Irannezhad et al., 2015; Nalley et al., 2016; Hertig et al., 2015].

Low frequency variations are expected to affect CRE sources and their associated power generation. Consequently, the balance between electricity production and energy load is also likely to fluctuate over long periods. In this section, we aim to analyse how meteorological drivers and energy generation series fluctuated in the course of the 20^{th} century. The resulting low frequency fluctuations of penetration rates and characteristics of energy droughts will bring information about the reliability of the analysis performed in Chap.III. It will also illustrate the risks associated to assessing the ease of integration of CRE sources over a relatively short period.

With the recent development and release of climate reanalysis datasets of the 20^{th} century, it is now possible to analyse globally the low frequency variations of a variety of meteorological variables. In this study, these datasets provide gridded data of the large scale predictors required in the hybrid analogue downscaling method presented in Part III. SCAMP was used to reconstruct the regional multivariate weather time series in our 12 test zones. Subsequently, long series of river flow, power generation and penetration rate were generated and analysed in terms of low frequency fluctuations.

1. Reconstruction of the 20^{th} century regional climate conditions

Several 20^{th} century reanalysis datasets of the Earth System have been developed in the last few years. As part of the ERA-Clim project[1] and following the generation of the ERA40 and ERA-Interim datasets, which start respectively in 1957 and 1979, the ERA20C climate reanalysis was produced by the ECMWF. It extends from 1900 to 2010 and has a 1.125° grid (approximately 125 km horizontal resolution). Contrary to the previous datasets, the 4D-Var daily assimilation method only includes surface pressure and surface marine wind data [Poli et al., 2013]. Despite the increasing number of observations during the 20^{th} century, assimilating only pressure and wind data should guarantee on one hand a partial temporal homogeneity of this dataset and on the other hand a correct atmospheric circulation. However, other thermodynamic parameters, for which no supporting information based on observations is assimilated, could suffer from large biases.

The reconstruction of the 20^{th} century regional climate conditions using SCAMP implies extracting all large scale predictors from the ERA20C dataset. In the hybrid downscaling approach that we presented in Chap.V, the second analogy level is based on near surface humidity. SCAMP also requires a post-correction based on large-scale 2m temperature. The questionable quality of these two thermodynamic variables in ERA20C could lead to irrelevant downscaled series of predictands. The assimilation system used in ERA-Interim is much more complete. It includes a large panel of thermodynamic observations. In the following section, we will compare the large scale predictors from ERA20C with the ones from ERA-Interim in order to highlight some possible biases. We will also assess the repercussion of these potentially lower quality data on the reconstruction of regional climate.

1.1. ERA20C large-scale predictors: evaluation and correction

1.1.1. Correction of predictors

Fig.VI.1 presents the seasonal cycle of T-Td in ERA20C and in ERA-Interim for three representative regions (NO, GE and AN). For all regions, large biases exist. In northern regions, the shapes of the seasonal cycles are consistent between the two datasets but ERA20C systematically overestimates the low troposphere moisture (i.e. underestimation of T-Td values). On the opposite, near surface humidity is always underestimated in Mediterranean regions, especially in summer. The amplitude of the seasonal cycles is also too pronounced in these regions. For some locations (e.g. in GE) the sign of the bias changes from winter to summer due to the limited amplitude of T-Td seasonal cycles in ERA20C. These inadequacies between ERA-Interim and ERA20C databases are weaker but still significant for temperature (not shown).

The variety of bias features and their high magnitudes emphasise the necessity of correcting thermodynamic predictors. A bias correction of GCMs outputs is classically applied in climate impact studies (e.g. Ines and Hansen, 2006; Piani et al., 2010; Hagemann et al., 2011). However, the

[1] http://www.era-clim.eu/

correction of multiple variables/predictors is generally not satisfactory. Indeed, a multivariate bias correction is likely to deteriorate the cross-correlations between the corrected variables. Nevertheless, using raw data as inputs of impact models is often considered to be even less relevant, especially when the studied system is non-linear. Thus, we chose to perform a correction of both T-Td and T in ERA20C before using these data as large scale predictors. Many correction methods exist from the simple delta change approach to more complex ones such as linear scaling, power transformation and distribution mapping [Teutschbein and Seibert, 2012].

Distribution mapping is also referred to as quantile-quantile correction (Q-Q correction). It is based on the comparison between observed and simulated cumulative distribution functions. It consist in identifying and correcting the bias associated to each simulated percentile so that the corrected CDF fits the observed one. Here, we applied a Q-Q correction using ERA-Interim data as reference.

To tackle the change in bias sign and magnitude across the year, the correction is performed separately for the four seasons. The Cumulative Distribution Functions (CDF) are computed on a regional basis mixing the data from all grid cells within the analogy domains used in SCAMP (cf. Part III Fig.V.11, T-Td - green window, T - red window). In England, for instance, all grid points of the ERA-Interim and ERA20C datasets within the green windows are used to compute the reference and uncorrected CDFs of T-Td. The results of this regional correction approach are similar to the ones of a local correction method, for which all grid cells are considered and corrected independently. The corrected cycles of T-Td are presented on Fig.VI.1. The seasonal Q-Q correction is able to balance the imprecisions of ERA20C.

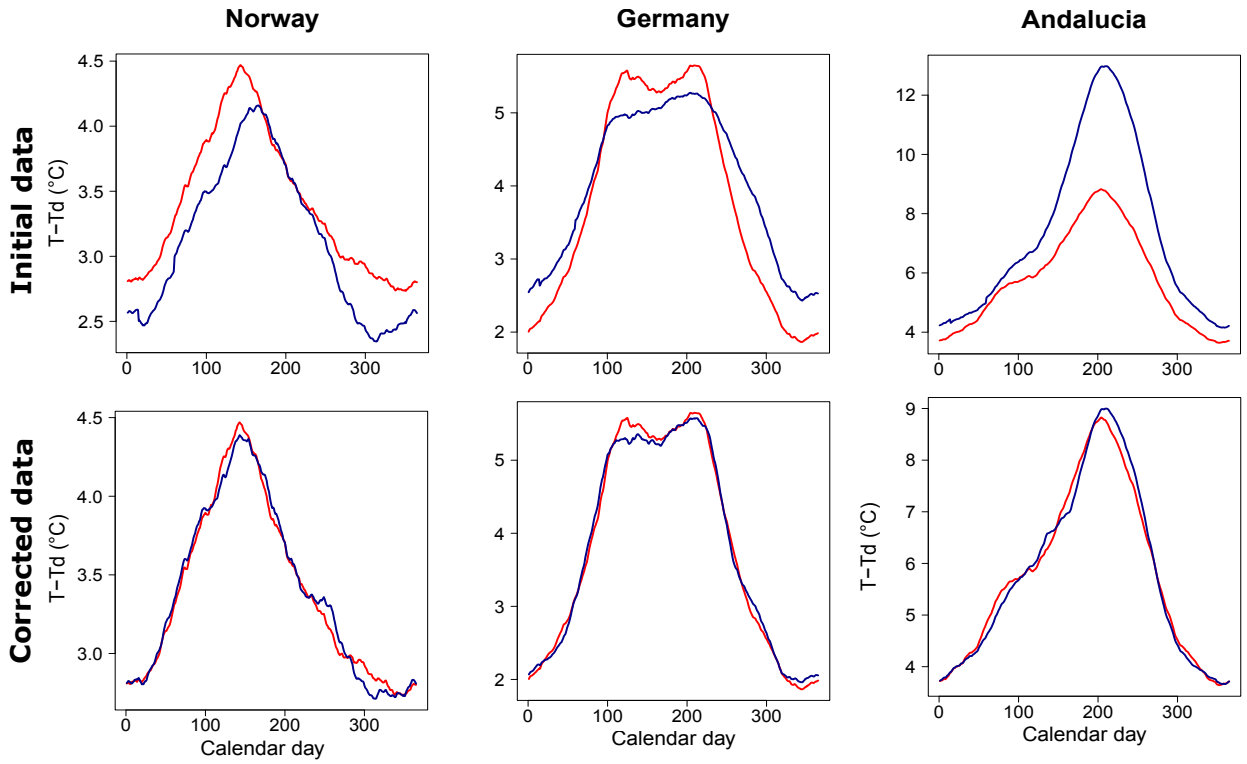

Figure VI.1 – **Raw versus corrected ERA20C thermodynamic predictors**. Mean seasonal cycle of T-Td in ERA-Interim (red) and ERA20C (blue) for 3 of the 12 test regions. The first row corresponds to the uncorrected data for ERA20C. The second one presents the results of a seasonal Q-Q correction. The cycles have been computed over the 1983-2012 period.

1.1.2. Effects on downscaled data

Region weather series of the 20^{th} century have been generated with both uncorrected and corrected predictors from ERA20C. Significant differences between the associated downscaled data are obtained, especially for temperature and precipitation. They directly impact the simulated hydro-meteorological and energy variables. Fig.VI.2 illustrates these differences on simulated river discharge in NO, GE and AN. The reference cycles (black curves) have been obtained simulating river discharge with observed data while the blue ones are associated either to corrected or uncorrected ERA20C input data. The blue shade represents the dispersion between the 50 simulated discharge cycles issued from the ensemble of downscaled weather scenarios.

The reference seasonal cycles of discharge are poorly reproduced using uncorrected weather data. In regions where snow-pack has a strong influence on river flow (e.g NO), the peak in simulated discharge is always overestimated and late compared as a consequence of a temperature bias. The simulated cycles after correction of predictors are much more consistent with the reference ones. In other regions, the bias in discharge obtained with the uncorrected data is mainly due to smaller rainfall amounts. Downscaled precipitation and discharge are generally underestimated from early summer to early winter in central/western Europe and during spring and autumn in Mediterranean regions. These biases in discharge in southern Europe are also reduced after correction.

Apart for some specific and rare cases (e.g. in GE, with winter flow becoming slightly overestimated after correction) removing the predictors biases in ERA20C leads to a much more accurate reproduction of the reference variables. Thus, the following results and evaluations of the 20^{th} century climate will be only based on the downscaled weather variables resulting from the corrected ERA20C input data.

2. Low frequency fluctuations

2.1. Hydro-meteorological variables

The internal variability of climate and its low frequency fluctuations have impacted weather conditions in Europe in the course of the 20^{th} century. With an increasing influence since the 1950s, Climate Change came into play and contributed to the final hydro-meteorological series. The main objective of this chapter is to assess the low-frequency temporal variability of weather variables under "stationary" climate conditions. Performing such an analysis based on the 20^{th} century observations is not straightforward as climate change likely resulted in long-term trends from some meteorological variables. A preliminary consideration for a robust variability analysis consists in identifying and characterising these possible trends.

2.1.1. Linear trends

Separating the climate change signal from the natural variability of climate is not an easy task, especially when the natural variability is large with respect to the magnitude of change [Deser et al., 2012]. Depending on the meteorological variable and on the region, the onset and the trend

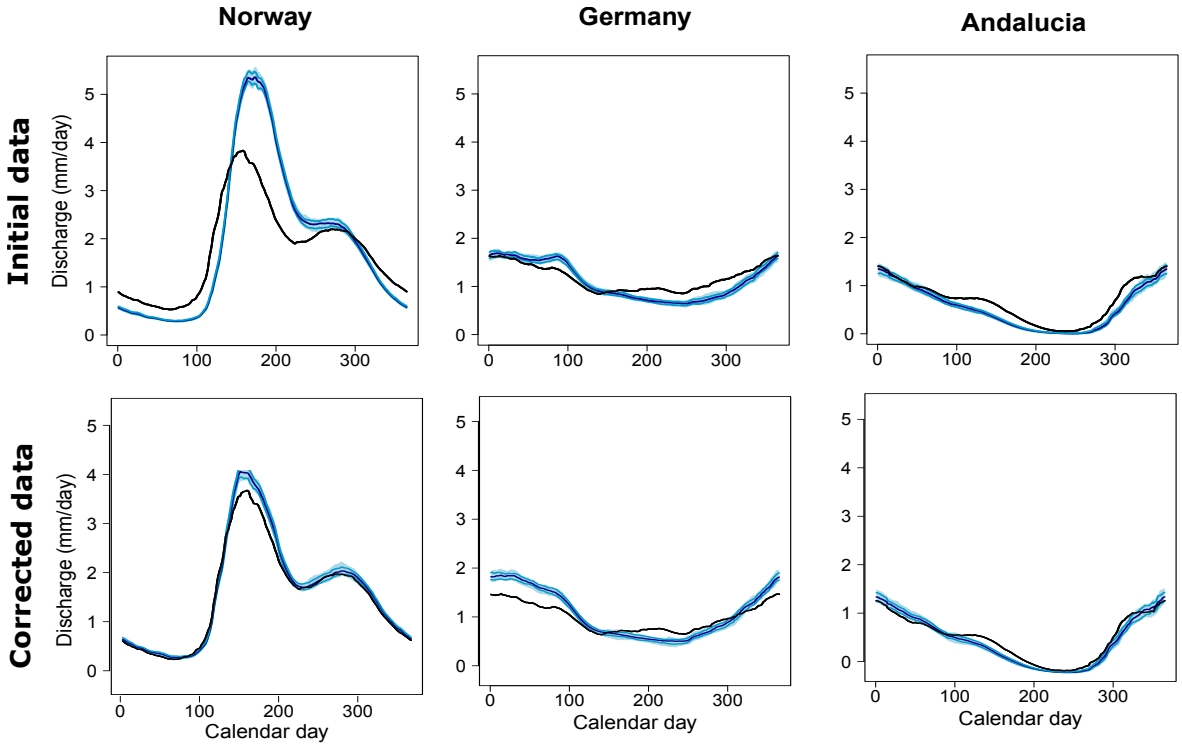

Figure VI.2 – **Raw versus corrected ERA20C predictors: impact on simulated hydrological cycles**. Mean annual cycle of discharge in observed series (black) and after downscaling with ERA20C (blue). The first row corresponds to the uncorrected data for ERA20C. The second one presents the results after a seasonal Q-Q correction of the T-Td predictor. The cycles have been computed over the 1983-2012 period.

characteristics can change greatly. In this analysis, we chose to search only for simple linear trends in the series. Restricting ourself to this unique and simple trend type is obviously not optimal for temperature, as global warming has experienced a drastic acceleration for the last 30 years. A robust analysis would require testing also non-linear trend models. However, for the sake of simplicity, only linear trend models have also been applied to temperature series.

Trends are looked for over the entire period, from 1900 to 2010. Statistically significant trends are identified using the 95% confidence interval (Student's t-test). When a significant trend is detected, it is removed from the time series before performing the analysis on low-frequency variations. Fig.VI.3 presents the regression coefficients of the linear trend fit for all four hydro-meteorological variables. It leads to the following main conclusions:

- River discharge series exhibit positive trends for latitudes higher than 45° and negative ones elsewhere. However, the slope coefficients are significant for only five regions (NO, BE, GE, IT and TU). The Tunisian region presents the strongest negative trend with a drop of 30% in mean daily river flow, from 1900 to 2010.
- The ERA20C downscaled series indicate an increase in temperature during the 20^{th} century for the whole European continent. In AN, the simulated temperature has increased by +1.1°C over the whole 111-year period.

- For 11 out of 12 test regions, simulated wind presents a significant increase since 1900 (Up to 6% in EN). This result is quite surprising. To our knowledge, no such trend has been established by previous observation-based studies for Europe. Actually, similar (or even stronger) trends exist in the large scale wind speed data from ERA20C. All regions and seasons are concerned but the British Isles seem to be more impacted especially in spring and autumn ($+3m \cdot s^{-1}$ in 110 years). Considering the resolution of ERA20C, the increase in wind speed is due, for the most part, to a stronger geostrophic wind component. It can result either from stronger gradients (i.e. deeper lows and stronger high pressure systems) or from a modification of the synoptic circulation. Such changes could be physically consistent and relevant but some additional tests seem necessary to check that they are not an artefact from the assimilation system. Indeed, only marine wind and sea level pressure observations are assimilated in ERA20C. Their increasing number from 1900 to 2010 could lead to more pronounced pressure features at the end of the simulation period.

- Finally, according to the downscaled simulations, Southern Europe got more sun radiation at the end of the 20^{th} century. No significant linear trend is found for northern and central European regions.

2.1.2. Low frequency fluctuations

The fluctuations of downscaled weather variables and simulated river discharge from 1900 to 2010 are presented on figure Fig.VI.4 for 3 out of 12 regions (NO, GE, AN). To facilitate the comparison between variables and regions, the figure displays the 10-yr moving average series of anomalies obtained by subtracting the 111-yr mean value to the initial series. Red and blue colours discriminate between positive and negative anomalies around the long-terms trend identified in the previous section.

The duration and intensity of positive and negative phases change from one variable to the other. Temperature has rather long and sometimes strong (up to $\pm$ 0.8°C) anomalies. A synchrony between some regions is manifest (e.g. NO and GE, negative long-duration anomaly from 1950 to 1990). However, one must recall that the last 30 years have undergone global warning and that the linear trend removal did not take its acceleration since 1980 into account. Wind variations have a limited duration (10-15 years max) and a maximum amplitude of 1.5 $m.s^{-1}$. These results are in agreement with the ones presented for France in Jourdier, 2015. Few anomalies last more than 20 years, indicating that wind speed mainly fluctuates at smaller time scales. For both radiation and river discharge, the characteristics of the anomalies seem to change greatly not only from one event to the other but also between regions. Some long duration negative phases occurred (e.g. GE, Discharge, 1920-1960 ; AN, Radiation, 1930-1970) while brief (10 to 20 years) oscillations can be seen in some other cases (NO, Discharge ; GE, Radiation). The amplitude of the anomalies is very weak for radiation ($\pm 4W \cdot m^2$, less than 3% of the mean annual radiation) and large for river discharge (up to about 10%).

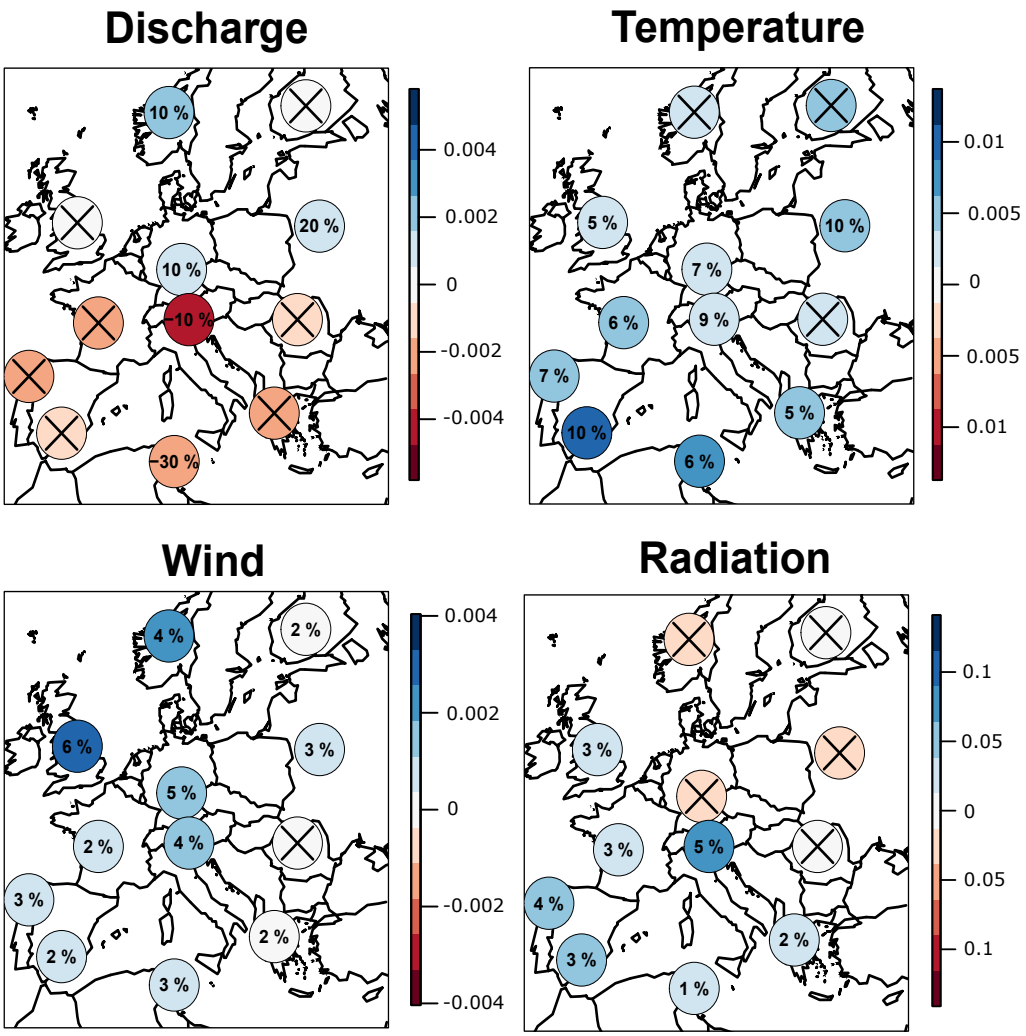

Figure VI.3 – **20^{th} century trend in annual hydro-meteorological drivers**. Slope coefficients (colors) of a linear regression on discharge ($mm.day^{-1}.yr^{-1}$), temperature($°C.yr^{-1}$), wind ($m.s^{-1}.yr^{-1}$) and radiation ($W.m^{-2}.yr^{-1}$) for the 12 European test regions. Non-significant linear trends (95% confidence interval) are highlighted with the cross symbol. When it is relevant, the relative change from 1900 to 2010 is displayed.

2.2. Electricity production

The low frequency variations of climate directly impact the renewable power generation. Thus, wind, solar and hydro power together with energy demand are also expected to fluctuate at a multi-decadal time scale.

To illustrate these variations, the hydro-meteorological time series of the 20^{th} century and the weather-energy conversion models presented in Chap.II are used to simulate both power generation energy load series. In order to focus only on climate-related fluctuations, the different parametrisations of all conversion models are kept constant over the whole simulation period. Hence, the relationship between hydro-meteorological drivers and energy generation/load are assumed to be invariant in time from 1900 to 2010.

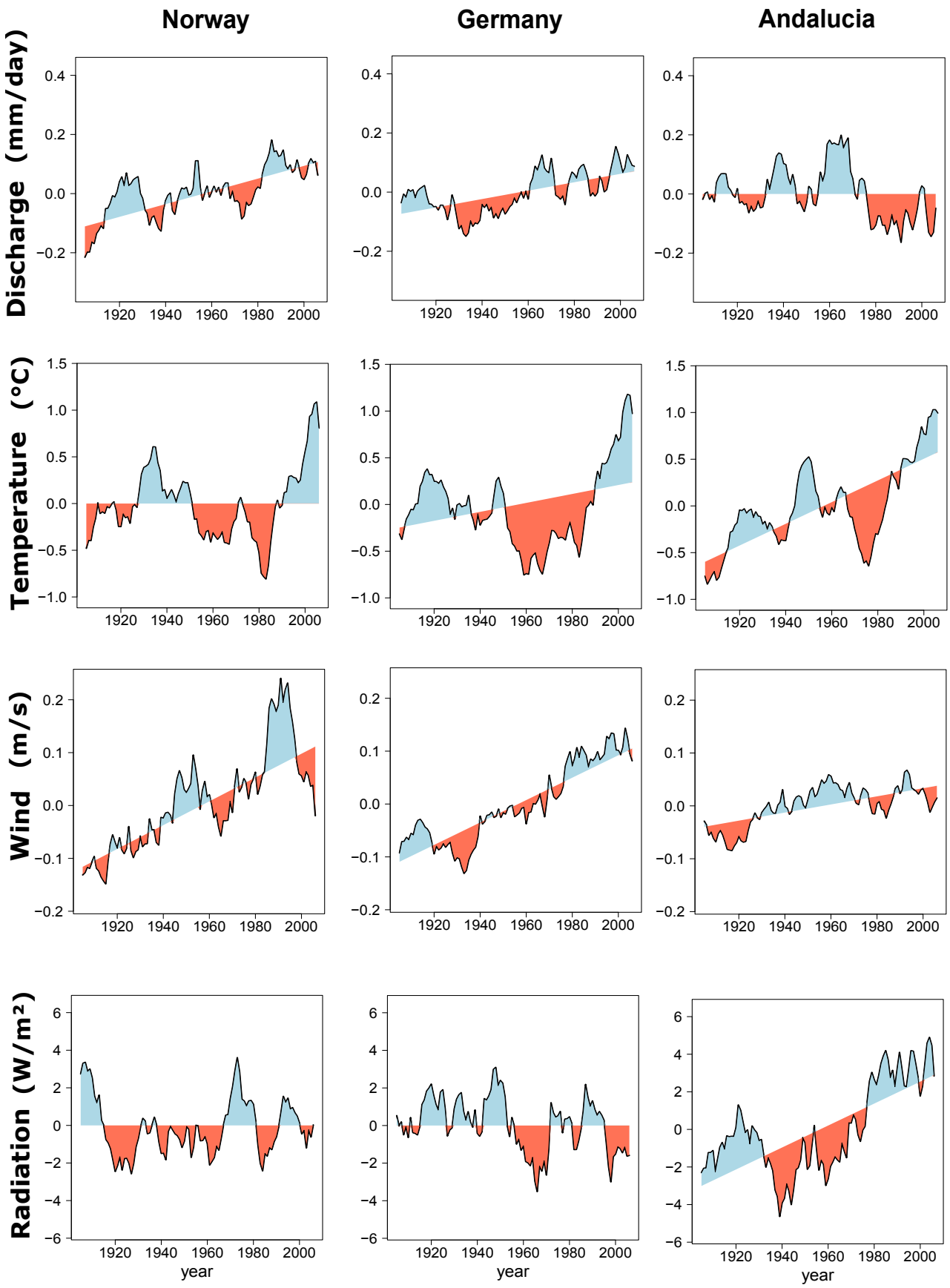

Figure VI.4 – **Multidecadal variations of hydro-meteorological drivers**. 10-yr moving average series of standardized discharge, temperature, wind and radiation in 3 out of the 12 test regions. Blue (respectively red) color highlights positive (respectively negative) low-frequency fluctuations around then mean value (0) or around the statistically-significant linear trend.

2.2.1. Trend in production/demand

The close relationships between meteorological drivers and power generation/load lead to similar trends in both types of series. We discuss here the main results and the associated figure is presented in Appendix.D:

- As a direct consequence of the changes in simulated discharge, the simulated hydro power resource has decreased in Mediterranean regions (significant negative trends in GA, AN and TU). It has risen in Scandinavia (significant in NO and BE).
- As a result of an increasing simulated wind speed, wind power has increased significantly from 1900 to 2010 in all regions.
- Simulated solar power has significantly increased in South western Europe (TU, AN, GR, GA, IT, FR and EN).
- At an annual time scale, the simulated energy demand has been relatively constant (appart from a slight negative trend in EN, FR and GA). However, this result hides some seasonal disparities. In winter and spring, negative trends are detected but they are generally not significant. On the other hand, Fig.VI.5 presents the slope coefficients of linear regression applied to summer and autumn series. It highlights two opposite contributions in Europe. Firstly, there is a drop in energy load in autumn for north western regions due to a delay in the arrival of colder temperature (less heating systems). In summer and in most regions, an increasing frequency of heat waves leads to more simulated electricity consumption due to air conditioning.

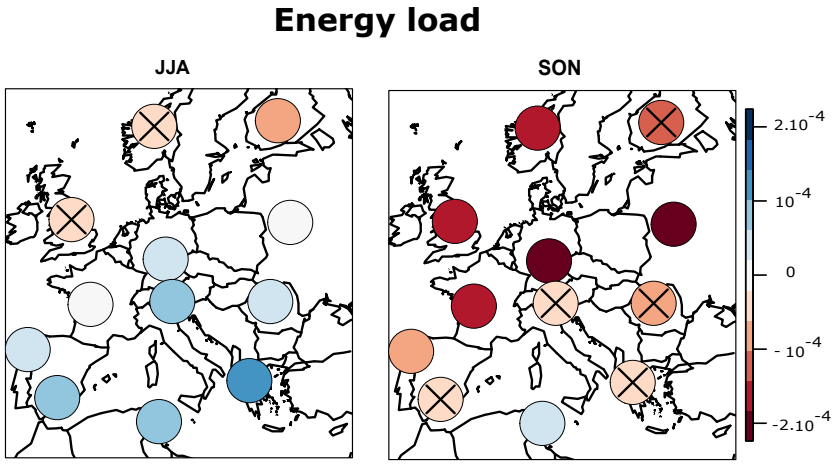

Figure VI.5 – **20^{th} century trend in summer an autumn energy load**. Slope coefficients (colors) of a linear regression on summer and autumn energy load (yr^{-1}) for the 12 European test regions. Non-significant linear trends (95% confidence interval) are highlighted with a cross symbol.

2.2.2. Low frequency fluctuations

Low frequency fluctuations of power generation series are highly dependent on the characteristics of their meteorological drivers. We just present, for illustration, the low-frequency fluctuations of power series in NO (Fig.VI.6). The following comments are valid for all 12 test regions. In order to compare the intensity of anomalies from on source to the other, we present the relative variations compared to the average regional production from 1900 to 2010.

- It clearly appears that hydro power undergoes the strongest fluctuations in terms of intensity and duration of anomalies. In this particular case, the differences between positive and negative phases reach 15% and they can exceed 30% in other regions (not shown).
- Jourdier, 2015 highlighted the strong multidecadal variations of wind power generation in France. Here, these fluctuations are also significant (2 to 5%), but much smaller than the ones of RoR hydro power.
- Solar power also exhibits very weak variations (1 to 2%).
- Finally, the low-frequency fluctuations of temperature have limited effect on energy load. The intensity of anomalies never exceed 3% and is slightly more pronounced in northern Europe (not show).

The combination of these various characteristics in low-frequency fluctuations of energy sources and energy load is likely to affect the penetration rate. We will now focus on this parameter and evaluate the reliability, in terms of multidecadal stability of PE rate, of each CRE source and of OM1.

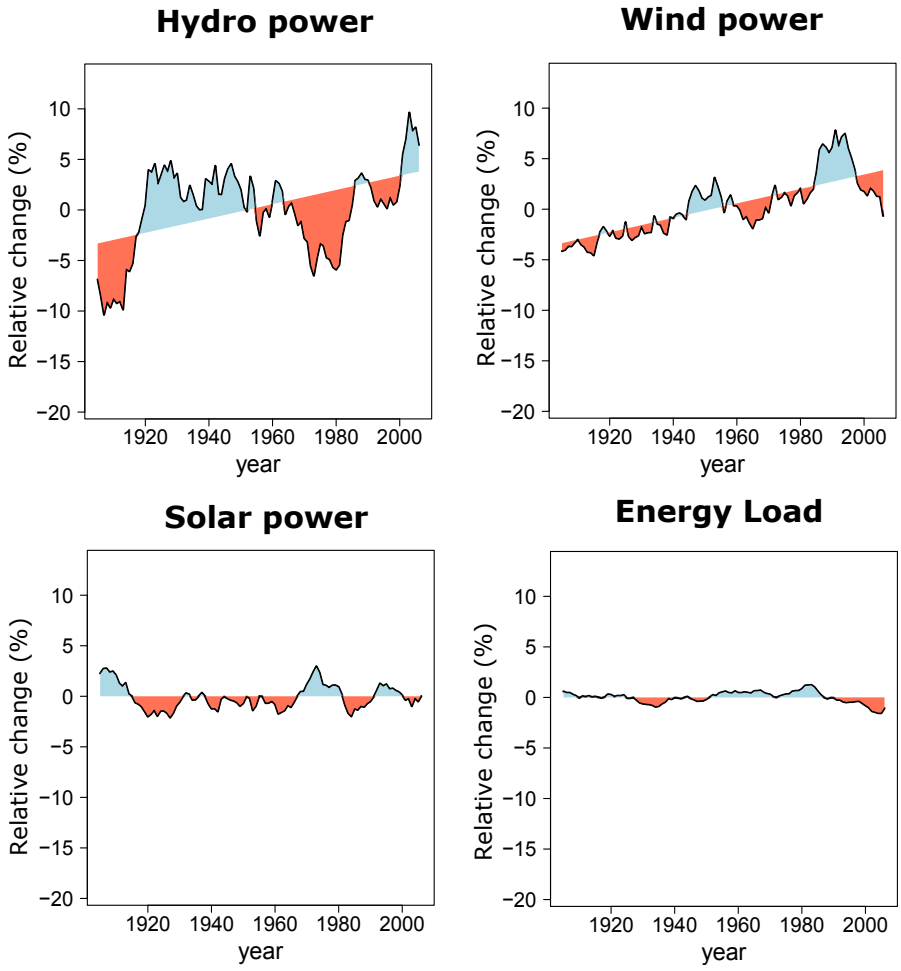

Figure VI.6 – **Multidecadal variations of energy generation**. 10-yr moving average series of relative change in hydro, wind, solar power and energy load in NO. Blue (respectively red) color highlights positive (respectively negative) low-frequency fluctuations around then mean value (0) or the linear trend when it is statistically significant.

2.3. Penetration rates and energy droughts

2.3.1. Long-term trend

In Chap.III, the ability of single energy sources and of energy mixes to meet the energy demand was evaluated on a 30 year period (1983-2012) via the penetration rate (PE, Eq.III.1). This criterion is estimated comparing a power generation series (either from a single source or a mix) with the energy load one. For the PE analysis, power generation series are normalized so that the mean productions equal the mean load over the entire period of interest (1983-2012 in Chap.III). In this way, it only accounts for the temporal production/demand mismatch and not for the level of equipment.

As shown in Chap.III.5, the penetration rate is greatly affected by the level of equipment. In other words, it largely depends on the ratio between mean electricity production and mean energy load over the considered period. In this analysis of the 20th century, we also assume invariant climate-energy relationships (i.e constant level of equipment and temperature-to-demand links). Thus, we only focus on the effects of the low frequency variability of climate on PE.

As highlighted in previous sections, There are some strong low frequency fluctuations in both production and energy load. These fluctuations will likely impact the PE time series and lead to important differences from one decade to the other. However, variations in PE could also result from a long-term change in the power generation/load match driven by climate change. Indeed, the simulated fluctuations in PE for 20^{th} century strongly emphasise their dependence on the long-term trends of electricity production series. As mentioned in Sec.2.1.1, some of those trends (wind) are also likely resulting from a temporal heterogeneity in the input weather data (geopotential - ERA20C dataset). The predominance of the trend signal in some series makes the analysis of PE low frequency fluctuations potentially misleading.

A possibility to get rid of (or at least reduce) the trends contributions is to remove the long term trends in all meteorological variables series and to use the corrected data as inputs of the weather-energy conversion models. However, this is a rather demanding task, which necessitates re-running all ERA-20C regional energy scenarios. We adopted another method to solving this issue: For each CRE source, we scale the daily production time series with a coefficient assumed to vary linearly with time. The rate of change of this coefficient is estimated so that the mean average production roughly fits the mean average load in the course of the 20^{th} century. Obviously, this method is not optimal but it should lead to a reasonable estimate of the low-frequency variations of PE. The coefficients associated the three single CRE sources are presented for NO, GE and AN in Fig.VI.7. For all regions, the scaling coefficients of wind power are decreasing from 1900 to 2010. It is relatively constant for solar power. More regional disparities exist for the coefficient associated to hydro power with on one hand, a strong rise in Southern Europe and on the other hand, constant or decreasing coefficients elsewhere.

2.3.2. Low-frequency fluctuations

The 1101-year long time series of de-trended penetration rates are presented on Fig.VI.8, for all energy sources and mixes and for NO, GE and AN. Firstly, despite various characteristics in term of

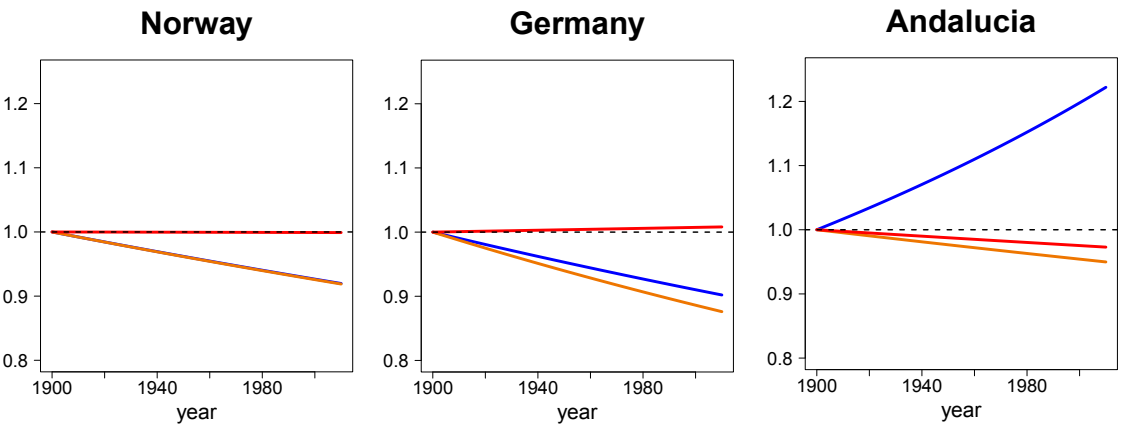

Figure VI.7 – **Scaling coefficients used to guarantee a constant electricity production from 1900 to 2010** (based on a 30-yr moving average) for hydro-power (blue), solar-power (red), wind-power (orange) and OM1 (green). These coefficients are used to remove the trend signal in the penetration rate series and only consider the 10-yr period fluctuations.

low-frequency fluctuations, the ranking of energy sources does not change in the course of the 20^{th} century. OM1 is always the unquestionable best options regarding the mean penetration rate.

Low frequency fluctuations in PE must be taken into account to decide on the size of CRE power plants. Basing it on an estimation of PE rates using a limited period could result in an under or over-sizing. Regarding this criterion, the different energy sources and mix are not equivalent. Solar power is always the most reliable energy. Indeed, its associated regional PE series are almost constant over the whole period and their low frequency variations are limited. The same comment applies to wind power which does not fluctuate much around its mean penetration rate. The strong variations of hydro power prevent it from being a reliable energy sources at a multidecadal scale. Let us take the example of hydro power in NO. Estimating the PE rate of this energy source from 1960 to 1980 leads to an underestimation of its mean value and thus to a costly over-sizing. On the other hand, considering the 1990-2010 period which presents a positive anomaly in PE, the associated hydro power plant would be too small to adequately meet the energy load on "normal" or negative anomaly periods. Finally, the results of OM1 are uneven from one region to the other and depend on the proportion of each single energy source in the regional energy mix.

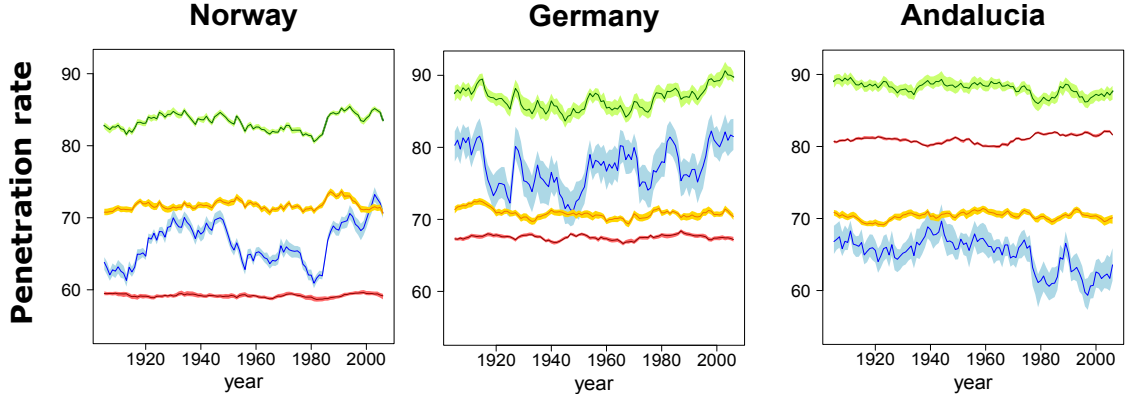

Figure VI.8 – **Multidecadal variations in global penetration rate (PE - %)**. 10-year moving average de-trended series of PE for hydro-power (blue), solar-power (red), wind-power (orange) and OM1 (green) from 1900 to 2010. Results are presented for NO, GE and AN.

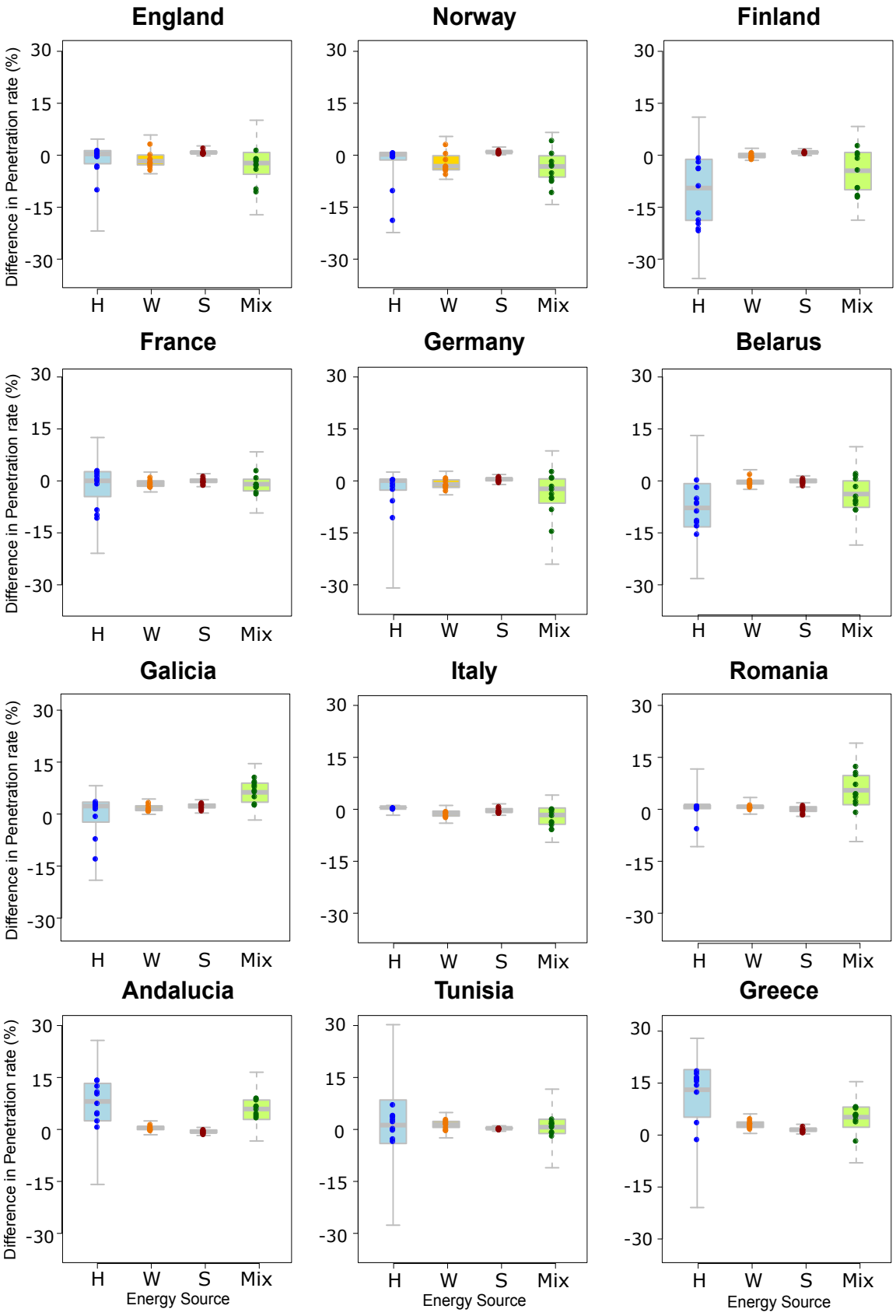

Figure VI.9 – **Multidecadal variations in the estimation of PE (%)**. Each dot corresponds to the mean PE value associated to a given 10-year period compared to the reference one (2001-2010). The box-plots illustrate the total dispersion computed from the 50 downscaled series from the 10 decades of the 1900-2000 period compared to the 50 reference ones from 2001 to 2010. Results are displayed for hydro-power (blue), solar-power (red), wind-power (orange) and OM1 (green).

These Multidecadal fluctuations are also highlighted on Fig.VI.9, which shows for all regions and energy sources/mix, the differences in penetration rate from all 10-year sub-period of the 20th century to a reference period (2001-2010). Each dot corresponds to the mean value associated to a given 10-year period and the box-plots illustrate the total dispersion computed from the 50 downscaled series of all 11 decades of the 1900-2010 period. This information quantifies the risks associated to the evaluation of the penetration rate of an energy source based on a short period (10 years).

In all regions, the percentage of satisfied demand using solar power does not depend on the 10-year sub-period choice. Differences in penetration rate never exceed 2%. Using a short period to estimate the mismatch between wind power and energy load is rather reasonable for most regions. However, the penetration rates seem to be more impacted by low frequency variations in EN and NO, resulting in an over or under-estimation of about 7% for some decades.

Hydro power undergoes strong Multidecadal fluctuations. Assessing its ability to meet the energy demand on a few years leads to high risks of under or over-estimation. For a given 10 year period, there is also a strong inter-scenarios dispersion, resulting in total differences reaching 30% in some regions (TU, GR, FI, BE). Italy stands out of the crowd; weak differences in penetration rate exist from on decade to the other for this region.

Finally, mixing different energy sources leads to important differences between the 10-yr based estimations of PE, especially for regions where hydro power prevails in OM1. The total dispersion even exceeds the sum of the contributions from hydro, solar and wind power in some regions (IT, RO). All in all, despite the appeal of combining different energy sources to fulfil a larger part of the energy demand, the Multidecadal variability of energy mixes should not be underestimated.

2.3.3. Energy droughts

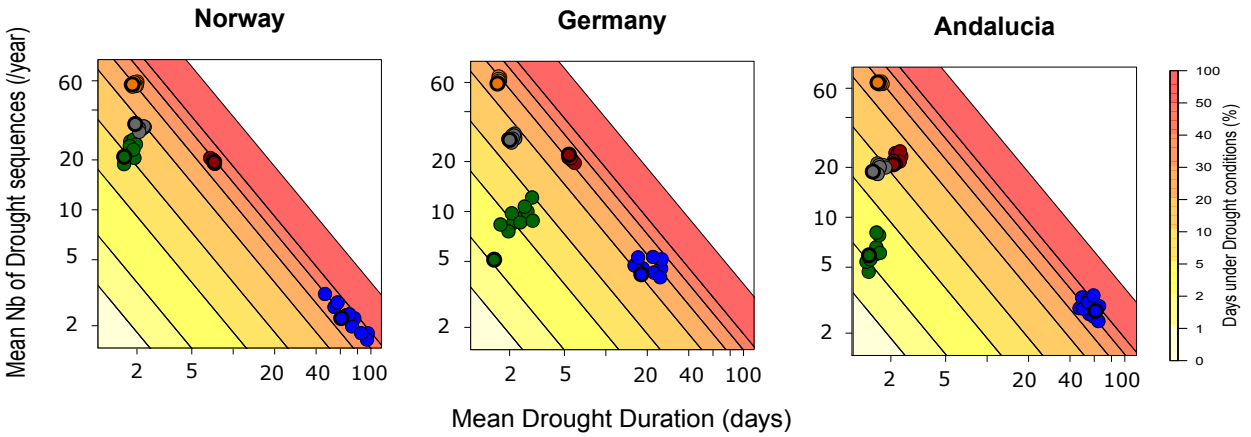

Figure VI.10 – **Multidecadal fluctuations of energy droughts characteristics**. Mean number of drought episodes versus mean drought duration. Results are displayed for hydro-power (blue), solar-power (red), wind-power (orange), OM1 (green) and OM2 (grey). Each dot correspond to a 10 years sub-period of the 1900-2010 one.

Due to the relatively short period for which weather observations are available, we did not account for the low-frequency fluctuations of the energy droughts in Part II. Estimating accurately both mean duration and frequency of the droughts episodes is an important step toward a relevant and efficient renewable power supply. Thus, we round off our analysis of the multidecadal variations of green

electricity production in Europe, assessing how energy droughts characteristics have changed in the course of the 20^{th} century. The results are presented on Fig.VI.10 for NO, GE and AN, and for all energy sources and mixes. Each dot corresponds to a given 10-year sub-period.

Following the results discussed previously for PE, the number of wind and solar power drought sequences and their mean durations do not fluctuate much from one decade to the other in the simulated series. Logically, the same comment is valid for OM2, combining only these two energy sources. The duration of drought episodes associated to hydro power varies greatly in some regions. It ranges, for instance, from 50 to 100 days in NO. Consequently, the risk of energy shortage for hydro power should be evaluated on long periods. Ultimately, the number of drought episodes related to the OM1 also changes and can be three times higher from one decade to the other in some regions (e.g. from 5 to 15 sequences per year in GE). However, these relatively high variations are counterbalanced by the much lower frequency and duration of drought events compared to single energy sources.

Chapter VII

Large scale oscillations of the climate system: effects on renewables

In Chap.III and Chap.VI we showed that all climate variables fluctuate at various time scales from inter-annual to multidecadal periods. These fluctuations are sometimes driven by large scale oscillations in sea surface temperature or sea level pressure. El Nino-Southern Oscillation (ENSO) [Ropelewski and Halpert, 1986] has an unquestionable impact on both temperature and precipitation amounts in a number of regions worldwide. The Atlantic Mutidecadal Oscillation (AMO) [Enfield et al., 2001] and the North Atlantic Oscilation (NAO) determine respectively the long-term and the inter-annual variability of the European climate [Trigo et al., 2002; Rogers, 1997; Hurrell and Van Loon, 1997]. We examine how the low frequency variability of weather and energy variables can be related to such large scale climate phenomena.

1. Presentation of the Climate indices

Some climate fluctuations are known to be driven by large-scale or global oceanic and atmospheric oscillations. The ENSO (El Nino-Southern Oscillation), which consists of fluctuations of the Ocean temperature in the equatorial Pacific [Ropelewski and Halpert, 1986], has a strong impact on both temperature and precipitation patterns in many regions worldwide. However, its influence on the European climate is less certain [Scaife, 2010] even if some studies highlighted several connections [Brönnimann, 2007].

The Atlantic Ocean temperature also fluctuates on a multidecadal scale [Enfield et al., 2001]. The AMO index is computed as the area-weighted average temperature over the Northern Atlantic (0° to

70°N). It has an approximate period of 70 years and its influence on the European climate has been proven in winter [Rodwell et al., 1999].

The atmospheric patterns of the northern Atlantic, despite their fixed average locations (Azores High, Iceland Low), switch positions from daily to annual scales. This oscillation, known as the North Atlantic Oscillation (NAO) [Hurrell and Van Loon, 1997], influences greatly the European climate, especially in winter [Trigo et al., 2002; Rogers, 1997]. The NAO index quantifies the anomaly in position and intensity of the usual north Atlantic pressure patterns[1].

Using the long time series (starting in the 19^{th} century), provided by the NOAA[2], we analyse the correlation between two of these indices (AMO and NAO) with the regional hydro-meteorological series. We aim to confirm the results of past studies focusing on the impact of these natural oscillations on the European climate and to extend them to CRE sources.

The annual time series of AMO and NAO indices from 1900 to 2010 are presented on Fig.VII.1. Both series have a high inter-annual variability, with consecutive years of strong opposite anomalies often observable. However, the long-term variations of the AMO index (70-year period) already appear on the annual data. It is highlighted on the 10-yr moving average series. Conversely, no clear periodicity in long-term variations of the NAO index can be identified. Stronger and numerous years with a positive NAO index occurred until 1960 but more variability exists since then. Some past studies also suggested that the AMO could impact the NAO, particularly in winter [Rodwell et al., 1999]. The Spearman correlation coefficients, computed on annual series, proved that a significant anti-correlation (-0.26) exists between both indices. Nevertheless, large disparities between seasons have been found with anti-correlation in winter and spring (-0.19 and -0.45 respectively) but no significant correlation coefficients for other seasons.

2. Correlation with hydro-meteorological parameters

Fig.VII.2 and Fig.VII.3 present the regional Spearman correlation coefficients between the two climate indices (NAO and AMO respectively) and the annual series of surface weather variables in winter, summer and for the whole year.

- Firstly, one can notice that the correlation coefficients are low and often not statistically significant in summer for all variables and most regions. Nevertheless, there is a weak negative correlation between the NAO and summer wind, radiation and discharge in Europe.
- Following the results of previous studies, a positive phase of the NAO leads to a warmer year and particularly a warmer winter for northern European regions. Conversely, Mediterranean regions experience temperature colder than usual. The same dipole exists for wind speed with positive correlations (stronger wind with NAO+) for latitude higher than 50°. The warmer and windier conditions for a positive NAO index are associated with a succession of weather

[1] A description of how monthly and annual time series of NAO index have been computed is available on the NOAA website http://www.cpc.ncep.noaa.gov/products/precip/CWlink/daily_ao_index/history/method.shtml

[2] http://www.esrl.noaa.gov/psd/data/climateindices/list

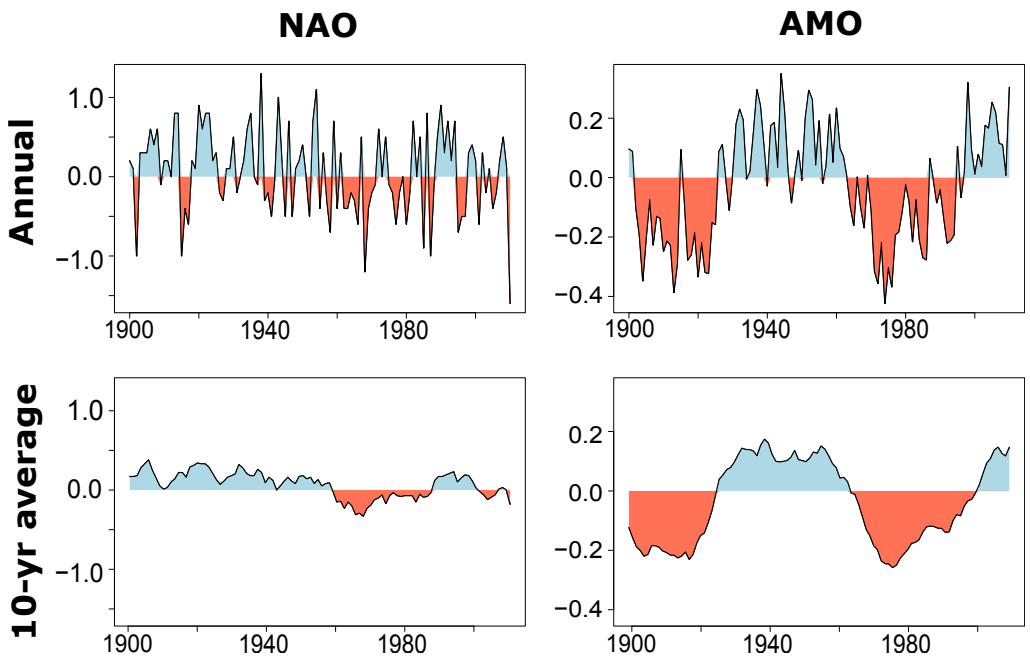

Figure VII.1 – **Time series of NAO and AMO**. Annual and 10-yr moving averaged series of North Atlantic Oscillation (NAO) and Atlantic Multidecadal Oscillation(AMO) from 1900 to 2010. Positive (respectively negative) phases are displayed in blue (respectively red).

disturbances, in northern Europe. Logically, solar radiation is lower than usual whereas discharge increases as a consequence of more precipitation and less snow accumulation (in winter for Scandinavian regions).

The surface temperature of the Atlantic Ocean also impacts the European climate. The correlation coefficients between the AMO and continental temperatures are high and positive in summer, especially in Western Europe. In winter, the correlation sign changes and positive phases of the AMO are generally associated to colder winter seasons.

For the other variables, no systematic relationship can be established, particularly in winter, for which many correlation coefficients are not statistically significant. Moreover important regional differences exist. For instance, the results for winter discharge are very uneven with a change in correlation sign from one region to the neighbouring one. Yet, some spatial consistency is noticeable with, for instance, positive correlation coefficients in Mediterranean regions in summer and from EN to TU at an annual time scale. Annual discharge also has slight but significant anti-correlation with the AMO index in Eastern Europe. A negative correlation between summer/annual wind speed and the AMO is detectable for a majority of regions. The same comment is valid for to radiation. Finally, a positive winter correlation between radiation and the AMO index exist in Western Europe.

3. Relationships with CRE sources and energy load

The correlation coefficients between the climate indices and regional power generation series can almost be directly deduced from the ones presented for their hydro-meteorological drivers. For this reason, the associated figures are only presented in Appendix.D. We summarize here the main results:

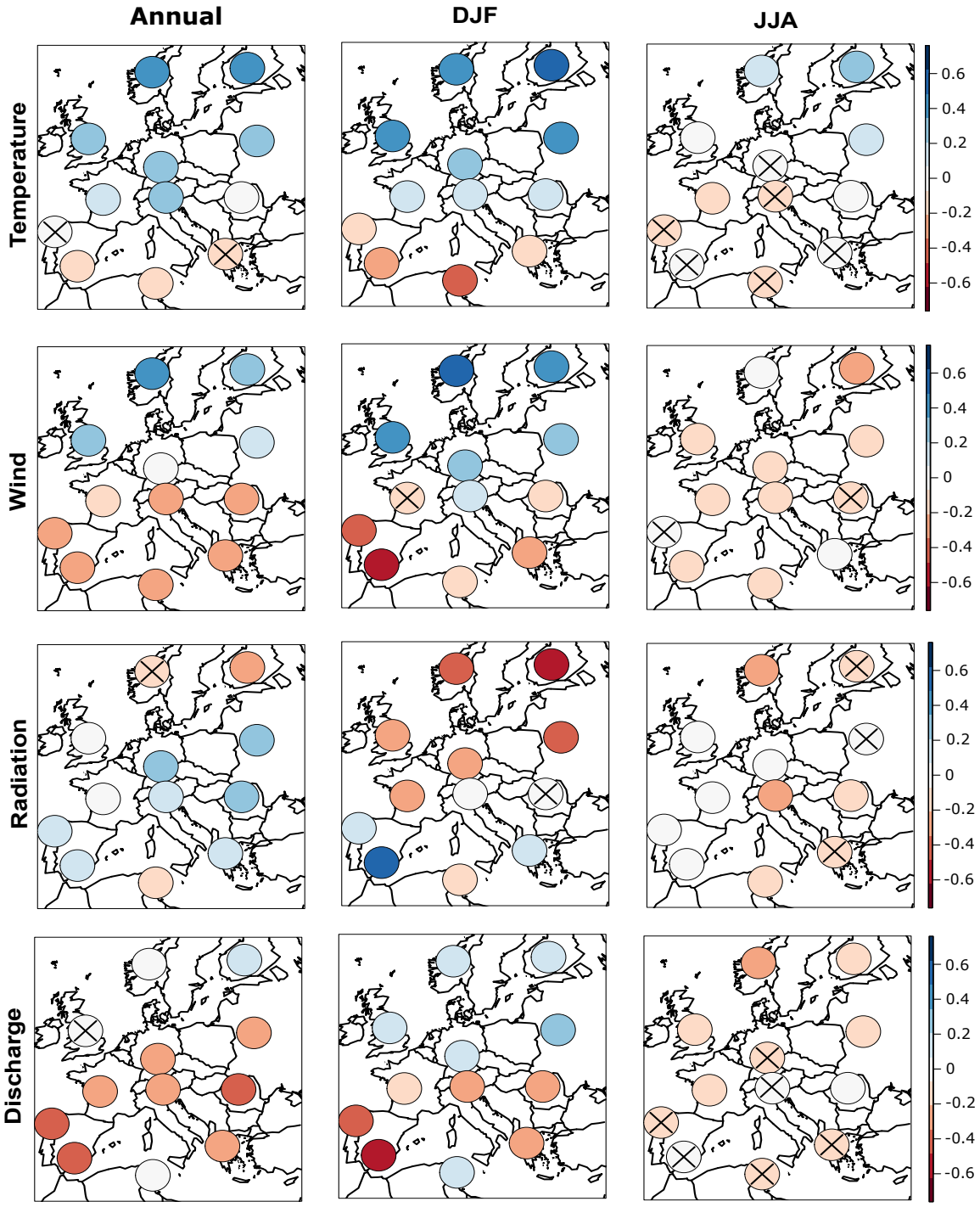

Figure VII.2 – **Connections between the NAO and meteorological drivers**. Spearman correlation coefficients between the NAO index and regional series of temperature, wind, radiation and discharge. Non-significant correlation coefficients (95% confidence interval) are highlighted with the cross symbol. Results are displayed for annual, winter and summer data.

Winter

- Positive NAO phases result in higher wind and hydro power in Northern Europe but lower production values in the Mediterranean basin
- The energy demand is lower in most regions during positive anomalies of the NAO except in AN and TU.
- The electricity production from solar panels is generally lower for NAO+ in north-eastern Europe. A positive correlation exists for some other regions especially AN and GA.

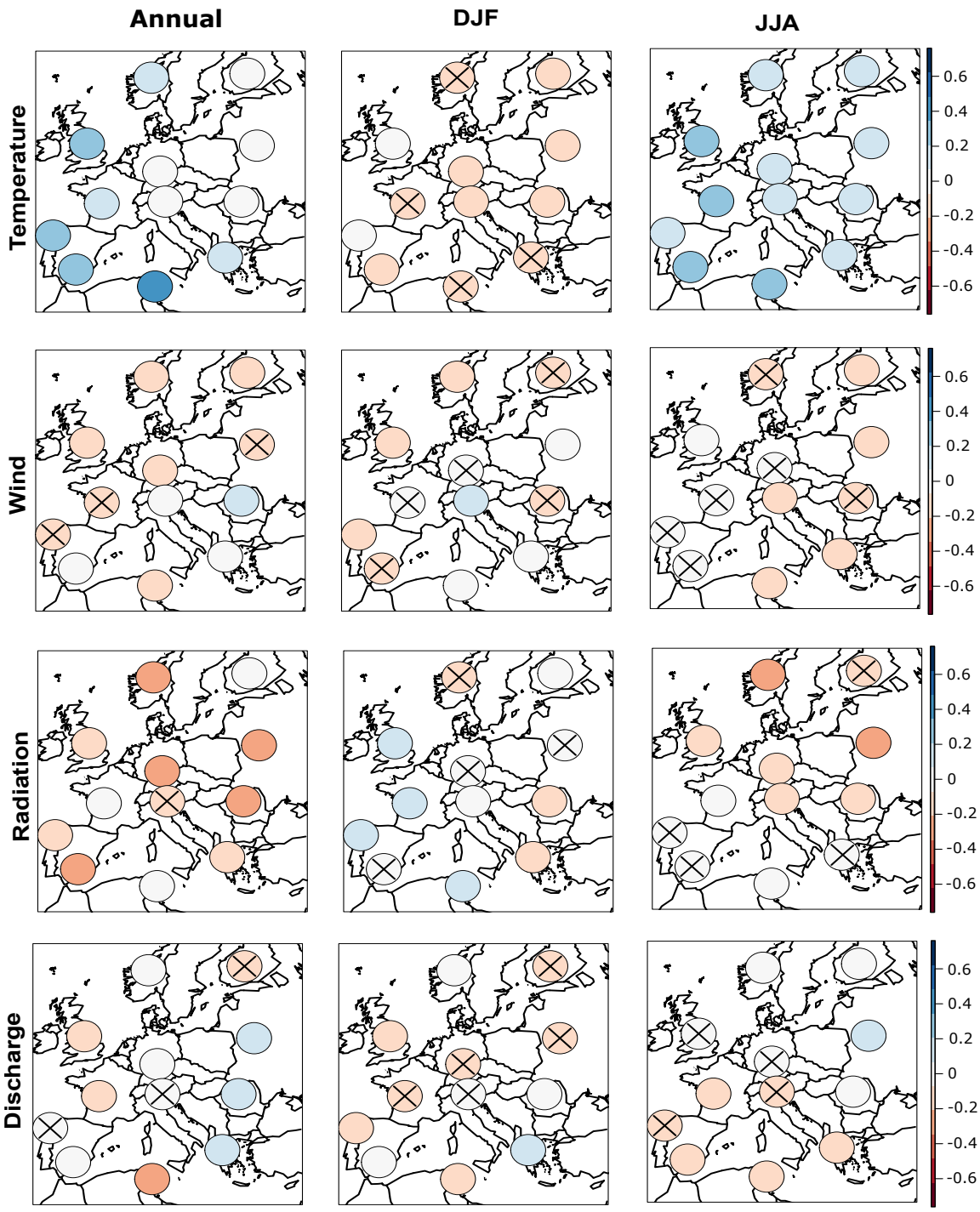

Figure VII.3 – **Connections between the AMO and meteorological drivers**. Spearman correlation coefficients between the AMO index and regional series of temperature, wind, radiation and discharge. Non-significant correlation coefficients (95% confidence interval) are highlighted with the cross symbol. Results are displayed for annual, winter and summer data.

- The correlation coefficients between the AMO and energy generation/load are weak and often not statistically significant. No spatial pattern is noticeable.

Summer

- The relationships between the NAO and energy generation/load are weaker in summer. The correlation coefficients are either not significant or slightly negative (energy load and wind power).

- Small but significant positive correlations exist between the AMO and hydro power in North-eastern Europe. There is a negative correlation from GR and TU to FR.
- For Solar/Wind power, the correlation coefficients assocated to both climate indices are also low. Regrading solar power, they are positive in most region. In the case of wind power, one can notice a weak opposition between western and eastern Europe with a positive correlation in AN, GA and EN and a negative one in Scandinavia, BE, TU and GR.
- Energy load presents a much higher correlation with the AMO than all CRE sources. In summer, the correlation coefficients are negative for northern regions (EN, NO, FI) and positive for all southern regions. Note also than some significant correlations also exist in spring and autumn (not shown). Correlation coefficients between the AMO and spring energy load are negative in EN, FR, GA and AN, positive elsewhere. There is more spatial homogeneity in autumn with positive correlations for most regions (apart from TU and AN).

4. Relationships with annual PE and energy droughts

4.1. Annual PE

The connections between the NAO and the penetration rates of CREs sources has been presented by François, 2016 (Fig.5) on a 30-yr period. We extend part of this study to the entire 20^{th} century, giving a more robust evaluation.

The relationships between the penetration rates of CRE sources and their meteorological drivers is less straightforward. However, the same spatial patterns of correlation with the NOA/AMO are emphasised again. Hence, we only summarise the main results (see the associated figure in Appendix.D):

- Correlation coefficients between the NAO and summer penetration rates and between the AMO and winter PE are weak and often not significant.
- For wind and hydro power, higher winter penetration rates occur during positive phases of the NAO in northern Europe but during negative phases in Mediterranean regions.
- The spatial pattern of correlations between the winter NAO and solar PE is similar to the ones of wind and hydro power PE but with opposite signs: Negative correlation coefficients in Northern Europe, positive ones in Mediterranean regions.
- The most significant correlation between the AMO and summer penetration rates are found in eastern Europe for wind power (negative correlations) and in Mediterranean regions for hydro power (negative correlations).

4.2. Energy droughts

We performed the same analysis on the annual duration and frequency of occurrence of energy droughts, defined in Chap.III. In many cases, no spatial pattern emerges or most of the correlation coefficients are not significant. We only present here the most noteworthy results.

The Spearman correlation coefficients between climate indices and annual drought frequency series are presented on Fig.VII.4. A mentioned previsouly, correlations are generally weak and few spatial consistency exists. However, a stronger relationship is found between the NAO and wind power droughts which are less numerous in Northern Europe during positive phases of NAO.

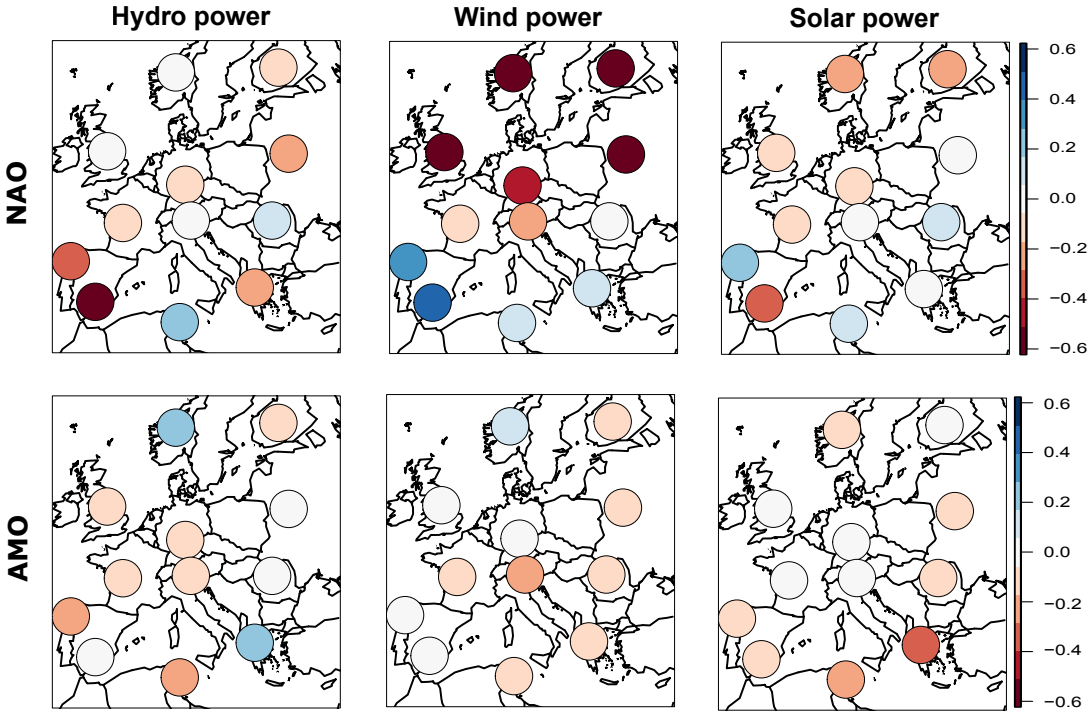

Figure VII.4 – **Connections between the NAO/AMO and energy droughts frequency in winter**. Spearman correlation coefficients between the NAO/AMO index and regional series of energy droughts frequency in winter. Non-significant correlation coefficients (95% confidence interval) are highlighted with the cross symbol

No significant correlation between the AMO and mean annual droughts duration could be highlighted. Fig.VII.5 only presents the winter correlation of these series with the NAO (no significant correlation in summer). Once again, the most noteworthy result is associated to wind power with long energy droughts in the Mediterranean and shorter one in Scandinavia during NAO+ phases. Significant positive correlations also exist for hydro power in FI and BE and for solar power in Iberian peninsula (GA and AN).

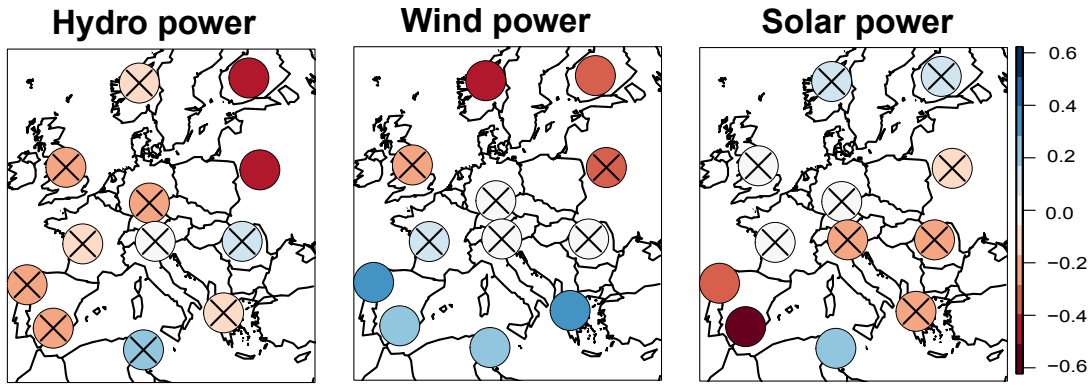

Figure VII.5 – **Connections between NAO and energy droughts duration in winter**. Spearman correlation coefficients between the NAO index and regional series of energy droughts duration in winter. Non-significant correlation coefficients (95% confidence interval) are highlighted with the cross symbol

Overview

The two previous chapters aimed to illustrate and quantify the low-frequency fluctuations of weather, electricity production and penetration rate series. Using the recently released ERA20C climate reanalysis from the ECMWF and the multivariate analogue method developed in Part III (SCAMP), downscaled regional weather series were generated from 1900 to 2010. A bias correction based on the quantile-mapping method was necessary for some predictors (T-Td and Temperature) to ensure relevant and correct hydro-meteorological simulated series.

- For all regions, simulated temperature and discharge have strong and long-lasting multidecadal anomalies. Conversely, low-frequency fluctuations are rather limited and short lasting for wind indicating that this variable varies at shorter time scales. Solar radiation can be lengthy but their magnitude are weaker and never exceed $3W \cdot m^2$.
- The variations of hydro-meteorological variables directly impact the power generation and energy load series. Consequently, hydro power undergoes strong fluctuations in all European regions with anomalies lasting several decades and generally being from 5 to 20% higher (or lower) than the mean production. Wind and solar power have more reasonable multidecadal variations. The strong and lengthy fluctuations of temperature have a rather limited impact energy load (fluctuation below 3%).
- The analysis of penetration rate fluctuations confirmed the important variations of hydro power compared to the other energy sources. Its penetration rate should be evaluated on long periods to avoid irrelevant power plant dimensions and recurrent over/under-production periods. Moreover, attention should be paid to hydro-power droughts characteristics which present strong multidecadal fluctuations in both frequency and duration. Finally, when the share of hydro-power in an energy mix is high, the resulting energy and penetration series suffer from similar low-frequency variations.

We also explored the possible relationships between hydro-meteorological/energy/penetration series and two climate indices known to influence the European climate. The North Atlantic Oscillation (NAO) and the Atlantic Multidecadal Oscillations (AMO) strongly impacts the hydro-meteorological drivers. The most noticeables connections are:
1) NAO+ leading warmer, winder, cloudier and rainier conditions in Northern Europe while the opposite anomalies exist in Mediterranean regions.
2) AMO+ resulting in warmer summer temperature over the entire continent.

These results impact directly energy/load and penetration series but the connections with both the NAO and the AMO get weaker (lower correlation coefficients). However, wind power PE rates and energy droughts characteristics remain strongly related to the NAO in winter.

Part V

EXPLORING FUTURE REGIONAL CLIMATE: SCENARIOS AND LIMITS OF THE ANALOGUE METHOD

Chapter VIII

The 21st century climate using analogues

The ongoing global warming and its effects on local meteorology will likely modify the characteristics of regional power generation time series. Many studies already assessed the possible impacts of climate change on the hydro-meteorological drivers of CRE sources or on the mean ressources in renewables (e.g. in Jerez et al., 2015; Reyers et al., 2016; Segal et al., 2001; Tobin et al., 2015). However, the mean electricity productions are not sufficient to evaluate the possible future changes in CRE sources. Indeed, they do not describe the modification of the match between production and demand. To perform such an evaluation, regional multivariate time series, with accurate co-variations are required.

In this chapter we will use SCAMP to downscale large scale simulations from a selection of climate models, generated as part of the last CMIP phase [Taylor et al., 2012]. These GCMs have been used to simulate the past and current climate (historical runs) and its future evolution until 2100. Four Representative Concentration Pathways (RCP), corresponding to different scenarios of greenhouse gas emissions, force these climate simulations from 2005. We will here focus on the RCP4.5 and RCP8.5 scenarios. This GHG emissions peak in 2040 in the RPC4.5 case while they keep on increasing until 2100 in the more pessimistic RCP8.5 [Taylor et al., 2012].

After evaluating and sometimes correcting the large scale predictors from the selected GCMs, the downscaled series of predictands will be compared with each other. Moreover, the relevance and agreement of these downscaled simulations with the findings of similar studies will be assessed.

1. GCMs presentation

1.1. Description of CMIP5 smilations

In 2008, the World Climate Research Programme (WCRP) agreed to promote a 5^{th} phase of the Coupled Model Inter-comparison Project (CMIP)[1]. This project aimed to coordinate and gather climate simulations from numerous research centres worldwide. All these simulations follow a set of common rules in order to be comparable and to bring useful information about the three following questions:

- How can GCMs can efficiently reproduce and predict both past and future climate conditions?
- What are the uncertainties related to these simulations and what are the reasons for the wide range of different simulations using similar model forcings.
- What are the reasons for the strong model differences in the feedbacks between clouds and the carbon cycles?

A detailled description of the CMIP5 framework and of the associated climate simulations is provided by Taylor et al., 2012.

In this study, we selected and extracted data from 4 GCMs for which all the large scale variables used as predictors in SCAMP were available, that is to say: HGT500, HGT1000, T-Td and T. However, for most GCMs, the geopotential height is not extrapolated when its value is lower that the surface elevation in the model. In Europe, HGT1000 is not available over the highest mountain ranges (e.g Alps, Scandinavian mountains). Moreover, the deepest low pressure systems often have negative HGT1000 leading to more missing values. To tackle this issue, we replaced the HGT1000 predictor by the pressure at sea level (PSL) which gives a very similar information, in terms of gradients and positions of highs and lows. The dew point temperature (Td) is a variable which is usually not provided as part of the GCMs outputs. The near-surface relative humidity (RHS), available for all models, was used to computed Td and construct T-Td (second-level predictor of SCAMP), following Lawrence, 2005.

The general characteristics of the selected GCMs are presented in Tab.VIII.1. 3 of them are European models and the last one has been developed in Japan. All of them have 3 members for the historical run giving a more detailed and accurate description of the simulated past climate conditions. Apart from the IPSL-CM5A-MR model, multiple runs have been used for one of the RCPs: 3 members with RCP8.5 for MIROC and HadGEM, 3 members with RCP4.5 for MPI-ESM.

Table VIII.1 – Characteristics of the selected General Circulation Models

Historical				**RCP**			
Country	**Model**	**Resolution**	**Members**	**From-To**	**RCP**	**Members**	**From-To**
France	IPSL-CM5A-MR	2.5°-1.25°	3	1850-2005	4.5|8.5	1|1	2006-2100
UK	HadGEM2-CC	1.875°-1.25°	3	1950/60/60-2005	4.5|8.5	1|3	2006-2099
Japan	MIROC5	1.4°-1.4°	3	1850-2009	4.5|8.5	1|3	2006-2100
Germany	MPI-ESM-MR	1.9°-1.9°	3	1950-2005	4.5|8.5	3|1	2006-2100

[1] cmip-pcmdi.llnl.gov/cmip5

1.2. Evaluation and correction of predictors

Historical climate simulations are only constrained with non-meteorological forcing (GHG emission, solar radiation...) and thus cannot be considered as climate reanalysis datasets. However, they are supposed to efficiently simulate the past climate conditions and the statistical properties of atmospheric variables for any region of interest. Yet, the low resolution of these models and the numerous parametrisations that are involved in the simulations could result in large inaccuracies or biases. As an illustration, we will present the simulated humidity predictors (T-Td) and HGT500 fields of some of the selected GCMs.

The seasonal cycles of T-Td in ERA-Interim and in the HadGEM2-CC model are presented on Fig.VIII.1 for NO, GE and AN. The cycles have been computed using the data from 1979 to 2005 (largest common period) and gathering all three historical members of each GCM. It allows us to partly free ourself from the low-frequency fluctuations in the GCMs and to use a 27x3 year period to describe the simulated past climate. In all regions, T-Td cycles are poorly simulated by the GCMs (biased shapes and amplitudes). In most cases (apart from Scandinavian regions, here NO), summer moisture is too low but winter is too humid. Applying the same quantile-mapping seasonal bias correction as for ERA-20C in Part IV partly remove these large biases. Even if the cycles shapes are not entirely corrected (e.g in Germany with a lower peak in summer), the range of T-Td values is much more consistent with the ERA-Interim data. As explained in Chap.VI, performing a bias correction on predictors is not entirely satisfying. However, this correction seems necessary before downscaling the GCMs simulations.

Unlike ERA20C, no surface wind or pressure observations are assimilated in GCMs making the simulated atmospheric circulation potentially biased. Thus, we also performed a comparison of the PSL and HGT500 fields between the selected GCMs and ERA-Interim. Firtly, Fig.VIII.2 presents the mean seasonal (winter and summer) biases in HGT500 for all GCMs. Most of the following comments are valid for PSL. For all models, the biases are generally stronger in winter. Both MPI and IPSL models present a strong negative bias in 500hPa geopotential height located over the British Isles. There is a better agreement between HadGEM2, MIROC and ERA-Interim with weak negative biases mainly located in western or central Europe. However, these two models are less consistent with the climate reanalysis data in summer. This is particularly the case of MIROC whose mean geopotential height is overestimated over Scandinavia. No significant bias between MPI, IPSL and ERA-Interim can be seen in summer. All in all, the characteristics of the GCMs biases in HGT500 are very model and season-dependent.

The mean seasonal bias in geopotential height or sea level pressure does not give information on the origin of these differences. They could come either from deeper of weaker pressure features in the model or from a bias in the atmospheric circulation and in the usual trajectory of mid-latitude cyclones. To estimate the extent to which GCMs are able to accurately simulate the atmospheric circulation over Europe, we performed an Empirical Orthogonal Functions (EOF) analysis (also known as Principal Components analysis). EOFs identify the spatial modes of variability (ie, the most characteristic spatial patterns) and quantify their contributions to the total variablity of weather patterns. This method has been widely used to characterise the atmopheric circulation or to establish

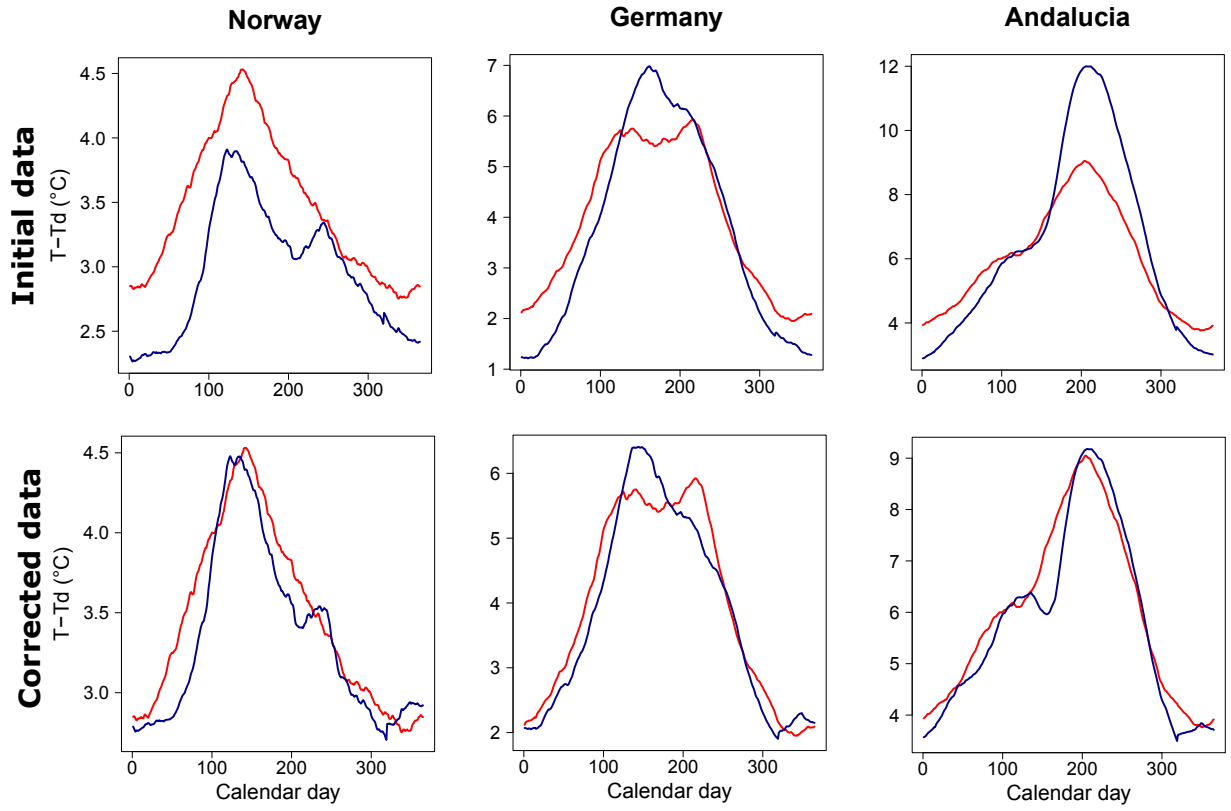

Figure VIII.1 – **T-Td bias in HadGEM2-CC.** Mean seasonal cycle of T-Td in ERA-Interim (red) and HadGEM-CC model (blue) for 3 of the 12 test regions. The first row corresponds to the uncorrected data for HadGEM-CC. The second one presents the results of a seasonal Q-Q correction. The cycles have been computed over the 1979-2005 period.

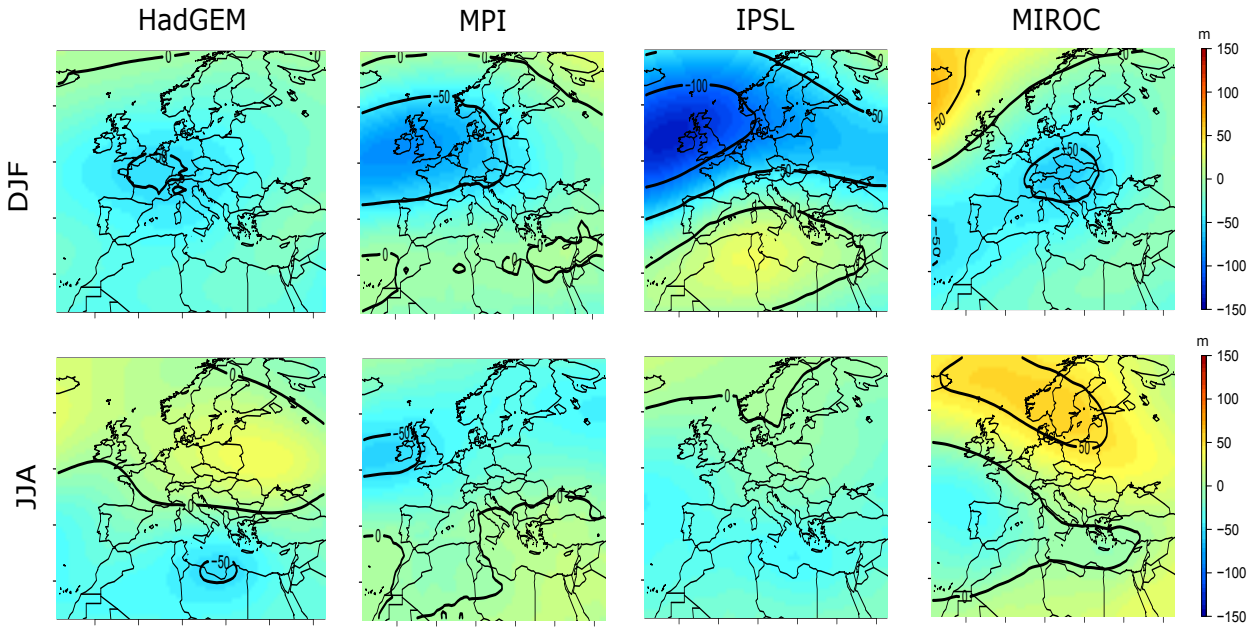

Figure VIII.2 – **Bias in mean seasonal 500hPa geopotentiel height for the four selected GCMs** over the 1979-2005 period. Results are presented for both winter (DJF) and summer (JJA).

a classification of synoptic situations into weather types [Esteban et al., 2006; Huth et al., 2008; Beck and Philipp, 2010; Bower et al., 2007; Hurrell and Deser, 2015; Lafaysse et al., 2014; Boe, 2007].

A detailed description of the functionning and developpment of an EOF analysis can be found in Von Storch and Zwiers, 2001; Bjornsson and Venegas, 1997.

We performed an EOFs analysis on an enlarged European domain. The boundaries of this domain have been set such as all the analogy domains used for HGT500 and PSL in SCAMP would be included, that is to say: 23.25°W-42.75°E / 24°N-69°N. As an illustration of the spatial bias in the GCMs, we present on Fig.VIII.3 a comparison between the first three EOFs in MPI-ESM and in ERA-Interim. Winter and summer have been considered separately to account for a possible seasonality in bias.

Regarding the winter reference modes in ERA-Interim, 41% of the total variance is explained by westerlies (NAO). The second mode consists of a strong anomaly located over the British Isles and represents 28% of the variability. Finally the third mode (14%) is characterised by a W-E dipole with one anomaly located over the Atlantic Ocean and the other one in central Europe. The MPI-ESM model has difficulties to simulate accurately the winter westerlies. The positions of the anomalies are shifted south-westward and they account for only 32% of the total variance. EOF2 and EOF3 are relatively well simulated in the model but their order is reversed (EOF3 is more frequent than EOF2). EOF3 is also slightly shifted in the MPI-ESM model giving a NO-SE dipole.

In summer, the first mode (33%) consists of an anomaly in geopotential height located over the North Sea. A new dipole (British Isles vs Scandinavia) comes next and represents 26% of the total summer variability. Finally, the third EOF presents two anomalies of the same sign over the Atlantic and in Western Russia while an opposite one is located in Northern Atlantic. Both order and associated explained variance of the three reference summer EOFs are well simulated by the MPI-ESM model. However some imprecisions exist in the location and intensity of the anomalies (eg. weak maximum in EOF2 shifted south-westward).

Speaking generally, the spatial bias in EOF modes is very model-dependent and changes greatly from one season to the other. This comment is in agreement with some previous studies [Lafaysse et al., 2014]. It is not possible to make general comments that are valid for all the GCMs selected in this study. We presented the results associated the MPI-ESM model to illustrate the magnitude of the biases and how they could affect the global atmospheric circulation in GCMs. Yet, performing a spatial correction of HGT500 and PSL in our climate simulation is far from being straightforward. To our knowledge, no satisfactory bias correction method have been developed and evaluated for the correction of multivariate spatial fields from GCMs. Such a correction would require, on one hand to modify the spatial structure of the inaccurate simulated EOFs modes and, on the other hand to adjust the explained variance of each of these modes. The development of a relevant correction method, which would not worsen the first analogy level of SCAMP based on shapes and gradients of HGT500 and PSL, is beyond the scope of this study. Moreover, the reference EOFs from ERA-Interim have been computed on a relatively short period (from 1979 to 2005) giving more uncertainty to their estimation. Considering all these limitations and difficulties, no correction of SLP and HGT500 from the selected GCMs was made before downscaling.

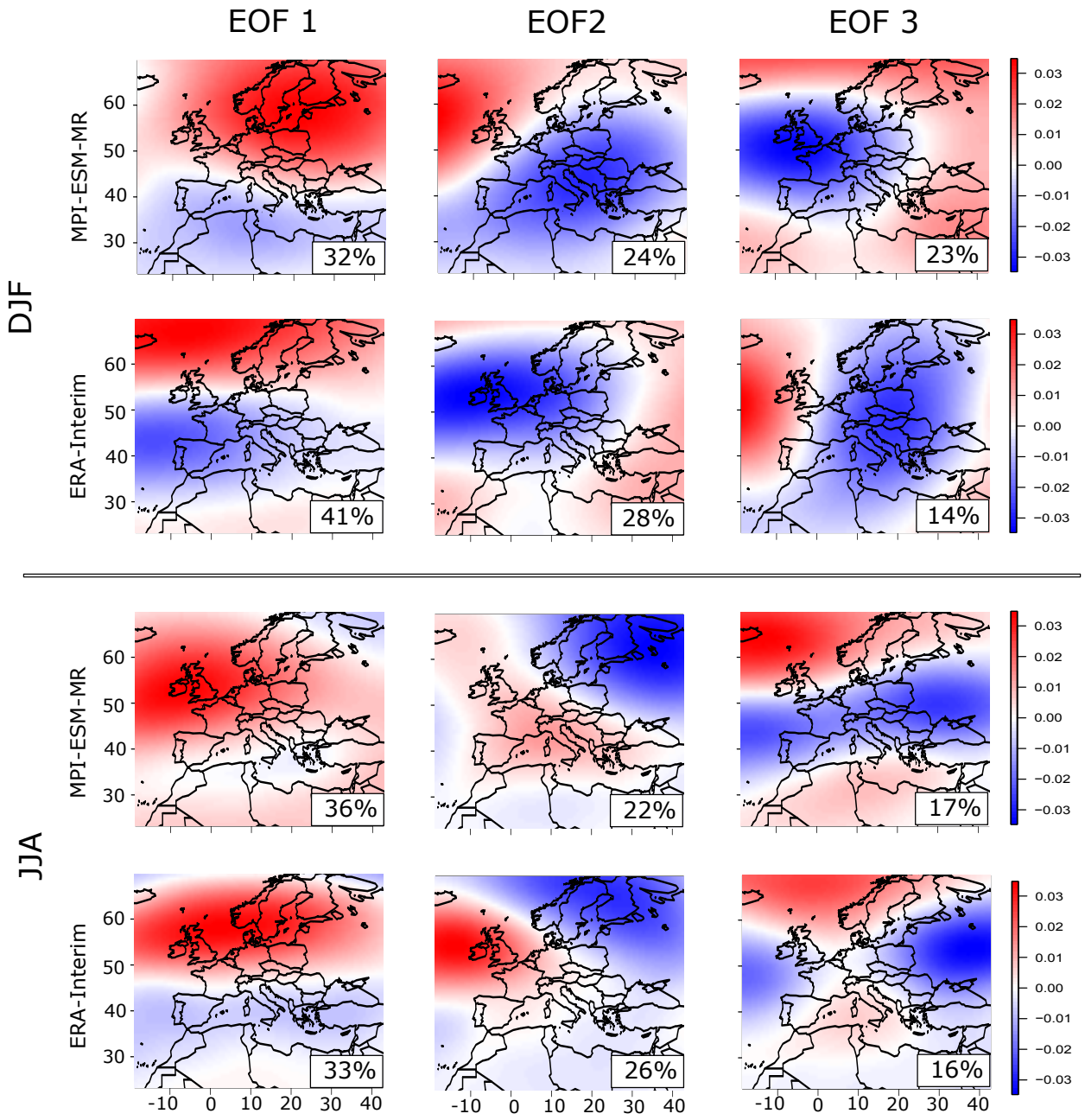

Figure VIII.3 – **Comparison between the first three EOFs of 500hPa geopotential height in the MPI-ESM and in ERA-Interim.** Results are presented for both winter (DJF) and summer (JJA).

2. Downscaled future climate

2.1. Future trends and modifications

Using SCAMP and the corrected GCMs data, daily series of regional predictands were generated from 1960 to 2100. We will first present the time series associated to the HadGEM2-CC model. The results obtained with this model are similar to the ones of the three other GCMs.

The 20-year moving averaged series of predictands from the downscaled simulations of the HadGEM2-CC model are presented on Fig.VIII.4, for three representative regions (NO, GE and AN). It gathers all runs (historical, RCP4.5 and RCP8.5) and members. The dark line represents the median downscaled scenario and the inter-scenarios dispersion (90^{th} and 10^{th} percentiles distance) is shown thanks to the color shading.

For temperature, the increase begins at the starting date of the historical time series in all regions. In the first half of the 21^{st} century the RCP8.5 and RCP4.5 are very similar. They move apart from 2050 with the RCP4.5 temperature still increasing but more reasonably. Conversely, all RCP8.5 members present a continuous and strong rise until the end of the 21^{st} century. These results are consistent with GHG emissions peaking in 2040 in the RPC4.5 case while they keep on increasing for RCP8.5. For all regions and runs, the inter-scenarios dispersion is small (90^{th} and 10^{th} percentiles distance <0.5°C). All members (historical and RCP8.5) are also very consistent with each other (distance between median downscaled scenarios < 1°C).

Both precipitation and wind are expected to decrease in the course of the 21^{st} century according to the HadGEM2 model. However, the large inter-downscaled scenarios and inter-members dispersion gives lower confidence in the amplitude of the decrease. Moreover, in most cases, it is not possible to discriminate between the RCP45 and RCP85, as their time series do not diverge significantly, even at the end of the century.

Finally, and despite the still large small scale variability, the trends are less questionable for radiation. Sun radiation is expected to increase significantly especially for the RCP8.5. Such as for temperature, the RCPs split after 2050 and there is a stabilisation of the radiation series with the RCP4.5.

From a spatial point of view, Fig.VIII.5 shows the absolute changes from the 1970-2000 period to the 2070-2100 one. The downscaled weather series associated to the RCP85 are presented for all the selected GCMs. When several members are available (HadGEM2, MIROC), the displayed change is the mean value from all three members. For precipitation, wind and radiation the relative change is also indicated. Generally speaking, there is a strong agreement between the downscaled series obtained with the 4 selected GCMs. However, some spatial disparities or difference in the magnitude of the change are noticeable.

All GCMs simulations downscaled with SCAMP agree on an important increase in temperature until the end of the 21^{th} century. The strongest changes are obtained for the HadGEM2 model which gives up to +7°C in IT and RO. On the other hand, the smallest changes are given by MPI with a maximum rise of +4°C. However, this model only has a single member for the RCP8.5 giving less reliability to its results. The spatial structure of change in downscaled temperature is very similar from one GCM to the other. Regions close to the Atlantic Ocean would experience a more reasonable increase while Mediterranean regions and central Europe get a much warmer climate.

The approximately same comments are valid for regional precipitation. Everywhere in Europe, downscaled precipitation projections present an almost systematic decrease in annual precipitation. These drops can reach from -40 to -50% in some cases (IPSL, RO-GR ; HadGEM, IT-RO-BE ;

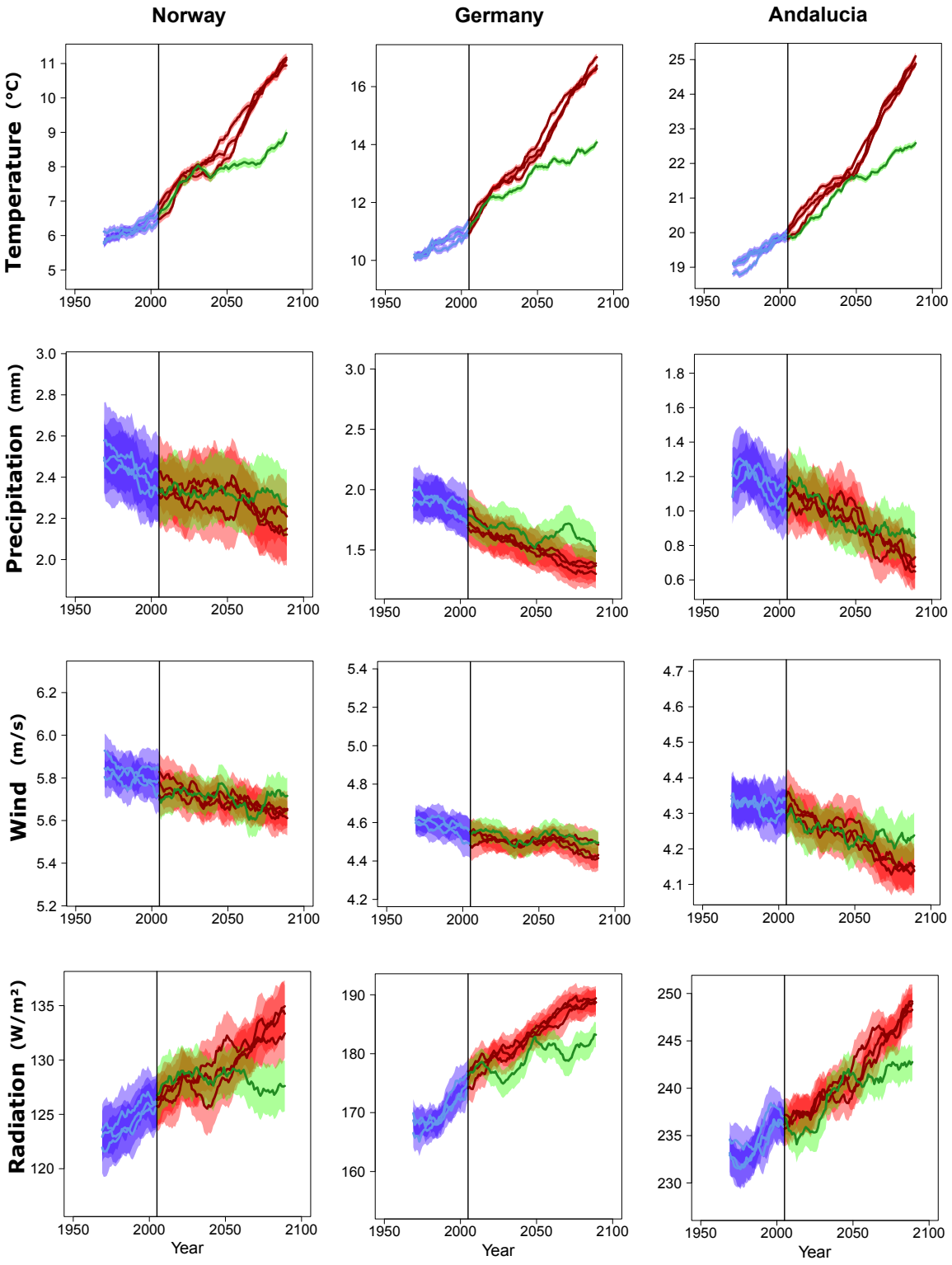

Figure VIII.4 – **Time series of predictands from downscaled HadGEM2-CC.** 20-year moving averaged series of predictands from the downscaled simulations of the HadGEM2-CC model, including all run (historical, RCP4.5 and RCP8.5) and members, and for three representative regions (NO, GE and AN). The dark lines represent the median downscaled scenario and the inter-scenarios dispersions (90^{th} and 10^{th} percentiles distance) are shown thanks to the color shading.

MIROC, IT-RO). The Atlantic regions (GA, EN, NO) are again showing less significant changes while south-eastern Europe undergo much rarer rainfall.

Generally speaking, all 4 downscaled GCM simulations seem to indicate that wind speed is going to decrease in Europe. However, these changes are weak. The most significant results is for TU, where all models agree on a reduction of wind speed from 4 to 6%.

The regional changes in downscaled radiation are once again very similar in the selected GCMs, apart from the MPI model which presents lower values. Near-surface sun radiation increases during the 21^{st} century. In addition to regions close to the Ocean, for which less modifications are expected, the Mediterranean basin also shows moderated changes.

Some of these results are consistent with other studies focusing on the effect of global warning on the European climate. This is the case for temperature which is expected to strongly increase until the end of the century under the RCP8.5 [Rogelj, 2013; Harris et al., 2010]. Heat waves and extreme hot temperature will also become more frequent and intense [Ballester et al., 2010a; Ballester et al., 2010b; Kjellström et al., 2007; Schär et al., 2004]. The downscaled future wind speed in our 12 test regions also follows the results of some past study, suggesting a decrease in wind speed in Mediterranean regions [Tobin et al., 2015]. However, all GCM-SCAMP chains indicate a global decrease in precipitation for the whole European continent. These results are not always consistent with the outcomes of several recent studies.

2.2. The case of precipitation

Many climate change studies have not only focused on the likely temperature increase but also on its possible effect on precipitation [Tapiador, 2010; Trenberth, 2011]. Despite a more complex context related to the variability of precipitation on many temporal and spatial scales, there is a growing consensus on what can be expected for Europe in the next decades. The last IPCC report [IPCC, 2013] already suggested that most GCMs from CMIP5 agreed on two opposite precipitation trends in Europe (RCP8.5): An increasing scarcity of rainfall in the Mediterranean basin on one hand, and a strong rise in annual precipitation in Scandinavia on the other hand. From western to central Europe, the uncertainty is higher and there is less confidence in the limited trends proposed by the models [IPCC, 2013; Jacob et al., 2014].

Many regional studies, using dynamically downscaled GCMs data came to the same conclusion on annual or seasonal precipitation [May, 2008; Ruosteenoja et al., 2007; Tapiador, 2010; Jacob et al., 2014]. Some additional work on intense precipitation (which was not evaluated in this study) indicate an increase of both frequency and intensity of extreme events [Fowler et al., 2007; Kyselỳ and Beranová, 2009; Madsen et al., 2014]. Supporting the developpement of numerous downscaled climate scenarios, EURO-CORDEX gave a more robust assessment of the future change in precipitation for Europe. The high resolution simulations (0.11°or 0.44°) issued from 10 regional models gave a more accurate spatial evaluation of these trends. Fig.VIII.6, extracted and adapted from Jacob et al., 2014, presents the multi-model change in precipitation in Europe between 1971-2000 and 2071-2100 for the RCP4.5 and RCP8.5. For both scenarios, the increase in precipitation is robust and significant in Central Europe, Scandinavia and in the British Isles (RCP85). Similarly, there is a high confidence in the drop in annual precipitation for the Mediterranean basin with the most pessimistic RCP. The projected changes in annual precipitation reach +30% with the RCP8.5 in Scandinavia and -20% in AN, TU and GR.

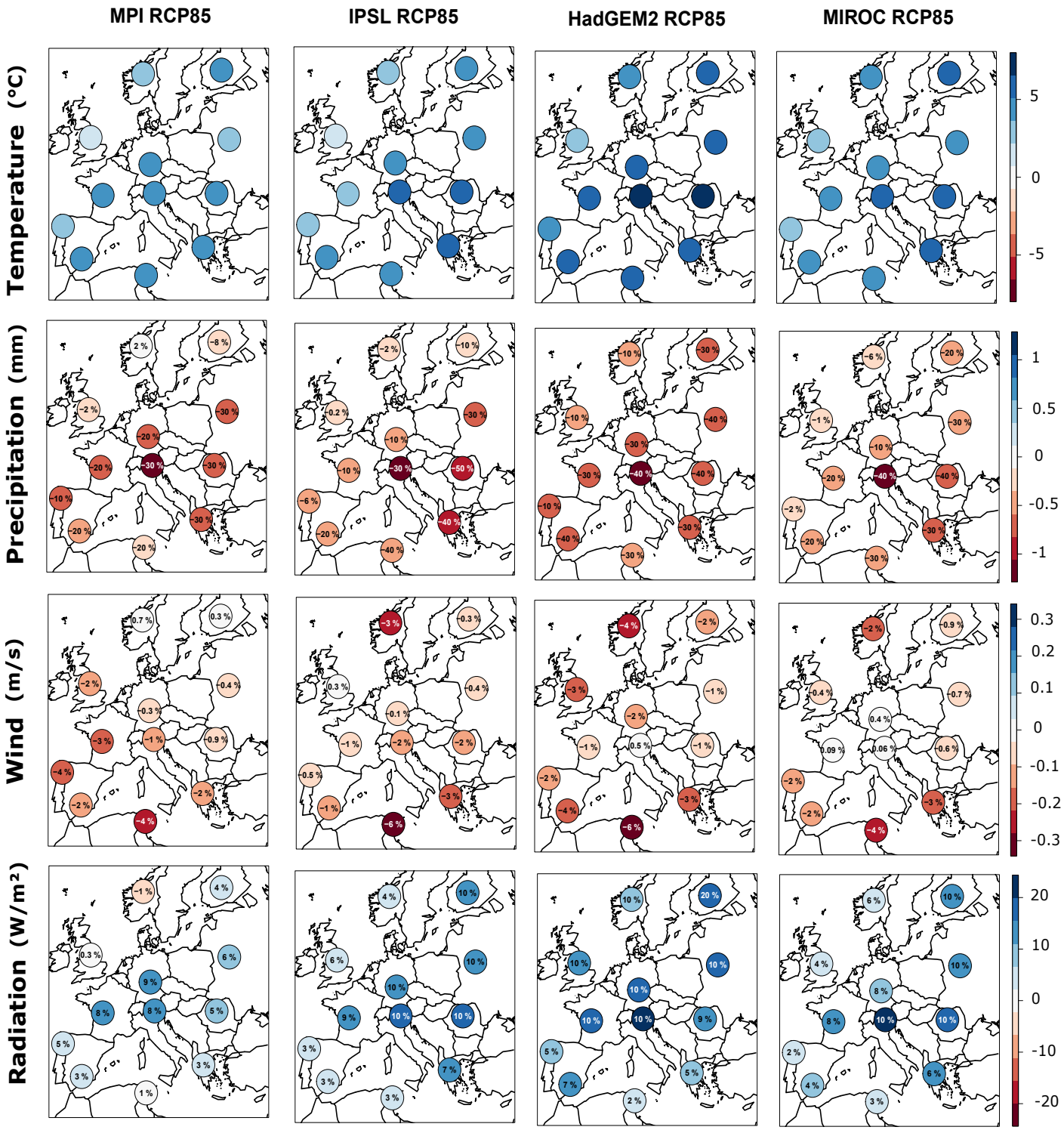

Figure VIII.5 – **Absolute change in annual mean of predictands from the 1970-2000 period to the 2070-2100 one.** The results associated to the RCP85 are presented for all the selected GCMs. When several members are available (HadGEM2, MIROC), the displayed change is the mean values from all three members. For Precipitation Wind and Radiation the relative change is also indicated.

This wide agreement on future trends in precipitation for Europe makes the results of our downscaled scenarios questionable. For all our 12 regions and 4 GCMs, SCAMP predicts a reduction in annual precipitation. Thus, it seems that the downscaling method, optimised for past and current climate conditions, fails to simulate accurately the regional series of precipitation. Despite the likely correct results for temperature and wind speed, it is not possible to use SCAMP to produce the

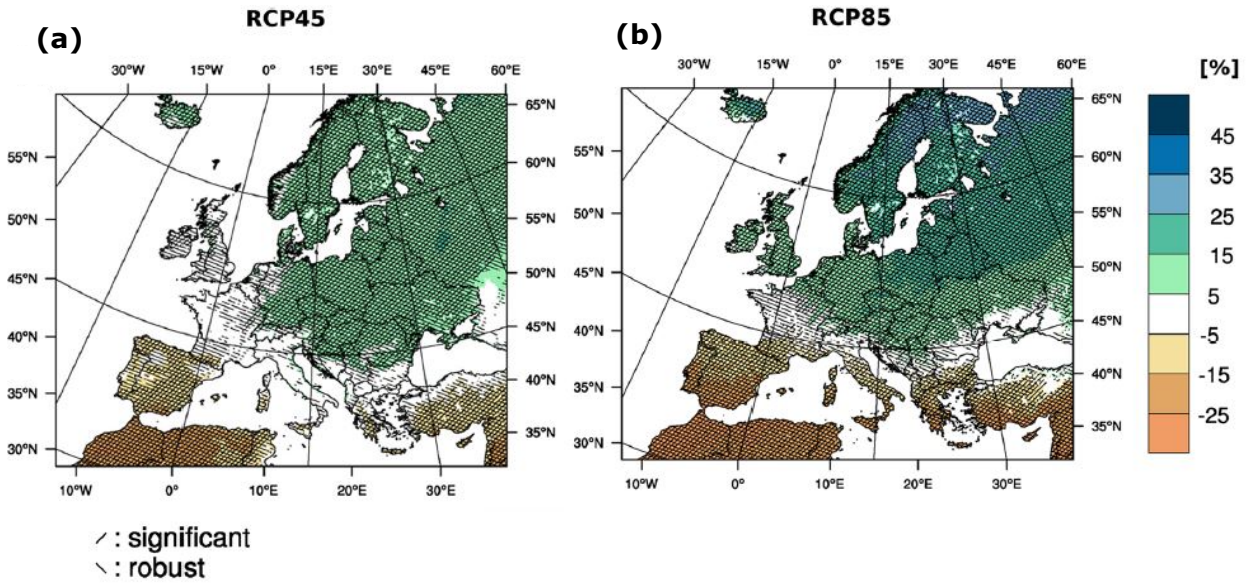

Figure VIII.6 – **EURO-CORDEX results on European precipiation changes.** Projected changes of total annual precipitation (%) for 2071-2100 compared to 1971-2000, for RCP4.5 (a) and RCP8.5 (b) scenarios. Hatched areas indicate regions with robust and/or statistical significant change. Extracted and adapted from Jacob et al., 2014.

multivariate scenarios of predictands we are interested in. Moreover, few studies on the projected change in sun radiation exist. We also have little confidence in the pan-European increase in sun radiation suggested by our downscaled series. Indeed, there are some common atmospheric mechanisms between precipitation and cloud cover. It is very probable that our results on radiation are similarly biased.

In the next chapter, we will try to identify some possible reasons of this inability of SCAMP to simulate relevant precipitation series under climate change conditions.

Chapter IX

SCAMP under Climate Change: The precipitation issue

In Chap.VIII, SCAMP was used to generate regional series of surface weather variables for a selection of GCMs until 2100. For temperature and wind, the simulated trends and changes were in good agreements with previous studies. However, the results associated to precipitation are more questionable for many European regions. SCAMP predicts a drop in annual precipitation for the whole continent whereas most past studies agreed on an strong increase of this variable for all regions except in the Mediterranean basin [Jacob et al., 2014].

Here, we attempt to identify some of the reasons for the inability of SCAMP to simulate relevant precipitation projections. Using a perfect-model approach, described hereafter, we evaluate and analyse some key features that could contribute to this issue.

1. Statistical downscaling methods and future scenarios

Statistical downscaling methods take advantage of the strong relationship between synoptic atmospheric conditions and local weather. A number of studies worldwide have used those links to generate downscaled projections of regional weather [Boé et al., 2006; Lafaysse et al., 2014; Willems and Vrac, 2011]. The application of downscaling methods for future projections relies on 4 main hypotheses that have to be accepted to guarantee the relevance of region scenarios [Musy et al., 2014].

H1 The large scale predictors are accurately simulated in the selected datasets.
First and foremost, the quality of input data to the downscaling method must be ensured. If a GCM is unable to simulate correctly the selected predictors (statistical distributions, multi-

scale spatio-temporal variability, inter-variables co-variations), one cannot expect the associated downscaled projections to be relevant. This idea is often referred to as the "Garbage-in, garbage-out" (GIGO [1]) concept, coming for the field of computer sciences but transferable to many other applications, especially to hydro-meteorology.

In Chap.VIII, we evaluated the ability of a selection of GCMs to simulate all the predictors involved in the downscaling of precipitation. The associated results highlighted the large biases in atmospheric circulation and in thermodynamic parameters. In such cases, a correction of GCMs outputs is classically performed for climate impact studies (e.g. Ines and Hansen, 2006; Piani et al., 2010; Hagemann et al., 2011). This was done for T-Td in order to ensure that the ranges of predictors values are comparable in both GCMs and reanalysis datasets. On the other hand, as the analogy of geopotential is based on shapes and gradients, HGT500 and PSL fields from GCMs were not modified. None of these options is entirely satisfactory. Indeed, performing a bias correction could deteriorate the predictors-predictand relationship while no correction could prevent from finding close analogues. It is likely that the biases in the predictors set partly contribute to the inconsistency of our precipitation scenarios. However, there are probably some other elements that come into play. To free ourselves from the bias contribution, we use SCAMP in a perfect-model approach. It consists in extracting both predictands and predictors from the outputs of unique general circulation or regional climate model. Then, analogues are searched for in the "climate model world". We will describe in details the functioning of SCAMP in a perfect-model approach together with the selected data in Sec.2.

H2 The selected predictors have a strong physical relationship with the predictands of interest and their predictive skills are strong

In Part III, a lot of effort has been put into building a multivariate analogue downscaling that guarantees both good predictive skills and correct inter-variable correlations. The final predictors set is a combination of HGT500, HGT1000 and T-Td. For precipitation, selecting T-Td rather than VV600 or a combination of relative humidity at 700 and 1000hPa, does not lead an important drop in predictive skills. The additional evaluation of seasonality and inter-annual variability confirmed the relevance of the multi-variate predictors for the simulation of regional precipitation. Therefore, H2 appears to be valid under current climate conditions.
In the following, we will assume that this hypothesis is also valid in a perfect model approach, meaning that the predictors set has a strong predictive skill for precipitation "in the climate model world". This hypothesis can be partly evaluated by comparing the raw simulated precipitation from the model with the outputs of SCAMP in perfect-model approach for past decades.

H3 The selected predictors carry the climate change signal and gather enough information to describe its effects on predictands

Climate Change is expected to impact not only local weather parameters but also synoptic meteorological features [Graff and LaCasce, 2012]. The optimal predictors set which has been identified in SCAMP from observations, has a strong predictive skill for precipitation. However,

[1] https://www.techopedia.com/definition/3801/garbage-in-garbage-out-gigo

the information on synoptic meteorology that the predictors bring, may not be enough to assess how climate change will impact this variable in the future. There is no evaluation method that can satisfactorily confirm that the simulated changes in the predictors set will suffice to catch the change in precipitation that will occur in the coming decades. We will partly address this question with the perfect model approach, by comparing the long-term trends from raw RCMs data and from reconstructed precipitation series. In addition, we will present how the simulated HGT500 and T-Td change from past climate conditions to the late 21^{st} century. As SCAMP is based on the analogue method, we will check that the future (2070-2100) ranges of simulated predictors/predictand values do not exceed the past ones (before 2000). If this condition is not fulfilled, SCAMP can have difficulties to find close analogues or to sample relevant precipitation values.

H4 The strong predictors-predictand relationships are still relevant and not modified by climate change

As mentioned for H2, the statistical relationship that has been established between HGT500, HGT1000, T-Td and precipitation is valid under past/current climate conditions. However, strong modifications of the climate system can result in a modification or a simple rupture of the predictor-predictand relationship. Another set of predictors could then be more relevant in a much warmer climate.

To highlight some possible modifications of the predictors-predictand relationship, we propose to compare two different ways of using SCAMP in a perfect-model approach. The first one, named SCAMP-FX, mimics the classic SCAMP and reconstructs the entire series of precipitation, looking for analogue dates on a fixed period (late 20^{th} century). The second one, SCAMP-MV, consists in adapting the positioning of the archive period to the target day by using a moving temporal window. We will discuss in detail the differences between these methods in the next section.

Precipitation can have different origins. Fronts and synoptic disturbances mostly result in stratiform precipitation. Convective processes are smaller scale phenomena which can bring a large contribution to the total precipitation amount, especially in summer. The large scale predictors of SCAMP have been selected to optimise the prediction of total precipitation. However, the predictors-predictand relationship could be different for the stratiform and convective contributions. Consequently, we will evaluate, for one of the GCM-RCM chain, some possible modifications of predictors-convective and predictors-stratiform precipitation relationships by using both SCAMP-FX and SCAMP-MV.

2. Perfect-model approach

2.1. Description of the method

The perfect model approach consists in applying SCAMP in the "GCM/RCM world". All physical processes (either simulated or parametrised) in climate models and all their meteorological outputs are considered as representative of the climate system. Of course, this modelling is incomplete and

many phenomena are roughly simulated or even not taken into account. However, since the perfect model method involves data from a unique model and no observations, no bias correction is required.

When using SCAMP, the perfect model approach implies that all predictors and predictands are extracted from the climate model (GCM-RCM chain in our particular case). For a given target day, analogues are searched for within a variety of simulated large-scale situations from the climate model. Similarly to what was done with observations, we define a model archive which sets the first and last dates that can be used as analogues. Then, the predicted values are simply the precipitation data simulated by the RCM on the selected analogue dates. Such a method has been already applied, for instance, by Dayon et al., 2015 to test the transferability of an analogue downscaling of precipitation in France. In their study, the authors generated a single time series by using the daily nearest analogues. Here, we will use the ensemble analogue approach, already presented for SCAMP in Chap.IV3.3, which consists in generating multiple downscaled series from the 30 nearest analogues identified for each prediction day.

We now describe the two different versions of SCAMP that will be used in the following analysis.

2.1.1. SCAMP-FX

SCAMP-FX (SCAMP-Fixed archive), uses a 30-yr long fixed archive period to identify analogue dates and reconstructs the entire series of precipitation until 2100. This archive extends from 1970 to 1999 as illustrated in Fig.IX.1.a. This first method mimics the downscaling of GCMs with SCAMP in Chap.VIII for which the archive period is constrained by the observations availability from 1983 to 2012.

2.1.2. SCAMP-MV

In SCAMP (resp. SCAMP-FX), the local weather conditions of a given target day are reconstructed using analogues and their associated observed (resp. simulated) values of predictands from a past reference period. Consequently, the range of possible predictions is limited to what has been observed (resp. simulated) in the past. Moreover, the predictors-predictand relationship used to downscale precipitation remains constant for the entire simulation period and is imposed by the archive period.

SCAMP-MV (SCAMP-Moving archive) makes use of the availability of simulated precipitation data for the whole 21^{th} century and proposes an adaptive archive period which is always centred on the target day. In order to compare its results to SCAMP-FX and to depend only on the positioning of the archive and not its length, analogues dates are also searched for within a 30-yr period ($\pm$15 years around the target day), as illustrated on Fig.IX.1.b. SCAMP-MV guarantees that all analogues are selected in a climatically homogeneous period. If the predictors-predictand relationship is modified but still relevant under warmer conditions, this method is expected to accurately simulate the fluctuations and the long-term trends of precipitation series.

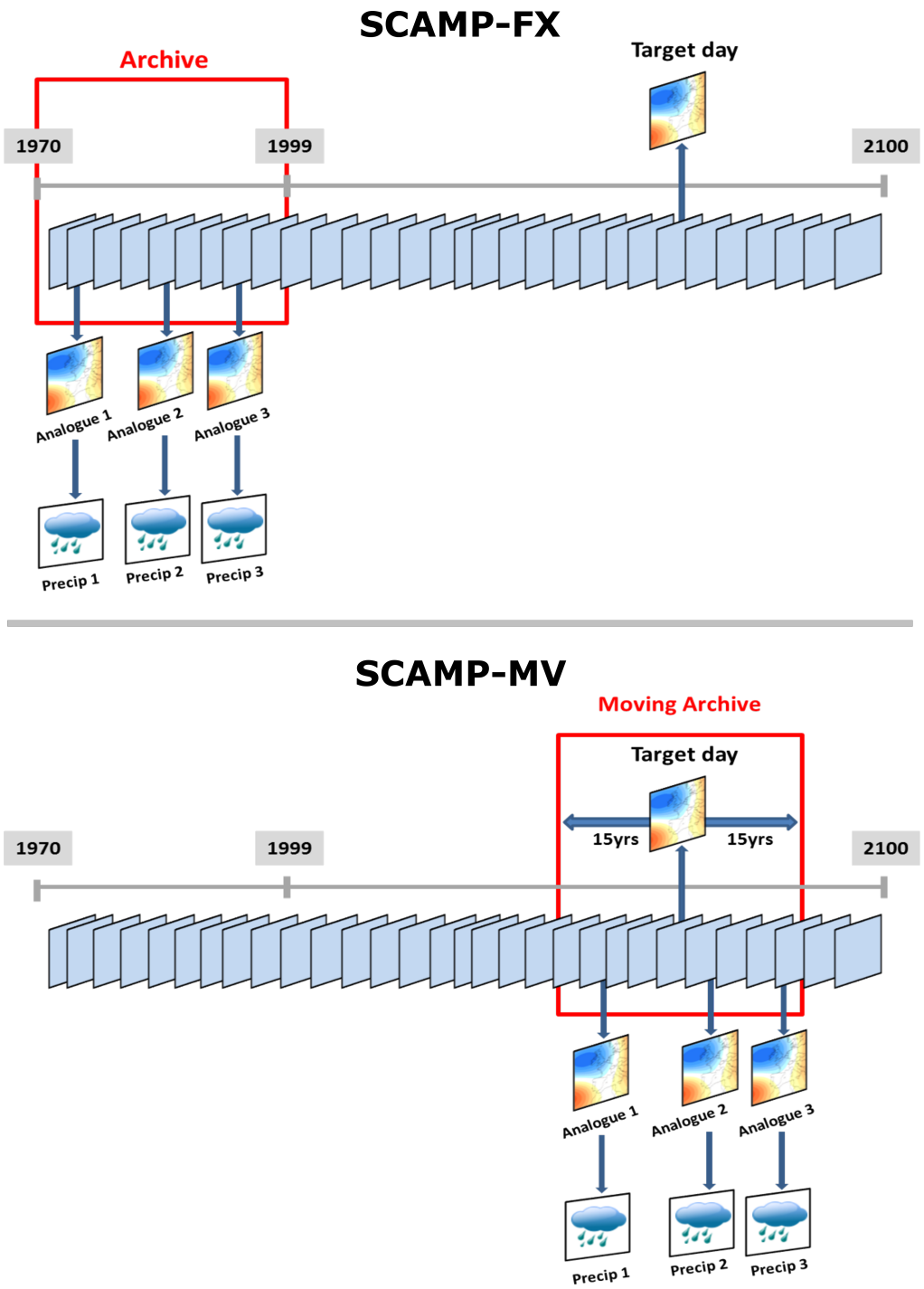

Figure IX.1 – **Comparative diagrams of SCAMP-FX (fixed archive) and SCAMP-MV (adaptive moving archive)** for the reconstruction of precipitation series in perfect model approach.

2.2. Data

Three GCM-RCM chains, developed as part of the EURO-CORDEX project, were selected as input data of SCAMP-FX and SCAMP-MV (cf. Tab.IX.1). They involve two of the GCMs already used in Chap.VIII (IPSL-CM5A-MR and MIROC5). We also performed this analysis for both RCP4.5 and RCP8.5. In order to mimic the simulations of SCAMP presented in Chap.VIII, the predictors data from the selected RCMs are spatially degraded from their initial resolution (0.11 or 0.44°) to a 0.75° grid, corresponding to the spatial resolution of ERA-Interim. We worked with HGT500, PSL

(which replaces HGT1000) and HURS (near surface relative humidity) which gives a very similar information to T-Td. The daily regional series of precipitation are computed by averaging precipitation fields within the regions boundaries illustrated in Fig.II.1.

In the following analysis, some figures will only present the results associated to IPSL-WRF. The good agreement between the 3 GCM-RCM chains makes all comments based on this single chain pretty much transferable to all the other selected models. Similarly, a combination of regions NO-AN, NO-FI-BE or FI-AN is often used to illustrate the most noteworthy outcomes of this analysis. Finally, the changes in precipitation are often stronger for the RCP8.5. We will present the downscaled simulations issued from this scenario to make their analysis easier.

In addition to the classic precipitation data, the convective part of daily precipitation has also been downloaded for the IPSL-CM5A-MR & WRF331F chain. As small scale processes related to convection cannot be explicitly solved by RCMs due to their spatial resolution, this variable results from the activation of the convection parametrisation. Gathering both total and convective precipitation, we can separate the convective from the stratiform contributions and highlight some possible modifications of predictors-predictand relationship for both of them.

Table IX.1 – Characteristics of the selected GCM-RCM chains

GCM	**RCM**	**Resolution**	**RCP**	**From-To (hist + RCP)**
IPSL-CM5A-MR	RCA4	0.11°	4.5|8.5	1970-2100
IPSL-CM5A-MR	WRF331F	0.11°	4.5|8.5	1951-2100
MIROC5	RCA4	0.44°	4.5|8.5	1951-2100

3. Results

3.1. Predictors and Predictands samples

In Sec.1, we mentioned that one hypothesis made when using statistical downscaling methods for future projections is that the selected predictors carry enough information on climate change to describe its effects on the predictand of interest (H3). Even if it is not possible to verify this statement as there is still a lot of uncertainty related the modifications due to global warming, we propose, as a first step, to compare the simulated characteristics of predictors between two periods: 1970-1999 and 2070-2099.

The first analogy level in SCAMP is only based on shapes and gradients of geopotential. Fig.IX.2 compares the simulated spatial modes of variability, of past and future winter atmospheric circulation in IPSL-WRF, thanks to an EOF analysis. For this model, the three first simulated modes under past climate conditions are still prevailing for the 2070-2099 period. They explain most of the spatial variability in HGT500 fields for both past (83%) and future (85%) periods. However, some important changes are noticeable in proportions of explained variance and positioning of the different anomalies. EOF1 is responsible for a similar percentage of simulated HGT500 variability for both periods but the centring of the associated anomalies is shifted earthward. The North Atlantic - central Europe dipole in past EOF2 is also shifted eastward at the end of the 21^{th} century. Moreover, the percentage of explained variance drops from 29 to 15% making this pattern third EOF in the future. Finally,

simulated past westerlies (EOF3) have a very similar structure from past to future climate conditions but are much more frequent (from 13 to 33% of explained variability). The IPSL-WRF model seems to simulate changes in atmospheric circulations mainly due to some modifications of the frequencies of past atmospheric regimes. The same type of comments can be made for PSL, other seasons and other GCM-RCM chains (not shown). However, despite some modifications of the main EOFs and some changes in their ranking, the search for relevant HGT500-PSL analogues for the 21^{st} century seems possible, at first sight.

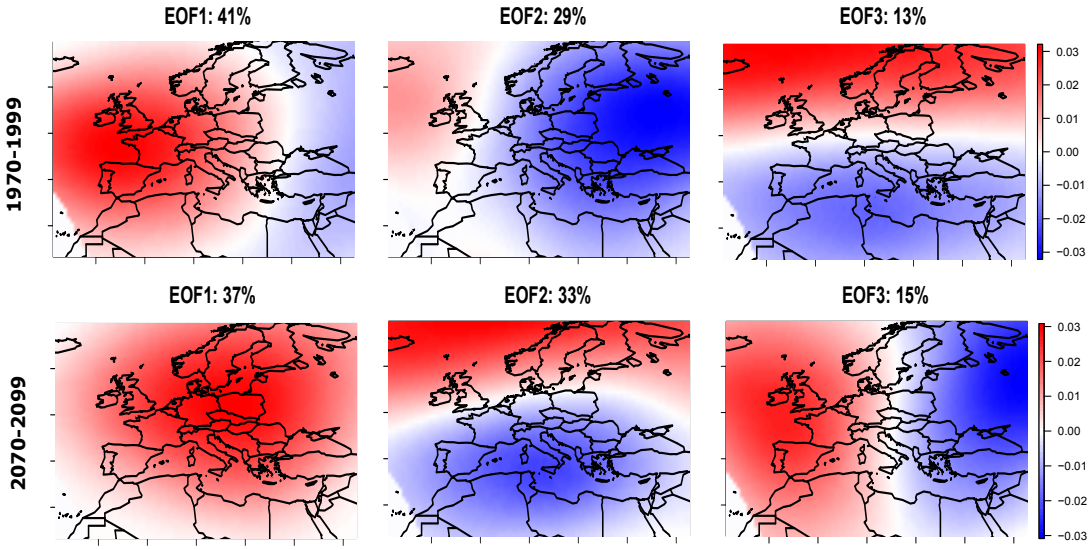

Figure IX.2 – **Simulated change in HGT500 first EOFs**. Comparison between the first three winter EOFs of 500hPa geopotential height in the IPSL-WRF chain from the 1970-1999 period to the 2070-2099 one.

Relative humidity takes part in the statistical downscaling for the second analogy level of SCAMP-FX (and SCAMP-MV). Fig.IX.3 presents the simulated probability density functions of this predictor for both past and future periods, the IPSL-WRF model and two representative regions (NO, AN). In Scandinavia, the model simulates more humid conditions at the end on the 21^{th} century. Conversely, the opposite change can be seen in Mediterranean regions (here AN). Despite these modifications in distribution shape, the ranges of both past and future simulated humidity are similar. Thus, it also seems possible to find relevant analogues based on HURS.

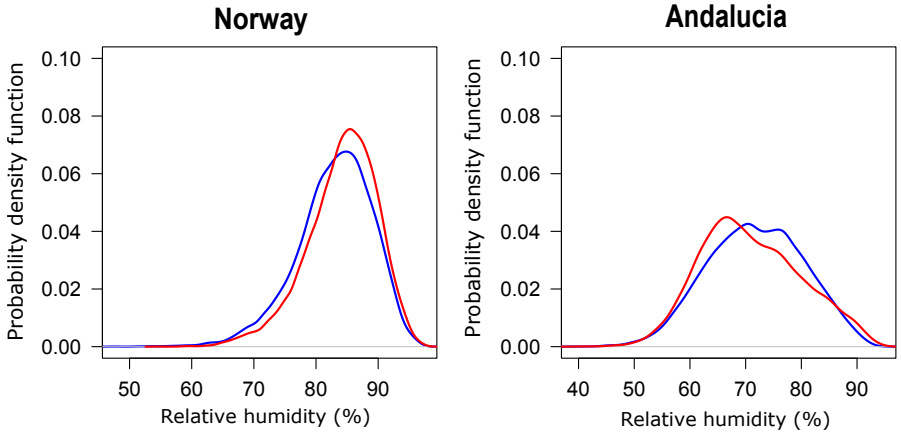

Figure IX.3 – **Simulated change in HURS**. Comparison between the probability density functions of 2m relative humidity in the IPSL-WRF chain from the 1970-1999 period to the 2070-2099 one. Results are presented for NO and AN.

Similarly to predictors, a drastic change in daily precipitation distribution (predictand) can deteriorate the performances of the analogue method. Indeed, using SCAMP, the range of predictions is constrained by the sample of precipitation values from the archive period. Fig.IX.4 illustrates the differences between past and future simulated cumulative distribution functions for the IPSL-WRF chain in NO and AN. Once again, Scandinavian and Mediterranean regions experience opposite simulated changes. High values of daily precipitation become more frequent in NO but rarer in AN. Nevertheless, the range of precipitation values is similar between past and future periods (e.g. in NO, only 9 daily precipitation values of the 2070-2099 period exceed the maximum precipitation from the 1970-1999 one). As a consequence, the reference precipitation sample (fixed archive) used in SCAMP-FX is not necessarily a limiting factor and all simulated future precipitation values can potentially be reconstructed.

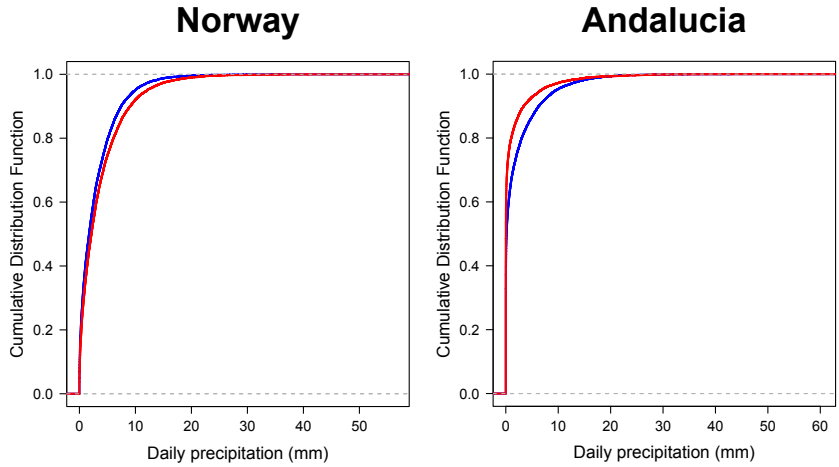

Figure IX.4 – **Simulated change in precipitation**. Comparison between the empirical Cumulative Distribution Functions of precipitation in the IPSL-WRF chain from the 1970-1999 (blue) period to the 2070-2099 one (red). Results are presented for NO and AN.

3.2. Analogy Scores

In Sec.3.1, we highlighted the modifications of both predictors and predictands in the RCM-GCM chains. Despite similar HGT500/PSL modes and comparable ranges of HURS values, it could be difficult to find as many relevant analogues (in terms of analogy scores) in the future as for a past period. Fig.IX.5 presents the 20-yr moving average series of analogy scores (TWS at level 1 and RMSE at level 2) with SCAMP-FX in FI and AN for the IPSL-WRF chain. In both regions the median value of the 1^{st} analogy score (ie. related to geopotential) remains constant with SCAMP-FX over the whole simulation period. The similarity between a given target day and its associated analogues (based on HGT500 and PSL) is as good in the future as under past atmospheric conditions. Likewise, the RMSE is mostly stable from 1960 to 2100 for both regions with a slight increase at the very end of the series. However, this modification is moderate and limited to the last 30 years of simulation. All in all, for this set of predictors and analogy scores, it seems that the "quality" of atmospheric analogues is not significantly deteriorating in the course of the 21^{st} century.

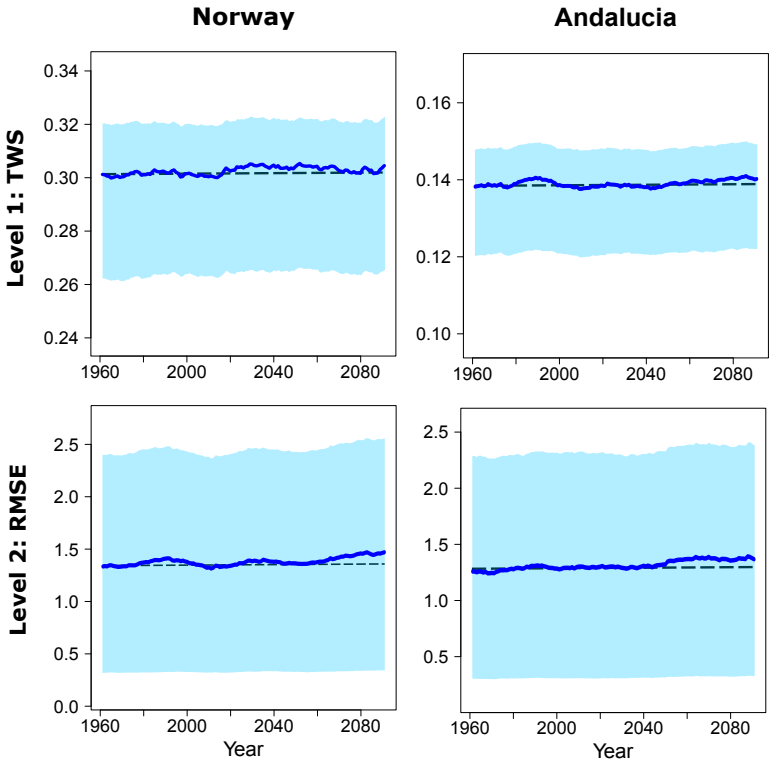

Figure IX.5 – **Time series of analogy scores.** 20-yr moving average series of analogy scores for both analogy levels (median) using SCAMP-FX (blue) in the IPSL-WRF model. The distance between the 10^{th} and the 90^{th} percentile of scores values is given thanks to the color shading. Results are presented for NO and AN. As a reminder: A perfect analogy is achieved for TWS=0 (identical HGT500/PSL fields) and RMSE=0 (same large-scale humidity).

3.3. Comparison between SCAMP-FX and SCAMP-MV

In this section, we explore some possible modifications of the predictors-predictand relationship which could deteriorate the prediction of precipitation in a climate change context (Hypothesis H4 from Sec.1). We use the two versions of SCAMP (SCAMP-FX and SCAMP-MV) presented in Sec.2.

Fig.IX.6 presents the 20-yr moving average series of simulated regional precipitation in the RCM and after downscaling by using both SCAMP-FX and SCAMP-MV. We present the simulations associated to all GCM-RCM chains forced by the RCP8.5 and to regions in north-eastern Europe (i.e. where the strongest increase in precipitation is expected by the end of the 21^{st} century). For a given GCM-RCM chain, SCAMP-FX and SCAMP-MV are forced by the same large scale information. Thus, the two methods are directly comparable and expected to presents similar high frequency fluctuations of precipitation. On the other hand, if the predictors-predictand relationship is valid, these variations should also follow the raw data from the GCM-RCM chain.

For both SCAMP versions, Fig.IX.6 highlights some bias between reference and downscaled precipitation series even during the "historical" period. Even if bias is a classic issue when using the analogue method [Young, 1994; Chardon et al., 2014], one should recall that both predictors set and analogy domains have been optimised in SCAMP by using observations and large scale reanalysis data of the late 20^{th} century. Each RCM has its own physics (equations, parametrisations) which describes the real atmospheric system but suffers from numerous imperfections. Hence, it would be necessary to re-optimise at least the positioning and dimension of the analogy domains. Moreover,

for some regions, the dimensions of the analogy windows associated to HGT500 had to be reduced as they were exceeding the RCMs boundaries. Non-optimal analogy windows could also result in a large bias as highlighted by several past studies (e.g. Chardon et al., 2014). In this study, our main interest is on the temporal fluctuations of precipitation. This systematic bias does not impact our analysis.

Despite some regional differences in precipitation amount, all RCMs agree on a large increase in mean daily precipitation for all regions in north-eastern Europe. SCAMP-FX is able, in a few cases to simulated part of this rise (NO, IPSL-RCA4 ; FI, MIROC-WRF). However, it generally greatly underestimates or fails to reproduce the long-term trends. The mismatch between RCM data and these reconstructed series gets more critical from the 2050s leading to differences exceeding 20% in some regions (BE, IPSL-RCA4 ; BE, IPSL-WRF). These results emphasise the inability of SCAMP-FX to simulate relevant series of precipitation when the European climate conditions have been modified by global warming. From the beginning of the simulation period to the 2000s, SCAMP-MV gives similar results to the ones of SCAMP-FX. However, for all models and regions the two curves move apart rapidly afterwards. The reconstructed precipitation series of SCAMP-MV, which adapts the archive period for the analogue days search, greatly correlate with the raw RCM data. SCAMP-MV is able to accurately simulate both low frequency fluctuations of precipitation and long term-trends resulting from climate change.

3.4. Predictive skills of the predictors set under Climate Change

The ability of SCAP-MV to reproduce the long-term trend and the low frequency fluctuations of precipitation is not sufficient to prove the relevance of the predictors set for future decades. Indeed, a simple moving-climatology model, which would use the same archive periods as SCAMP-MV, would definitely be able to catch these types of modification. Nevertheless, SCAMP-MV can provide a first assessment the predictive skills of the predictors set in a much warmer climate when looking at high frequency fluctuations (from daily to inter-annual) in the reconstructed series. Fig.IX.7 presents the annual series of precipitation anomalies from the raw MIROC-RCA4 data and after downscaling with SCAMP-MV. These anomaly series have been constructed by subtracting the low frequency fluctuations (30-yr moving average) of the RCM precipitation data to both initial RCM and downscaled series. The filtering does not remove the bias in the SCAMP-MV simulations, which is still visible for some regions (TU, AN), but it makes the comparison between the high frequency fluctuations of both reference and simulated series directly possible and much easier.

For all regions and the entire simulation period, there is a strong consistency between SCAMP-MV and the RCM. Both chronology and magnitude of the positive/negative anomalies in annual precipitation are accurately reproduced by the downscaling method. The Spearman correlation coefficients between the reference and simulated series range from 0.75 (TU) to 0.92 (GA). Therefore, the ability of SCAMP-MV to simulate accurately the inter-annual variability of precipitation does not change in the course of the 21^{st} century.

From these results, it appears the predictors set has a strong predictive skill for the whole 21^{st} century. Hence, the discordance between the simulations of SCAMP-FX and SCAMP-MV suggests

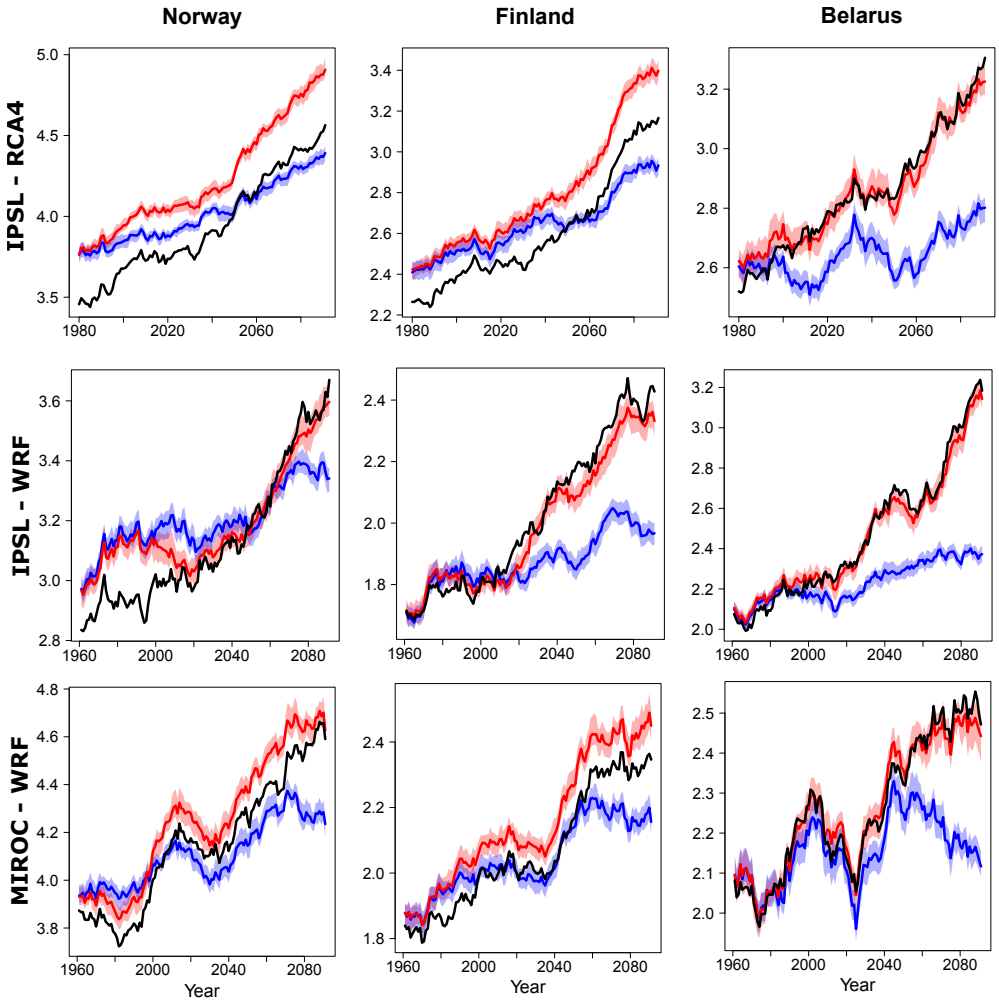

Figure IX.6 – **Time series of simulated precipitation (mm).** 20-yr moving average series of regional precipitation in RCM (back curve) and after downscaling (median scenario) with SCAMP-FX (blue) and SCAMP-MV (red). The distance between the 10^{th} and the 90^{th} percentile is given thanks to the color shading. Results are presented for all RCMs in NO, FI and BE.

that the predictors-predictand relationship is gradually but continuously modified in the course of the 21^{st} century, explaining the poor performances of SCAMP-FX.

3.5. Convective and stratiform precipitation

To further investigate the origins of the increasing discrepancy between SCAMP-FX and the RCM precipitation series, we apply the previous methodology to convective (Pc) and stratiform precipitation (Ps) for one of the GCM-RCM chain presented previously (IPSL-WRF). In practice, only total and convective precipitation are available as classic outputs of RCMs. The daily stratiform precipitation series can be directly generated from a simple difference (Eq.IX.1). Thus, we separate the part of precipitation amount due to convection from the stratiform one, related to synoptic fronts or non-convective orographic processes. Convective and stratiform precipitation series are then reconstructed in turns with both SCAMP-FX and SCAMP-MV by using the same methodology as for total precipitation in the previous section.

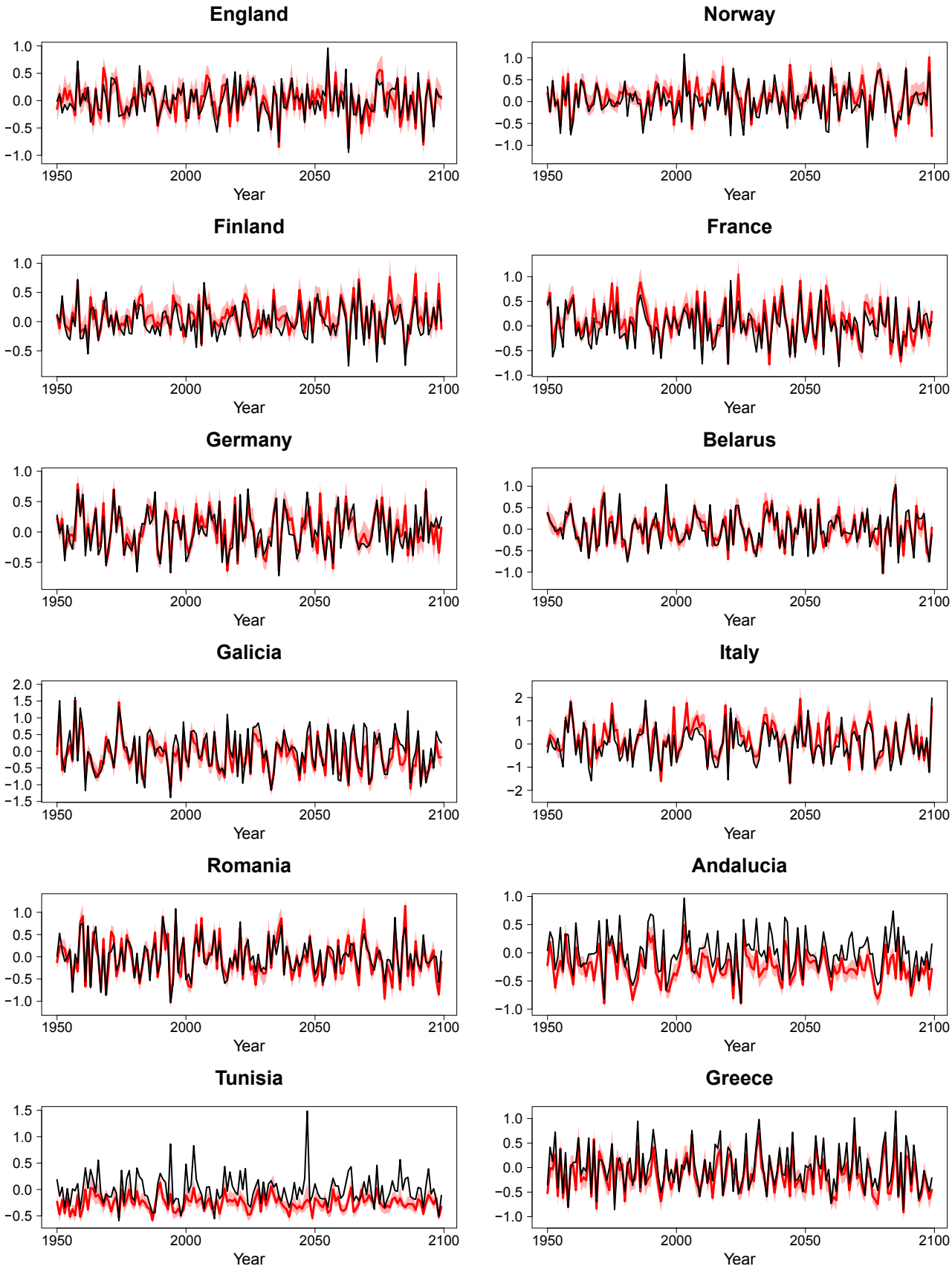

Figure IX.7 – **Precipitation inter-annual variability (mm) from MIROC-RCA4 and after downscaling with SCAMP-MV**. Annual series of precipitation anomalies from the raw MIROC-RCA4 (black) data and after downscaling with SCAMP-MV (red). These anomaly series have been constructed subtracting the low frequency fluctuations (30-yr moving average) of the RCM precipitation data to both initial RCM and downscaled series. The distance between the 10^{th} and the 90^{th} percentile is given thanks to the color shading.

$$Ps = P - Pc \tag{IX.1}$$

Where

- P: Total precipitation
- Pc: Convective precipitation
- Ps: Stratiform precipitation

Results will be presented only for two regions, one in Scandinavia (FI) and one in the Mediterranean (AN), illustrating two major and different types of precipitation regimes in Europe. The shares of convective/stratiform precipitation is radically different between these two regions. In the "GCM-RCM world", convective precipitation represents approximately 30% of the total amount in FI whereas it is about 50% in AN. Although both RCPs have been run, we will only focus on the RCP8.5 for which the strongest modifications in precipitation exist.

3.5.1. Precipitation amount

On Fig.IX.8 are presented the 20-yr moving average series of regional stratiform/convective precipitation in the IPSL-WRF model and after reconstruction with both SCAMP-FX and SCAMP-MV. In northern regions, IPSL-WRF simulates an increase in both stratiform and convective precipitation. Conversely, these two variables are expected to decrease strongly in AN.

In AN and FI and for both precipitation types, SCAMP-MV reproduces rather well the trend and low frequency fluctuations of the reference series. However, the simulated series get smoother for future decades and SCAMP-MV has more difficulties to simulate high frequency variations. Even if a similar evaluation as the one presented in Sec.3.4 would be necessary, it seems that the predictors-predictand relationship is weaker in the future for both Ps and Pc.

The results associated to SCAMP-FX demonstrate its inability to simulate either convective or stratiform precipitation changes in FI. Downscaled and reference precipitation amount diverges from 2000. In AN, SCAMP-FX seems to be more consistent with the IPSL-WRF convective precipitation, but the stratiform contribution is poorly reproduced. The conclusion for Pc and Ps is similar to the one of total precipitation: for both precipitation types, the predictors-predictand relationship seems to change under climate change.

3.5.2. Frequency of occurrence and intensity

In a warmer climate, both number of rainy days and precipitation intensity can be modified. To go one step further and understand better the reasons for the increasing discrepancy between initial and reconstructed RCM precipitation series, we analyse the ability of SCAMP-FX (and SCAMP-MV) to simulate the temporal evolution of intensity and frequency of "wet days". This analysis is performed separately for both convective and stratiform precipitation. We use a 1mm precipitation threshold to discriminate between wet and dry days. Consequently, wet days do not account for weak regional precipitation and very local events (the regional precipitation still being below 1mm). The associated results are presented on Fig.IX.9.

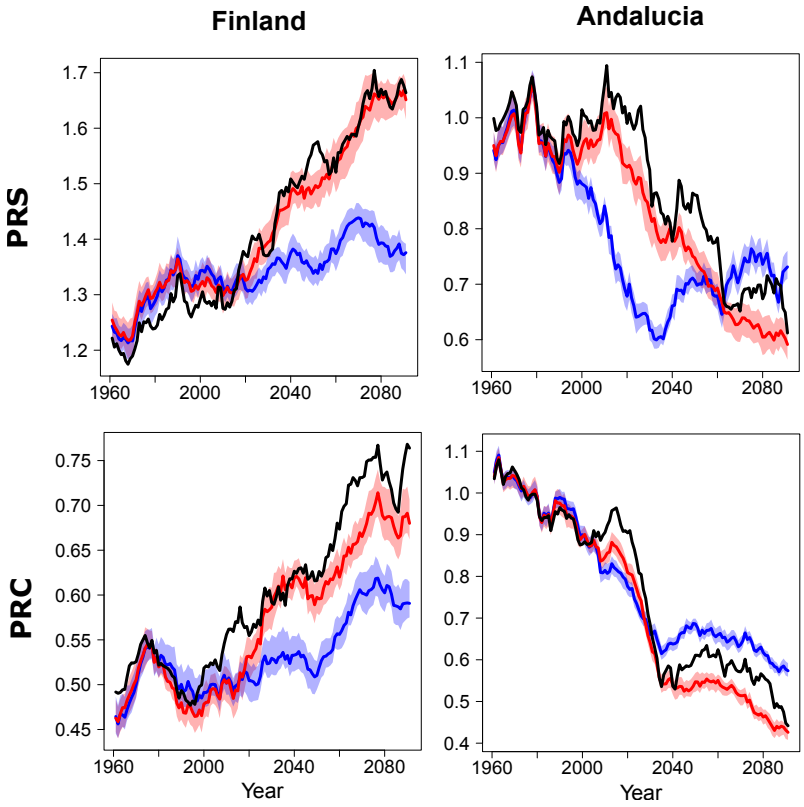

Figure IX.8 – **Simulated change in convective and stratiform precipitation (mm)**. 20-yr moving average series of regional stratiform (Ps) and convective (Pc) precipitation in RCM (back curve) and after downscaling (median scenario) using SCAMP-FX (blue) and the SCAMP-MV (red). The distance between the 10^{th} and the 90^{th} percentile is given thanks to the color shading. Results are presented for the IPSL-WRF model in FI and AN.

In FI, representing regions in North-eastern Europe, the frequency of occurrence of Ps and Ps is increasing in the model. This modification is relatively well simulated by both SCAMP-FX and SCAMP-MV. On the other hand, the mean intensity of wet days should also rise, especially for the stratiform part. In this case, SCAMP-FX fails to reproduce this increase, leading to the large bias in global precipitation described previously.

In AN, the bias seems to have a different origin. The frequency of occurrence of both convective and stratiform precipitation drops in the RCM raw data (-40%). SCAMP-FX is only able to simulate the modification associated to the stratiform contribution and presents a rather constant number of convective days. Considering the intensity of wet days, SCAMP-FX is able to simulate the right trends (reduction for Pc and no trend for Ps) but cannot reproduce low frequency fluctuations of any precipitation type (eg. positive anomalies for PRS from 2000 to 2060).

All in all, this analysis highlights the likely radical modifications in the triggering and intensity of convective/stratiform precipitation in the course of the 21^{st} century, leading to important biases for SCAMP-FX. In north-eastern Europe, the reconstructed series have a relevant number of wet days but the associated precipitation intensities are too low for both precipitation types in the future. In the Mediterranean, the most critical issue is the number of days for which convective precipitation is significant (>1mm). It remains roughly constant with SCAMP-FX while it drops for the raw model data.

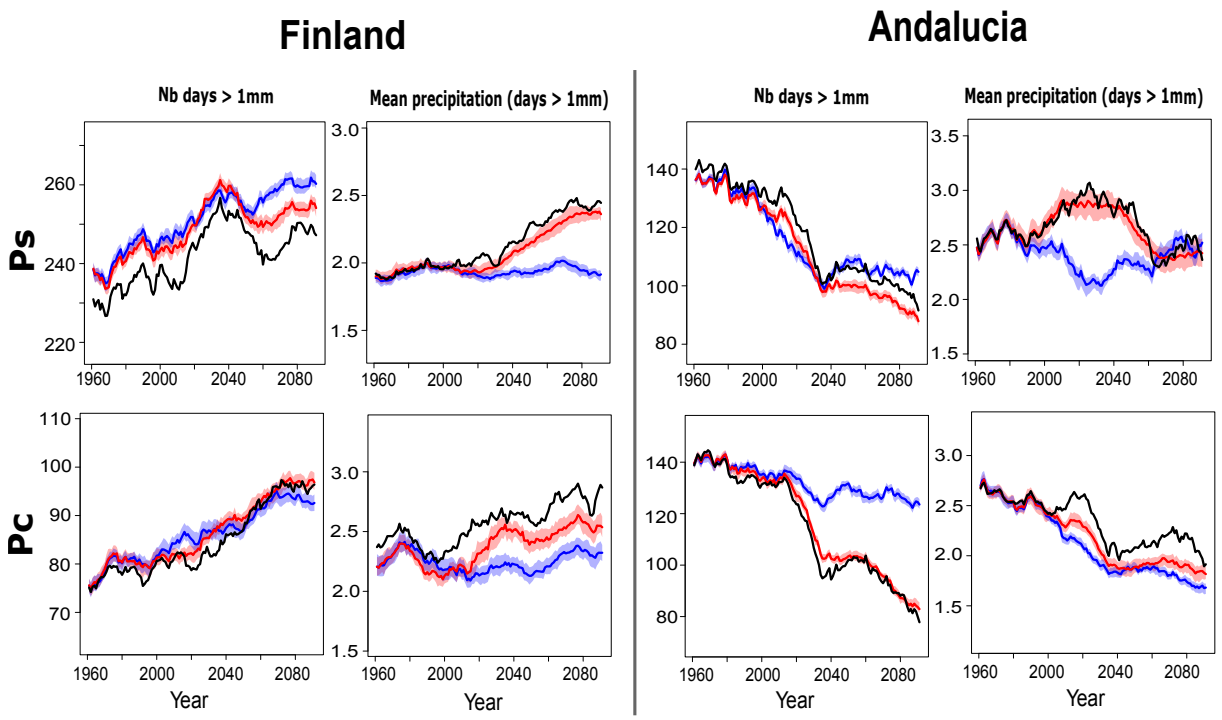

Figure IX.9 – **Simulated change in convective and stratiform precipitation characteristics.** 20-yr moving average series of number of days for which P>1mm (left) and mean precipitation amount (mm) for these rainy days (right) for regional stratiform (PRS) and convective (PRC) precipitation in RCM (back curve) and after downscaling (median scenario) using SCAMP-FX (blue) and SCAMP-MV (red). The distance between the 10^{th} and the 90^{th} percentile is given thanks to the color shading. Results are presented for the IPSL-WRF model in FI and AN.

3.6. Conclusion on this analysis

The previous results are obtained from the application of SCAMP in a perfect model approach. Therefore, their relevance is not guaranteed in a "real world" context (ie. using observations). However, they give some reasonable insight into the reasons for the discrepancy between SCAMP outputs and the results of numerous other studies [Jacob et al., 2014]. Moreover, there is a strong consistency between the results from the multiple GCM-RCMs used here. It also gives more confidence in the transferability of these conclusions to the issue highlighted in Chap.VIII for the "classic" SCAMP downscaling.

As a conclusion, we present the main outcomes of this analysis and some reasons that can contribute to the inconsistent precipitation projections presented in Chap.VIII:

1. The large scale predictors from the selected GCMs and required in SCAMP suffer from large biases which probably contribute to the inaccurate precipitation predictions. However, the perfect-model approach, which allows us to free ourself from these biases, proved that they cannot be the only contributors to the inconsistent simulations. Indeed, reconstructed series with SCAMP-FX present the same inability of simulating long-term changes in precipitation in a climate change context.

2. When analogue dates are identified based on HGT500/PSL and near-surface relative humidity, the "quality" of the analogues (in terms of analogy scores) seems to be constant in the course of the 21^{th} century. The characteristics/distributions of both predictors and predictand are mod-

ified by climate change but most future fields (HGT/PSL) or values (HURS and Precipitation) can be re-sampled from a past period. The precipitation issue does probably not result from the predictors or predictand samples.

3. Conversely to SCAMP-FX, a moving archive (SCAMP-MV) leads to relevant trend, low frequency fluctuations and more importantly accurate inter-annual variations of precipitation. Therefore, we can put forth the hypothesis that the predictors set still have strong predictive skills under future climate conditions but also that the predictor-predictand relationship is gradually modified for future decades.

4. Both convective and stratiform contributions to total precipitation are modified in the selected RCM for the coming decades. The issue of SCAMP-FX, which is likely transferable to SCAMP in Chap.VIII, is due to the mean precipitation intensity of wet days in Northern Europe and to their frequency of occurrence for Mediterranean regions.

Overview

In this part, we aimed to assess the effects of climate change on the co-variations of CRE sources and on their consistency with the energy demand. Using SCAMP and a selection of GCMs issued from the CMIP5, regional projections of CRE meteorological drivers were generated for the 21^{st} century. The associated series present a large increase in mean temperature for all regions (up to 7°C with the RCP8.5), a lessening of mean wind speed, more solar radiation and finally a drop in mean regional precipitation for the coming decades. This last result on precipitation runs counter to the findings of multiple studies focusing on European future climate scenarios [Jacob et al., 2014]. It gives little confidence in the ability of SCAMP to simulate relevant precipitation projections in a much warmer climate.

Using statistical downscaling method for future scenarios requires making some strong assumptions on predictors, predictands and on their statistical relationship:

H1 The large scale predictors are accurately simulated in the selected datasets.

H2 The selected predictors have a strong physical relationship with the predictands of interest and they predictive skills are strong.

H3 The selected predictors carry the climate change signal and gather enough information to describe its effects on predictands.

H4 The strong predictors-predictand relationship is still relevant and not modified by climate change.

We proposed to partly explore the validity of these hypotheses by using SCAMP in a perfect model approach. It consists in reconstructing the precipitation time series from a selection of RCMs by looking for analogues in the " climate model world" and using the associated simulated precipitation as local predictions. We introduced two different versions of SCAMP which either use a fixed past archive period for the analogue identification (SCAMP-FX) or a moving one (SCAMP-MV) for which the starting and ending date of the archive depend on the target day. SCAMP-MV gives an evaluation of the relevance of the predictors set under future climate conditions.

This analysis suggests that the predictors-predictand relationship is changing in the course of the 21^{st} century but that the selected predictors set still has strong predictive skills. Moreover, we separated the convective and stratiform contributions to the total simulated precipitation and showed that, for future decades:
- The daily intensities of convective and stratiform precipitation are underestimated in Northern European regions.
- The number of convective days is over-estimated for Mediterranean regions.
-The predictors-predictand relationship seems to change for both convective and stratiform precipitation.

Part VI

CONCLUSION

1. Main outcomes of this thesis

The integration of renewables in regional electric power systems will be one of the main challenges of the coming decades. The multi-scale variations of climate strongly impact some of these renewable energy sources and make their integration not straightforward.

This thesis proposed to study the ease of integration of climate-related-energy (CRE) sources in Europe (solar, wind and RoR hydro power). To perform this analysis, we developed a suite of models, named CRE-Mix, able to convert weather conditions into power generation and energy load series. CRE-Mix also assesses the temporal mismatch between production and demand.

Additionally, in order to extend this work to the entire 20^{th} and 21^{th} centuries, we set up a statistical downscaling method (SCAMP) capable of providing physically-consistent multivariate weather series from climate reanalysis or climate models data. We present here the main outcomes of these analyses, focusing on the multi-scale fluctuations of CRE sources and on their possible contribution to a sustainable electricity supply in Europe.

1.1. Variability and the ease of integration of CRE sources in Europe

The variety of European hydro-climatic conditions is large. The hydro-meteorological drivers of CRE sources (temperature, wind, solar radiation and river discharge) vary greatly at multiple time and space scales. It results in large temporal weather-driven fluctuations of solar, wind and RoR power series. The study of the 20^{th} century climate also showed that the inter-annual and low frequency fluctuations driven by large atmospheric/oceanic patterns play a key role for all energy sources and should not be neglected, especially for RoR hydro power.

Then we evaluated the ease of integration of single energy sources by using two criteria measuring the temporal match between electricity generation and energy load series. The first one, referred to as the penetration rate (PE), quantifies the proportion of energy demand that is fulfilled over a long period. Then, we focused on the characteristics of low energy production periods which are defined as one or several consecutive days for which the proportion of satisfied demand is bellow a given threshold. By analogy with hydrological droughts, we referred to these problematic periods as "energy droughts". The analysis is carried out in turn for 12 European regions, firstly by assuming a complete disconnection between them (i.e no inter-regions exchange of electricity).

Assuming a balance between mean production and mean energy load (over a 30-yr reference period), the intermittency of single CRE sources and demand time series leads to the following results:

- The global penetration rate is generally limited and the proportion of satisfied demand rarely exceeds 80%. The most problematic cases are for solar power in Northern Europe and for hydro power in Mediterranean regions with PE $< 60\%$. Moreover, the large low-frequency fluctuations of hydro power lead to important changes in PE from one decade to the other.
- Low production periods and energy droughts have various characteristics from one CRE source to the other. For hydro power these periods are infrequent but very long lasting. Conversely,

they never exceed a few days but are very numerous for wind power. Low production periods and energy droughts have intermediate characteristics for solar power.

The strong variability of CRE sources, imposed by hydro-climatic conditions, prevents them from providing an efficient and reliable energy supply. However, some integrating factors exist and can improve the supply-demand balance. Among the large panel of possible methods, we tested the potential improvements associated to: 1) Combining different CRE sources 2) Performing a spatial integration allowing, regions to complement each other 3) Introducing storage facilities of different capacities 4) Deliberately over-sizing power plants.

These integrating factors all proved, to varying degrees, their ability to reduce the temporal mismatch between electricity production and energy demand and to lower both duration and frequency of low production periods and energy droughts:

- Combining energy sources leads to much higher regional PE rates ranging from 80 to 92%. The droughts associated to regional energy mixes are rare and short-lasting.
- Spatially integrating power and load series increases to proportion of satisfied demand for both hydro and wind power sources. The strong seasonality and spatial homogeneity of solar production series lead to limited improvements for solar power.
- Small storage systems can balance the high frequency variations of wind power and significantly increase its ability of meet the energy demand. Much larger storage systems are necessary to achieve similar improvements with both solar and hydro power.
- For all CRE sources, oversized power plants moderately improve the production-demand balance.

Finally, combining two of the previous integrating factors (e.g. Energy mix & Storage, Energy mix & Spatial integration) leads to a much more reliable CRE system with high penetration rates and rare energy droughts.

1.2. Multi-variate downscaling with the Analogue method

The extension of the previous study to the entire 21^{st} century and to future scenarios cannot be done without some adaptations. Indeed, the spatial resolution of climate reanalysis data and of climate models is not sufficient to use directly their outputs as regional weather scenarios. Among the various existing downscaling approaches, we chose the Analogue method, which already proved it ability to generate relevant meteorological scenarios. It is also easily implemented and can be adapted for the generation of multivariate weather data.

Analysis the co-variations of CRE sources, requires producing regional weather series which, on one hand, accurately simulate the local conditions, and on the other hand guarantee the physical consistency between the downscaled variables.

Using the ERA-Interim data, we developed and optimised a multi-variate downscaling method, named SCAMP (Sequential Constructive Atmospheric Analogues for Multivariate weather Predic-

tions), which meets these requirements. It is based on a common analogue model (geopotential at 500 and 1000hPa and near surface relative humidity T-Td) for precipitation, solar radiation and temperature and an independent analogue model (geopotential at 1000hPa) for wind.

SCAMP is able to reproduce regional observed series with good predictive skills for all predictands. Seasonal cycles and inter-annual variability are also accurately simulated. The comparison of observed and simulated inter-variables correlations proved that the downscaled scenarios are physically consistent.

The application of SCAMP for the reconstruction of the 20^{th} century regional weather series allowed us to highlight the low frequency variability of CRE resources resulting from the multidecadal fluctuations of climate. These long-term variations are rather negligible for solar power, energy load and to a lesser extent for wind power. Conversely, large multidecadal fluctuations exist for hydro power.

Applying SCAMP to several Global Circulation Models (GCM) gave questionable results. On one hand, the downscaled scenarios of wind and temperature are very consistent with other studies focusing on these variables. On the other hand, the regional projections of precipitation indicate drier conditions at the end of the 21^{st} century for all test regions in Europe, including Scandinavia. This result is in disagreement with many recent studies projecting wetter conditions in northern and central Europe in a climate change context. Thus, SCAMP simulations for precipitation could not be used to extend the previous study to the coming decades.

In order to identify some possible reasons for the inapplicability of SCAMP in the context of this study, we proposed to use it in a perfect model approach and to reconstruct precipitation series from a selection Regional Climate Models (RCM). Such an application does not guarantee that its outcomes are valid "in the real world" but it allows us to make some fair hypotheses on the analogue downscaling issue. The associated outcomes are the followings:

- In the "RCMs world", the downscaled series of precipitation suffer from the same problem with a large decrease for all European regions. They are in disagreement with raw precipitation data from the selected RCMs.
- Both predictors and predictands characteristics are modified from past to future decades but the ranges of values and of possible weather situations are similar.
- It seems possible to find relevant analogues for future decades (constant analogy scores)
- The comparison of a classic SCAMP method, having a fixed archive (SCAMP-FX) with another one adapting the archive period to the target day (SCAMP-MV), indicates that the predictors set is still relevant in the future. However, the predictors-predictand relationship changes in the course of the 21^{st} century.

2. Some perspectives for further research

2.1. Improving some components of CRE-Mix

The suite of chains developed as part of this study (CRE-Mix), gives a first assessment of the ease of integration of some renewables in Europe. It is based on a set of simplifying assumptions which only take into account the effects of hydro-climatic variability. Consequently, it puts aside many other determining factors in the fluctuations of CRE sources such as, for instance, the technical limitations for the installation of new equipments and the non-climate-related fluctuations of energy demand. However, CRE-Mix includes several modules that allow for storage, energy sources combinations and electricity transmission between regions.

For most of the components of CRE-Mix, the multiple simplifying assumptions leave room of improvement. We present some the most noteworthy developments that could contribute to a more realistic model:

- Into order to focus our analysis only on the CRE fluctuations and not to depend on the absolute electricity production values, simulated power series were normalized, assuming that mean production equals mean energy demand for a long reference period of 33 years. This assumption implicitly implies that the regional level of equipment is high enough to meet the energy load. For some energy sources and regions, such a statement is likely not realistic. In FI or BE, for instance, a balance between hydro power and energy demand would require numerous and large power plants to overcome the regional small water head (limited max-min altitude difference). In TU, the limited water resources from rivers also make the use of hydro power for electricity production difficult. The regional population density also influences the mean energy demand and its effect on the production-demand balance has not been taken into account in CRE-Mix.

- The parametrisation of the hydrological model and all weather-energy conversion models is unique for all European regions. It draws a picture of the regional differences in CRE due to spatial fluctuations of climate. A more realistic option would consist in taking on board some more regional specificities. For instance, Fig.II.8) proves that some large differences in the temperature-demand relationship exist from one region to the other. They could be easily included by considering region-specific models. The hydrological model used in this study could also benefit from a regional parametrisation if one in interested in producing accurate discharge simulations.

- The assessment of hydro power potential from river discharge is not straightforward. Conversely to solar and wind power, this energy sources is not fully distributed and is only concentrated along the river network. Moreover, the local hydro power production depends on the hydro-meteorological conditions affecting the whole upstream area and is also strongly impacted by past weather conditions (initial soil moisture, snow pack, etc.)
  In CRE-Mix, the assessment of hydro power is performed only for the RoR contribution (no reservoir) and avoiding water transfer from neighbouring catchments (test regions located at the upstream part of river basins). In many respects, RoR hydro power is, by itself, an interesting

CRE source which is becoming increasingly developed. Moreover, the storage module in CRE-Mix can be seen as a modelling of small to medium scale reservoirs that can balance the hydro power variability from daily to seasonal scale. Nonetheless the contribution of large reservoirs to the total hydro power production is large for some regions (e.g in NO) and can be used to balance the variations of river discharge over several years. Taking these reservoirs into account is complicated. It would require 1) working on real river basins 2) assessing the current regional equipments in water reservoirs 3) Considering their multiple other uses, such as irrigation water management or flood mitigation. Such models have already been developed and studied for some specific locations (e.g. [François, 2013]) but their application to other reservoirs/regions is demanding and not straightforward.

2.2. Inter-regions complementarity

As one of the possible integrating factors that can improve the electricity supply-demand balance, we tested the effect of a spatial integration of CRE sources at a European scale. This first step toward the analysis of spatial complementarity proved that European regions can complement each other. However, this integration was performed for the ideal grid configuration, known as the European copper plate. It assumes that a regional electricity production can be used instantaneously to meet the energy demand in another region without losses related to energy transmission. This strong assumption likely leads to a smoothing of both demand and production series and to an overestimation of the penetration rates.

A possible improvement consists in including in CRE-Mix a schematic representation of the European electrical grid that would take into account some of the limitations related to electricity transmission. To go further and place ourself in a more realistic situation, the spatial complementarity could also be analysed only between neighbouring regions, for which the electricity exchange is easily conceivable.

2.3. Low frequency fluctuations and trends in the 20th century climate series

The analysis of low-frequency variations of CRE sources necessitated using climate reanalysis data of the 20th century. The associated outcomes are very informative on the connections between CRE sources and some large scale climate indices (NAO, AMO). It also gives an assessment of the climate-related risks from the new point of view. As a complement to this work, on could evaluate the possible inter-regional synchronism between low-frequency fluctuations of CRE courses.

However, an extensive study would require to separate accurately the internal variability of climate from the climate change signal. In this study, we handled trends in a very simple way, testing only for linear changes in the time series. As mentioned in this thesis, some other trend models are probably more relevant, especially for temperature. Moreover, both ERA20C data and the reconstructed series of wind speed indicate positive and significant trends in mean annual wind speed in Europe. Some additional tests must be set up to check if this issue is only an artefact of the increasing number of wind/pressure assimilated data in the course of the 20th century, in ERA20C. This could be done

using some other climate reanalysis data such as the 20CR reanalysis [Compo et al., 2011] from NOAA or some (rare) long series of observed wind speed. Then, the significant trends in weather series should be removed before generating CRE sources and PE time series, in order not suffer from their contributions in the multidecadal variability assessment.

Another rather different but interesting way of characterising the low frequency fluctuations of CRE sources would be to downscale the pre-industrial runs of multiple GCMs which are supposed to be representative of stationary climate conditions.

2.4. SCAMP in a climate change context: some possible application

The downscaling of GCMs with SCAMP gave regional precipitation series in disagreements with most studies focusing on future trends in precipitation, in Europe. Using a perfect model approach, we showed that these differences are probably due to a modification of the predictor-predictand relationship for future decades ; not only for total precipitation but also for both convective and stratiform contributions. However, it appears that the predictors set still have good predictive skills as long as analogues are searched for within a climatologically homogeneous period.

As a result, SCAMP (with its current parametrisation) cannot be used to generate future series of precipitation in a classic way, using observations which are only representative of the current climate conditions. Some other predictors could be added in the analogue model (for example the ones proposed by Dayon et al., 2015: TTI - Totals Total Index) to improve the ability of SCAMP to simulate the modifications imposed by climate change. However, it would require optimising (analogy windows) and evaluating (skill scores, inter-variables correlations) this new set of predictors.

Nevertheless, SCAMP has some potential application in a climate change context. RCMs give scenarios of regional meteorological variables that could be used for an analysis of CREs co-fluctuations. However, they do take the small scale variability of local variables into account. As mentioned in Chap.IV, the analogue method gives an estimation of this source of variability when selecting several analogue dates for the same target day. In this whole study, we used 50 downscaled series of predictands to take this contribution on board. Applying SCAMP in a perfect model approach (cf. Chap.IX) and using a moving archive period to look for analogues (SCAMP-MV), is able to generate a set local scenarios from a single deterministic RCM simulation. As presented in Chap.VIII (e.g. Fig.VIII.4), the small scale variability obtained with such a re-sampling approach is not negligible. It would be interesting to apply SCAMP-MV to RCMs in order to take its contribution into consideration.

2.5. Extension to other continents

Most of the concepts and modelling choices of CRE-Mix, developed as part of the COMPLEX project and for an European study, could be applied to other regions worldwide. It would give an assessment of the ease of integration of CRE sources in other countries and provide some guidelines to policy makers, private companies and local communities, interested in developing renewable energy. For some developing countries, which still suffer from a limited electrical grid, CRE-Mix can estimate

the local CRE resources and find the optimal energy mix which could be used to meet the energy demand and improve the local electricity access.

However, as mentioned previously, some further improvements should be made to CRE-Mix if hydro power has to contribute to the energy mix. For instance, the hydrological model presented in this thesis, has been optimised for European hydro-climatic conditions and is probably not able to simulate relevant river discharge for very different catchments/weather conditions. Estimating hydro power in other regions could rely on site-specific and already existing hydrological models. Several models having a global coverage have been proposed in recent years. These models do not give a perfect representation of local hydrological systems but likely lead to a first reasonable estimate of the regional hydrological regimes.

Finally, the downscaling method proposed in this study is also partly applicable to other regions. We have high hopes that SCAMP would be relevant for any mid-latitude test area but its performances should be evaluated anyway. Its transferability to sub-tropical and tropical zones is much more questionable and the current set of predictors is likely to be sub-optimal as a consequence of radically different atmospheric processes.

BIBLIOGRAPHY

Abatzoglou, J. T. and Brown, T. J. [2012]. "A comparison of statistical downscaling methods suited for wildfire applications". *International Journal of Climatology*. Vol. 32. no. 5, pp. 772–780.

Abdulharis, A, Khan, M., Chhabra, V., Biswas, S., Pratap, A., et al. [2010]. "Evaluation of LARS-WG for generating long term data for assessment of climate change impact in Bihar." *Journal of Agrometeorology*. Vol. 12. no. 2, pp. 198–201.

Adams, A. S. and Keith, D. W. [2013]. "Are global wind power resource estimates overstated?": *Environmental Research Letters*. Vol. 8. no. 1, p. 015021.

Ailliot, P., Allard, D., Monbet, V., and Naveau, P. [2015]. "Stochastic weather generators: an overview of weather type models". *Journal de la Société Française de Statistique*. Vol. 156. no. 1, pp. 101–113.

Alaya, B., Ali, M., Chebana, F., and Ouarda, T. B. [2014]. "Probabilistic Gaussian Copula Regression Model for Multisite and Multivariable Downscaling." *Journal of Climate*. Vol. 27. no. 9, pp. 3331–3347.

Albadi, M. and El-Saadany, E. [2010]. "Overview of wind power intermittency impacts on power systems". *Electric Power Systems Research*. Vol. 80. no. 6, pp. 627–632.

Arent, D. J., Wise, A., and Gelman, R. [2011]. "The status and prospects of renewable energy for combating global warming". *Energy Economics*. Vol. 33. no. 4, pp. 584–593.

Ballester, J., Giorgi, F., and Rodó, X. [2010a]. "Changes in European temperature extremes can be predicted from changes in PDF central statistics". *Climatic change*. Vol. 98. no. 1-2, pp. 277–284.

Ballester, J., Rodó, X., and Giorgi, F. [2010b]. "Future changes in Central Europe heat waves expected to mostly follow summer mean warming". *Climate Dynamics*. Vol. 35. no. 7-8, pp. 1191–1205.

Bartók, B. [2010]. "Changes in solar energy availability for south-eastern Europe with respect to global warming". *Physics and Chemistry of the Earth, Parts A/B/C*. Vol. 35. no. 1, pp. 63–69.

Basso, S and Botter, G [2012]. "Streamflow variability and optimal capacity of run-of-river hydropower plants". *Water Resources Research*. Vol. 48. no. 10.

Beaudin, M., Zareipour, H., Schellenberglabe, A., and Rosehart, W. [2010]. "Energy storage for mitigating the variability of renewable electricity sources: An updated review". *Energy for Sustainable Development*. Vol. 14. no. 4, pp. 302–314.

Beck, C. and Philipp, A. [2010]. "Evaluation and comparison of circulation type classifications for the European domain". *Physics and Chemistry of the Earth, Parts A/B/C*. Vol. 35. no. 9, pp. 374–387.

Bindoff, N. L., Stott, P. A., AchutaRao, M, Allen, M. R., Gillett, N, Gutzler, D., Hansingo, K., Hegerl, G, Hu, Y., Jain, S., et al. [2013]. "Detection and attribution of climate change: from global to regional".

Bjornsson, H and Venegas, S. [1997]. "A manual for EOF and SVD analyses of climatic data". *CCGCR Report*. Vol. 97. no. 1, pp. 112–134.

Blenkinsop, S and Fowler, H. [2007]. "Changes in European drought characteristics projected by the PRUDENCE regional climate models". *International Journal of Climatology*. Vol. 27. no. 12, pp. 1595–1610.

Boberg, F., Berg, P., Thejll, P., Gutowski, W. J., and Christensen, J. H. [2009]. "Improved confidence in climate change projections of precipitation evaluated using daily statistics from the PRUDENCE ensemble". *Climate dynamics*. Vol. 32. no. 7-8, pp. 1097–1106.

Boé, J, Terray, L, Habets, F, and Martin, E [2006]. "A simple statistical-dynamical downscaling scheme based on weather types and conditional resampling". *Journal of Geophysical Research: Atmospheres*. Vol. 111. no. D23.

Boe, J. [2007]. "Changement global et cycle hydrologique: Une étude de régionalisation sur la France". PhD thesis. Université Paul Sabatier-Toulouse III.

Bogdanov, D. and Breyer, C. [2016]. "North-East Asian Super Grid for 100% renewable energy supply: Optimal mix of energy technologies for electricity, gas and heat supply options". *Energy Conversion and Management*. Vol. 112, pp. 176–190.

Bontron, G. [2004]. "Prévision quantitative des précipitations: Adaptation probabiliste par recherche d'analogues. Utilisation des Réanalyses NCEP/NCAR et application aux précipitations du Sud-Est de la France". PhD thesis. Institut National Polytechnique Grenoble (INPG).

Bower, D., McGregor, G. R., Hannah, D. M., and Sheridan, S. C. [2007]. "Development of a spatial synoptic classification scheme for western Europe". *International Journal of Climatology*. Vol. 27. no. 15, pp. 2017–2040.

Brönnimann, S [2007]. "Impact of El Niño–Southern Oscillation on European climate". *Reviews of Geophysics*. Vol. 45. no. 3.

Brown, T. A. [1974]. "Admissible Scoring Systems for Continuous Distributions."

Budischak, C., Sewell, D., Thomson, H., Mach, L., Veron, D. E., and Kempton, W. [2013]. "Cost-minimized combinations of wind power, solar power and electrochemical storage, powering the grid up to 99.9% of the time". *Journal of Power Sources*. Vol. 225, pp. 60–74.

Buishand, T. A. and Brandsma, T. [2001]. "Multisite simulation of daily precipitation and temperature in the Rhine basin by nearest-neighbor resampling". *Water Resources Research*. Vol. 37. no. 11, pp. 2761–2776.

Caillouet, L., Vidal, J.-P., Sauquet, E., and Graff, B. [2016]. "Probabilistic precipitation and temperature downscaling of the Twentieth Century Reanalysis over France". *Climate of the Past*. Vol. 12. no. 3, pp. 635–662.

Casanueva, A., Frías, M. D., Herrera, S., San-Martín, D., Zaninovic, K, and Gutiérrez, J. [2014]. "Statistical downscaling of climate impact indices: testing the direct approach". *Climatic change*. Vol. 127. no. 3-4, pp. 547–560.

Cattiaux, J., Vautard, R, and Yiou, P [2009]. "Origins of the extremely warm European fall of 2006". *Geophysical Research Letters*. Vol. 36. no. 6.

Cavazos, T. and Hewitson, B. C. [2005]. "Performance of NCEP–NCAR reanalysis variables in statistical downscaling of daily precipitation". *Climate Research*. Vol. 28. no. 2, pp. 95–107.

Change, I. C. [2014]. "Mitigation of Climate Change. Contribution of Working Group III to the Fifth Assessment Report of the Intergovernmental Panel on Climate Change". *Cambridge University Press, Cambridge, UK and New York, NY*.

Chardon, J., Hingray, B., Favre, A.-C., Autin, P., Gailhard, J., Zin, I., and Obled, C. [2014]. "Spatial similarity and transferability of analog dates for precipitation downscaling over France". *Journal of Climate*. Vol. 27. no. 13, pp. 5056–5074.

Charles, A., Timbal, B., Fernandez, E., and Hendon, H. [2013]. "Analog downscaling of seasonal rainfall forecasts in the Murray darling basin". *Monthly Weather Review*. Vol. 141. no. 3, pp. 1099–1117.

Chen, H., Cong, T. N., Yang, W., Tan, C., Li, Y., and Ding, Y. [2009]. "Progress in electrical energy storage system: A critical review". *Progress in Natural Science*. Vol. 19. no. 3, pp. 291–312.

Christensen, J. H. and Christensen, O. B. [2007]. "A summary of the PRUDENCE model projections of changes in European climate by the end of this century". *Climatic change*. Vol. 81. no. 1, pp. 7–30.

Christidis, N., Stott, P. A., Zwiers, F. W., Shiogama, H., and Nozawa, T. [2010]. "Probabilistic estimates of recent changes in temperature: a multi-scale attribution analysis". *Climate Dynamics*. Vol. 34. no. 7-8, pp. 1139–1156.

Christidis, N., Stott, P. A., and Brown, S. J. [2011]. "The role of human activity in the recent warming of extremely warm daytime temperatures". *Journal of Climate*. Vol. 24. no. 7, pp. 1922–1930.

Church, J. A., Clark, P. U., Cazenave, A., Gregory, J. M., Jevrejeva, S., Levermann, A., Merrifield, M. A., Milne, G. A., Nerem, R. S., Nunn, P. D., et al. [2013]. "Sea level change". Tech. rep. PM Cambridge University Press.

Compo, G. P., Whitaker, J. S., Sardeshmukh, P. D., Matsui, N., Allan, R. J., Yin, X., Gleason, B. E., Vose, R., Rutledge, G, Bessemoulin, P, et al. [2011]. "The twentieth century reanalysis project". *Quarterly Journal of the Royal Meteorological Society*. Vol. 137. no. 654, pp. 1–28.

Daoud, A. B., Sauquet, E., Bontron, G., Obled, C., and Lang, M. [2016]. "Daily quantitative precipitation forecasts based on the analogue method: improvements and application to a French large river basin". *Atmospheric Research*. Vol. 169, pp. 147–159.

Dayon, G, Boé, J, and Martin, E [2015]. "Transferability in the future climate of a statistical downscaling method for precipitation in France". *Journal of Geophysical Research: Atmospheres.* Vol. 120. no. 3, pp. 1023–1043.

De Vries, B. J., Van Vuuren, D. P., and Hoogwijk, M. M. [2007]. "Renewable energy sources: Their global potential for the first-half of the 21st century at a global level: An integrated approach". *Energy policy.* Vol. 35. no. 4, pp. 2590–2610.

Dee, D., Uppala, S., Simmons, A., Berrisford, P., Poli, P, Kobayashi, S, Andrae, U, Balmaseda, M., Balsamo, G, Bauer, P, et al. [2011]. "The ERA-Interim reanalysis: Configuration and performance of the data assimilation system". *Quarterly Journal of the royal meteorological society.* Vol. 137. no. 656, pp. 553–597.

Denault, M., Dupuis, D., and Couture-Cardinal, S. [2009]. "Complementarity of hydro and wind power: Improving the risk profile of energy inflows". *Energy Policy.* Vol. 37. no. 12, pp. 5376–5384.

Déqué, M, Jones, R., Wild, M, Giorgi, F, Christensen, J., Hassell, D., Vidale, P., Rockel, B, Jacob, D, Kjellström, E., et al. [2005]. "Global high resolution versus Limited Area Model climate change projections over Europe: quantifying confidence level from PRUDENCE results". *Climate Dynamics.* Vol. 25. no. 6, pp. 653–670.

Deser, C., Phillips, A., Bourdette, V., and Teng, H. [2012]. "Uncertainty in climate change projections: the role of internal variability". *Climate Dynamics.* Vol. 38. no. 3-4, pp. 527–546.

Duffie, J. and Beckman, W. [1991]. "Solar engineering of termal process".

Ely, C. R., Brayshaw, D. J., Methven, J., Cox, J., and Pearce, O. [2013]. "Implications of the North Atlantic Oscillation for a UK–Norway Renewable power system". *Energy policy.* Vol. 62, pp. 1420–1427.

Enfield, D. B., Mestas-Nuñez, A. M., and Trimble, P. J. [2001]. "The Atlantic multidecadal oscillation and its relation to rainfall and river flows in the continental US". *Geophysical Research Letters.* Vol. 28. no. 10, pp. 2077–2080.

ESHA [2012]. "Small Hydropower Roadmap. Condensed research data for EU-27".

Esteban, P., Martin-Vide, J., and Mases, M. [2006]. "Daily atmospheric circulation catalogue for Western Europe using multivariate techniques". *International journal of climatology.* Vol. 26. no. 11, pp. 1501–1515.

Fan, Z., Kulkarni, P., Gormus, S., Efthymiou, C., Kalogridis, G., Sooriyabandara, M., Zhu, Z., Lambotharan, S., and Chin, W. H. [2013]. "Smart grid communications: Overview of research challenges, solutions, and standardization activities". *IEEE Communications Surveys & Tutorials.* Vol. 15. no. 1, pp. 21–38.

Fant, C., Schlosser, C. A., and Strzepek, K. [2016]. "The impact of climate change on wind and solar resources in southern Africa". *Applied Energy.* Vol. 161, pp. 556–564.

Farajzadeh, M, Oji, R, Cannon, A., Ghavidel, Y, and Bavani, A. M. [2015]. "An evaluation of single-site statistical downscaling techniques in terms of indices of climate extremes for the Midwest of Iran". *Theoretical and Applied Climatology.* Vol. 120. no. 1-2, pp. 377–390.

Fatichi, S., Ivanov, V. Y., and Caporali, E. [2011]. "Simulation of future climate scenarios with a weather generator". *Advances in Water Resources.* Vol. 34. no. 4, pp. 448–467.

Fealy, R. and Sweeney, J. [2008]. "Statistical downscaling of temperature, radiation and potential evapotranspiration to produce a multiple GCM ensemble mean for a selection of sites in Ireland". *Irish Geography.* Vol. 41. no. 1, pp. 1–27.

Fogt, R. L., Perlwitz, J., Monaghan, A. J., Bromwich, D. H., Jones, J. M., and Marshall, G. J. [2009]. "Historical SAM variability. Part II: twentieth-century variability and trends from reconstructions, observations, and the IPCC AR4 models*". *Journal of Climate.* Vol. 22. no. 20, pp. 5346–5365.

Fowler, H., Ekström, M, Blenkinsop, S, and Smith, A. [2007]. "Estimating change in extreme European precipitation using a multimodel ensemble". *Journal of Geophysical Research: Atmospheres.* Vol. 112. no. D18.

François, B. [2013]. "Gestion optimale d'un réservoir hydraulique multi usages et changement climatique. Modèles, projections et incertitudes. Application à la réserve de Serre-Ponçon". PhD thesis. Université de Grenoble, France.

François, B [2016]. "Influence of winter North-Atlantic Oscillation on Climate-Related-Energy penetration in Europe". *Renewable Energy*. Vol. 99, pp. 602–613.

François, B, Hingray, B, Raynaud, D, Borga, M, and Creutin, J. [2016]. "Increasing climate-related-energy penetration by integrating run-of-the river hydropower to wind/solar mix". *Renewable Energy*. Vol. 87, pp. 686–696.

Gallagher, J., Styles, D., McNabola, A., and Williams, A. P. [2015]. "Current and future environmental balance of small-scale run-of-river hydropower". *Environmental science & technology*. Vol. 49. no. 10, pp. 6344–6351.

Goodess, C. M. and Palutikof, J. P. [1998]. "Development of daily rainfall scenarios for southeast Spain using a circulation-type approach to downscaling". *International Journal of Climatology*. Vol. 18. no. 10, pp. 1051–1083.

Goulden, M., Bedwell, B., Rennick-Egglestone, S., Rodden, T., and Spence, A. [2014]. "Smart grids, smart users? The role of the user in demand side management". *Energy research & social science*. Vol. 2, pp. 21–29.

Goyal, M. K., Ojha, C. S. P., et al. [2010]. "Evaluation of various linear regression methods for downscaling of mean monthly precipitation in arid Pichola watershed". *Natural Resources*. Vol. 1. no. 01, p. 11.

Graabak, I. and Korpås, M. [2016]. "Variability Characteristics of European Wind and Solar Power Resources-A Review". *Energies*. Vol. 9. no. 6, p. 449.

Graff, L. S. and LaCasce, J. [2012]. "Changes in the extratropical storm tracks in response to changes in SST in an AGCM". *Journal of Climate*. Vol. 25. no. 6, pp. 1854–1870.

Guilbaud, S. and Obled, C. [1998]. "Prévision quantitative des précipitations journalières par une technique de recherche de journées antérieures analogues: optimisation du critère d'analogie". *Comptes Rendus de l'Académie des Sciences-Series IIA-Earth and Planetary Science*. Vol. 327. no. 3, pp. 181–188.

Guivarch, C. and Hallegatte, S. [2011]. "Existing infrastructure and the 2 C target". *Climatic Change*. Vol. 109. no. 3-4, pp. 801–805.

Gutmann, E., Pruitt, T., Clark, M. P., Brekke, L., Arnold, J. R., Raff, D. A., and Rasmussen, R. M. [2014]. "An intercomparison of statistical downscaling methods used for water resource assessments in the United States". *Water Resources Research*. Vol. 50. no. 9, pp. 7167–7186.

Hagemann, S., Chen, C., Haerter, J. O., Heinke, J., Gerten, D., and Piani, C. [2011]. "Impact of a statistical bias correction on the projected hydrological changes obtained from three GCMs and two hydrology models". *Journal of Hydrometeorology*. Vol. 12. no. 4, pp. 556–578.

Hänggi, P. and Weingartner, R. [2012]. "Variations in discharge volumes for hydropower generation in Switzerland". *Water resources management*. Vol. 26. no. 5, pp. 1231–1252.

Hannaford, J, Lloyd-Hughes, B., Keef, C, Parry, S, and Prudhomme, C [2011]. "Examining the large-scale spatial coherence of European drought using regional indicators of precipitation and streamflow deficit". *Hydrological Processes*. Vol. 25. no. 7, pp. 1146–1162.

Hanssen-Bauer, I, Achberger, C, Benestad, R., Chen, D, and Førland, E. [2005]. "Statistical downscaling of climate scenarios over Scandinavia". *Climate Research*. Vol. 29. no. 3, pp. 255–268.

Harris, G., Collins, M, Sexton, D., Murphy, J., and Booth, B. [2010]. "Probabilistic projections for 21st century European climate". *Natural Hazards and Earth System Sciences*. Vol. 10. no. 9, pp. 2009–2020.

Haylock, M., Hofstra, N, Klein Tank, A., Klok, E., Jones, P., and New, M [2008]. "A European daily high-resolution gridded data set of surface temperature and precipitation for 1950–2006". *Journal of Geophysical Research: Atmospheres*. Vol. 113. no. D20.

Hertig, E, Seubert, S, Paxian, A, Vogt, G, Paeth, H, and Jacobeit, J [2014]. "Statistical modelling of extreme precipitation indices for the Mediterranean area under future climate change". *International Journal of Climatology*. Vol. 34. no. 4, pp. 1132–1156.

Hertig, E., Beck, C., Wanner, H., and Jacobeit, J. [2015]. "A review of non-stationarities in climate variability of the last century with focus on the North Atlantic–European sector". *Earth-Science Reviews.* Vol. 147, pp. 1–17.

Hofstra, N., Haylock, M., New, M., Jones, P., and Frei, C. [2008]. "Comparison of six methods for the interpolation of daily, European climate data". *Journal of Geophysical Research: Atmospheres.* Vol. 113. no. D21.

Hoogwijk, M. and Graus, W. [2008]. "Global potential of renewable energy sources: a literature assessment". *Background report prepared by order of REN21. Ecofys, PECSNL072975.*

Horton, P, Jaboyedoff, M, Metzger, R, Obled, C, and Marty, R [2012]. "Spatial relationship between the atmospheric circulation and the precipitation measured in the western Swiss Alps by means of the analogue method". *Natural Hazards and Earth System Sciences.* Vol. 12, pp. 777–784.

Hurrell, J. W. and Deser, C. [2015]. "Northern Hemisphere climate variability during winter: Looking back on the work of Felix Exner". *Meteorologische Zeitschrift.* Pp. 113–118.

Hurrell, J. W. and Van Loon, H. [1997]. "Decadal variations in climate associated with the North Atlantic Oscillation". Climatic Change at High Elevation Sites. Springer, pp. 69–94.

Huth, R., Beck, C., Philipp, A., Demuzere, M., Ustrnul, Z., Cahynova, M., Kyselỳ, J., and Tveito, O. E. [2008]. "Classifications of atmospheric circulation patterns". *Annals of the New York Academy of Sciences.* Vol. 1146. no. 1, pp. 105–152.

Hwang, S. and Graham, W. D. [2013]. "Development and comparative evaluation of a stochastic analog method to downscale daily GCM precipitation". *Hydrology and Earth System Sciences.* Vol. 17. no. 11, pp. 4481–4502.

Imbers, J, Lopez, A, Huntingford, C, and Allen, M. [2013]. "Testing the robustness of the anthropogenic climate change detection statements using different empirical models". *Journal of Geophysical Research: Atmospheres.* Vol. 118. no. 8, pp. 3192–3199.

Ines, A. V. and Hansen, J. W. [2006]. "Bias correction of daily GCM rainfall for crop simulation studies". *Agricultural and forest meteorology.* Vol. 138. no. 1, pp. 44–53.

IPCC [2013]. "The physical science basis. Contribution of working group I to the fifth assessment report of the intergovernmental panel on climate change". *K., Tignor, M., Allen, SK, Boschung, J., Nauels, A., Xia, Y., Bex, V., Midgley, PM, Eds.* P. 1535.

Irannezhad, M., Ronkanen, A.-K., and Kløve, B. [2015]. "Effects of climate variability and change on snowpack hydrological processes in Finland". *Cold Regions Science and Technology.* Vol. 118, pp. 14–29.

Isaac, M. and Van Vuuren, D. P. [2009]. "Modeling global residential sector energy demand for heating and air conditioning in the context of climate change". *Energy policy.* Vol. 37. no. 2, pp. 507–521.

Jacob, D., Petersen, J., Eggert, B., Alias, A., Christensen, O. B., Bouwer, L. M., Braun, A., Colette, A., Déqué, M., Georgievski, G., et al. [2014]. "EURO-CORDEX: new high-resolution climate change projections for European impact research". *Regional Environmental Change.* Vol. 14. no. 2, pp. 563–578.

Jacobeit, J., Hertig, E., Seubert, S., and Lutz, K. [2014]. "Statistical downscaling for climate change projections in the Mediterranean region: methods and results". *Regional Environmental Change.* Vol. 14. no. 5, pp. 1891–1906.

Jakob, M., Holm, K., Lange, O., and Schwab, J. W. [2006]. "Hydrometeorological thresholds for landslide initiation and forest operation shutdowns on the north coast of British Columbia". *Landslides.* Vol. 3. no. 3, pp. 228–238.

Jeong, D. I., St-Hilaire, A., Ouarda, T. B., and Gachon, P. [2012]. "CGCM3 predictors used for daily temperature and precipitation downscaling in Southern Québec, Canada". *Theoretical and applied climatology.* Vol. 107. no. 3-4, pp. 389–406.

Jerez, S, Thais, F, Tobin, I, Wild, M, Colette, A, Yiou, P, and Vautard, R [2015]. "The CLIMIX model: A tool to create and evaluate spatially-resolved scenarios of photovoltaic and wind power development". *Renewable and Sustainable Energy Reviews.* Vol. 42, pp. 1–15.

Jomelli, V., Delval, C., Grancher, D., Escande, S., Brunstein, D., Hetu, B., Filion, L., and Pech, P. [2007]. "Probabilistic analysis of recent snow avalanche activity and weather in the French Alps". *Cold Regions Science and Technology.* Vol. 47. no. 1, pp. 180–192.

Jourdier, B. [2015]. "Ressource éolienne en France métropolitaine: méthodes d'évaluation du potentiel, variabilité et tendances". PhD thesis. Ecole Doctorale Polytechnique.

Khalili, M., Van Nguyen, V. T., and Gachon, P. [2013]. "A statistical approach to multi-site multivariate downscaling of daily extreme temperature series". *International Journal of Climatology.* Vol. 33. no. 1, pp. 15–32.

Kirchmeier, M. C., Lorenz, D. J., and Vimont, D. J. [2014]. "Statistical downscaling of daily wind speed variations". *Journal of Applied Meteorology and Climatology.* Vol. 53. no. 3, pp. 660–675.

Kjellström, E., Bärring, L., Jacob, D., Jones, R., Lenderink, G., and Schär, C. [2007]. "Modelling daily temperature extremes: recent climate and future changes over Europe". *Climatic Change.* Vol. 81. no. 1, pp. 249–265.

Kotlarski, S., Keuler, K., Christensen, O. B., Colette, A., Déqué, M., Gobiet, A., Goergen, K., Jacob, D., Lüthi, D., Meijgaard, E. van, et al. [2014]. "Regional climate modeling on European scales: a joint standard evaluation of the EURO-CORDEX RCM ensemble". *Geoscientific Model Development.* Vol. 7. no. 4, pp. 1297–1333.

Kuentz, A., Mathevet, T., Cœur, D., Perret, C., Gailhard, J., Guérin, L., Gash, Y., and Andréassian, V. [2014]. "Hydrométrie et hydrologie historiques du bassin de la Durance". *La Houille Blanche-Revue internationale de l'eau.* no. 4, pp. 57–63.

Kuentz, A., Mathevet, T, Gailhard, J, and Hingray, B [2015]. "Building long-term and high spatio-temporal resolution precipitation and air temperature reanalyses by mixing local observations and global atmospheric reanalyses: the ANATEM model". *Hydrology and Earth System Sciences.* Vol. 19. no. 6, pp. 2717–2736.

Kyselỳ, J. and Beranová, R. [2009]. "Climate-change effects on extreme precipitation in central Europe: uncertainties of scenarios based on regional climate models". *Theoretical and Applied Climatology.* Vol. 95. no. 3-4, pp. 361–374.

Lafaysse, M, Hingray, B, Mezghani, A, Gailhard, J, and Terray, L [2014]. "Internal variability and model uncertainty components in future hydrometeorological projections: The Alpine Durance basin". *Water Resources Research.* Vol. 50. no. 4, pp. 3317–3341.

Lawrence, M. G. [2005]. "The relationship between relative humidity and the dewpoint temperature in moist air: A simple conversion and applications". *Bulletin of the American Meteorological Society.* Vol. 86. no. 2, pp. 225–233.

Lazzaro, G. and Botter, G. [2015]. "Run-of-river power plants in Alpine regions: Whither optimal capacity?": *Water Resources Research.* Vol. 51. no. 7, pp. 5658–5676.

Leckebusch, G. C., Weimer, A., Pinto, J. G., Reyers, M., and Speth, P. [2008]. "Extreme wind storms over Europe in present and future climate: a cluster analysis approach". *Meteorologische Zeitschrift.* Vol. 17. no. 1, pp. 67–82.

Lehner, B., Czisch, G., and Vassolo, S. [2005]. "The impact of global change on the hydropower potential of Europe: a model-based analysis". *Energy Policy.* Vol. 33. no. 7, pp. 839–855.

Linden, M. van der [2009]. "ENSEMBLES: Climate Change and its Impacts: Summary of research and results from the ENSEMBLES project". 160pp.

Lorenz, E. N. [1969]. "Atmospheric predictability as revealed by naturally occurring analogues". *Journal of the Atmospheric sciences.* Vol. 26. no. 4, pp. 636–646.

Luo, X., Wang, J., Dooner, M., and Clarke, J. [2015]. "Overview of current development in electrical energy storage technologies and the application potential in power system operation". *Applied Energy.* Vol. 137, pp. 511–536.

Madsen, H., Lawrence, D., Lang, M., Martinkova, M., and Kjeldsen, T. [2014]. "Review of trend analysis and climate change projections of extreme precipitation and floods in Europe". *Journal of Hydrology.* Vol. 519, pp. 3634–3650.

Makkonen, L., Ruokolainen, L., Raisanen, J, and Tikanmaki, M [2007]. "Regional climate model estimates for changes in Nordic extreme events". *Geophysica.* Vol. 43. no. 1-2, pp. 19–42.

Maraun, D., Wetterhall, F, Ireson, A., Chandler, R., Kendon, E., Widmann, M, Brienen, S, Rust, H., Sauter, T, Themeßl, M, et al. [2010]. "Precipitation downscaling under climate change: Recent developments to bridge the gap between dynamical models and the end user". *Reviews of Geophysics.* Vol. 48. no. 3.

Maraun, D., Osborn, T. J., and Rust, H. W. [2012]. "The influence of synoptic airflow on UK daily precipitation extremes. Part II: regional climate model and E-OBS data validation". *Climate dynamics.* Vol. 39. no. 1-2, pp. 287–301.

Martín, M., Valero, F, Pascual, A, Sanz, J, and Frias, L [2014]. "Analysis of wind power productions by means of an analog model". *Atmospheric Research.* Vol. 143, pp. 238–249.

Marty, R, Zin, I, and Obled, C. [2013]. "Sensitivity of hydrological ensemble forecasts to different sources and temporal resolutions of probabilistic quantitative precipitation forecasts: flash flood case studies in the Cévennes-Vivarais region (Southern France)". *Hydrological Processes.* Vol. 27. no. 1, pp. 33–44.

Marty, R., Zin, I., Obled, C., Bontron, G., and Djerboua, A. [2012]. "Toward real-time daily PQPF by an analog sorting approach: Application to flash-flood catchments". *Journal of Applied Meteorology and Climatology.* Vol. 51. no. 3, pp. 505–520.

Marzeion, B., Cogley, J. G., Richter, K., and Parkes, D. [2014]. "Attribution of global glacier mass loss to anthropogenic and natural causes". *Science.* Vol. 345. no. 6199, pp. 919–921.

Mason, I., Page, S., and Williamson, A. [2010]. "A 100% renewable electricity generation system for New Zealand utilising hydro, wind, geothermal and biomass resources". *Energy Policy.* Vol. 38. no. 8, pp. 3973–3984.

Matheson, J. E. and Winkler, R. L. [1976]. "Scoring rules for continuous probability distributions". *Management science.* Vol. 22. no. 10, pp. 1087–1096.

May, W. [2008]. "Potential future changes in the characteristics of daily precipitation in Europe simulated by the HIRHAM regional climate model". *Climate Dynamics.* Vol. 30. no. 6, pp. 581–603.

Mezghani, A and Hingray, B [2009]. "A combined downscaling-disaggregation weather generator for stochastic generation of multisite hourly weather variables over complex terrain: Development and multi-scale validation for the Upper Rhone River basin". *Journal of Hydrology.* Vol. 377. no. 3, pp. 245–260.

Min, S.-K., Zhang, X., Zwiers, F. W., and Hegerl, G. C. [2011]. "Human contribution to more-intense precipitation extremes". *Nature.* Vol. 470. no. 7334, pp. 378–381.

Monteith, J. L. [1965]. "Evaporation and Environment. 19th Symposia of the Society for Experimental Biology". University Press, Cambridge, 19:205–234.

Müller, R, Pfeifroth, U., Träger-Chatterjee, C, Cremer, R, Trentmann, J, and Hollmann, R [2015]. "Surface Solar Radiation Data Set - Heliosat (SARAH) - Edition 1". *Satellite Application Facility on Climate Monitoring.*

Musy, A., Hingray, B., and Picouet, C. [2014]. "Hydrology: a science for engineers". CRC Press.

Nalley, D, Adamowski, J, Khalil, B, and Biswas, A [2016]. "Inter-annual to inter-decadal streamflow variability in Quebec and Ontario in relation to dominant large-scale climate indices". *Journal of Hydrology.* Vol. 536, pp. 426–446.

Nash, J. E. and Sutcliffe, J. V. [1970]. "River flow forecasting through conceptual models part I-A discussion of principles". *Journal of hydrology.* Vol. 10. no. 3, pp. 282–290.

Obled, C., Bontron, G., and Garçon, R. [2002]. "Quantitative precipitation forecasts: a statistical adaptation of model outputs through an analogues sorting approach". *Atmospheric research.* Vol. 63. no. 3, pp. 303–324.

Olsson, J, Uvo, C., and Jinno, K [2001]. "Statistical atmospheric downscaling of short-term extreme rainfall by neural networks". *Physics and Chemistry of the Earth, Part B: Hydrology, Oceans and Atmosphere.* Vol. 26. no. 9, pp. 695–700.

Omondi, P, Awange, J., Ogallo, L., Okoola, R., and Forootan, E [2012]. "Decadal rainfall variability modes in observed rainfall records over East Africa and their relations to historical sea surface temperature changes". *Journal of Hydrology.* Vol. 464, pp. 140–156.

Peel, M. C., Finlayson, B. L., and McMahon, T. A. [2007]. "Updated world map of the Köppen-Geiger climate classification". *Hydrology and Earth System Sciences Discussions Discussions.* Vol. 4. no. 2, pp. 439–473.

Perpinan, O, Lorenzo, E, and Castro, M. [2007]. "On the calculation of energy produced by a PV grid-connected system". *Progress in Photovoltaics: research and applications.* Vol. 15. no. 3, pp. 265–274.

Piani, C, Weedon, G., Best, M, Gomes, S., Viterbo, P, Hagemann, S, and Haerter, J. [2010]. "Statistical bias correction of global simulated daily precipitation and temperature for the application of hydrological models". *Journal of Hydrology.* Vol. 395. no. 3, pp. 199–215.

Pierce, D. W., Cayan, D. R., and Thrasher, B. L. [2014]. "Statistical Downscaling Using Localized Constructed Analogs (LOCA)*". *Journal of Hydrometeorology.* Vol. 15. no. 6, pp. 2558–2585.

Poli, P., Hersbach, H., Tan, D., Dee, D., Thepaut, J.-N., Simmons, A., Peubey, C., Laloyaux, P., Komori, T., Berrisford, P., et al. [2013]. "The data assimilation system and initial performance evaluation of the ECMWF pilot reanalysis of the 20th-century assimilating surface observations only (ERA-20C)".

Pulquério, M., Garrett, P., Santos, F. D., and Cruz, M. J. [2015]. "On using a generalized linear model to downscale daily precipitation for the center of Portugal: an analysis of trends and extremes". *Theoretical and Applied Climatology.* Vol. 120. no. 1-2, pp. 147–158.

Pustitrarini, H. D. [2015]. "Climate-related energy scarcity analysis in Europe: A threshold based approached".

Radanovics, S., Vidal, J.-P., Sauquet, E., Daoud, A. B., and Bontron, G [2013]. "Optimising predictor domains for spatially coherent precipitation downscaling". *Hydrology and Earth System Sciences.* Vol. 17, p–4189.

Rahmstorf, S. and Coumou, D. [2011]. "Increase of extreme events in a warming world". *Proceedings of the National Academy of Sciences.* Vol. 108. no. 44, pp. 17905–17909.

Rasmussen, M. G., Andresen, G. B., and Greiner, M. [2012]. "Storage and balancing synergies in a fully or highly renewable pan-European power system". *Energy Policy.* Vol. 51, pp. 642–651.

Raynaud, D., Hingray, B., Zin, I., Anquetin, S., Debionne, S., and Vautard, R. [2016]. "Atmospheric analogues for physically consistent scenarios of surface weather in Europe and Maghreb". *International Journal of Climatology.*

Rehman, S., Al-Hadhrami, L. M., and Alam, M. M. [2015]. "Pumped hydro energy storage system: a technological review". *Renewable and Sustainable Energy Reviews.* Vol. 44, pp. 586–598.

Reyers, M., Moemken, J., and Pinto, J. G. [2016]. "Future changes of wind energy potentials over Europe in a large CMIP5 multi-model ensemble". *International Journal of Climatology.* Vol. 36. no. 2, pp. 783–796.

Riihelä, A., Carlund, T., Trentmann, J., Müller, R., and Lindfors, A. V. [2015]. "Validation of CM SAF Surface Solar Radiation Datasets over Finland and Sweden". *Remote Sensing.* Vol. 7. no. 6, pp. 6663–6682.

Ring, M. J., Lindner, D., Cross, E. F., Schlesinger, M. E., et al. [2012]. "Causes of the global warming observed since the 19th century". *Atmospheric and Climate Sciences.* Vol. 2. no. 04, p. 401.

Rodríguez-Fonseca, B., Mohino, E., Mechoso, C. R., Caminade, C., Biasutti, M., Gaetani, M., Garcia-Serrano, J., Vizy, E. K., Cook, K., Xue, Y., et al. [2015]. "Variability and predictability of west African droughts: a review on the role of sea surface temperature anomalies". *Journal of climate.* Vol. 28. no. 10, pp. 4034–4060.

Rodwell, M. J., Rowell, D. P., and Folland, C. K. [1999]. "Oceanic forcing of the wintertime North Atlantic Oscillation and European climate". *Nature.* Vol. 398. no. 6725, pp. 320–323.

Rogelj, J [2013]. "Long-term climate change: projections, commitments and irreversibility".

Rogers, J. C. [1997]. "North Atlantic storm track variability and its association to the North Atlantic Oscillation and climate variability of northern Europe". *Journal of Climate.* Vol. 10. no. 7, pp. 1635–1647.

Ropelewski, C. F. and Halpert, M. S. [1986]. "North American precipitation and temperature patterns associated with the El Niño/Southern Oscillation (ENSO)". *Monthly Weather Review*. Vol. 114. no. 12, pp. 2352–2362.

Ruosteenoja, K., Tuomenvirta, H., and Jylhä, K. [2007]. "GCM-based regional temperature and precipitation change estimates for Europe under four SRES scenarios applying a super-ensemble pattern-scaling method". *Climatic Change*. Vol. 81. no. 1, pp. 193–208.

Scaife, A. A. [2010]. "Impact of ENSO on European Climate".

Schaefli, B, Hingray, B, Niggli, M, and Musy, A [2005]. "A conceptual glacio-hydrological model for high mountainous catchments". *Hydrology and Earth System Sciences Discussions*. Vol. 9. no. 1/2, pp. 95–109.

Schaefli, B., Hingray, B., and Musy, A. [2007]. "Climate change and hydropower production in the Swiss Alps: quantification of potential impacts and related modelling uncertainties". *Hydrology and Earth System Sciences Discussions*. Vol. 11. no. 3, pp. 1191–1205.

Schär, C., Vidale, P. L., Lüthi, D., Frei, C., Häberli, C., Liniger, M. A., and Appenzeller, C. [2004]. "The role of increasing temperature variability in European summer heatwaves". *Nature*. Vol. 427. no. 6972, pp. 332–336.

Scheff, J. and Frierson, D. [2012]. "Twenty-first-century multimodel subtropical precipitation declines are mostly midlatitude shifts". *Journal of Climate*. Vol. 25. no. 12, pp. 4330–4347.

Segal, M., Pan, Z., Arritt, R. W., and Takle, E. S. [2001]. "On the potential change in wind power over the US due to increases of atmospheric greenhouse gases". *Renewable Energy*. Vol. 24. no. 2, pp. 235–243.

Shields, M. A., Payne, A. I., et al. [2014]. "Marine renewable energy technology and environmental interactions". Springer.

Smith, A., Lott, N., and Vose, R. [2011]. "The integrated surface database: Recent developments and partnerships". *Bulletin of the American Meteorological Society*. Vol. 92. no. 6, p. 704.

Srivastav, R. K. and Simonovic, S. P. [2015]. "Multi-site, multivariate weather generator using maximum entropy bootstrap". *Climate Dynamics*. Vol. 44. no. 11-12, pp. 3431–3448.

Steinke, F., Wolfrum, P., and Hoffmann, C. [2013]. "Grid vs. storage in a 100% renewable Europe". *Renewable Energy*. Vol. 50, pp. 826–832.

Steinschneider, S. and Brown, C. [2013]. "A semiparametric multivariate, multisite weather generator with low-frequency variability for use in climate risk assessments". *Water resources research*. Vol. 49. no. 11, pp. 7205–7220.

Stige, L. C., Stave, J., Chan, K.-S., Ciannelli, L., Pettorelli, N., Glantz, M., Herren, H. R., and Stenseth, N. C. [2006]. "The effect of climate variation on agro-pastoral production in Africa". *Proceedings of the National Academy of Sciences of the United States of America*. Vol. 103. no. 9, pp. 3049–3053.

Stocker, T., Field, C., Dahe, Q., Barros, V., Plattner, G.-K., Tignor, M., Midgley, P., and Ebi, K. [2009]. "IPCC Expert Meeting on Detection and Attribution Related to Anthropogenic Climate Change".

Stott, P. A., Christidis, N., Otto, F. E., Sun, Y., Vanderlinden, J.-P., Oldenborgh, G. J. van, Vautard, R., Storch, H. von, Walton, P., Yiou, P., et al. [2016]. "Attribution of extreme weather and climate-related events". *Wiley Interdisciplinary Reviews: Climate Change*. Vol. 7. no. 1, pp. 23–41.

Stroeve, J. C., Kattsov, V., Barrett, A., Serreze, M., Pavlova, T., Holland, M., and Meier, W. N. [2012]. "Trends in Arctic sea ice extent from CMIP5, CMIP3 and observations". *Geophysical Research Letters*. Vol. 39. no. 16.

Surmaini, E., Hadi, T. W., Subagyono, K., and Puspito, N. T. [2015]. "Prediction of drought impact on rice paddies in west Java using analogue downscaling method". *Indonesian Journal of Agricultural Science*. Vol. 16. no. 1, pp. 21–30.

Swanson, K. L., Sugihara, G., and Tsonis, A. A. [2009]. "Long-term natural variability and 20th century climate change". *Proceedings of the National Academy of Sciences*. Vol. 106. no. 38, pp. 16120–16123.

Szarka, N., Scholwin, F., Trommler, M., Jacobi, H. F., Eichhorn, M., Ortwein, A., and Thrän, D. [2013]. "A novel role for bioenergy: a flexible, demand-oriented power supply". *Energy*. Vol. 61, pp. 18–26.

Tapiador, F. J. [2010]. "A joint estimate of the precipitation climate signal in Europe using eight regional models and five observational datasets". *Journal of Climate*. Vol. 23. no. 7, pp. 1719–1738.

Taylor, K. E., Stouffer, R. J., and Meehl, G. A. [2012]. "An overview of CMIP5 and the experiment design". *Bulletin of the American Meteorological Society*. Vol. 93. no. 4, p. 485.

Teutschbein, C. and Seibert, J. [2012]. "Bias correction of regional climate model simulations for hydrological climate-change impact studies: Review and evaluation of different methods". *Journal of Hydrology*. Vol. 456, pp. 12–29.

Teweles, S and Wobus, H [1954]. "Verification of prognostic charts". *Bull. Amer. Meteor. Soc.* Vol. 35, pp. 455–463.

Tian, D. and Martinez, C. J. [2012]. "Comparison of two analog-based downscaling methods for regional reference evapotranspiration forecasts". *Journal of hydrology*. Vol. 475, pp. 350–364.

Timbal, B and McAvaney, B. [2001]. "An analogue-based method to downscale surface air temperature: application for Australia". *Climate Dynamics*. Vol. 17. no. 12, pp. 947–963.

Timbal, B, Dufour, A, and McAvaney, B [2003]. "An estimate of future climate change for western France using a statistical downscaling technique". *Climate Dynamics*. Vol. 20. no. 7-8, pp. 807–823.

Timbal, B, Fernandez, E, and Li, Z [2009]. "Generalization of a statistical downscaling model to provide local climate change projections for Australia". *Environmental Modelling & Software*. Vol. 24. no. 3, pp. 341–358.

Tobin, I., Vautard, R., Balog, I., Bréon, F.-M., Jerez, S., Ruti, P. M., Thais, F., Vrac, M., and Yiou, P. [2015]. "Assessing climate change impacts on European wind energy from ENSEMBLES high-resolution climate projections". *Climatic Change*. Vol. 128. no. 1-2, pp. 99–112.

Trenberth, K. E. [2011]. "Changes in precipitation with climate change". *Climate Research*. Vol. 47. no. 1-2, pp. 123–138.

Trigo, R. M., Osborn, T. J., and Corte-Real, J. M. [2002]. "The North Atlantic Oscillation influence on Europe: climate impacts and associated physical mechanisms". *Climate Research*. Vol. 20. no. 1, pp. 9–17.

United-Nations [2015]. "Adoption of the Paris Agreement: United Nations, 21st Conference of the Parties, Paris". United Nations.

Uvo, C. B. and Berndtsson, R. [2002]. "North Atlantic Oscillation; a climatic indicator to predict hydropower availability in Scandinavia". *Hydrology Research*. Vol. 33. no. 5, pp. 415–424.

Valero, F, Pascual, A, and Martín, M. [2014]. "An approach for the forecasting of wind strength tailored to routine observational daily wind gust data". *Atmospheric Research*. Vol. 137, pp. 58–65.

Vautard, R. and Yiou, P. [2009]. "Control of recent European surface climate change by atmospheric flow". *Geophysical Research Letters*. Vol. 36. no. 22.

Vautard, R., Thais, F., Tobin, I., Bréon, F.-M., Lavergne, J.-G. D. de, Colette, A., Yiou, P., and Ruti, P. M. [2014]. "Regional climate model simulations indicate limited climatic impacts by operational and planned European wind farms". *Nature communications*. Vol. 5.

Vidal, J.-P., Martin, E, Kitova, N, Najac, J, and Soubeyroux, J.-M. [2012]. "Evolution of spatio-temporal drought characteristics: validation, projections and effect of adaptation scenarios". *Hydrology and Earth System Sciences*. Vol. 16. no. 8, pp. 2935–2955.

Von Bremen, L. [2010]. "Large-scale variability of weather dependent renewable energy sources". Pp. 189–206.

Von Storch, H. and Zwiers, F. W. [2001]. "Statistical analysis in climate research". Cambridge university press.

Vrac, M, Marbaix, P., Paillard, D, Naveau, P, et al. [2007]. "Non-linear statistical downscaling of present and LGM precipitation and temperatures over Europe". *Climate of the Past*. Vol. 3. no. 4, pp. 669–682.

Weitemeyer, S., Kleinhans, D., Vogt, T., and Agert, C. [2015]. "Integration of Renewable Energy Sources in future power systems: The role of storage". *Renewable Energy*. Vol. 75, pp. 14–20.

Westra, S., Alexander, L. V., and Zwiers, F. W. [2013]. "Global increasing trends in annual maximum daily precipitation". *Journal of Climate*. Vol. 26. no. 11, pp. 3904–3918.

Wetterhall, F., Halldin, S., and Xu, C.-y. [2005]. "Statistical precipitation downscaling in central Sweden with the analogue method". *Journal of Hydrology*. Vol. 306. no. 1, pp. 174–190.

Wilby, R. L. and Quinn, N. W. [2013]. "Reconstructing multi-decadal variations in fluvial flood risk using atmospheric circulation patterns". *Journal of Hydrology*. Vol. 487, pp. 109–121.

Wilks, D. S. and Wilby, R. L. [1999]. "The weather generation game: a review of stochastic weather models". *Progress in Physical Geography*. Vol. 23. no. 3, pp. 329–357.

Willems, P. and Vrac, M [2011]. "Statistical precipitation downscaling for small-scale hydrological impact investigations of climate change". *Journal of Hydrology*. Vol. 402. no. 3, pp. 193–205.

Xydis, G. [2013]. "Comparison study between a renewable energy supply system and a supergrid for achieving 100% from renewable energy sources in Islands". *International Journal of Electrical Power & Energy Systems*. Vol. 46, pp. 198–210.

Yiou, P [2014]. "Anawege: a weather generator based on analogues of atmospheric circulation". *Geoscientific Model Development*. Vol. 7. no. 2, pp. 531–543.

Young, K. C. [1994]. "A multivariate chain model for simulating climatic parameters from daily data". *Journal of Applied Meteorology*. Vol. 33. no. 6, pp. 661–671.

Zorita, E., Hughes, J. P., Lettemaier, D. P., and Storch, H. von [1995]. "Stochastic characterization of regional circulation patterns for climate model diagnosis and estimation of local precipitation". *Journal of Climate*. Vol. 8. no. 5, pp. 1023–1042.

APPENDICES

Appendix A

Evaluation of the WRF wind simulations. Based on Raynaud et al., 2016

We performed a complementary evaluation of the model outputs comparing them with available wind stations. The observed series have been collected from the ECA& D and ISD-Lite databases. A total number of 137 stations with data available, at least partially, from 1983 to 2012 were selected. The geographical distribution of the stations is very uneven from one region to the other but all of them are represented. Similarly, the length of the series varies greatly between stations, going from a few months to the whole 1983-2012 period. At each location, the observed time series has been compared to the corresponding grid point from the WRF outputs. Firstly, the correlation coefficients were computed for all four seasons separately. Results for winter and summer are presented on Fig.A.1. For both seasons, strong differences in correlation from one region to the other can be seen. WRF simulations are greatly correlated with observations for regions located in plains (EN, GE, BE, FI, FR) with values exceeding 0.8. On the opposite, wind in mountainous regions is not as well simulated and the correlation coefficients are often below 0.5. Some seasonal disparities are also noticeable with higher correlations in winter at all sites. Fig.A.1 also presents the model bias. In most cases, slight positive biases exist with values ranging from 0 to 2 $m \cdot s^{-1}$. However, stronger differences between the WRF and on-site observations can be seen for some regions (NO and II), especially in winter. Speaking generally, the model outputs are more consistent with observations in summer with bias values close to 0.

Since the present study focuses on co-variations between climate-related energies, it is essential to check that inter-variables correlations are equally well reproduced using the WRF model. Using the temperature, precipitation and radiation data described previously, correlation coefficients between wind speed and the three other predictands have been computed for both observed and simulated series. The results are presented on A.2 as a function of the altitude difference between weather

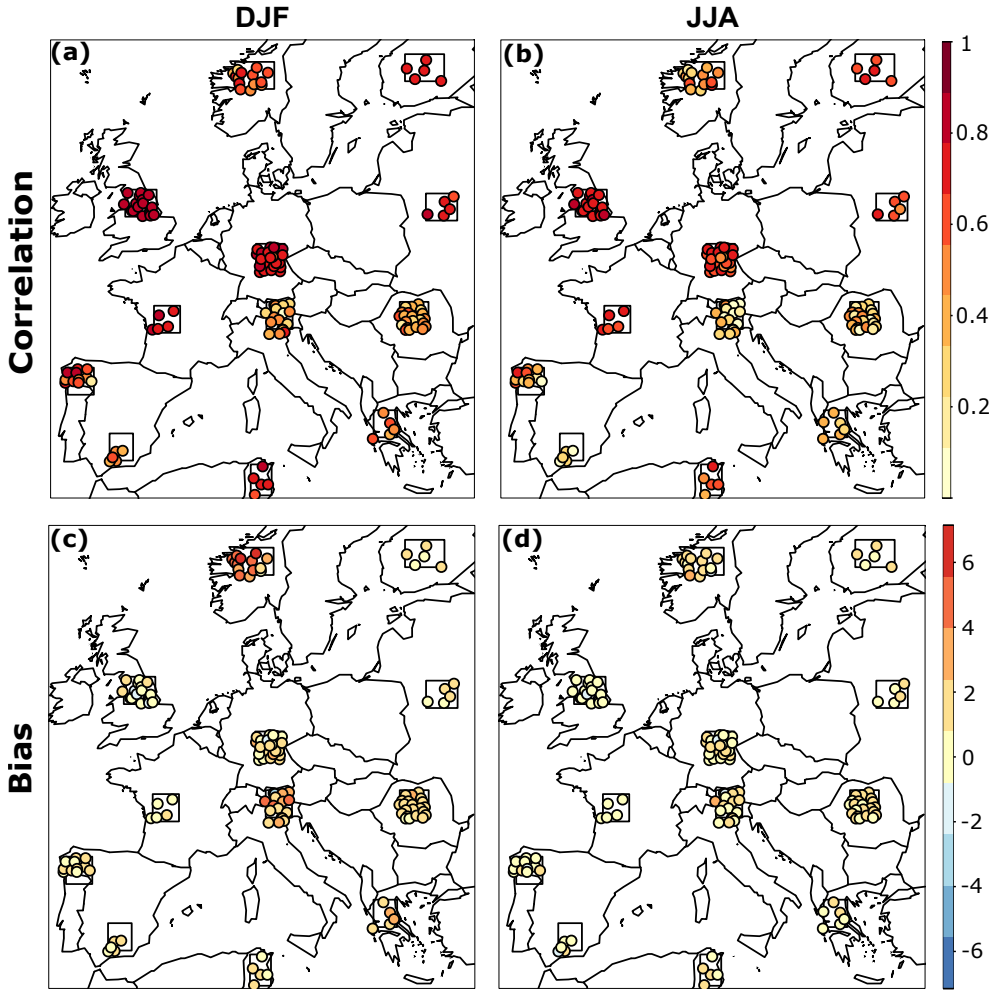

Figure A.1 – Correlation coefficients (a)-(b) and bias (c)-(d) of wind speed data from the WRF model compared to on-site observations at wind stations. Results are displayed for winter and summer seasons. All available weather stations are used regardless of their time series length which goes from a few months for some of them to the entire 1983-2012 period.

stations and their corresponding grid cells in the WRF model. For all pairs of variables, there is a clear relationship between the ability of WRF to simulate relevant inter-variables correlation coefficients and the accuracy of the topography in the model. For most stations, there are good agreements between observations and simulations for altitude differences below 50m. For higher values, WRF correlation coefficients tend to diverge from the observed ones and the confidence in the model simulations drops rapidly. The results are generally better in winter.

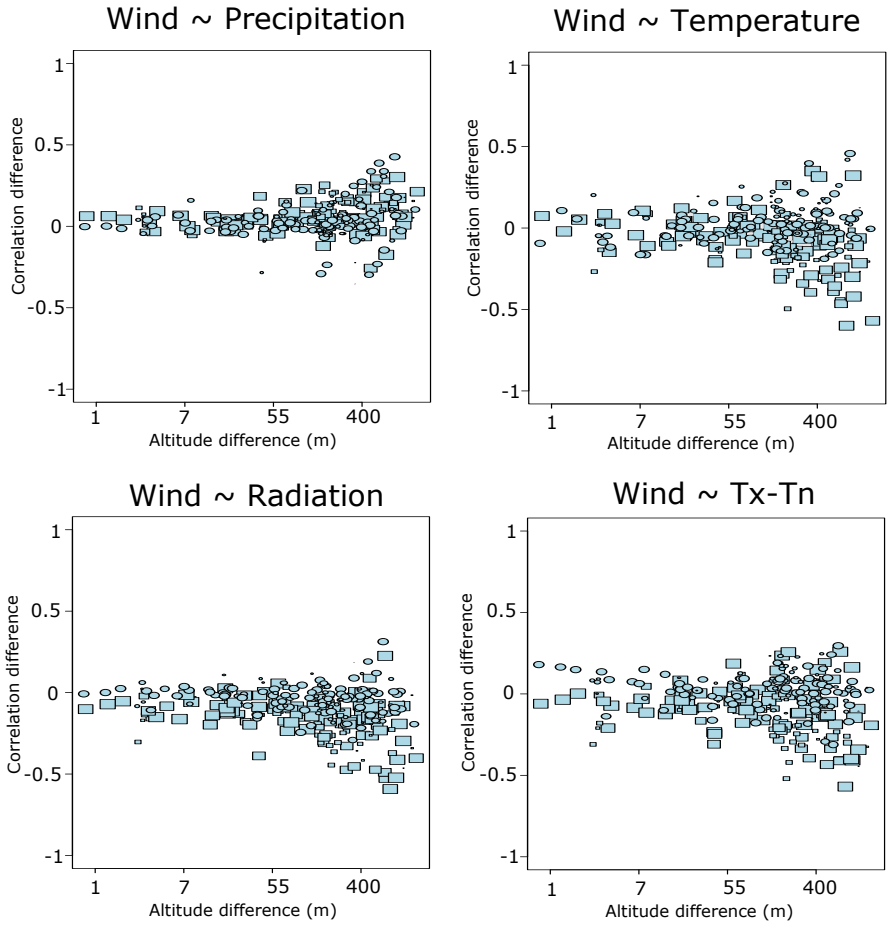

Figure A.2 – Ability of the hybrid WRF-observation dataset to reproduce correlations coefficients between variables. Results are presented in terms of inter-variable correlation difference where the reference correlation is that obtained between observations (for wind and the other variable) and where the simulated correlation is that obtained between WRF wind data and observations for the other variables (e.g. radiation). Difference in correlation is presented as a function of the difference in altitude between the station considered and the associated grid point from the WRF model. Results are displayed for winter (dots) and summer months (square). The size of each symbol is proportional to the length of the observed time series at the station of interests

Appendix B

Calibration of the hydrological model

For the calibration of the hydrological model, discharge data were collected from the Global Runoff Data Center (GRDC[1]) and from other research centres[2][3]. Unfortunately, data were available for only 6 out of our 12 regions. Therefore, the choice was made to look for an unique parametrisation for all regions, based on the calibration of the hydrological model for this subgroup. This parametrisation should lead to reasonable discharge simulations in all our European test areas.

Tab.B.1 presents the number of discharge stations used in each region, together with the total upstream area associated to the discharge measurements. One can notice the very uneven representation of the test regions. In some cases (EN, NO), the total upstream area corresponds to less than 20% of the surface area considered in the model (40000km^2). In GE and RO, the data also gather information from catchments in the surroundings of the test regions, giving total upstream area over 40000km^2.

Table B.1 – Regional characteristics of the stations used for the calibration of the hydrological model

Region	Nb of Stations	Total upstream area
EN	7	2000 km^2
FR	15	27000 km^2
FI	6	33000 km^2
NO	5	4500 km^2
GE	7	75000 km^2
RO	7	56000 km^2

[1] http://www.bafg.de/GRDC
[2] http://www.ceh.ac.uk
[3] www.ymparisto.fi

The calibration was performed in a very simple way:

1. For each region, a specific-discharge (q_{obs}) time series was computed for each sub-catchment (discharge divided by the upstream area). Then, a "regional" specific-discharge $q_{obs,r}$ series was generated by averaging the q_{obs} time series associated to each available station.

2. For each region, a Nash efficiency coefficient [Nash and Sutcliffe, 1970] is then computed by comparing the observed regional time series $q_{obs,r}$ with the simulated one $q_{sim,r}$.

3. A "European" Nash coefficient (mean value of regional coefficients) is finally used to optimise the parameters of the hydrological model (K_1, K_2, K_r, S_1, and degree-day method for snowmelt, cf. Fig.II.5). Thus, the same set of parameters is used for all regions.

The comparison between "observed" and simulated seasonal cycles of discharge is presented on Fig.D.5. The cycles have been normalised using the regional mean "observed" discharge. For the majority regions (EN, GE, FR and NO), the simulated cycles are consistent with the observed ones. Some biases exit but both shape and amplitude are rather well simulated, even where complex processes are involved (e.g, NO, snowmelt-related peak). The results are less satisfactory in FI an RO (no early spring peak in RO, bias in autumn and winter in FI). The limited quality and representativeness of discharge series may be one reason for these inaccurate simulations, especially in RO. Another potential reason is the rough representation of the regional hydrological systems: In FI, there are some large lakes, which reduce the temporal variability and the seasonality of discharge. The hydrological model considered in this study does not take their effect into account.

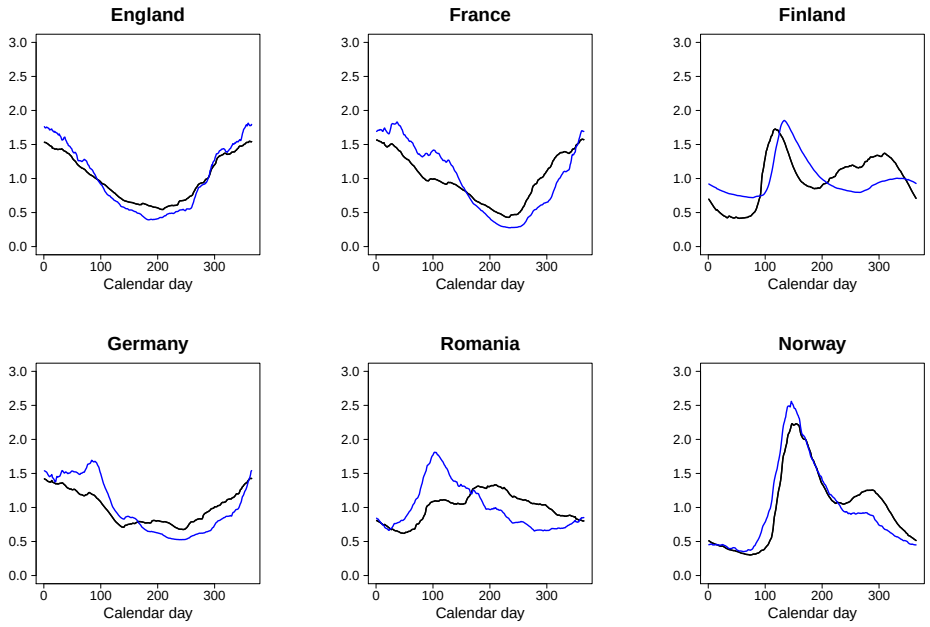

Figure B.1 – **Comparison between observed and simulated discharge (mm/day).** Normalised seasonal cycles of discharge from observations (blue) and using the hydological model (black).

Appendix C

Hydro, wind and solar power mix in Europe: François et al., 2016

Increasing Climate-Related-Energy penetration by integrating run-of-the river hydropower to wind/solar mix

François, B.[1,2], B. Hingray[1,2], D. Raynaud[1,2], M. Borga[3] and J.D. Creutin[1,2]

[1]Université de Grenoble-Alpes, LTHE, 38041 Grenoble, France
[2]CNRS, LTHE, 38041 Grenoble, France
[3]University of Padova, Dept. Land, Environment, Agriculture and Forestry, Padova, Italy

Corresponding author: Baptiste FRANCOIS

Phone: +334 76 82 67 28

Email: baptiste.francois@ujf-grenoble.fr

This article was published in Renewable Energy journal

Reference: François, B., Hingray, B., Raynaud, D., Borga, M., and Creutin, J.D. (2016). Increasing climate-related-energy penetration by integrating run-of-the river hydropower to wind/solar mix. Renew. Energy 87, 686–696. doi:10.1016/j.renene.2015.10.064

Abstract

The penetration rate of Climate Related Energy sources like solar-power, wind-power and hydro-power source is potentially low as a result of the large space and time variability of their driving climatic variables. Increased penetration rates can be achieved with mixes of sources. Optimal mixes, i.e. obtained with the optimal share for each source, are being identified for a number of regions worldwide. However, they often consider wind and solar power only.

Based on 33 years of daily data (1980-2012) for a set of 12 European regions, we re-estimate the optimal mix when wild run-of-the-river energy is included in the solar/wind mix. It is found to be highly region dependent but the highest shares are often obtained for run-of-the-river, ranging from 35% to 65% in Belarus and England. High solar shares (>40%) are found in southern countries but solar shares drop to less than 15% in northern countries. Wind shares range from 10 to 35% with the exception of Norway where it reaches 50%. These results put in perspective the optimal 60% - 40% wind/solar mix currently used for Europe. For all regions, including run-of-the-river in the mix allows increasing the penetration rate of CREs (from 1 to 8 percentage points).

Key words: Climate-Related Energy, Penetration, Energy mix, Complementarity

1. Introduction

Installed capacity of Climate Related Energy (CRE), i.e. solar-power, wind-power and hydro-power, is growing quickly across Europe. A new goal of 27 % of renewable share by

2030 has been defined by the EU (European Council, 2014). For some European countries such as Austria, Spain, Norway or Sweden, this objective is already achieved (Sturc, 2012). On the other hand, the European Climate Foundation states that 100 % renewable is an objective to be achieved by 2050 (ECF, 2010). This scenario is physically realistic even at the global scale since the technical potential of renewable energies covers several times the energy demand (Hoogwijk and Graus, 2008). However, it is well-known that this available potential is not equally distributed over space (von Bremen, 2010). In Europe, solar power potential is much higher in Southern countries than in the Northern ones. For wind power, it is the opposite with higher potential in the north and along the shores. Lehner et al., (2005) show that the space distribution of hydropower potential relates with the mountain ranges in Europe: higher is the altitude, the higher the hydropower potential. Heide et al., (2010) illustrated that Europe could take advantage of combining different CREs allowing a limited use of conventional power.

Even though it is not yet clear what will look like such a 100 % renewable energy mix, solar and wind energy sources are expected to be important contributors. The main reason is that, contrary to biomass, their weather driving variables (i.e. wind, solar irradiance and temperature) are exploitable everywhere in Europe (Steinke et al., 2013).

For a 100 % scenario at the European scale, von Bremen (2010) shows that the mix composed by 60 % of wind and 40 % of Photo-Voltaic (PV) minimizes the monthly energy balance variance which governs the balancing costs related to energy transport and storage. The hourly energy balance variance is however minimized with a lower share of solar due to its diurnal cycle. Heide et al., (2010) show that even if a certain rate of fossil-nuclear still remains in activity (for instance covering lower than 50 % of the energy demand on average), the optimal share between wind and solar would not differ significantly. Heide et al., (2011) find that oversizing solar and wind power capacities modifies the optimal mix minimizing the storage requirement. Following these studies, Weitemeyer et al., (2015) show that the highest penetration rate is obtained in Germany for a wind power share ranging from 60 to 80 %.

In some ways, hydropower is never explicitly included in the mix computation but considered as a storage facility. Indeed, large hydropower storage is used for balancing production and load mismatches. In this sense, the term of ‘blue battery’ is used when referring to the huge energy storage capacity provided by Scandinavian or Alpine reservoirs (Piria and Junge, 2013). Less attention is paid to small run-of-the-river power (hereafter denoted as RoR power), even if the amount of energy produced is important in several places. In Italy for instance, small run-of-the-river hydropower plants (i.e. with a power capacity lower than 3 MW) provide 22 % of the annual hydropower energy which reached 45,823 GWh in 2011, i.e. about 24 % of the electricity consumption (GSE, 2011). In Switzerland, 26 % of the generated power is generated by run-of-the river power plants (BFE, 2013). Even though RoR potential is already significant in Europe, new RoR power plants are under-construction or planned. For instance, an increase of about 33 % of small RoR power capacity is under-study in Scotland (Sample, 2015).

In Northern Italy, the challenge of integrating run-of-the river power into the combination with solar energy source starts to be investigated (François et al., 2016). Different degrees of complementarity are obtained, depending on the hydrological regime of the considered catchments (snow- or rainfall-dominated regimes) and on the time scales (e.g. hourly, monthly).

This study investigates how the use of RoR hydropower coming from uncontrolled river flows may increase the global penetration of climate related energies under the hypothesis that only solar, wind and RoR power are used to meet the demand. We use a benchmark set of 12 regions spread across Europe and covering a wide variety of climates. Neither storage nor transport among regions is considered in this study.

The paper is organized as follows: The description of the study areas and the databases are given in Section 2. The analysis framework is detailed in Section 3. Results are presented in Section 4. Section 5 concludes and gives some outlooks for future research directions.

2. Study areas and dataset used

Figure 1 locates the different areas selected for this study. In the following, although the areas do not match country border, they will be referred for convenience with country or region names. As the surface area of each domain is roughly 40,000km² (Table 1), we assume that they are large enough for being representative of the in-situ climate, both in terms of weather variable average and time variability. These domains are chosen for two main reasons. First, they represent a variety of climates in Europe moving along two climatic gradients: the north-south gradient mainly explores changes from Scandinavian to Mediterranean hydro-climatic regime. The west-east gradient explores changes from oceanic to continental climate. Second, they correspond to watershed heads. There is therefore no contribution of upstream areas to river flow within the considered domain and the whole hydropower production that can be harvested within the domain does only depend from runoff production within the domain.

Hydro-meteorological data used to assess energy production and demand for the 1980-2012 period are obtained from different observational datasets and models. Daily temperature and precipitation data come from the European Climate Assessment & Dataset (ECAD, Haylock et al., 2008) with a 0.25° space resolution.

In the present study, wind and solar radiation data are pseudo-observations obtained from climate simulations with the Weather Research and Forecasting Model when forced with large scale atmospheric fields from the ERA-Interim atmospheric reanalyses (hereafter noted as WRF, Vautard et al., 2014). Wind power generation is estimated at a daily time step from mean daily wind speed with a daily production function identified in a preliminary step from 3 hourly wind speed data (see Section 3).

Gathering long time series of runoff observations for unregulated watersheds is also challenging, if not impossible in populated areas. Only seven water discharge time series could actually be obtained for seven out of twelve regions thanks to the Global Runoff Data Center (GRDC, 1999). Unregulated runoff are thus obtained via simulation, for each grid cell of each region with a distributed version of the GSM-Socont hydrological model (Schaefli et al. 2005). This model simulates the snowpack dynamic (snow accumulation and melt), water abstraction from evapotranspiration, slow and rapid components of river flow from infiltrated and effective rainfall respectively. It uses daily precipitation, temperature, and wind speed from above cited databases. A unique set of parameters is used for all regions. It was calibrated from comparisons of simulations and GRDC discharge data.

Observed electricity demand data are obtained from the European Network of Transmission Systems Operators of Electricity (ENTSOE, https://www.entsoe.eu/home/). Data are however only available from 2006. Tunisia and Belarus are not members of the ENTSOE network; and, to our knowledge, there is no auxiliary database available for these two countries. We therefore also reconstructed electricity demand time series for all regions

and for the whole analysis period (back to 1980) with a climate-driven demand model developed from regions and periods with observations (Section 3).

3. Study framework

This section describes the computation of the different elements needed in our analysis: i) the power time series obtained from PV solar, wind and RoR, ii) the energy load time series and iii) the penetration rate for a given energy mix. Power generation from solar, wind and RoR are computed for each grid cell *i* and are then summed for each region. For the sake of simplicity, we assume that all grids have the same power capacity, i.e. the same level of equipment for each energy source. We further assume that each region is autonomous: there is no energy import/export with neighboring regions. We consider energy mixes based on solar photovoltaic, wind and RoR hydro only. In other words, we assume that the regional demand can be only satisfied (or not) with the production obtained within the region from these three energy sources. The study framework is applied to the 12 regions presented on Figure 1.

Solar power (photovoltaic)

The solar power generation from a photovoltaic generator (P_{PV}) at a given time *t* and from the grid cells indexed by *i* depends on the global solar irradiance I_{eff} (Wm^{-2}) and the air temperature T_a (°C) (Hanif et al. 2012) through the following expression (Perpiñan et al., 2007):

$$P_{PV}(t) = \sum_i B\, I_{eff}(t,i)\left(1 - \mu\left(T_a(t,i) - T_{c,STC}\right) - \mu\, C\, I_{eff}(t,i)\right), \qquad 1$$

with *B* a constant production parameter, defined as the product of the surface area of the PV array (m²) by the generator and invertor efficiencies (%), and with μ and *C* respectively the temperature and the radiation dependent efficiency reduction factors (%). $T_{c,STC}$ (°C) is the photovoltaic cell temperature corresponding to standard test conditions (Duffie and Beckman, 1991).

Wind power

Figure 2 presents a sketch of a wind power curve giving the power produced by a 1 MW power capacity windmill P_W for a given wind speed u (m s^{-1}). This relationship is nonlinear. Below a given threshold (e.g. 3 m s^{-1}), the wind speed is not sufficient to enable the power generation. Above this threshold, the power generation increases like the power 3 of the wind speed up to a second threshold from which the maximum wind turbine efficiency is reached (e.g. 13 m s^{-1}). Above a third threshold (e.g. 25m s^{-1}), the power generation has to be stopped in order to avoid any damages on the wind turbine. The nominal power curve needs to be adapted to estimate the power generation from daily average wind speed values using the infra-daily probability density distribution of wind speed values.

If the probability density function of the infra-daily wind speed p_{Um} is known for a daily average *Um* (m s^{-1}), the wind power generation for the corresponding day is given by the convolution of this function with the instantaneous power curve *W(u)* (W).

$$P_W(U_m) = \sum_i \int_0^\infty p_{Um}(u,i)W(u)du, \quad (2)$$

with $P_W(U_m)$ the daily wind-power (W) obtained for the daily average wind speed U_m , with u the instantaneous wind speed (m s^{-1}).

In our study, we evaluated this integral over a set of average daily wind *Um* classes from 0 to 35 m s^{-1} with 1 m s^{-1} step. The infra-daily variability required to evaluate this integral was obtained from the 3 hour time step data available from the WRF model for each day. A Weibull density function was finally used to model the empirical distribution functions $p_{Um}(u,i)$. The resulting wind power curve $P_W(U_m)$, allowing estimating daily production from mean daily wind speed is given in Figure 2. The 80 meter altitude wind speed time series used for computing wind power time series were estimated from 10 meter altitude WRF wind speed following the scaling equation:

$$u_1 = u_2\left(\frac{h_1}{h_2}\right)^\alpha, \quad (3)$$

with u_1 and u_2 the wind speeds (m s^{-1}) at the altitude h_1 and h_2 (m). α is an air friction coefficient chosen equal to 1/7 (no dimension) (Johnson, 1985).

Run-of-the-river power generation

Run-of-the-river power is derived from the energy of falling water along the river network. For a given region, the production is first computed for each grid cell. We consider that the power at a given time *t* is generated from a fraction of the river flow diverted from the natural river bed following:

$$P_{RoR}(t) = \sum_i \eta_H g h \rho\, q(t,i), \quad (4)$$

where P_{RoR} is the power delivered by the plant generator (kW), η_H the efficiency of the generator (%), q the water flow through the turbine ($m^3 s^{-1}$), g the acceleration of gravity (=9.81 m s^{-2}), ρ the water density (=1000 kg m^{-3}), h the failing height (m). h is simply defined as the difference between the cell altitude and the minimum altitude of the region.

Note that we here fully disregard the structure of the hydrographic network within the region, which in reality determines where rivers flow and where RoR power can be harnessed. For any given cell and whatever its location regarding the river network, we actually consider that all the runoff it produces will be harnessed along its path to the outlet of the region. Though this crude simplification, we expect that the sum of the production from each cell is a good indicator for what could be the regional hydropower generation, in terms of temporal organization especially.

As illustrated by the Figure 3, the generation is bounded by three characteristic flows corresponding to technical and environmental constraints. The design flow Q_d is the maximum river discharge that can be diverted to the power plant. The minimum flow Q_{min} is defined as the lowest acceptable flow. It can be either constant or variable in time. The maximum flow Q_{max} is the upper limit beyond which the production is interrupted to prevent any potential damages to the power plant. As discussed by Hänggi and Weingartner (2012),

Q_{min}, Q_d and Q_{max}, depend on the purpose of the hydropower plant. In this study, values of Q_{min}, Q_d and Q_{max}, are constant in time and fixed equal to the 95th, 25th and 2nd percentiles of the natural flows. Those values are usual for RoR power plant operated in a network of other power plants (Hänggi and Weingartner, 2012).

Energy load

As illustrated by François et al. (2016), the energy load may be modeled regarding the meteorological variables (e.g. outside temperature, cloud cover, humidity, etc.) and various socio-economic factors implying, for instance, lower consumptions during weekends and holidays. In this study, we assume that the climate driven part of the energy load can be estimated as a function of temperature only. We also disregard the influence of the socio-economic factors; all days are simulated as week days (i.e. the energy load model does not account for the difference between weekdays, weekends and holiday periods). This choice has the advantage to facilitate the interpretation, making comparable the results obtain over the different regions (which do not otherwise have the same holidays for instance). For the same reason, a same daily demand model is used for all regions. It is based on a piecewise linear regression aiming to represent needs for heating (respectively cooling) when the air temperature decreases below (resp. increases above) a given heating (resp. cooling) threshold. The model reads:

$$\begin{cases} L(t) = a_{T_{Heat}} \times [T_{Heat} - T(t)] + b \quad if\ T(t) < T_{Heat} \\ \quad L(t) = \ b \qquad if\ T_{Heat} < T(t) < T_{Cool} \\ L(t) = a_{T_{Cool}} \times [T(t) - T_{Cool}] + b \quad if\ T(t) > T_{Cool}, \end{cases} \tag{5}$$

where L is the simulated energy load (Wh) T_{Heat} and T_{Cool} are the heating and cooling thresholds (°C), a_{Theat} (Wh °C^{-1}), a_{TCool} (Wh °C^{-1}) and b (Wh) are model parameters. Parameters were estimated from regions and periods with available demand data.

Energy mix and penetration rate PE

For each energy source and each region, the power generation time series generated from previous models is normalized sothat the temporal mean production equals the temporal mean energy load over the 1980-2012 period:

$$p(t) = \frac{P(t)}{\langle P(t) \rangle} \langle L(t) \rangle, \tag{6}$$

with P the energy generated from one energy sources in one given region (Wh), L the in situ energy load (Wh) and p the normalized energy production (Wh). $\langle \quad \rangle$ is the temporal mean operator. For a given region, an energy mix scenario can be generated using a weighted sum of the three normalized power time series obtained for each of the three energy sources, respectively:

$$Pmix(t, \gamma) = \gamma [s_{PV} p_{PV}(t) + s_W p_W(t) + s_{RoR} p_{RoR}(t)], \tag{7}$$

where $Pmix$ is the energy generated from the energy mix (Wh), p_{PV}, p_W and p_{RoR} are the normalized time series of solar (photovoltaic), wind and run-of-the river power (Wh), and s_{PV}, s_W, s_{RoR} the related sharing coefficients (no dimension). As mentioned earlier, we only

consider these three different energy sources to supply the energy load L, so the sum of the sharing coefficients s_{PV}, s_W, s_{RoR} equals 1. The factor γ (no dimension) represents the average CRE production factor and corresponds to the ratio between the energy produced by the energy mix and the energy demand over the considered period:

$$\langle p(t) \rangle = \gamma \langle L(t) \rangle. \quad 8$$

It equals 1 when the mean energy production fits the mean energy load. It is greater than 1 when the mean inter-annual production exceeds the mean inter-annual load. This coefficient, further referred to as the average CRE production factor, allows exploring scenarios of over under- (respectively over-) production. In the following, we explored all scenarios of energy mix with sharing coefficients s_{PV}, s_W, and s_{RoR} ranging respectively from 0 to 1 with a regular step of 0.05. We additionally explored over and under production scenarios with average production factor ranging from 0 to 3.

Several definitions have been proposed for the penetration rate of a considered CRE. In this study we define the penetration as the percentage, over the full 1989-2012 period, of the total energy load that is instantaneously supplied by the CRE mix. We compute its value from daily time series. For a given value of the average CRE production factor γ, the penetration rate PE (%) is given by:

$$PE(\gamma) = \left[1 - \frac{\sum(max[L(t) - Pmix(t,\gamma), 0])}{\sum L(t)}\right] \times 100, \quad 9$$

where max [ ] is the maximum operator. In other words, the penetration rate corresponds to the percentage of the instantaneous load that can be satisfied by the mix, on average, without any storage or backup facility. In the present analysis, the maximum possible value of the penetration ratio is 100%. When γ equals 1, a penetration ratio equal to 100 % would be obtained for a configuration where the temporal organization of the load is exactly the same than that of the production. If the temporal organization of the production and the load differ, such a ratio is obtained when the production exceeds the load at any time and can only be obtained with an average CRE production factor γ higher than 1. In the following, the penetration function will refer to the function PE(γ), defined with PE values obtained for different values of γ.

4. Results

Seasonal opposition between wind and solar power

Solar power presents in all regions a similar seasonal pattern with a high production period during the summer (Figure 4). The patterns have larger amplitude in Northern areas like Norway and Finland due to the important daylight time changes along the years. The consequence for these regions is twofold: i) an almost nil solar generation during winter while it remains significant over this period in Southern regions such as Andalucía, Greece and Tunisia; ii) on the opposite, longer daylight times during summer with a solar power production higher than in the Southern areas. The envelope curves shown Figure 4 and the coefficients of variation (hereafter denoted as CV) reported in Table 2 illustrate how the time

variability of solar power decreases with decreasing the latitude (CV of daily data ranging from 0.89 to 0.35, Table 2).

As shown by several past studies over Europe (e.g. von Bremen, 2010; Heide et al., 2010, 2011), seasonal wind power pattern is anti-correlated with the seasonal solar power pattern (Figure 4). On average, high wind power generation is observed during winter and low generation during summer. Wind power seasonality is more important in the Northern regions than in the Southern ones. Contrary to solar power, wind power time variability is more homogeneous in space (CV ranging from 0.77 to 0.92, Table 2).

Singularity of run-of-the river power variability

Run-of-the river power seasonal patterns result from precipitation seasonality and snow pack dynamics. The latter is influenced by both the altitude and the latitude. As a result, the spatial variability of the seasonal pattern is more pronounced for RoR power than for wind and solar power. RoR seasonal patterns in regions with either high altitudes or located at high latitudes show important production during the snowmelt period from spring to early summer. Conversely, the production is lower during winter, when the main fraction of the precipitation is solid and runoff is low. For other regions, where the hydrological regime is rainfall dominated, the RoR seasonal patterns follow more or less the rainfall seasonality, with, in this part of the world, higher values during winter (e.g. France, Germany, Spain). In both regimes, the integrating effect of the hydrological cycle makes the RoR high frequency time variability smoother than for solar and wind power (CV of daily data ranging from 0.35 to 0.55, Table 2).

Load fluctuations and correlation with the CREs

As described in Section 2, the climate driven part of energy load is expected to be sensitive to high and low temperatures. As illustrated on Figure 4, the magnitude of the average seasonal patterns for the different CRES out-ranges the one observed for the energy load. Daily energy load variability is very low for all regions. This highlights that climate driven part of the energy load is weak regarding its average. Looking at the CV, the load seems roughly 3 to almost 20 times less variable than the different CRE power generation considered (Table 2). The ratio between the CV values of the CRE power and the load depends on the region and the energy source (Table 2). It is maximum for wind power in the Southern region (where the energy load time variability is low and the wind power variability is high).

In addition, power generation from the different CREs is poorly correlated with the energy load. The wind-load correlation is almost nil for all regions and represents less than 4 % of explained variance in all areas but for Italy where it represents 10 % of explained variance (Table 3). The solar-load correlation is negative for all regions except for the southernmost areas (i.e. Andalucía and Tunisia) where summer demand relating with cooling out-ranges demand for heating during winter. In Southern areas such as Greece, Galicia, Andalucía and Tunisia, the correlation is low with less than 15% of explained variance. The anti-correlation is more significant for the other regions even though the explained variance remains lower than 50 %. RoR-load anti-correlation appears to be significant in the areas where the hydrological regime is snow-melt dominated as Norway and Italy (around 50 % of explained variance for both regions). On the opposite, in areas where the hydrological regime is driven by precipitation seasonality with high flow period during winter (e.g. Germany and France), the correlation is positive but not significant (16 and 14 % of explained variance respectively).

Variability of the penetration of solar, wind, and RoR power

Figure 5 shows penetration functions for Italy, Galicia and Norway and for solar, wind and RoR power. For low production factors (i.e. from 0 to 0.4), the daily power generation from all CREs never exceed the daily energy demand (not shown). In such a case, there is no waste of energy and the penetration rate equals the factor γ. When increasing the power capacity, i.e. increasing the γ factor, the power generation can exceed the energy load during some time periods. If no storage facility is available, the fatal generation is next wasted or simply not produced by shutting down the plants for security reasons. As a consequence, the penetration rate becomes lower than the average CRE penetration. For very high values of γ, the penetration rate of a given CRE reaches a sill corresponding to the configuration where the generation is always higher than the load.

The penetration rate function can be significantly different for one energy source to another (Figure 5). In Galicia for instance, wind penetrates the least and RoR penetrates the most. This difference in penetration cannot come from a difference in correlation. Indeed in Galicia, the three considered CREs are uncorrelated with the energy load (15, 1 and 3 % of explained variance respectively for solar, wind and RoR hydro power, Table 3). However, we note that the CRE penetration rates are ordered regarding the time variability of the CRE power generation (illustrated with the CV on Table 2). In other words, the time variability of the CRE generation looks like the main driver of the penetration rate in Galicia. This result is due to the almost nil time variability of the energy load (CV = 0.05). It would not be valid anymore if the load were fluctuating with a similar magnitude than the CRE power. In such a case, a high correlation would be required for matching the demand.

In Figure 5, we additionally note that the penetration rate also differ from one region to another. As discussed previously, wind power penetrates the least in Galicia but the most in Norway. Solar power penetrates the least in Norway but the most in Italy. It is interesting to note that in Italy solar and RoR powers have similar time variability in term of CV (i.e. 0.5 and 0.51 respectively). However, we observe a higher penetration rate for solar than for RoR power, especially for high CRE production factor γ. This might be explained looking at the significant anti-correlation of RoR with the energy load (r=-0.71). In such a case, it seems such a significant anti-correlation (50 % of explained variance) handicaps the RoR power penetration. Solar power penetration seems less handicapped by a lower anti-correlation (r=0.51, 26 % of explained variance).

Similar situation is also noted in Norway where wind penetrates more than RoR hydro power while its time variability is higher (CV = 0.79 for wind and CV = 0.55 for RoR power). Again, RoR power penetration seems limited by its anti-correlation with the energy which, in addition is significant (48 % of explained variance) while wind power is positively correlated with the load, even though this correlation is not significant (4 % of explained variance). As a first conclusion, we can note that, considering a low variable energy load (Table 2), time variability of CRE power generation seems to be the main driving factor of the penetration rate. This penetration rate is however modulated by the correlation between load and generation, especially when the latter is significant.

Looking now at the optimal mix suggested by past studies such as the one of von Bremen (2010), namely 40 % of solar power and 60 % of wind power, we note that the penetration of this mix exceeds the penetration rates obtained with a single energy source (Figure 5). This results from lower time variability of the generation produced by the mix (Table 2) and from the reduced anti-correlation obtained from solar power (Table 3).

Increasing penetration with RoR hydropower integration

We now focus on the 100 % generation scenario (i.e. considering an average CRE production factor γ equal to 1). Figure 6 shows the penetration rate for each possible mix among wind, solar and RoR hydro power in Galicia. It highlights that in this region, the penetration rate increases when integrating RoR hydropower with solar and wind. The black arrow in Figure 6 goes from the optimal wind-solar power mix to the optimal wind-solar-RoR power mix. The orientation of the arrows indicates whether RoR replaces more solar than wind power, or conversely. An angle between the arrow and the horizontal axis (i.e. the axis showing a constant share of wind power) lower than 30°, means that RoR hydro power substitutes more solar power than wind power (and conversely when this angle is greater than 30°). For instance, Figure 6 shows for Galicia that the optimal integration of RoR hydro power would replace more wind than solar power.

Similar triangle plots are presented for all regions in Figure 7. We first note that the optimal wind-solar mix penetrates more in Southern than in Nordic Europe. Table 4 gives the penetration rates obtained with the "optimal" wind-solar mix for the different regions. These optimal shares maximize the penetration rate and thus differ from the one obtained by von Bremen (2010) the latter being obtained minimizing the monthly residual load variance (the von Bremen optimal share was also obtained considering Europe as a whole and for a much smaller time period). We note that the optimal share obtained for each region may have higher time variability than the one suggested by von Bremen (2010), as it is the case for Finland for instance. However in such a case, the optimal share allows to limit the significant anti-correlation brought by solar power (see CV and correlation coefficient Tables 2-4).

Not surprisingly, the optimal combination of wind and solar power seems correlated in space. In other words, the optimal mixes observed at two neighbor regions are more similar than the ones observed for two regions located at the two edges of a climate transect. Thanks to its low time variability, the share of solar power is high in Southern Europe, such as Greece, Galicia, Andalucía and Tunisia (i.e. $s_{PV} > 60$ %). It is lower in Northern Europe ($s_{PV} <$ 40 % for Norway and Finland) where wind power is more favorable (indeed, in Northern countries solar power is highly variable and significantly anti-correlated with the energy load).

When integrating RoR hydropower, the global penetration rate increases for all regions (Table 4). The lowest penetration increase is observed for Italy and Tunisia (+1 %) and the highest for England and Germany (+8 %). The benefit from integrating RoR power into the power mix actually depends on the different complementarity in time between RoR hydropower and wind and solar power, i.e. the way RoR power integration may decrease the time variability of the power generation and to improve the correlation with the energy load. As a result, the optimal share of RoR hydropower into the energy mix differs from one region to another. However, it is always a significant fraction of the energy mix, ranging from 35 % (Norway and Italy) to 65 % (England and Belarus).

Such high share coefficients might be surprising since RoR power in Belarus and England are either anti-correlated or not correlated at all with the energy load (r=-0.57 and r = -0.01 for Belarus and England respectively). However, RoR power variability in time is much lower than for solar and wind power in these regions (see CV values on Table 2). This highlights that the penetration rate increase results from a trade-off between making closer the time variability of the generation and the load and improving the generation-load correlation.

RoR hydropower integration also modifies the relative weight of wind and solar energies within the mix as shown Figure 7 and Table 4. In Belarus, the solar power is almost left out the mix (its contribution goes from 45 to 5 % when integrating RoR). Wind power decreases significantly in Southern Europe (i.e. in Greece, Galicia and Andalucía). Two regions with roughly the same optimal wind-solar share can also move to two different optimal mixes when integrating hydropower. This is the case for France and Italy: RoR hydropower integration decreases wind power share by 25 % in France and by 5% only in Italy.

5. Conclusion

At the European scale, several past studies looked at the potential advantages of combining solar and wind power. Other renewable energies such as biomass and hydropower were considered, either directly or not, as storage facilities able to balance the mismatches between load, wind and solar power generation. The literature shows that the optimal share between wind and solar power varies according to the time scale. For Europe and at daily time scale, it is usually considered as a mix composed by 60 % of wind power and 40 % of solar power. In this study, we integrated run-of-the-river (RoR) power with solar and wind power.

We analyze RoR power integration over 12 different regions in order to take into account a wide range of climatic conditions in Europe. The penetration rates, defined as the percent of energy load directly supplied by the CRE power generation (i.e. without any storage requirement for balancing) is computed for all the possible combination of the three considered CREs. Taking into account a 100 % renewable scenario (i.e. an average CRE generation factor $\gamma=1$), we show that RoR power integration increases the overall CRE penetration (ranging from +1 to +8 percentage points, Table 4). Increasing penetration rate actually appears to result from a trade-off between i) decreasing the difference in time variability between generation and load, and ii) improving the generation-load correlation (which often means limiting the anti-correlation coming from either solar or RoR hydro power).

The optimal solar-wind-RoR mixes show a high rate of RoR power for all regions (from 35 to 65 %). One could rightly point out that such a high share of RoR hydropower is not realistic in some areas, for both technical and economic reasons. However, our results show that i) it is worth integrating even a small amount of RoR hydropower into a solar-wind mix since the penetration always increase and ii) it is possible to optimize the RoR hydropower integration for each climate region by 'replacing' more solar or wind power contribution.

Our work is based on a number of assumptions, data and modelling choices, which potentially lead to some uncertainty in our results and interpretations. If a comprehensive uncertainty analysis was obviously out of the scope of the study, the following uncertainty sources are nevertheless worth being mentioned. A first difficulty concerns the dataset of hydro-meteorological observations required for the analysis. In the present case, a number of needed time series have been derived from weather pseudo-observations downscaled with the WRF regional model. Such data present of course limitations, for some types of meteorological events and/or in specific areas especially, where atmospheric processes are classically poorly simulated (e.g. convective and orographic precipitation, wind fields in mountainous regions). Conversely to observed data, pseudo-observations are however available at high space – time resolution. They are moreover complete over rather long

periods of time, even in regions with no observations, which is obviously a strength. As they are downscaled from the ERA-Interim atmospheric reanalyses, using these data instead of observed ones (when available) is finally not expected to drastically impact the results, especially in terms of temporal organization (and next co-fluctuations) of the different energy sources. In all cases, improved analyses of climate driven energy sources will be possible in the next decades, owing to the ongoing progresses in regional climate modelling which will allow producing more reliable reanalyses of meteorological variables for a number of region worldwide.

Another potentially critical source of uncertainty lies in the different models used to convert weather variables into energy load and power production. Better parametrizations and modelling schemes are obviously possible for more relevant simulations. The choice of a same parametrization for all studied regions could be for instance relaxed. The way runoff is harnessed for hydropower production could include information on the topological structure of the hydrographic network within each region. Further works should explore how such model refinements could influence our results, but the main conclusions of our work are not expected to drastically change. For instance, a major assumption made along this study was to consider that a fraction of the electricity consumption was temperature sensitive (see equation 5). This is not necessarily true for some European countries where heating needs are supplied by biomass burning or gas, for instance. When the present study is carried out with a constant energy load instead of a temperature sensitive one, results are rather unchanged. For all regions very similar 'triangles' and very similar optimal mixes are obtained (changes by few percent points only for the optimal mixes).

Future works should also consider few additional questions. The first relate to the RoR power integration for other time scales than daily. Von Breman (2010) show that the optimal solar-wind mix depends on the considered time scale (it goes from 20 % of solar power at hourly time scale to 40 % at monthly time scale). One can easily guess that RoR power would be also valuable at sub-daily time scales especially for smoothing the well-known high time variability of wind and solar power at those scales. The space integration is also an important question. Steinke et al. (2013) divided Europe in several 'copper plates', meaning that there are no energy transport losses within each region. They show that the sizes of these cooper plates implies different strategies in term of oversizing CRE power capacity, storage and backup facilities requirement. The approach used in this study is similar since each region is autonomous and considered as a cooper plate. Analyzing the effect of the grid extension at the regional scale (i.e. the size of each region/cooper plate) and at the European scale (i.e. allowing energy transport from one region to another), on the penetration rate and the corresponding optimal strategies of CRE mix would help stakeholders to design future network.

Storage facilities also matters. Weitemeyer et al. (2015) show that storage facilities increase the penetration of the 60 % wind 40 % solar mix in Germany. The increase amplitude however depends on the storage distribution (centralized with high efficiency vs distributed with lower efficiency). It would be worth analyzing such an increase for different climatic conditions than Germany and for different energy mixes, including RoR. Large time scales (i.e. monthly, yearly, decades) are also important. François et al. (2016) highlight that variability at larger time scales is a good proxy of the storage required for balancing. For these large time scales, variability of RoR might differ regarding the precipitation variability in Europe. Succession of either wet or dry years should be critical for the share of RoR power within the energy mix, and needs to be investigated. Such study would for instance benefit of the new large-scale reanalysis data (Compo et al., 2011). Large time scale study also

highlights the need to account for climate change impact on weather variable driving both the CRE generation and the energy load (François et al., 2014a).

Acknowledgements. This work is part of the FP7 project COMPLEX (Knowledge based climate mitigation systems for a low carbon economy; Project FP7-ENV-2012 number: 308601; http://www.complex.ac.uk/). This paper also benefited from comments and suggestions from two anonymous reviewers.

References

BFE, Bundesamt für Energie (Office fédéral de l'énergie) (2013). Schweizerische Elektrizitätsstatistik 2013 - Statistique suisse de l'électricité 2013, Bern, Switzerland, Technical report, 56pp, available online at http://www.bfe.admin.ch/. Last access: 22 april 2015 (in German and French)

(von) Bremen, L. (2010). Large-scale variability of weather dependent renewable energy sources. In Management of Weather and Climate Risk in the Energy Industry, (Springer), pp. 189–206.

Compo, G.P., Whitaker, J.S., Sardeshmukh, P.D., Matsui, N., Allan, R.J., Yin, X., Gleason, B.E., Vose, R.S., Rutledge, G., Bessemoulin, P., Brönnimann, S., Brunnet, M., Crouthamel, R.I., Grant, A.N., Groisman, P.Y., Jones, P.D., Kruk, M.C., Kruger, A.C., Marshall, G.J., Maugeri, M., Mok, H.Y., Nordli, Ø., Ross, T.F., Trigo, R.M., Wang, X.L., Woodruff, S.D., Worley. S.J (2011). The Twentieth Century Reanalysis Project. Q. J. R. Meteorol. Soc. 137, 1–28.

ECF (2010). Roadmap 2050: A practical guide to a prosperous, low-carbon Europe. Eur. Clim. Found. Volume 1, 100pp (Available online: http://www.roadmap2050.eu/, Last access November 2014).

European Council (2014). Conclusions of the European Council (Brussels). 16pp (Available online: http://ec.europa.eu/clima/policies/2030/documentation_en.htm, Last access: 26 November 2014).

François, B., Borga, M., Creutin, J.D., Hingray, B., Raynaud, D., and Sauterleute, J.F. (2016). Complementarity between Solar and Hydro Power: Sensitivity study to climate characteristics in Northern-Italy. Renew. Energy. 86, 543-553. doi:10.1016/j.renene.2015.08.044

François, B., Borga, M., Anquetin, S., Creutin, J.D., Engeland, K., Favre, A.C., Hingray, B., Ramos, M.H., Raynaud, D., Renard, B., Sauquet, E., Sauterleute, J.F., Vidal, J;P. and Warland, G.. (2014a). Integrating hydropower and intermittent climate-related renewable energies: a call for hydrology: Hydrol. Process. 28, 5465–5468.

GRDC (Global Runoff Data Center), 1999. Long-term mean monthly discharges of selected GRDC stations, Global Runoff Data Centre, Koblenz, Germany.

Hanif, M., Ramzan, M., Rahman, M., Khan, M., Amin, M., Aamir, M., 2012. Studying Power Output of PV solar Panels at different Temperatures and Tilt Angles. OSESCO journal of science and technology 8, 9–12.

Haylock, M.R., Hofstra, N., Tank, A.M.G.K., Klok, E.J., Jones, P.D., New, M., 2008. A European daily high-resolution gridded data set of surface temperature and precipitation for 1950-2006. J. Geophys. Res.-Atmos. 113. doi:10.1029/2008JD010201

Heide, D., von Bremen, L., Greiner, M., Hoffmann, C., Speckmann, M., and Bofinger, S. (2010). Seasonal optimal mix of wind and solar power in a future, highly renewable Europe. Renew. Energy *35*, 2483–2489.

Heide, D., Greiner, M., von Bremen, L., and Hoffmann, C. (2011). Reduced storage and balancing needs in a fully renewable European power system with excess wind and solar power generation. Renew. Energy *36*, 2515–2523.

Hoogwijk, M., and Graus, W. (2008). Global potential of renewable energy sources: a literature assessment. Backgr. Rep. Prep. Order REN21 Ecofys PECSNL072975.

Johnson, G.L. (1985). Wind characteristics. In Wind Energy Systems, (Prentice-Hall Englewood Cliffs (NJ)), 32-99.

Lehner, B., Czisch, G., and Vassolo, S. (2005). The impact of global change on the hydropower potential of Europe: a model-based analysis. Energy Policy 33, 839–855.

Perpiñan, O., Lorenzo, E., Castro, M.A., 2007. On the calculation of energy produced by a PV grid-connected system. Progress in Photovoltaics: Research and Applications 15, 265–274.

Piria, R., and Junge, J. (2013). Norway's Key Role in the European Energy Transition, Smart Energy for Europe Platform, Berlin, Germany. 11p, Available online: http://jointdeclaration.org/wp-content/uploads/2013/06/Norway-key-role-energy-transition_web.pdf

Sample, J. (2015). Interactions between land use, climate and hydropower in Scotland. In EGU General Assembly Conference Abstracts, p. 3351.

Schaefli, B., Hingray, B., Niggli, M., and Musy, A. (2005). A conceptual glacio-hydrological model for high mountainous catchments. Hydrol Earth Syst Sci 9, 95–109.

Steinke, F., Wolfrum, P., and Hoffmann, C. (2013). Grid vs. storage in a 100% renewable Europe. Renew. Energy *50*, 826–832.

Sturc, M. (2012). Renewable energy: Analysis of the latest data on energy from renewable sources (Eurostat - European Union). 8pp (Available online: http://epp.eurostat.ec.europa.eu/, Last access: November 2014).

Vautard, R., Thais, F., Tobin, I., Bréon, F.-M., de Lavergne, J.-G.D., Colette, A., Yiou, P., and Ruti, P.M. (2014). Regional climate model simulations indicate limited climatic impacts by operational and planned European wind farms. Nat. Commun. 5, 3196.

Weitemeyer, S., Kleinhans, D., Vogt, T., and Agert, C. (2015). Integration of Renewable Energy Sources in future power systems: The role of storage. Renew. Energy 75, 14–20.

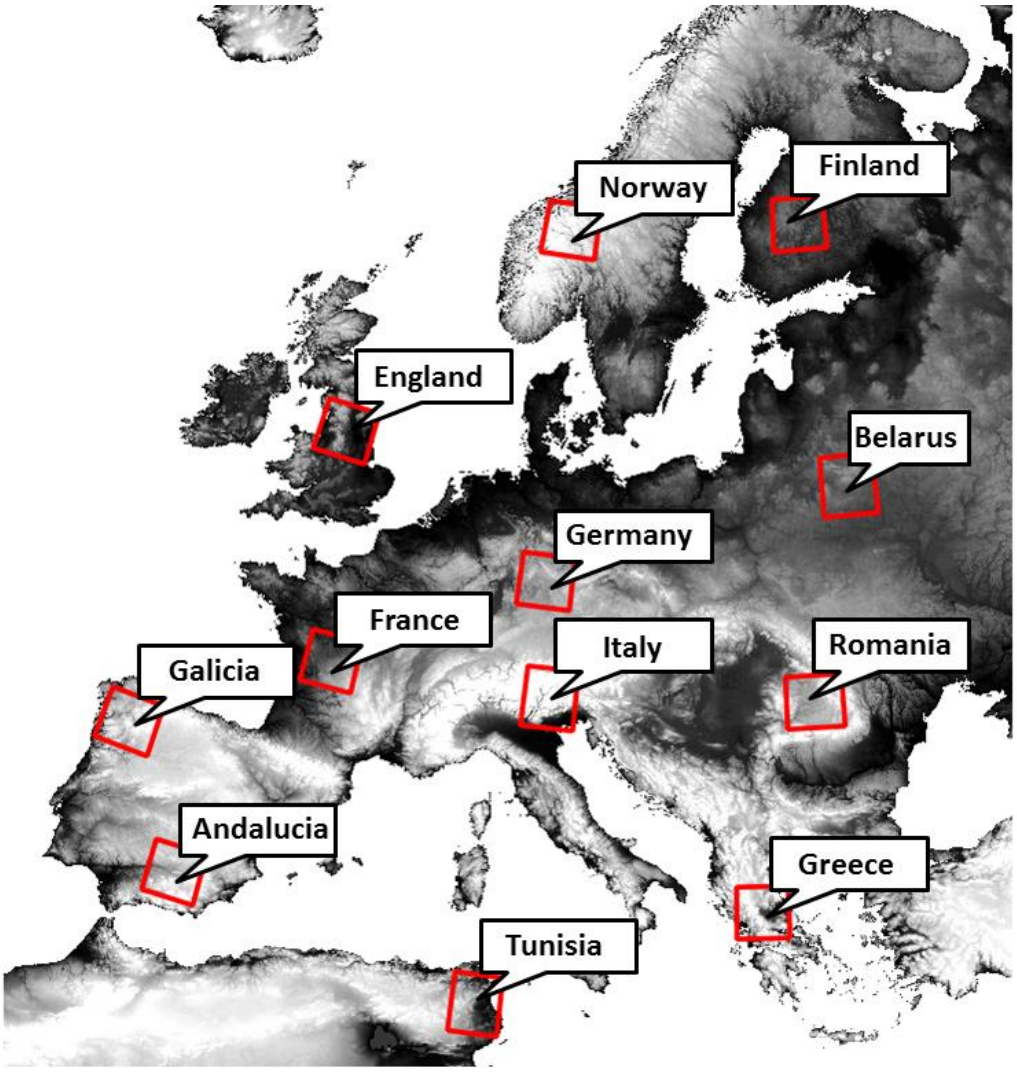

Figure 1: Map of the 12 regions selected across Europe and North Africa with their name used in this study. This selection explores two climate transects, the first one going from the Northern regions (Norway, Finland) to the Southern ones (Greece, Andalucía, Tunisia) and the second one going from the oceanic climate (England, France, Galicia) to the continental one (Romania, Belarus).

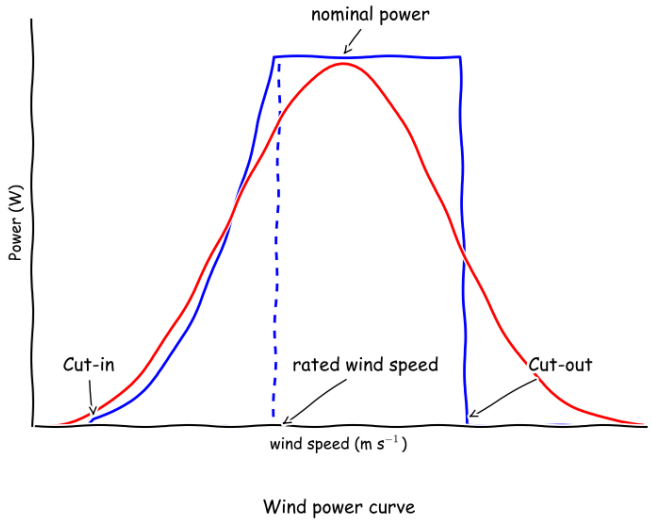

Figure 2: Sketch of the wind power curve. The blue curve is the nominal windmill power curve illustrating the different wind speed thresholds governing power generation. The red curve is the modified daily power curve according to the 3 hour time scale resolution and the statistical distribution of sub-daily wind velocities.

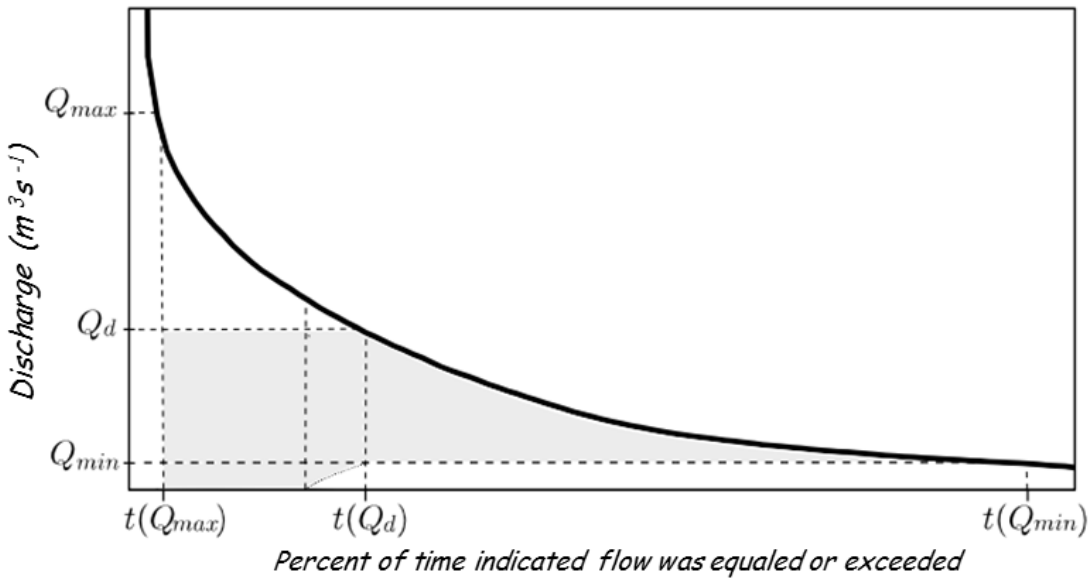

Figure 3: Flow duration curve and characteristic discharges used to simulate power generation from the run-off-the-river plant. Qmin, Qmax are the minimum and maximum discharge above which and below which the generation has to be stopped. Qd is the design flow. The ligh gray area represents the design volume used for the considered power plant generation.

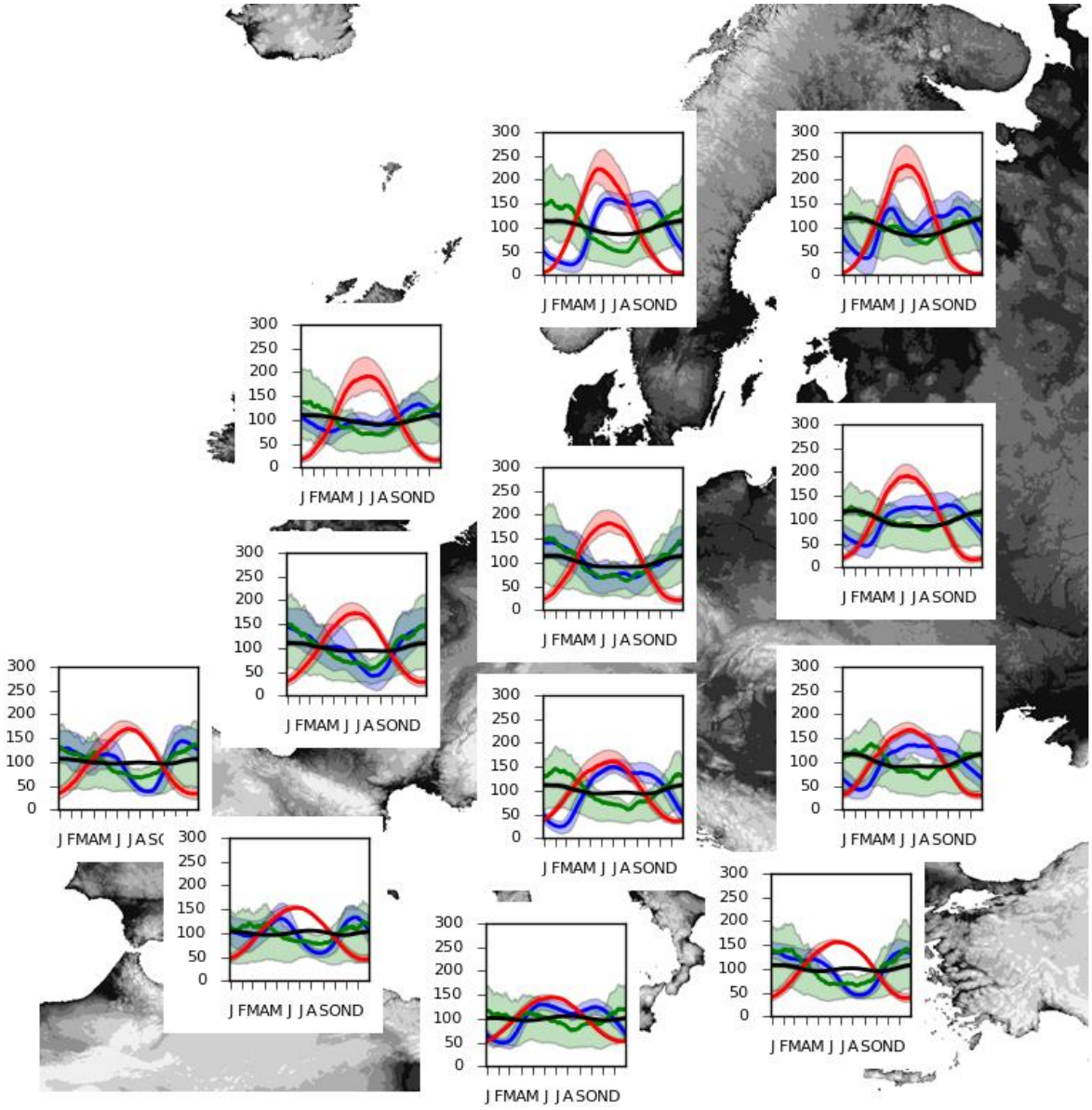

Figure 4: Normalized inter-annual average cycle of CRE power generation (solar- (red), wind- (black) and RoR hydro- (blue) power) and load (green) in each studied region over the period 1980-2012 (see equation 6 for the normalization procedure); For information only, light shaded areas show the distance between the 25th and 75th percentiles of the variable obtained for the 1980-2012 period for each calendar day; the x-axis gives the initial letters of the months of the year; the value of each variable on the y-axis is given in percentage of the average load.

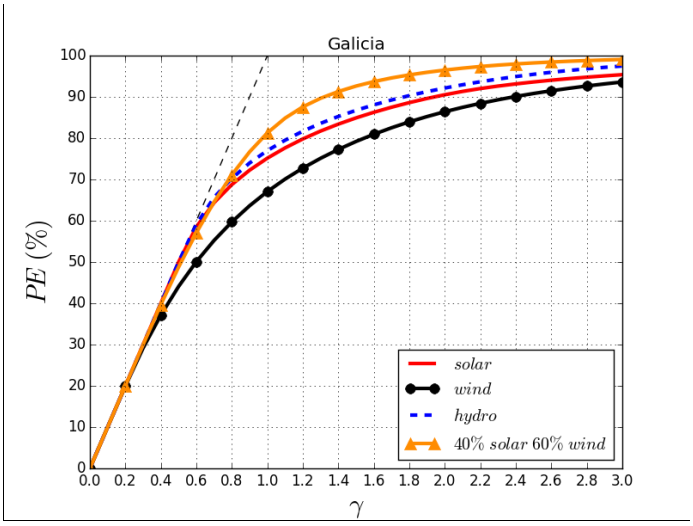

(a)

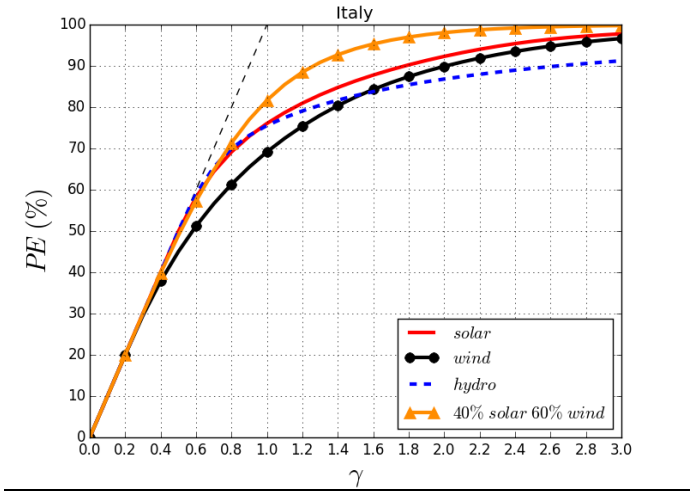

(b)

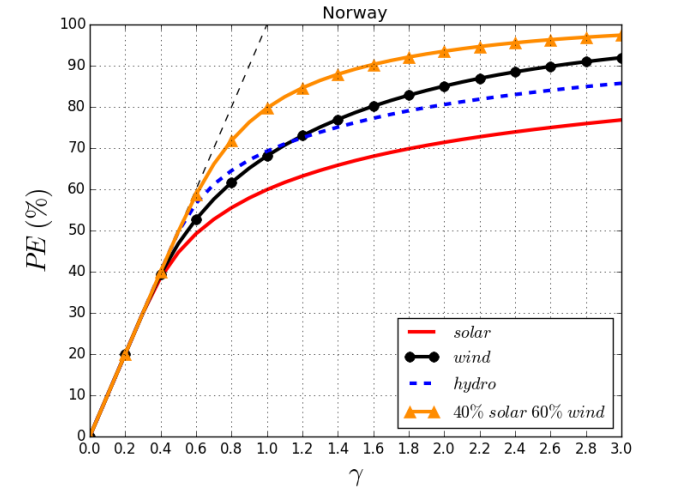

(c)

Figure 5: Evolution of the penetration rate PE with the average CRE generation factor γ for a) Galicia, b) Italy and c) Norway and for solar (red), wind (black), hydro (blue) CREs and the von Bremen optimal mix (60% wind, 40% solar, orange)

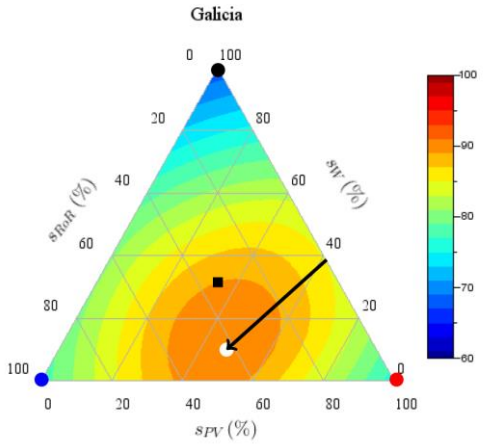

Figure 6: CRE penetration rate (%) for all wind/solar/hydro mix configurations in Galicia when a 100 % CRE production scenario is considered (the average CRE generation factor for the 1980-2012 period is γ=1). The x-axis gives the share of solar power (s_{PV} [%]), the left axis gives the share of RoR power (s_{RoR} [%]), and the right axis gives the share of wind power (s_W [%]). Red, black and blue bullets correspond respectively to a 100% solar, 100% wind and 100% hydro mix scenario. Horizontal gray lines show mix with the same wind share. 60° increasing (resp. decreasing) gray lines show mix with the same solar power share (resp. RoR power share). The black square corresponds to an equal share of each energy source. The white dot corresponds to the optimal mix, i.e. the mix giving the highest penetration rate. The black arrow shows the shift of the optimal CRE share and of the corresponding penetration rate when replacing a fraction of solar and wind power by RoR hydro power. It goes from the optimal wind-solar mix to the optimal wind-solar-RoR mix. The orientation of the arrows indicates what RoR replaces more wind than solar or conversely. For instance, a horizontal arrow indicates that RoR only replaces solar power (with no change in the wind rate). Conversely, an angle of 60° between the arrow and the wind axis indicates that RoR only replaces wind power (with no change in the solar rate).

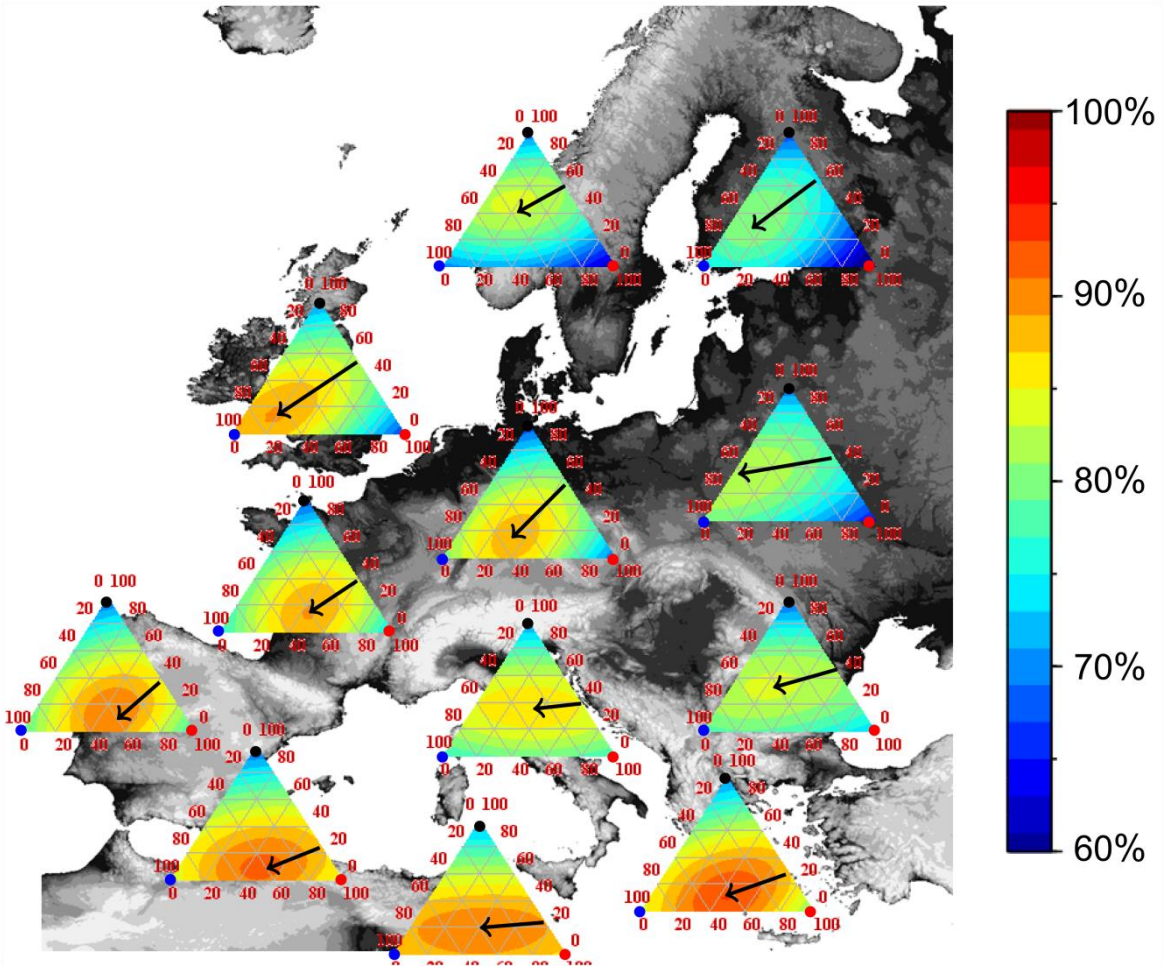

Figure 7: CRE penetration rate (%) as a function of the wind/solar/hydro mix for all 12 European regions. See Figure 6 for caption details.

Table 1: Location (Latitude, Longitude limits), size and elevation (average [min, max]) of the 12 regions

Region	Lat Min (°)	Lat Max (°)	Lon Min (°)	Lon Max (°)	Area (km²)	Elevation (m a.s.l.)
Finland	61.625	63.375	23.625	27.375	37465	137 [84 – 207]
Norway	61.125	62.875	7.375	11.125	38091	952 [171 – 1660]
Belarus	52.625	54.375	25.625	28.625	38610	176 [116 – 287]
England	52.875	54.625	-3.125	-0.125	38381	133 [0 – 450]
Germany	49.375	51.125	9.375	12.125	38047	379 [174 – 619]
France	45.375	47.125	-0.375	2.125	37405	217 [44 – 784]
Italy	45.625	47.375	10.375	12.875	37234	1348 [2 – 2701]
Romania	45.625	47.375	23.125	25.875	40957	675 [253 – 1410]
Greece	38.625	40.375	20.625	22.875	37564	666 [74 – 1411]
Galicia	41.375	43.125	-8.625	-6.125	40039	683 [79 – 1496]
Andalucia	37.125	38.875	-4.625	-2.375	38362	813 [228 – 1964]
Tunisia	34.875	36.875	8.875	10.875	40073	306 [19 – 880]

Table 2: Coefficient of variation (CV) of the daily power time series from each CRE (CV = standard deviation / mean) and for the von Bremen solar/wind optimal mix (von Bremen, 2010). CV of daily energy load in last column. Numbers within brackets give the ratio values between CV from each CRE and the load ‘s CV.

Region	PV Power	Wind Power	Hydro Power	60% wind 40% solar	Energy load
Finland	0.89 (6)	0.88 (6)	0.55 (3)	0.58 (4)	0.16
Norway	0.84 (7)	0.79 (7)	0.60 (5)	0.46 (4)	0.12
Belarus	0.70 (5)	0.83 (6)	0.43 (3)	0.52 (4)	0.14
England	0.73 (8)	0.79 (9)	0.36 (4)	0.48 (5)	0.09
Germany	0.65 (6)	0.92 (8)	0.55 (5)	0.52 (5)	0.11
France	0.57 (7)	0.90 (11)	0.60 (8)	0.51 (6)	0.08
Italy	0.50 (6)	0.87 (11)	0.51 (6)	0.51 (6)	0.08
Romania	0.53 (4)	0.92 (8)	0.46 (4)	0.55 (5)	0.12
Greece	0.45 (8)	0.86 (14)	0.41 (7)	0.48 (8)	0.06
Galicia	0.54 (11)	0.91 (18)	0.53 (11)	0.51 (10)	0.05
Andalucía	0.41 (8)	0.92 (18)	0.40 (8)	0.54 (11)	0.05
Tunisia	0.35 (9)	0.77 (19)	0.35 (9)	0.47 (12)	0.04

Table 3: Pearson correlation coefficient between daily power and daily energy load; values in bracket give the percentage of explained variance, computed as the squared value of the correlation coefficient).

Region	PV Power	Wind Power	Hydro Power	60% wind 40% solar
Finland	-0.65 (42 %)	0.05 (< 1 %)	-0.32 (10 %)	-0.36 (13 %)
Norway	-0.58 (34 %)	0.21 (4 %)	-0.69 (48 %)	-0.21 (4 %)
Belarus	-0.69 (48 %)	0.07 (< 1 %)	-0.57 (32 %)	-0.30 (9 %)
England	-0.61 (37 %)	0.12 (1 %)	-0.01 (< 1 %)	-0.25 (6 %)
Germany	-0.65 (42 %)	0.13(2 %)	0.40 (16 %)	-0.19 (4 %)
France	-0.57 (32 %)	0.08 (< 1 %)	0.37 (14 %)	-0.17 (3 %)
Italy	-0.51 (26 %)	0.32 (10 %)	-0.71 (50 %)	0.12 (1 %)
Romania	-0.67 (45 %)	0.09 (< 1 %)	-0.60 (36 %)	-0.17 (3 %)
Greece	-0.35 (12 %)	0.19 (4 %)	0.20 (4 %)	0.07 (< 1 %)
Galicia	-0.39 (15 %)	0.02 (< 1 %)	0.18 (3 %)	-0.13 (2 %)
Andalucía	0.11 (1 %)	-0.09 (< 1 %)	-0.29 (8 %)	-0.06 (< 1 %)
Tunisia	0.21(4 %)	-0.07 (< 1 %)	-0.04 (< 1 %)	0.00 (< 1 %)

Table 4: Optimal shares and corresponding CV, correlation coefficient *r* and penetration rate PE_{opt} for a wind / solar mix and for a wind / solar / hydro mix. Shares are given for solar (S_{PV}), wind (S_W) and RoR (S_{RoR}) power for the 12 regions. The numbers in brackets give the penetration increase when integrating RoR hydro power into the solar/wind mix.

	Wind-Solar mix					Wind-Solar-RoR mix					
Region	**S_{PV} (%)**	**S_W (%)**	**CV**	**r**	**PE_{opt} (%)**	**S_{PV} (%)**	**S_W (%)**	**S_{RoR} (%)**	**CV**	**r**	**PE_{opt} (%)**
Finland	35	65	0.60	-0.30	74	15	35	50	0.42	-0.38	80 (+6)
Norway	40	60	0.46	-0.21	80	15	50	35	0.38	-0.35	82 (+2)
Belarus	45	55	0.50	-0.37	77	5	30	65	0.37	-0.45	82 (+5)
England	45	55	0.46	-0.32	80	20	15	65	0.27	-0.29	88 (+8)
Germany	50	50	0.46	-0.33	79	35	15	50	0.30	-0.06	87 (+8)
France	60	40	0.40	-0.41	82	45	15	40	0.28	-0.17	88 (+6)
Italy	60	40	0.39	-0.11	84	30	35	35	0.35	-0.3	85 (+1)
Romania	55	45	0.45	-0.35	80	25	35	40	0.38	-0.45	82 (+2)
Greece	65	35	0.33	-0.14	86	45	10	45	0.20	-0.09	92 (+6)
Galicia	60	40	0.39	-0.30	84	45	10	45	0.25	-0.2	89 (+5)
Andalucía	75	25	0.34	0.04	86	50	10	40	0.24	-0.13	90 (+4)
Tunisia	75	25	0.31	0.14	88	40	20	40	0.27	0.06	89 (+1)

Appendix D

Supplementary figures for Part IV

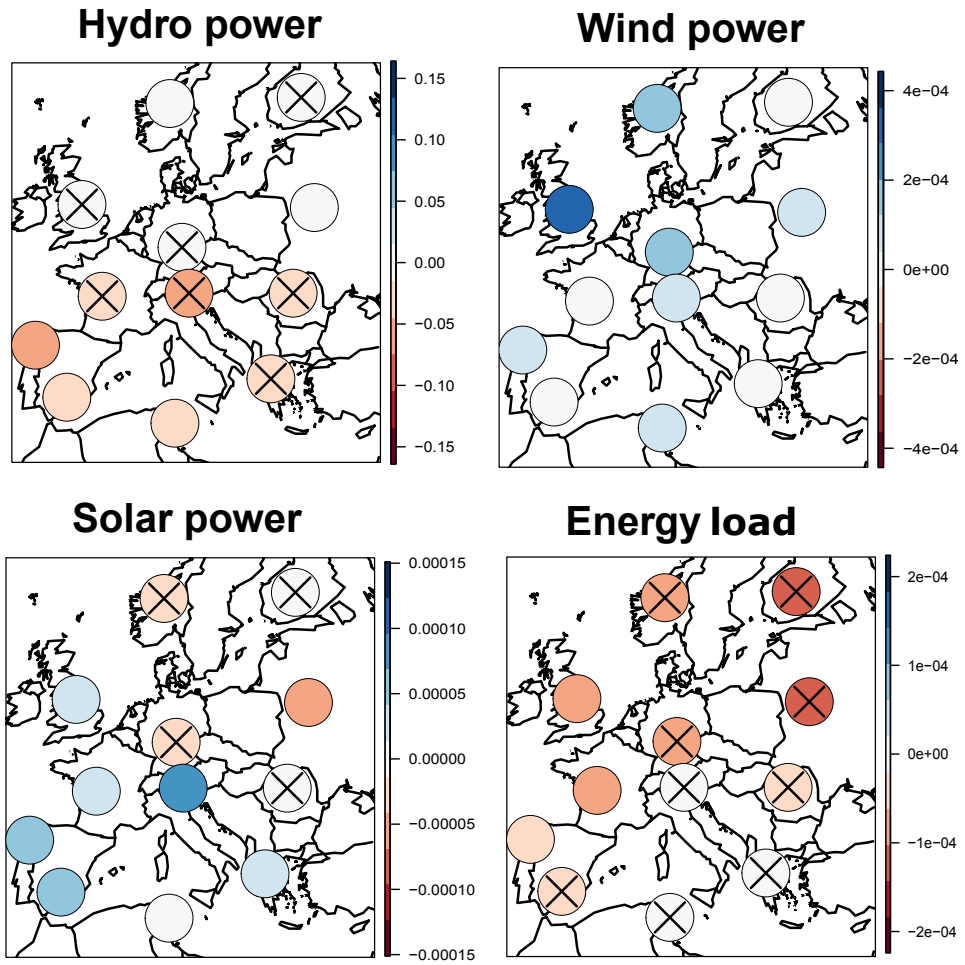

Figure D.1 – **20^{th} century trend in annual CRE sources and energy load**. Slope coefficients (colors) of a linear regression on hydro, solar, wind power (MW.yr^{-1}) and energy load (yr^{-1}) for the 12 European test regions. Non-significant linear trends (95% confidence interval) are highlighted with the cross symbol. When it is relevant, the relative change from 1900 to 2010 is displayed.

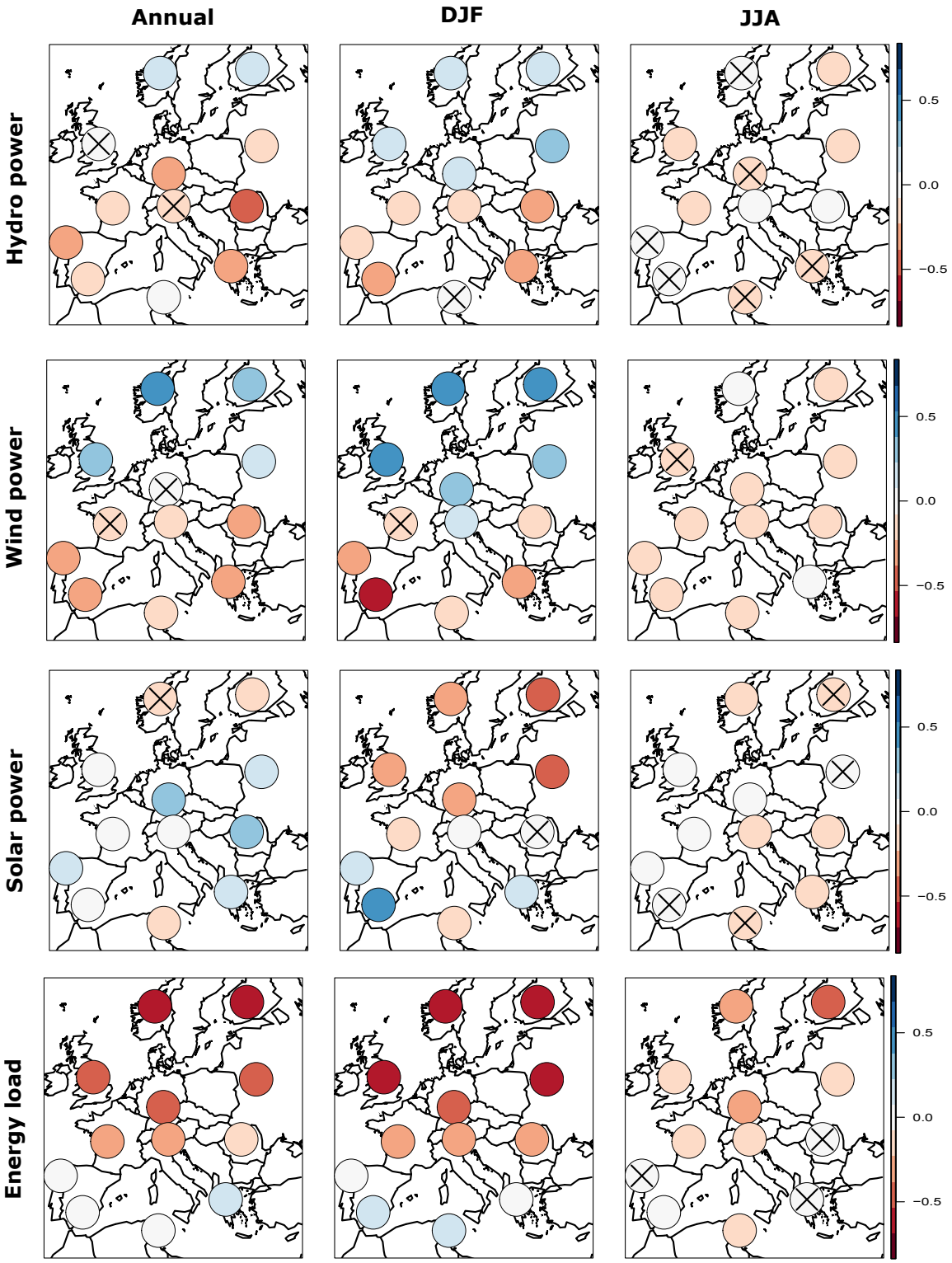

Figure D.2 – **Connections between the NAO and CRE sources/energy load**. Spearman correlation coefficients between the NAO index and regional series of hydro, wind, solar power and energy load. Non-significant correlation coefficients (95% confidence interval) are highlighted with the cross symbol. Results are displayed for annual, winter and summer data.

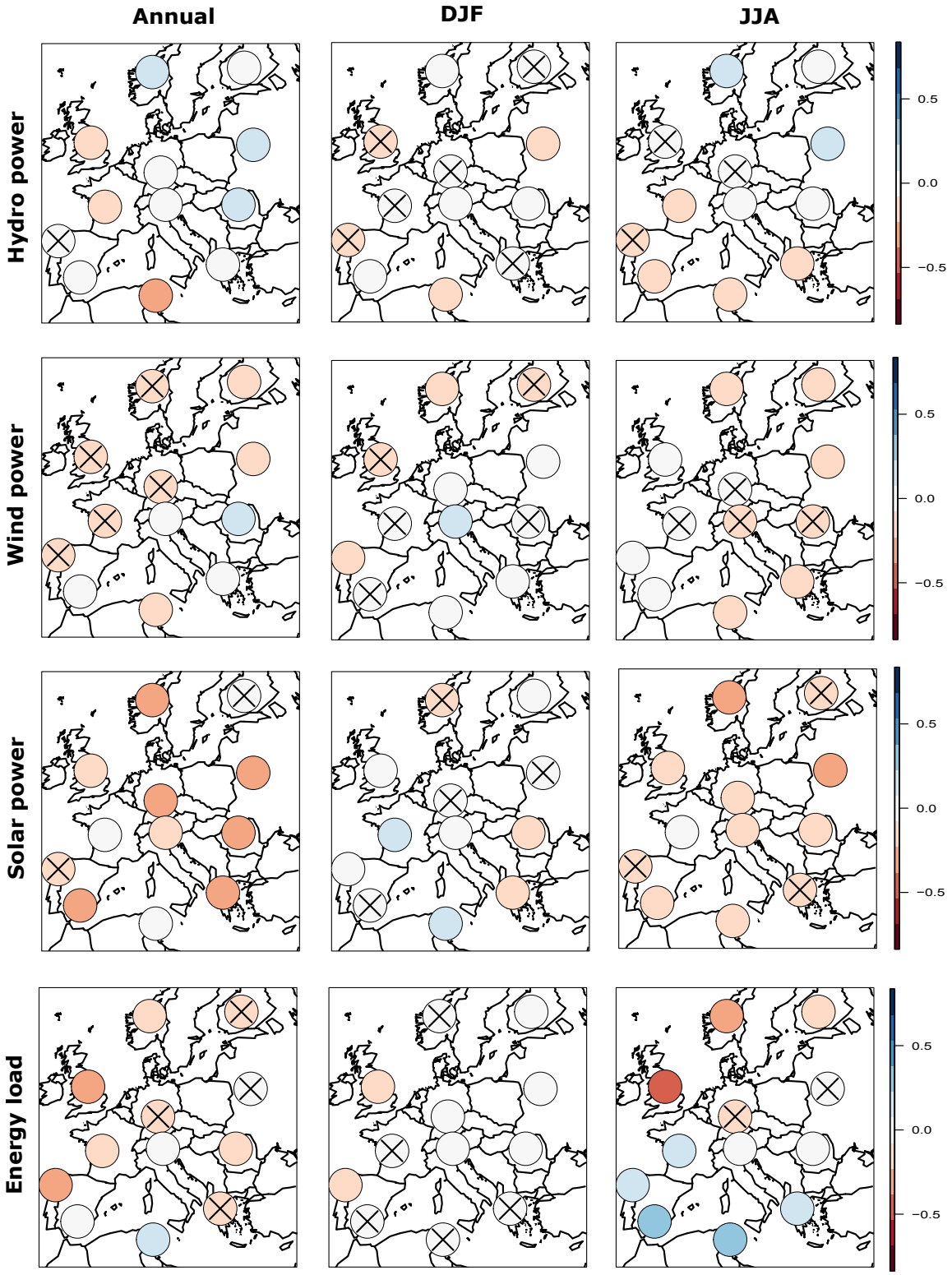

Figure D.3 – **Connections between the AMO and CRE sources/energy load**. Spearman correlation coefficients between the AMO index and regional series of hydro, wind, solar power and energy load. Non-significant correlation coefficients (95% confidence interval) are highlighted with the cross symbol. Results are displayed for annual, winter and summer data.

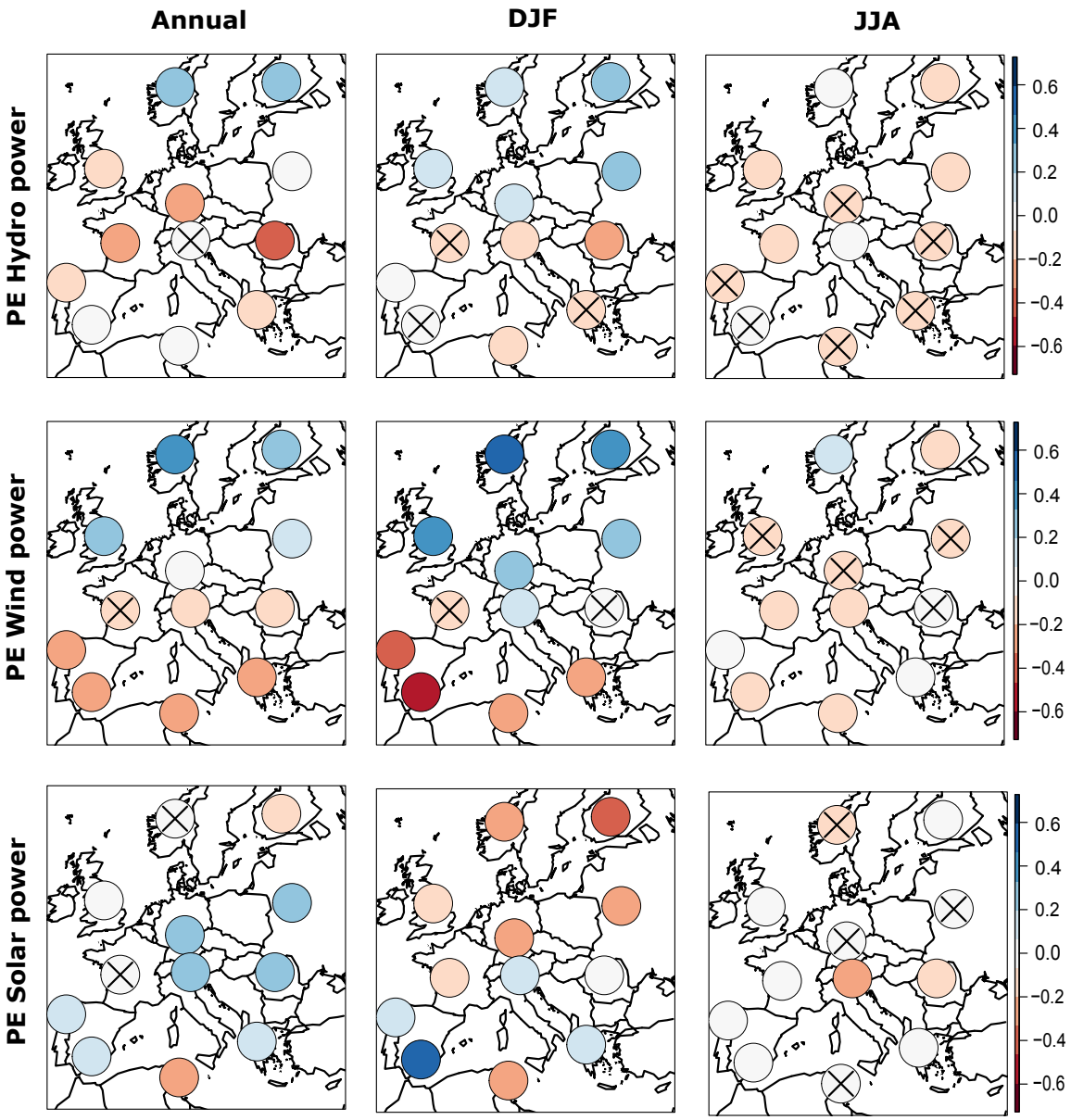

Figure D.4 – **Connections between the NAO and penetration rates of CRE sources**. Spearman correlation coefficients between the NAO index and PE regional series associated to hydro, wind and solar power. Non-significant correlation coefficients (95% confidence interval) are highlighted with the cross symbol. Results are displayed for annual, winter and summer data.

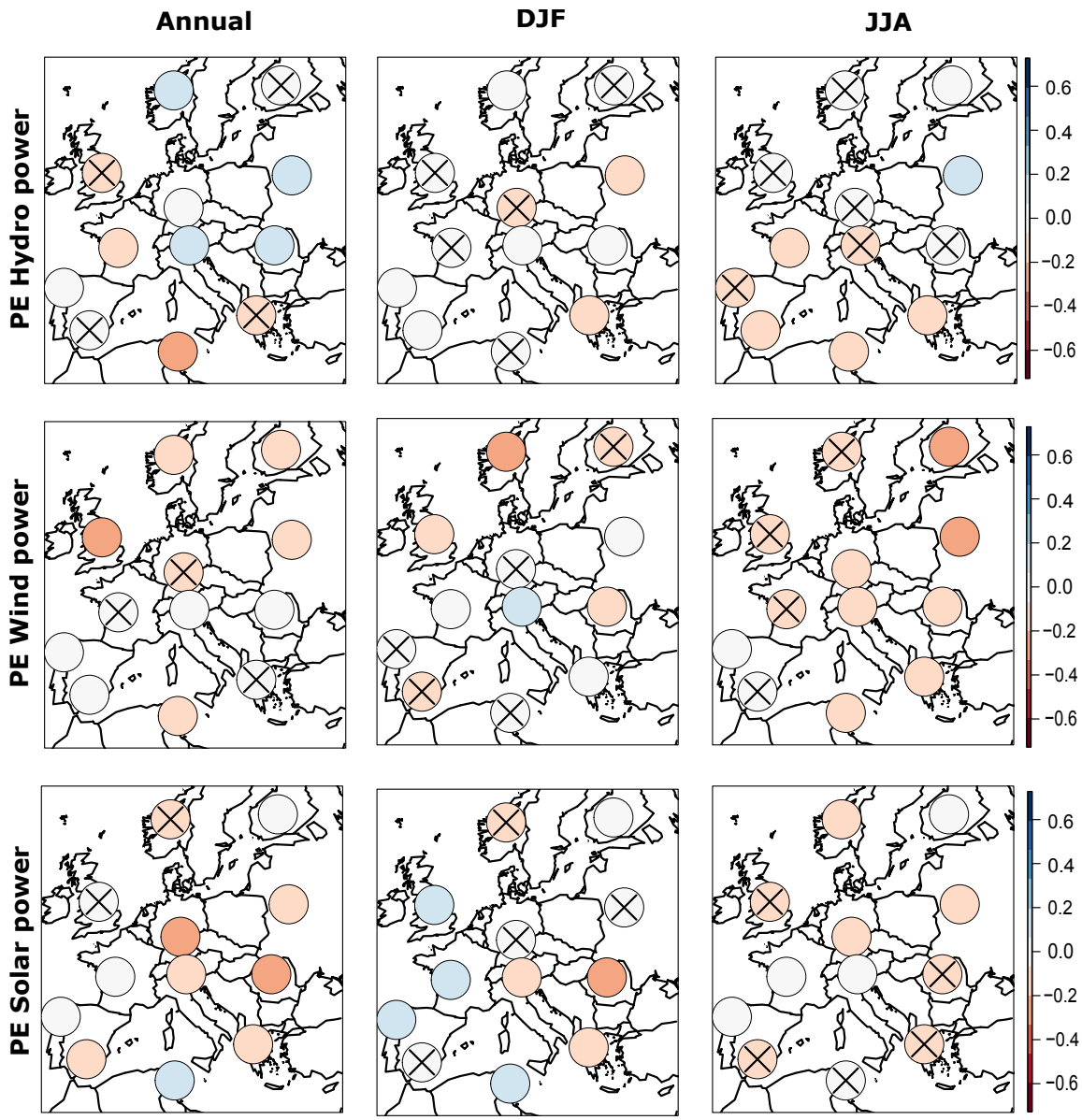

Figure D.5 – **Connections between the AMO and penetration rates of CRE sources**. Spearman correlation coefficients between the AMO index and PE regional series associated to hydro, wind and solar power. Non-significant correlation coefficients (95% confidence interval) are highlighted with the cross symbol. Results are displayed for annual, winter and summer data.

Variabilité hydro-climatique et intégration d'énergies renouvelables en Europe: Evaluation multi-échelle de l'équilibre production-demande pour différentes sources et combinaisons d'énergies

Dans un contexte de changement climatique, l'intégration des énergies renouvelables aux systèmes électriques est un enjeu majeur des décennies à venir. Les énergies liées au climat (photovoltaïque, éolien et hydro-électricité) peuvent contribuer à une réduction des émissions de gaz à effet de serre. Cependant, elles sont fortement intermittentes et la production électrique associée peine à répondre à la demande. Cette étude vise à évaluer la faisabilité météorologique du développement d'un système de production électrique basé sur les sources d'énergie liées au climat (CRE - Climate-Related Energy). Nous considérons uniquement leurs variations spatiotemporelles et supposons un équilibre entre production et demande moyennes. Nous avons développé CRE-Mix, une chaîne de modèles permettant de convertir les variables météorologiques en chroniques énergétiques. Cet outil permet l'estimation des fluctuations spatiotemporelles de production et de demande énergétiques résultant de la variabilité hydro-climatique. Pour une sélection de régions en Europe, nous évaluons la facilité d'intégration des CRE en fonctions de leur cohérence temporelle avec la demande. Pour chaque source d'énergie et de multiples mix énergétiques nous estimons successivement (i) le taux de pénétration moyen (PE), qui quantifie la proportion de demande satisfaite sur une longue période et (ii) les caractéristiques des périodes de faible pénétration pour lesquelles le taux journalier de demande satisfaite reste bas pendant plusieurs jours consécutifs. Les résultats montrent que les systèmes basés sur une seule source ont du mal à répondre à la demande et souffrent de longues périodes de faible PE, en raison de leur variabilité temporelle. Cependant, une combinaison d'énergies, l'utilisation de systèmes de stockage ou l'échange d'énergie entre régions, permettent d'augmenter fortement la fiabilité des CRE (PE proche de 100% et rares/courtes périodes de faible pénétration).

Cette étude, basée sur 30 ans, a été étendue à l'ensemble de XXème siècle afin d'évaluer les fluctuations basse fréquence des CRE résultant de la variabilité interne du climat. De longues chroniques régionales de production et de demande ont été générées grâce au développement d'une méthode de descente d'échelle statistique basée sur les analogues atmosphériques (SCAMP). Cet outil génère des scenarios météorologiques multivariés physiquement cohérents. Les résultats montrent que les variations basse fréquence des CRE sont influencées par les grandes oscillations océano-climatiques. De plus, on montre que les variations multi-décennales de l'hydro-électricité sont particulièrement importantes avec notamment une différence en PE supérieure à 15% d'une décade à l'autre et des périodes de faible pénétration aux caractéristiques très irrégulières. Enfin, nous évaluons la pertinence de systèmes électriques basés sur les CRE en climat futur. SCAMP permet de produire des scenarios régionaux de variables météorologiques à partir des modèles climatiques issus des simulations CMPI5. Pour les précipitations, les tendances simulées par SCAMP sont en désaccord avec de nombreuses études. L'application de SCAMP en "modèle parfait" semble indiquer que le lien entre les situations atmosphériques de grande échelle et les précipitations totales, mais également convectives et stratiformes, change en climat futur.

Hydro-climatic variability and the integration of renewable energy in Europe. Multi-scale evaluation of the supply-demand balance for various energy sources and mixes.

In the context of climate change, the integration of renewables in electric power systems is one of the main challenges of the coming decades. Climate-Related-Energy sources (CRE - solar, wind and hydro power) can contribute to reduce the greenhouse gas emissions. However, they exhibit large spatio-temporal fluctuations and the associated intermittent electricity generation often leads to an incomplete supply-demand balance. This study aims to evaluate the meteorological feasibility of developing an electric power system that would only rely on CRE sources. We focus on the multi-scale spatio-temporal fluctuations of these renewables by assuming a balance between mean electricity production and mean energy load. We develop and use CRE-mix, a suite of models able to convert meteorological conditions into CRE time series. It gives an assessment the spatio-temporal fluctuations of power production and energy demand, resulting from the multi-scale hydro-climatic variability. For a set of European regions, we assess the ease of integration of CRE sources, regarding their temporal consistency with energy demand. For each CRE source and multiple CRE mixes, we consider in turn (i) the mean penetration rate (PE), which quantifies the proportion of satisfied demand over a long period and (ii) the characteristics of low penetration periods, defined as sequences of days for which the penetration rate is lower than a given threshold. This study proves that single CRE sources have difficulty to meet the energy demand and suffer from long low penetration periods, due to their multi-scale temporal variations. However, using some integrating factors (multi-sources, storage systems, inter-regions electric power transmission), efficiently improves the reliability of CRE-based power systems with PE rates close to 100% and rare low penetration periods.

These analyses, based on a 30-yr period, are extended to the entire 20^{th} century in order to assess the low frequency fluctuations of CRE sources resulting from the internal variability of climate. Long regional series of production and demand, were generated thanks to the development of a statistical downscaling method based on atmospheric analogues (SCAMP). It simulates physically-consistent multivariate series of meteorological parameters. The results demonstrate that these fluctuations are related to some large scale oceano-climatic oscillations. Moreover, the multi-decennial variations of hydro power are particularly large: changes in PE rates exceeding 15% from one decade to the other and uneven energy droughts characteristics. Finally, we evaluate the relevance of the CRE sources under future climate conditions. SCAMP is used to produce downscaled projections of meteorological drivers of CRE sources for the 21^{st} century from a selection of CMIP5 climate models. The resulting scenarios for precipitation are not consistent with other studies focusing of the future modifications of this variable in Europe. The application of SCAMP in a perfect-model approach seems to indicate that the large-scale-meteorology/local-precipitation relationship is changing in the course of the 21^{st} century, for all total, convective and stratiform precipitation.